The Monophosphaamidine Functional Group

JASON DOUGLAS MASUDA

B.Sc., University of Lethbridge, 2000

A Thesis
Submitted to the School of Graduate Studies
of the University of Lethbridge
in Partial Fulfillment of the
Requirements for the Degree

MASTER OF SCIENCE

LETHBRIDGE, ALBERTA
May, 2002

For my wife Raechelle, who with her love and

support, has guided me in the right direction.

Abstract

The synthesis and characterization of two new bulky *N*,*P*-monophosphaamidines (also known as C-aminophosphaalkenes) are described. These phosphorus analogues to amidines are shown to exhibit isomerism and tautomerism in solution that is characteristic to the amidine functional group. In addition, the nature of the P=C-N system is examined using DFT techniques. Metal complexes of the title compounds with Group 6 metal carbonyls (L-M(CO)$_5$, M = Cr, Mo, W) are also described. A new primary phosphane is reported that contains the sterically bulky 2,6-diisopropylphenyl (Dip) group, along with mono and disilylated derivatives. Also included is the synthesis and characterization of a new bulky *N*,*N*',*P*-monophosphaguanidine.

Acknowledgements

First and foremost I would like to thank my supervisor Prof. René Boeré, for taking me, a lost student, under his wing and providing me with a strong foundation for my future endeavors. His time and patience with all my work as an undergraduate and graduate student will not be forgotten.

I thank Dr. Peter Dibble for his witty conversations, helpful advice and for writing all of those pesky reference letters I have asked for. I also thank Dr. Marc Roussel for taking the time to guide me through the area of theoretical chemistry and helping me through the initial theoretical work on my side projects with Dr. Dibble.

To all of the members of the Dibble and Boeré labs, I thank all of you for the assistance and fun in the lab. The lab would have been much more dreary without you. First I would like to thank Tracey Rommele for being a wonderful co-worker and lunch companion for the first half of my degree. Second, I would like to thank Michelle Thibault for taking all of my quirks and idiosyncrasies with a grain of salt. You have made time in the lab pass without too much pain.

Dr. Gotthelf Wolmershäuser of the Fachbereich Chemie at the Universität Kaiserslautern, Germany deserves credit for obtaining the data sets for most of the crystal structures in my work. The University of Lethbridge is acknowledged for funding in the latter half of my program.

Finally, I would like to thank the people outside the university that have been important throughout my degree: my wife Raechelle, my parents, Betty Ann and Ron, my sister Kristie and my close friends (in no particular order) Fezz, Doug, Gomez, Dingo, Scuba and Brad.

Table of Contents

List of Tables

List of Figures

List of Abbreviations

AM1	Austin Model One
B3LYP	Becke's Three Parameter Hybrid Functional Using the Lee, Yang, and Parr Correlation Functional
^{n}Bu	*n*-butyl
^{t}Bu	*tert*-butyl
COD	1,5-cyclo-octadiene
COZY	homonulclear correlated spectroscopy
Cp	cyclopentadienyl
Cp^{*}	1,2,3,4,5-pentamethylcyclopentadienyl
Cy	cyclohexyl
DBU	1,8-diazabicyclo[5.4.0]undecene
DFT	density functional theory
Dip	2,6-diisopropylphenyl group
E	'Entgegen' (opposite)
Et	ethyl
EtOH	ethanol
eV	electron Volt
EXSY	exchange spectroscopy
[Fe]	$Cp^{*}Fe(CO)_2$
g	gram
Hz	Hertz
HOMO	highest occupied molecular orbital
IR	infrared
IUPAC	International Union of Pure and Applied Chemistry
LCAO	linear combination of atomic orbitals
LUMO	lowest unoccupied molecular orbital
Me	methyl
MeOH	methanol

Mes	2,4,6-tri-methylphenyl
Mes*	2,4,6-tri-tertbutylphenyl
mL	milliliters
mmol	millimole
MO	molecular orbital
MS	mass spectrum
NMR	nuclear magnetic resonance
ORTEP	Oakridge thermal ellipsoid plot
Ph	phenyl
^{i}Pr	isopropyl
SCF	self-consistent field
STO	Slater-type orbital
TBDMS	*tert*-butyl-dimethylsilyl
THF	tetrahydrofuran
Trip	2,4,6-triisopropylphenyl
p-tolyl	4-$CH_3C_6H_4$
UV	ultraviolet
VT	variable temperature
Z	'Zusammen' (together)

Compound Numbering Scheme
1 - 15

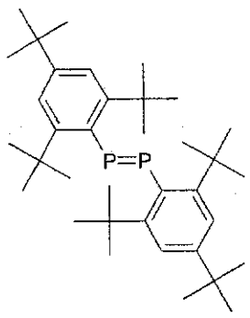

1

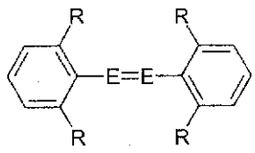

R = Mes (C_6H_2-2,4,6-CH_3), Trip (C_6H_2-2,4,6-$^iPr_3$)

2. E = P
3. E = As
4. E = Sb
5. E = Bi

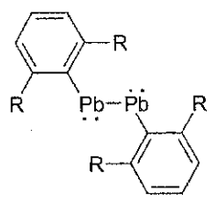

R = Trip (C_6H_2-2,4,6-$^iPr_3$)

6

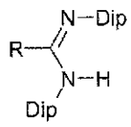

7. R = *p*-$CH_3C_6H_5$
8. R = *p*-$CH_3OC_6H_5$
9. R = CH_3
10. R = CF_3

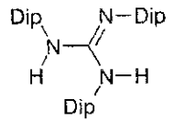

11.

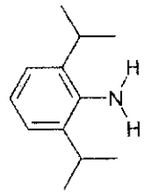

12

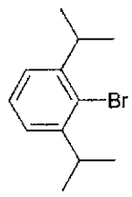

13

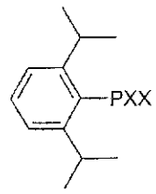

14
XX = Cl_2, ClBr, Br_2

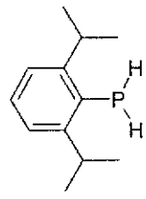

15

Compound Numbering Scheme
16 - 35

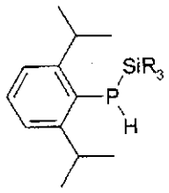

16. $R_3 = Me_3$
17. $R_3 = {}^tBuMe_2$

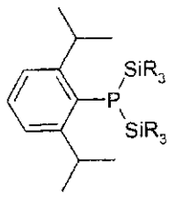

18. $R_3 = Me_3$
19. $R_3 = {}^tBuMe_2$

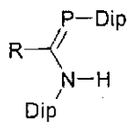

20. R = *p*-$CH_3C_6H_5$
21. R = *p*-$CH_3OC_6H_5$

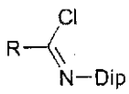

22. R = *p*-$CH_3C_6H_5$
23. R = *p*-$CH_3OC_6H_5$

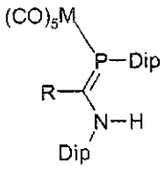

R = *p*-$CH_3C_6H_5$
24. M = Cr
25. M = Mo
26. M = W
R = *p*-$CH_3OC_6H_5$
27. M = Mo

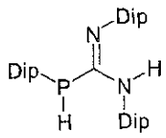

28

29

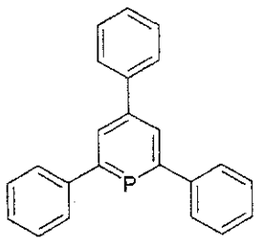

30

31

32

33

34

35

Compound Numbering Scheme

36 - 61

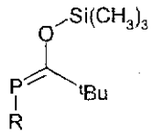

36. R = CH_3
37. R = ^{t}Bu
38. R = Cy
39. R = Ph

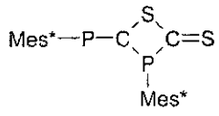

55

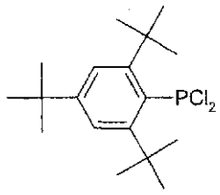

40

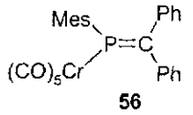

56

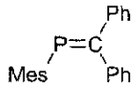

41

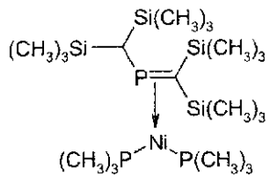

57

t-Bu—P=C=N—t-Bu

42

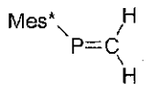

58

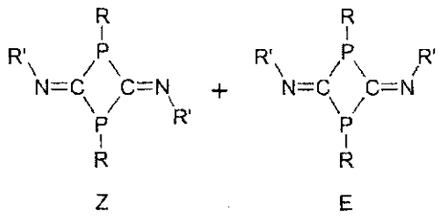

Z E

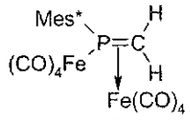

59

R = Ph
43. R' = 2-Cl-Ph
44. R' = 2,3-Cl-Ph
45. R' = 2-F-Ph
46. R' = 2,5-Cl-Ph

R' = Ph
47. R = Et
48. R = CH2Ph
49. R = Ph
50. R = t-Bu
51. R = Mes

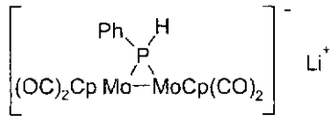

60

Mes*—P=C=N—Mes*

52

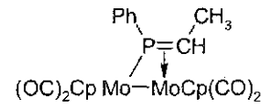

61

Mes*—P=C=O

53

Mes*—P=C=S

54

Compound Numbering Scheme
62 - 72

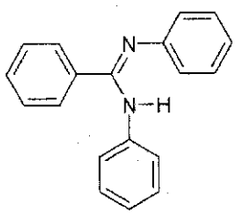

62

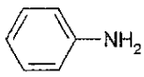

63

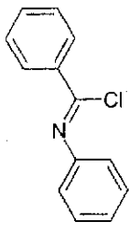

64

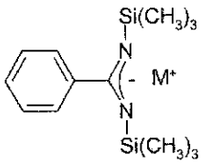

65 M = Li, Na, K

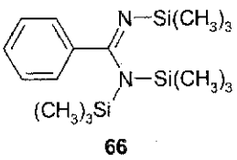

66

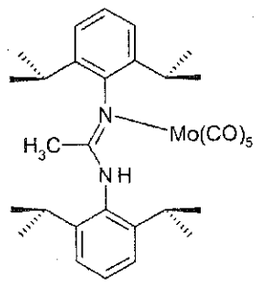

68

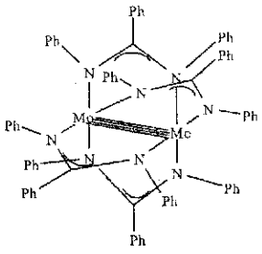

69

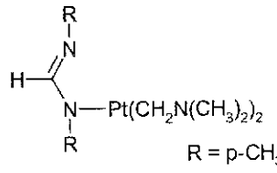

70

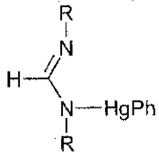

71

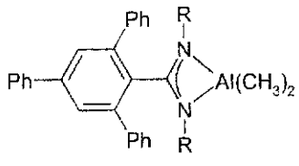

72 R = ^{i}Pr

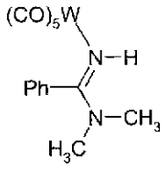

E isomer

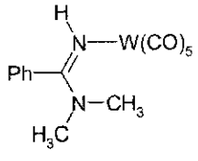

Z isomer

67

Compound Numbering Scheme
73 - 100

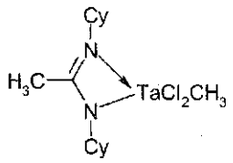

73

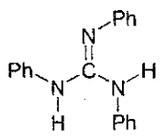

74

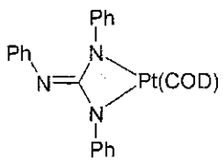

75

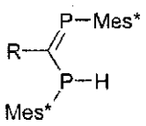

76. R = CH_3
77. R = Ph

Mes*—P=C=P—Mes*
78

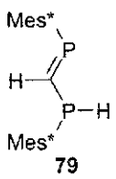

79

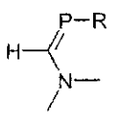

80. R = Ph
81. R = ^{t}Bu
82. R = Mes

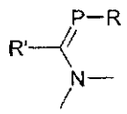

R' = H
83. R = Ph
84. R = Mes
R' = CH_3
85. R = Ph

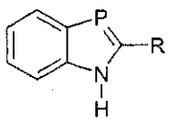

86. R = H
87. R = CH_3
88. R = Ph

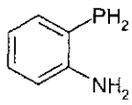

89

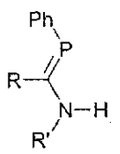

R = Ph
90. R' = Ph
91. R' = CH_3
92. R' = 2,6-Et_2Ph
93. R' = Cy
R' = Ph
94. R = ^{t}Bu
95. R = Mes

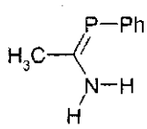

96

Ph_2PH
97

p-tolyl—N=C=N—*p*-tolyl
98

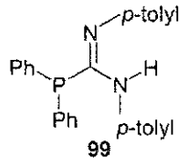

99

$PhPH_2$
100

Compound Numbering Scheme
101 – 123

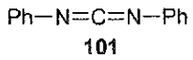

101

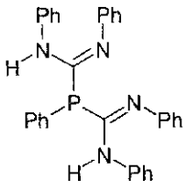

102

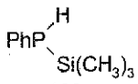

103

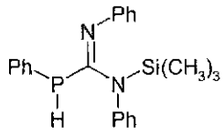

104

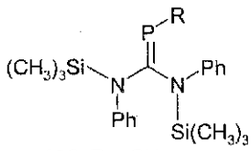

105. R = CH_3
106. R = Cy
107. R = ^{t}Bu
108. R = Ph
109. R = *p*-$(CH_3)_2$NPh

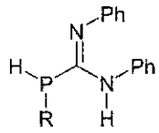

110. R = CH_3
111. R = Cy
112. R = ^{t}Bu
113. R = Ph
114. R = *p*-$(CH_3)_2$NPh

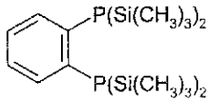

115

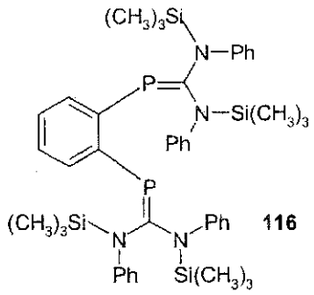

116

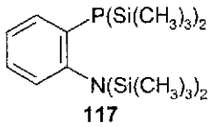

117

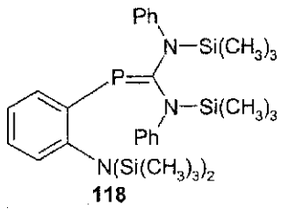

118

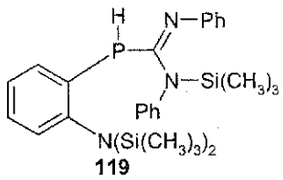

119

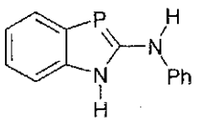

120

$PhP(Si(CH_3)_3)_2$
121

Cy–N=C=N–Cy
122

Cy–N=C=N–Ph
123

Compound Numbering Scheme
124 – 145

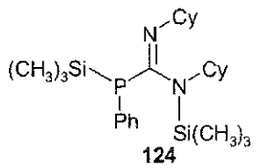
124

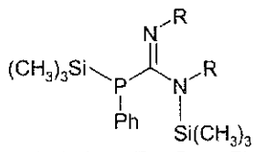
125 where R = Cy or Ph

$RP(Si(CH_3)_3)_2$
126. R = $Si(CH_3)_3$
127. R = H

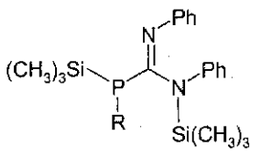
128. R = $Si(CH_3)_3$
129. R = H

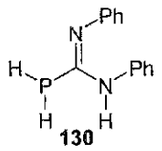
130

$^tBuNH_2$
131

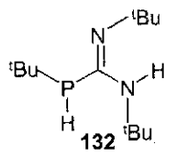
132

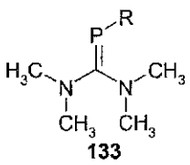
133

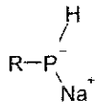
134. R = Ph
135. R = Mes

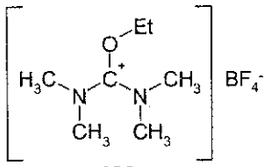
136

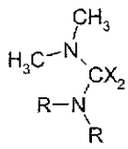
X = F, Cl
137. R = CH_3
138. R = Et

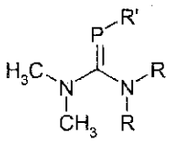
139. R = CH_3, R' = Ph
140. R = CH_3, R' = $Si(CH_3)_3$
141. R = Et, R' = $Si(CH_3)_3$

142. $^tBuC(O)Cl$

143. PhC(O)Cl

[Fe]Br
144

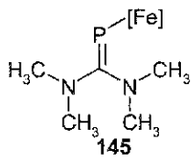
145

Compound Numbering Scheme
146 – 159

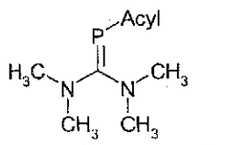

Acyl = 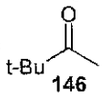 , 

146 **147**

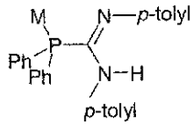

148. M = 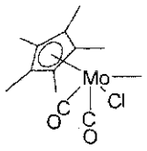

149. M = 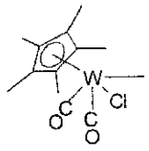

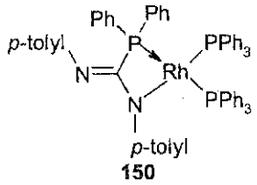

150

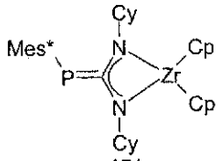

151

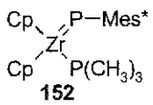

152

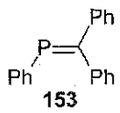

153

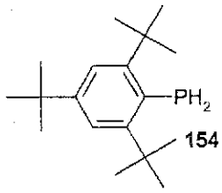

154

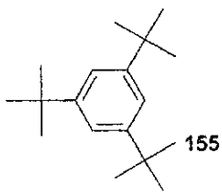

155

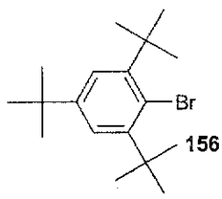

156

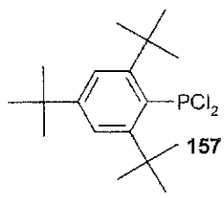

157

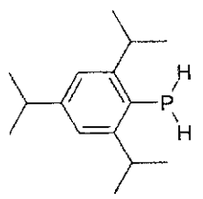

158

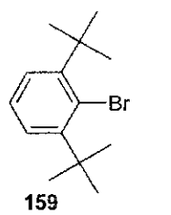

159

Compound Numbering Scheme
160 – 175

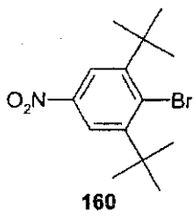

160

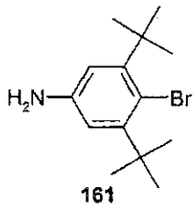

161

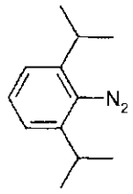

162

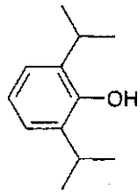

163

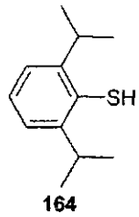

164

CH_3PBr_2

165

CH_3PBrCl

166

CH_3PCl_2

167

$Mes_2P(Cl,Br)$

168

*Trip*P(Cl,Br)

169

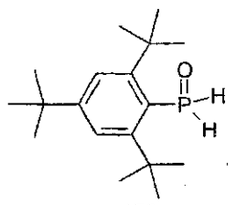

170

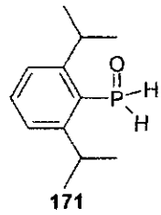

171

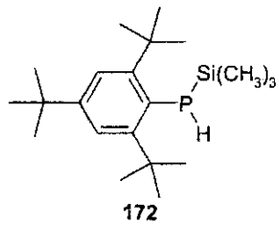

172

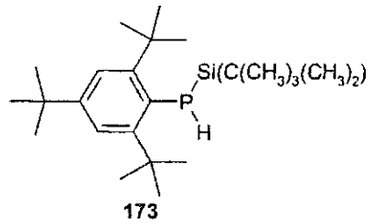

173

n $PhPCl_2$

174

Ph_nP_n

175

Compound Numbering Scheme
176 – 189

176

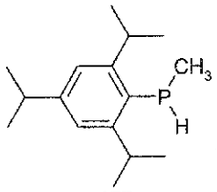

177

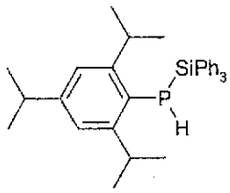

178

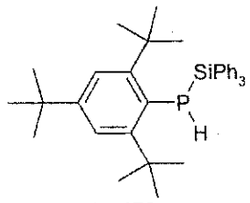

179

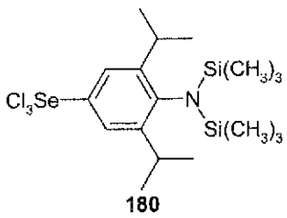

180

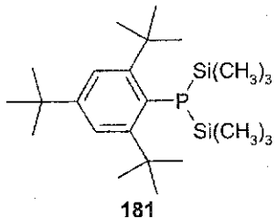

181

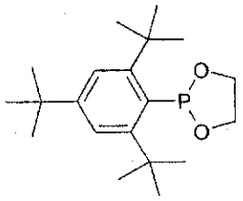

182

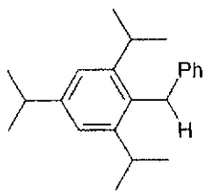

183

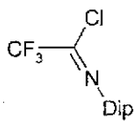

184

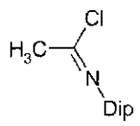

185

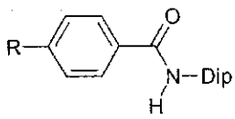

186. R = CH_3
187. R = CH_3O

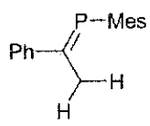

188

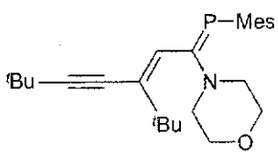

189

Compound Numbering Scheme
210 – 217

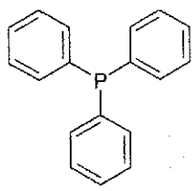

190

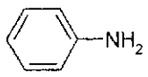

191

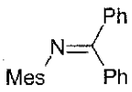

192

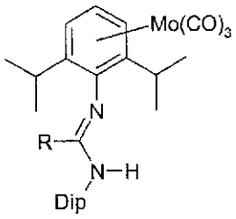

193. R = *p*-$CH_3C_6H_5$
194. R = *p*-$CH_3OC_6H_5$
195. R = CH_3
196. R = CF_3

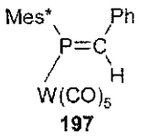

197

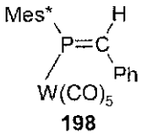

198

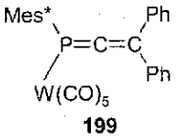

199

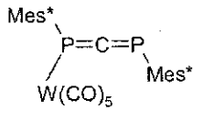

200

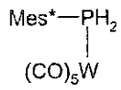

201

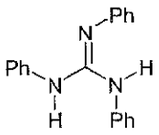

202

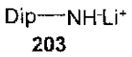

203

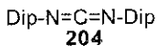

204

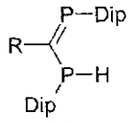

205

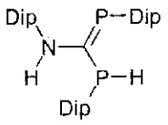

206

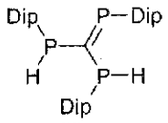

207

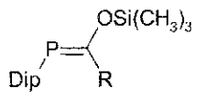

208

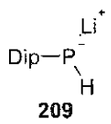

209

Compound Numbering Scheme
210 – 217

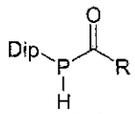

210

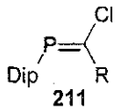

211

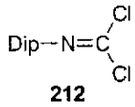

212

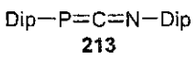

213

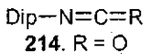

214. R = O
215, R = S

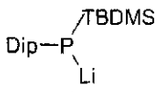

216

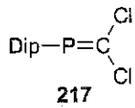

217

Chapter 1

Summary of the work

1.1 Introduction

Much work has been done on the use of sterically bulky substituents to kinetically and thermodynamically stabilize systems that would not otherwise be isolable. Twenty years ago Yoshifuji was able to isolate the first diphosphene, Mes*-P=P-Mes* (Mes* = 2,4,6-tritertbutylphenyl) **1**.[1,2] More recently, the heavier dipnictogens **2-5**,[3] as well as the multiply bonded Pb analogue of acetylene **6** were isolated through the use of bulky substituents (Figure 1.1).[4]

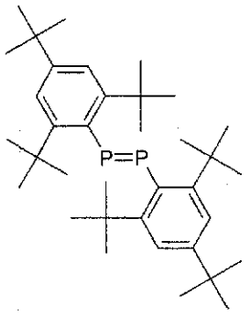

1

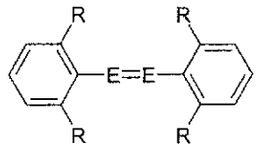

R = Mes (C_6H_2-2,4,6-CH_3), Trip (C_6H_2-2,4,6-$^iPr_3$)

2. E = P
3. E = As
4. E = Sb
5. E = Bi

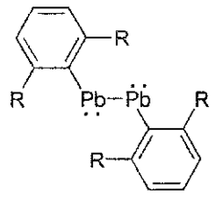

R = Trip (C_6H_2-2,4,6-$^iPr_3$)

6

Figure 1.1 Some of the low-coordinate systems stabilized through the use of sterically bulky substituents

The kinetic stabilization is a result of the bulky groups sterically shielding the low-coordinate center, thus slowing or preventing oligomerization from occurring. The bulky groups also enhance the thermodynamic stability of these systems by destabilizing the oligomerization product. By the well-known Hammond postulate[5], this will lead to an increase in the activation energy. For example, the cyclodimerization of ethylene **A** results in a more stable product **B**, whereas the cyclodimerization product **D** of 1,2-(Mes*)ethylene **C** is much less stable than the starting materials. By the Hammond postulate, the activation energy for the cyclodimerization of 1,2-(Mes*)ethylene $\mathbf{E_{A2}}$ will be higher than that of ethylene $\mathbf{E_{A1}}$, thus explaining the enhanced thermodynamic stability of these bulky systems (Figure 1.2).[6]

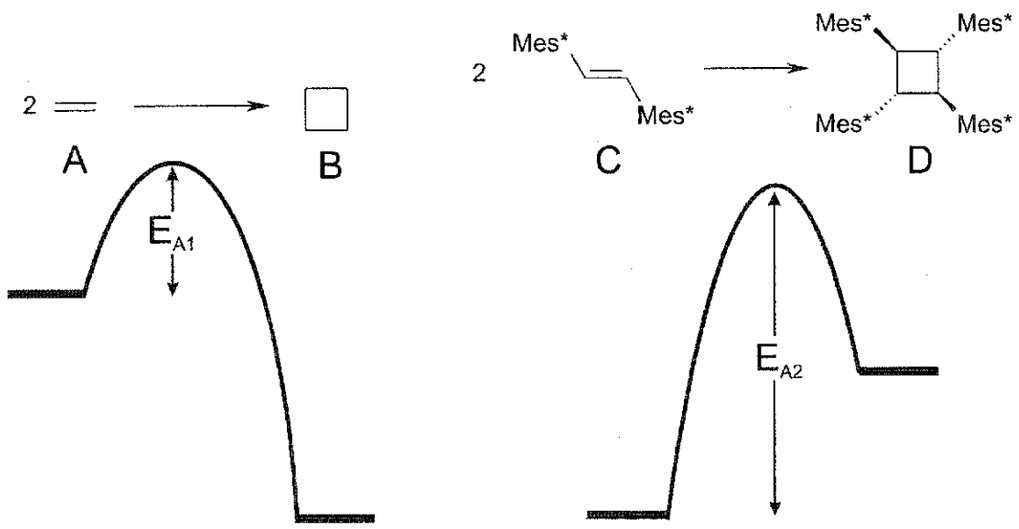

Figure 1.2 Reaction profiles for the cyclodimerization of ethylene and 1,2-(Mes*)ethylene

Interestingly, there has been less focus on examining the effects that these bulky substituents have on systems that do not necessarily need the kinetic and thermodynamic stabilization, e.g. compounds of carbon, oxygen and nitrogen. Because of this very reason, our group has isolated a series of amidines, **7-10**, and a guanidine, **11**, that contain

the sterically bulky 2,6-diisopropylphenyl (Dip) group on both the amino and imino nitrogens (Figure 1.3).[7,8,9] We have investigated in what way these bulky substituents alter the chemistry of the amidine core.

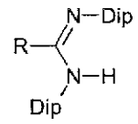

7. R = *p*-$CH_3C_6H_5$
8. R = *p*-$CH_3OC_6H_5$
9. R = CH_3
10. R = CF_3

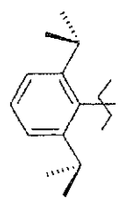

Dip = 2,6-diisopropylphenyl

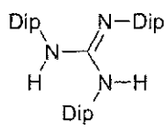

11.

Figure 1.3 Sterically bulky *N,N'*-amidines and *N,N',N"*-guanidine

1.2 The bulky 2,6-diisopropylphenyl (Dip) group

The bulky Dip group has many advantages over the more commonly used Mes* and the Trip (2,4,6-triisopropylphenyl) groups. At the cost of being slightly less sterically shielding than *ortho* ^{t}Bu groups, the use of *ortho* diisopropyl groups imparts to these substituents the advantage of providing a wealth of stereochemical information from the ^{1}H NMR signals via the often diastereotopic ^{i}Pr groups. In addition, we have avoided using the Mes* group because we have found that many of the nitrogen containing compounds were difficult, if not impossible to make, due to the extreme bulk of the ortho ^{t}Bu groups. A disadvantage of the Trip group is that the sterically unnecessary *para* ^{i}Pr substituent tends to obscure the often complex and always interesting ^{1}H NMR signals of the sterically essential *ortho* ^{i}Pr substituents. For example, in $TripPH_2$, chemical shifts of *ortho* and *para* ^{i}Pr-CH_3 groups are 1.23 and 1.24 ppm.[10] Thus there is considerable merit in the use of the Dip substituent and our group has used it as the group of choice in our studies.

1.3 Extensions to phosphorus chemistry

Since other work utilizing bulky substituents has focused on the synthesis of homologous series of molecules containing the heavier pnictogens, P, As, Sb and Bi,[3] we thought that it would be useful to produce the phosphorus homologues to our bulky amidines and guanidine (Figure 1.4). The systematic replacement of each nitrogen with phosphorus would allow us to follow the changes in the chemistry of the amidine core, to see differences solely caused by the change in pnictogen atom.

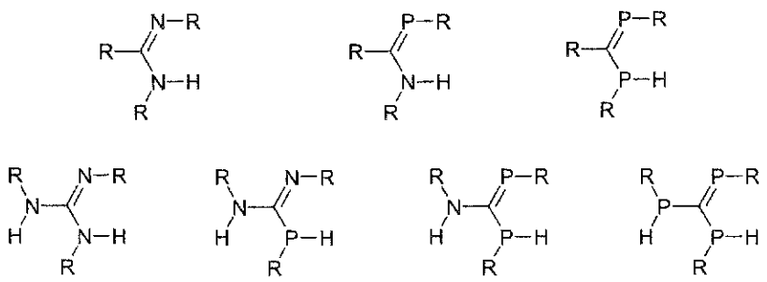

Figure 1.4 ***N,N'*-amidine, *N,N',N"*-guanidine and their phosphorus homologues**

This thesis deals with the synthesis and characterization of the mono-substituted phosphorus analogues of **7**, **8** and **11**, utilizing the sterically bulky Dip group to stabilize the reactive, low-coordinate phosphorus atom.

Chapter 2 is an introduction to amidine, phosphaalkene, guanidine and phosphaguanidine chemistry, providing the background to this work. Chapter 3 focuses on the density functional study of phosphaamidines and reasons as to why the P=C double bond is favored over the N=C double bond in these systems. Chapter 4 describes the synthesis of the novel 2,6-diisopropylphenylphosphane **15**, its precursors, **13**, **14**, and silylated derivatives, **16-19** (Figure 1.5). The primary phosphane **15** and the silylated phosphane **16** are essential to producing the exact phosphorus homologues to the bulky amidines and guanidine described earlier.

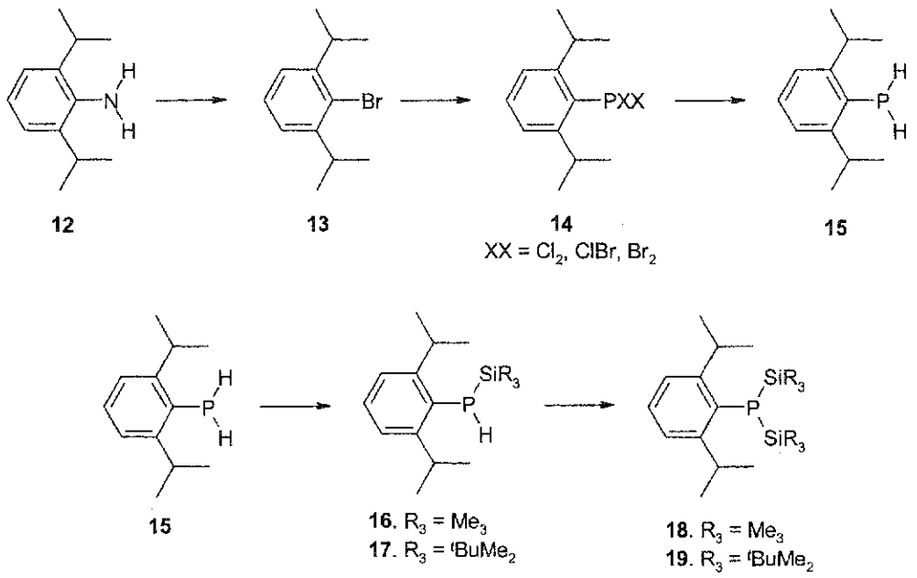

Figure 1.5 Sythetic route to $DipPH_2$ 15 and the silylated derivatives

Chapter 5 describes the synthesis of two new *N,P*-disubstituted phosphaamidines, **20** and **21** (Figure 1.6). Solid state structures are reported and their tautomerism in solution is proven, demonstrating that these systems differ substantially from regular phosphaalkenes, allowing us to properly assign them the name 'phosphaamidines'.

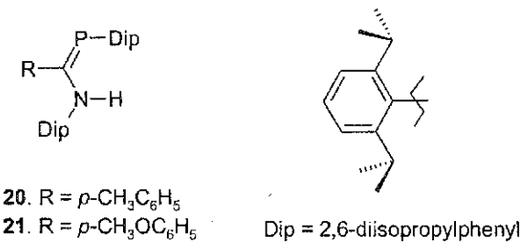

Figure 1.6 Phosphaamidine systems 20 and 21 containing the sterically bulky Dip group

These phosphaamidines are made by the reaction of the monosilylated primary phosphine, **16**, with imidoyl chlorides **22** and **23** (Figure 1.7).

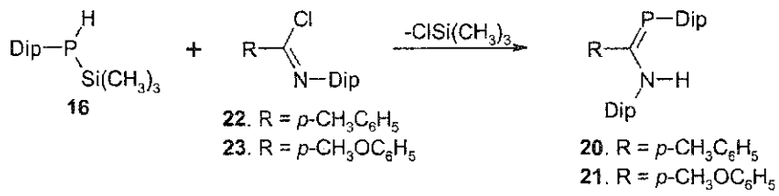

Figure 1.7 Synthetic route to phosphaamidines 20 and 21

Chapter 6 deals with the synthesis of Group 6 metal carbonyl complexes of **20** and **21**, made via reacting $Mo(CO)_6$ or $M(CO)_5$·THF (M = Cr, W) with one equivalent of phosphaamidine to give the σ-bonded metal pentacarbonyls **24-27** (Figure 1.8). With solution IR and crystallographic data we have established the *trans* influence of our phoshaamidines relative to other ligands. In addition, we have discovered that our phosphaamidines behave substantially different from the *N,N'*-amidines.

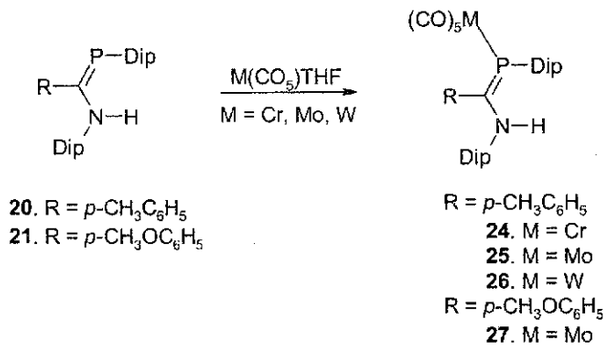

Figure 1.8 Group 6 metal carbonyl complexes of 20 and 21

In Chapter 7 the synthesis and characterization of the tri-substituted *N,N',P*-monophosphaguanidine, **28**, is also reported (Figure 1.9). Finally, Chapter 8 contains concluding remarks and possible future work.

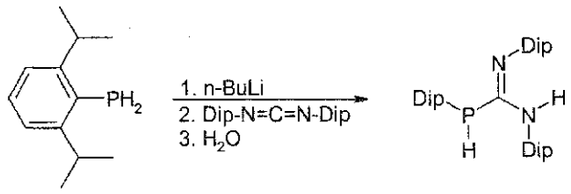

15 **28**

Figure 1.9 Synthesis of trisubstituted *N,N',P*-phosphaguanidine

All new molecules have been characterized by multi-nuclear NMR spectroscopy, IR spectroscopy, UV spectroscopy, high resolution mass spectroscopy, elemental analysis, and where applicable, single crystal X-ray diffraction.

1.4 Conclusion

The goal of this thesis is to thoroughly examine the *N,P*-phosphaamidines **20**, **21** and the *N,N',P*-phosphaguanidine **28**, in order to provide a good foundation for future work. In addition, this thesis will discuss and attempt to resolve many of the fundamental issues involving phosphaamidines that have never been addressed in the literature.

Reference List

1. Yoshifuji, M.; Shima, I.; Inamoto, N. *J. Am. Chem. Soc.* **1981**, *103*, 4587-4589.

2. Yoshifuji, M.; Shima, I.; Inamoto, N.; Hirotsu, K.; Higuchi, S. *J. Am. Chem. Soc.* **1982**, *104*(22).

3. Eshtiagh-Hosseini, H.; Kroto, H. W.; Nixon, J. F.; Maah, M. J.; Taylor, M. J. *J. Chem. Soc., Chem. Commun.* **1981**, 199-200.

4. Klebach, T. C.; Lourens, R.; Bickelhaupt, F.; Stam, C. H.; van Herk, A. *J. Organomet. Chem.* **1981**, *210*, 211-221.

5. Hammond, G. S. *J. Am. Chem. Soc.* **1955**, *77*, 334.

6. Burford, N.; Clyburne, J. A. C.; Chan, M. S. W. *Inorg. Chem.* **1997**, *36*, 3204-3206.

7. Boeré, R. T.; Klassen, V.; Wolmershauser, G. *J. Chem. Soc., Dalton Trans.* **1998**, 4147-4154.

8. Boeré, R. T.; Klassen, V.; Wolmershauser, G. *Can. J. Chem.* **2000**, *78*, 583-589.

9. Boeré, R. E.; Boeré, R. T.; Masuda, J.; Wolmershauser, G. *Can. J. Chem.* **2000**, *78*, 1613-1619.

10. Winkel, Y. v. d.; Bastiaans, H. M. M.; Bickelhaupt, J. *Chem.* **1991**, *405*, 183.

Chapter 2

Introduction to low-coordinate phosphorus chemistry

2.1 Introduction

In 1669, Hamburg physician and alchemist Hennig Brand discovered a substance in human urine that he named "kaltes Feuer" ("cold fire"). This substance was thought to be elemental light or fire due to the light it emitted. It was not known until later that it was the presence of oxygen that caused oxidation of phosphorus, releasing light in the process. Later in the 17th century the name had switched to phosphorus ("light bearer") and it was a key in the destruction of the phlogiston doctrine. Phosphorus-based compounds are not only essential to many life processes (e.g. adenosine triphosphate), but they can also be used in warfare, such as the deadly nerve gases used during WWII (e.g. Tabun, $(CH_3)_2N\text{-}P(=O)(\text{-}CN)(\text{-}OC_2H_5)$).[1] Until recently, phosphorus chemistry has focused on three, four and five coordinate, P(III) and P(V) compounds.

2.2 Low coordinate P(III) chemistry

Throughout the first half of the twentieth century, it was originally thought that it was impossible for low-coordinate, π-bonded phosphorus systems to exist.[2] However, in 1961, Gier[3] produced H-C≡P **29**, a highly reactive gas that is stable as a white solid at –170 °C. After much skepticism, the discovery of this acetylene analogue began the "second heyday" in phosphorus chemistry.[1]

The first non-ionic, two-coordinate P(III) system was 2,4,6-triphenyl phosphabenzene **30**, synthesized by Märkl in 1966.[4] In 1971, Ashe synthesized both

the parent phosphabenzene **31**, and arsabenzene **32**, the arsenic derivative being the first arsabenzene derivative isolated (Figure 2.1).[5]

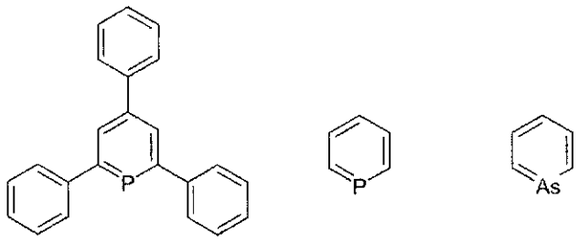

30 **31** **32**

Figure 2.1 2,4,6-Triphenylphosphabenzene, phosphabenzene and arsabenzene.

In 1976, Kroto[6,7] first reported a series of short-lived phosphaalkenes, **33**, **34** and **35**, detected by microwave spectroscopy. These were produced by pyrolysis of tertiary phosphanes, resulting in the elimination of methane or hydrogen halides (Figure 2.2).

$$(CH_3)_2PH \xrightarrow[-CH_4]{heat} HP{=}CH_2 \quad \mathbf{33}$$

$$CF_3PH_2 \xrightarrow[-HF]{heat} HP{=}CF_2 \quad \mathbf{34}$$

$$CH_3PCl_2 \xrightarrow[-HCl]{heat} ClP{=}CH_2 \quad \mathbf{35}$$

Figure 2.2 Synthesis of the first phosphaalkenes

In the same year, the first stable, acyclic phosphaalkenes **36**, **37**, **38** and **39** were isolated by Becker,[8] utilizing the silyloxy group to electronically stabilize the P=C double bond. This phosphaalkene was prepared from $RP(Si(CH_3)_3)_2$ + $^tBuC(O)Cl$ via $ClSi(CH_3)_3$ elimination, followed by 1,3-silyl migration (Figure 2.3).

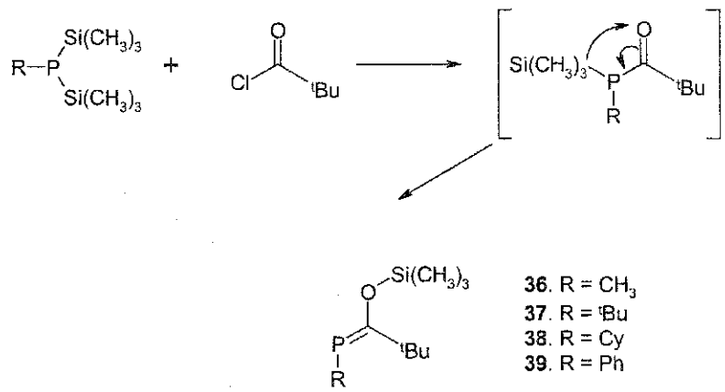

Figure 2.3 Synthesis of the first stable, non-cyclic phosphaalkene via 1,3-silyl migration

Systems that are stabilized by the '-O-R' group are classified as 'Becker' phosphaalkenes. The electronic stabilization comes from the two resonance structures that are possible (Figure 2.4).

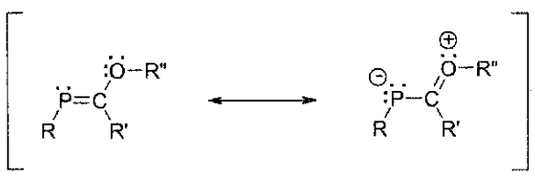

Figure 2.4 Resonance stabilized 'Becker' phosphaalkenes

Using sterically bulky substituents, low-coordinate systems can be kinetically stabilized, thus preventing oligomerization. Using the extremely bulky 2,4,6-tri-*tert*-butylphenyl (Mes*) substituent, Yoshifuji was able to isolate the first diphosphene **1** by Mg reduction of the phosphonous dichloride **40** (Figure 2.5).[9,10] This discovery, like the first report of H-C≡P **29**, was very controversial and many groups were determined to verify the results on their own.[11] It was found that the ^{31}P NMR signal (+493 ppm)[11] was significantly downfield from the signal in the original report (-59 ppm)[9] due to "signal fold-over" in the ^{31}P NMR spectrum.[10] Generally ^{31}P NMR is observed in a 500 ppm window between –250 and +250 ppm. When a signal is

outside of this region and the instrument is set-up for the normal spectral window, the true signal is folded over into the spectral window producing an artifact signal. Nevertheless, this system proved that bulky substituents could be used to stabilize low-coordinate heavy atoms. Recently, Yoshifuji[12] has written a review summarizing the protecting groups used to stabilize these low-coordinate systems.

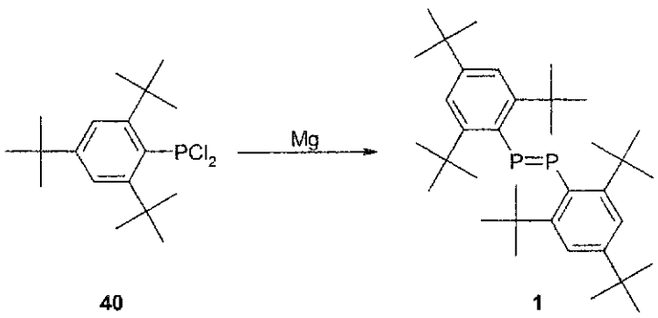

40 1

Figure 2.5 Synthesis of bis(2,4,6-tritertbutylphenyl)diphosphene

The first thermally stable phosphaalkene **41** with a localized, all-carbon substituted P=C double bond was made by Bickelhaupt in 1978 (Figure 2.6). By employing the bulky 2,4,6-trimethylphenyl (Mes) group, the P=C bond is kinetically stabilized, rather than electronically stabilized as with the 'Becker' phosphaalkenes.

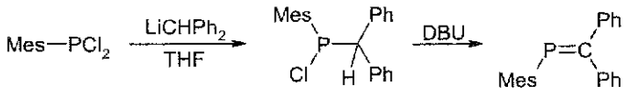

41

Figure 2.6 Kinetically stabilized phosphaalkene

In 1982, Kolodiazhnyi isolated the first stable phosphaazaallene **42**, a phosphorus analogue of carbodiimide, utilizing the bulky ^{t}Bu group (Figure 2.7).[13] Many other

1,3-phosphaazaallenes have since been isolated,[14] varying from yellow oils to red solids.

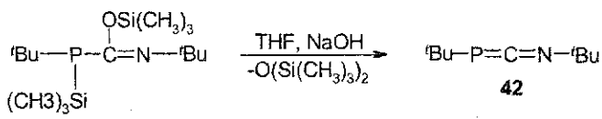

Figure 2.7 Synthesis of the first phosphaazaallene

Phosphaazaallenes can be made in a variety of ways, all of which have been compiled in a recent review by Escudié.[14] When less bulky substituents are used (R = Ph, R' = 2-Cl-Ph **43**, 2,3-di-Cl-Ph **44**, 2-F-Ph **45**, 2,5-di-Cl-Ph; R' = Ph, R = Et **47**, CH_2Ph **48**, Ph **49**, ^{t}Bu **50**, Mes **51**), these 1,3-phosphaazaallenes are only observable at low temperatures. Upon warming to room temperature, dimerization occurs in a head-to-tail fashion, via the P=C bond, to form 2,4-diimino-1,3-diphosphetanes (Figure 2.8).[14] When bulky substituents are present on nitrogen and phosphorus (i.e. **52**. R = R' = Mes*), purification can be done by column chromatography! This simple fact emphasizes the utility of these bulky substituents to kinetically stabilize low-coordinate phosphorus molecules.

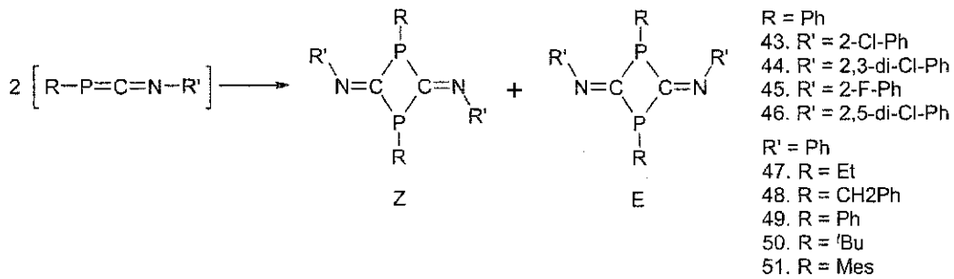

Figure 2.8 Dimerization of less bulky phosphaazaallenes

Appel isolated the phosphorus analogue of an isocyanate by using the bulky Mes* substituent to stabilize the -P=C=O fragment (Figure 2.9).[15] This first stable

phosphaketene **53** is not only a novel compound, but it has also found use in the synthesis of 1,3-phosphaazaallenes, -P=C=N-, and 1,3-diphosphaallenes, -P=C=P-.[14]

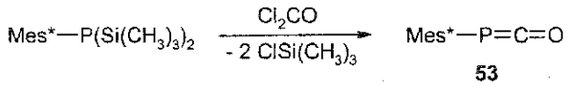

Figure 2.9 Synthesis of the first stable phosphaketene

The corresponding phosphathioketene, -P=C=S **54**, has only been isolated as the dimer **55**.[16] Here the Mes* substituent proved to be insufficiently bulky to stabilize the phosphathioketene group (Figure 2.10).

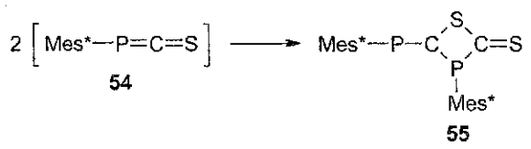

Figure 2.10 Dimerization of bulky phosphathioketene

2.3 Coordination chemistry of phosphaalkenes

Three coordination modes have been observed for phosphaalkenes (Figure 2.11).[17] Type **A**, η^1-coordination via the phosphorus lone pair, Type **B**, coordination via the π system, leading to two possible resonance structures and Type **C**, a combination of bonding modes **A** and **B**.

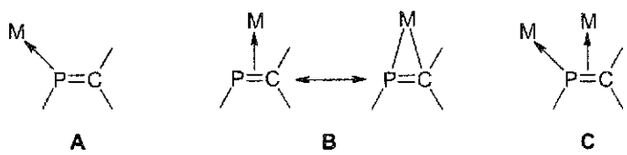

Figure 2.11 The three different modes of coordination for phosphaalkenes

Type **A** coordination compounds have been observed for Cr(0), Mo(0), W(0),[18] Fe(0), Ni(0), Rh(I), Pt(II) and Pd(0).[17] The metal-phosphorus bond is formed via σ-

bonding between the phosphorus lone pair and an empty valence orbital on the metal. This σ-bond is strengthened by $d\pi$-$p\pi$ back bonding from the filled metal *d*-orbitals to the empty π^*-orbital of the phosphorus atom (Figure 2.12).

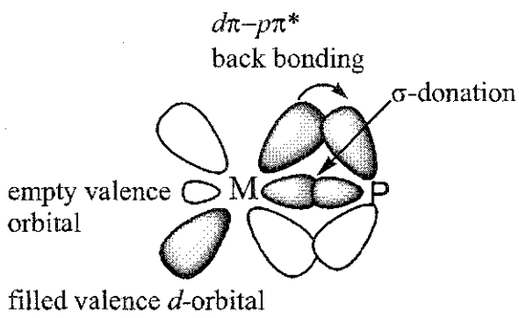

Figure 2.12 σ-bonding and $d\pi$-$p\pi^*$ backbonding in phosphorus-metal complexes

Type **A** complexes are most readily formed by ligand displacement from metal carbonyls. The chromium pentacarbonyl complex **56** was reported from the reaction of $Cr(CO)_5$·THF with phosphaalkene **41** (Figure 2.13).[19]

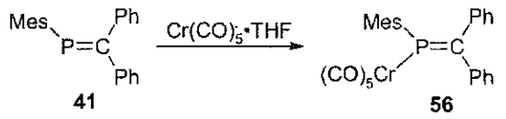

Figure 2.13 Synthesis of group 6 metal carbonyl phosphaalkene complexes

Complexes of type **B** are analogous to η^2-ethylene complexes with a dative metal bond. The filled π-orbital of the P=C system bonds to an empty valence orbital on the metal atom (Figure 2.14). Back donation of the filled *d*-orbitals of the metal into the π^* molecular orbital of the P=C system strengthens the metal-ligand bond, in turn weakening the P=C bond, causing the bond to lengthen.

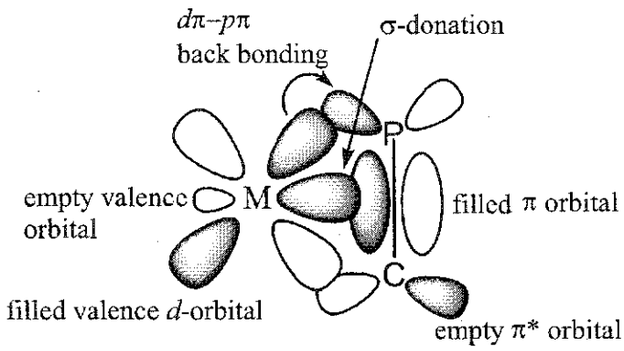

Figure 2.14 Metal bonding in dative ethylene-type complexes

One of the few examples of an η^2-phophaalkene complex **B** is shown in Figure 2.15.[20] The η^2-coordination by nickel has weakened the P=C bond, resulting in a phosphorus-carbon bond length of 1.77(3) Å, which is approximately midway between the average values for a P-C single bond (1.85 Å) and a P=C double bond (1.67 Å) for a standard phosphaalkene.[17]

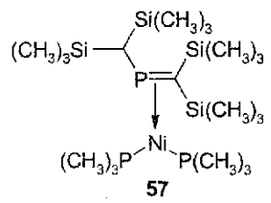

57

Figure 2.15 Phosphaalkene η^2-coordinated to $Ni(P(CH_3)_3)_2$.

The type of coordination can also change depending on the other ligands that are coordinated to the metal. For example, when Mes*-P=CPh_2 **58** is reacted with $Ni(CO)_4$, coordination of type **A** occurs. However, when 2,2'-bipyridyl-nickel is reacted with **58**, coordination type **B** occurs. This can be expected due to the fact that carbonyl ligands have good π-acceptor properties, resulting in an electron deficient metal center, therefore reducing the possible dative interaction of the metal with the π^* LUMO of the phosphaalkene.[17]

Coordination of type **C** is less common. One example is product **59** formed when Mes*-P=CH_2 **58** is reacted with iron nonacarbonyl (Figure 2.16).[17]

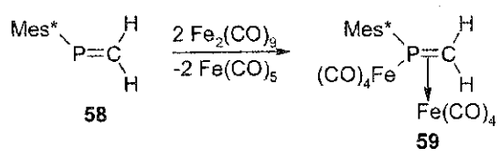

58 59

Figure 2.16 Reaction of phosphaalkene with ironnonacarbonyl to give coordination complex of type C

More recently, a phosphido-bridged dimolybdenum complex **60** was used to form phosphaalkene **61** with coordination type **C** (Figure 2.17).[21]

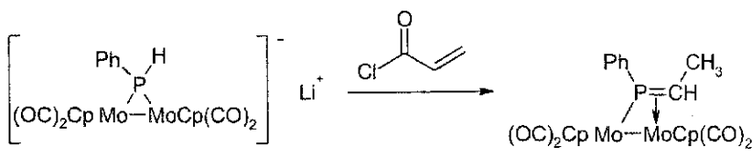

60 61

Figure 2.17 Phosphaalkene coordinating to dimolybdenum fragment to give coordination type C

2.4 Amidines

Amidines are the nitrogen analogues of carboxylic acids and esters (Figure 2.18). They are considered to be fairly strong Brønsted bases via the imino lone pair.

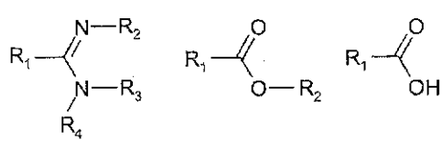

Figure 2.18 The amidine, ester and carboxylic acid functional groups

In 1858 the first amidine, bis-*N*,*N*'-diphenylbenzamidine **62**, was synthesized by Gerhardt[22,23] from the reaction of aniline **63** with *N*-phenylbenzimidoyl chloride **64** (Figure 2.19).

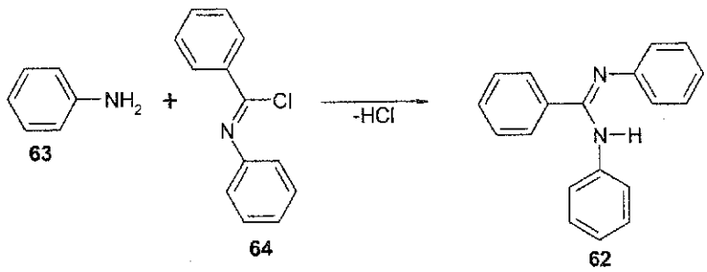

Figure 2.19 The synthesis of the first amidine, *N*,*N*'-diphenylbenzamidine

The many techniques that can be employed in the synthesis of amidines have been summarized by Gautier[24] and Boyd.[25]

There are 6 general types of amidines. Depending on the number and placement of the substituents they can be classified as unsubstituted **A**, imino **B** and amino-monosubstituted **C**, *N*,*N*- **D** and *N*,*N*'-disubstituted **E** and trisubstituted amidines **F** (Figure 2.20).

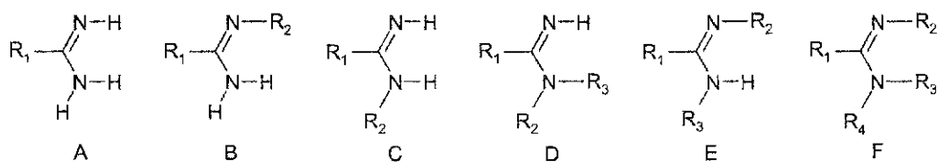

Figure 2.20 The six general types of amidines

For each derivative, there is a *cis-trans* isomerism that exists with respect to the C=N double bond as well as rotational isomerism around the C-N single bond. In addition to the isomerism, tautomerism can be exhibited in the monosubstituted and disubstituted forms. A naming system has been developed that uses the Cahn-Ingold-

Prelog sequence rules of the IUPAC nomenclature system.[26] This naming system specifies the exact orientation of the amidine based on the ranking of the R-groups and the corresponding E or Z orientation of the two highest ranking substituents. For example, there are four different stereochemical designations expected for *N,N'*-disubstituted amidines (Figure 2.21).

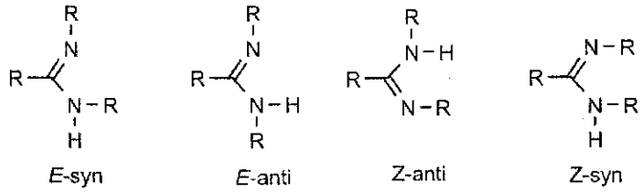

Figure 2.21 The four different stereochemical designations for *N,N'*-disubstituted amidines

There are two degenerate tautomeric forms of E-anti and Z-syn, while the Z-anti and E-syn isomers are related to each other by tautomerism (Figure 2.22).

New attention was brought to amidines in the 1980's when it was found that silylated benzamidines and silylated benzamidinates were not only easy to make, but they also reacted cleanly with metal halides. [27,28] The silylated benzamidinate **65** can be isolated as the Li, Na, K salts, or can be reacted with an equivalent of $ClSi(CH_3)_3$ to give the tris-substituted derivative **66** (Figure 2.23).[27]

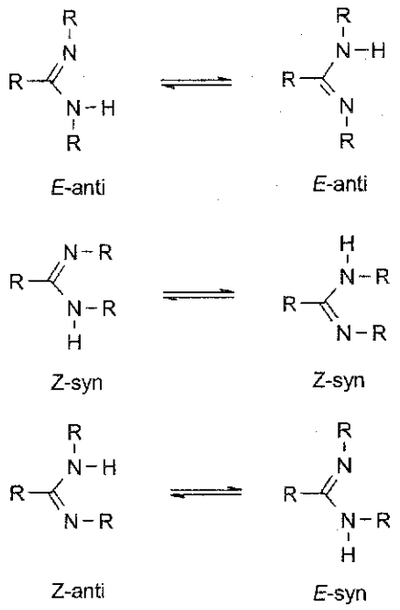

Figure 2.22 Tautomerism and isomerism exhibited by *N,N'*-disubstituted amidines

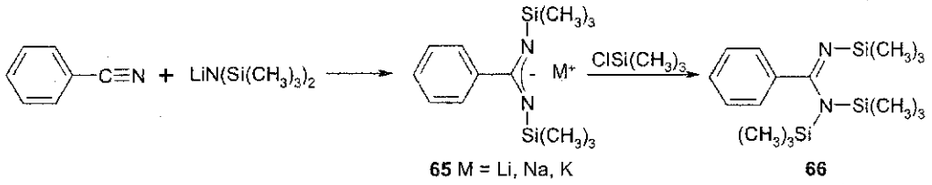

Figure 2.23 Synthetic route to silylated lithium benzamidinate and the fully silylated benzamidine

A significant portion of the metals in the periodic table have been isolated as their benzamidinate derivatives due to the utility of the silylated amidinate as a ligand.[28] Much interest has been devoted to the silylated benzamidinate ligand because it is said to be the steric and charge equivalent to an η^5-cyclopentadienyl (Cp) ligand (Figure 2.24). Thus, much work has been done on producing new homogeneous polymerization catalysts that incorporate the silylated amidinate, rather than the more commonly used Cp ligand.[28] As a result, there has recently been much interest in the

use of amidinate-metal complexes as olefin[29,30,31,32,33,34] and isocyanate[35] polymerization catalysts.

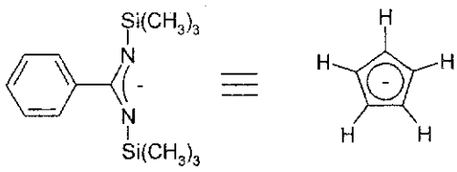

Figure 2.24 Silylated benzamidinate ligand is sterically and charge equivalent to the Cp ligand.

2.5 Guanidines

Guanidines can be thought of as amidines that contain an additional amino group connected to the central carbon atom (Figure 2.25). In general, guanidines are even stronger Brønsted bases than amidines, due to the electron donating effect of the second amino group attached to the central carbon.

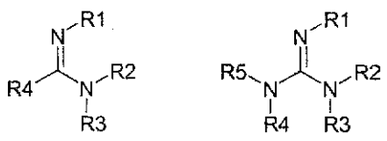

Figure 2.25 The amidine and guanidine groups

The synthesis of guanidines has been compiled in a recent work by Patai[36], and will not be discussed in detail because it is beyond the scope of this thesis. However, it is important to note that a common route to *N,N',N''*-trisubstituted guanidines is the reaction of amines with carbodiimides (Figure 2.26).

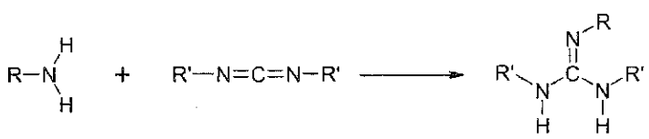

Figure 2.26 A common route to *N,N',N''*-trisubstituted guanidines

2.6 Coordination chemistry of amidines and guanidines

There are six possible coordination modes for amidines (Figure 2.27).

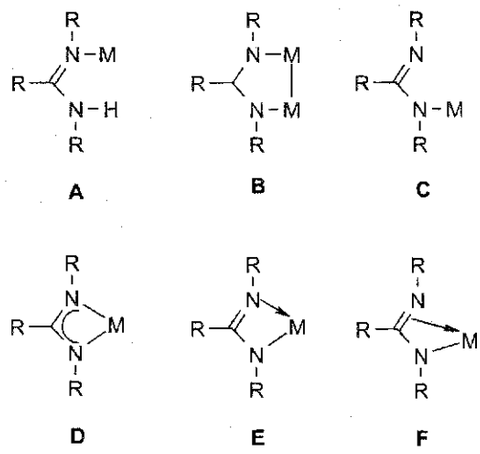

Figure 2.27 The six different coordination modes for amidines

Neutral amidines act as two-electron donors via the more basic and less sterically crowded imino lone pair. Very few neutral monodentate amidine complexes **A** are known (Figure 2.27). In 1987, $(OC)_5WNH=C(NMe_2)Ph$ **67** was made in both the E and Z isomers, via insertion of NH into the metal-carbene bond (Figure 2.28).[37] Over ten years later, our group isolated a monodentate amidine-$Mo(CO)_5$ complex **68** directly from the amidine (Figure 2.28).[38] This will be further discussed in Chapter 6.

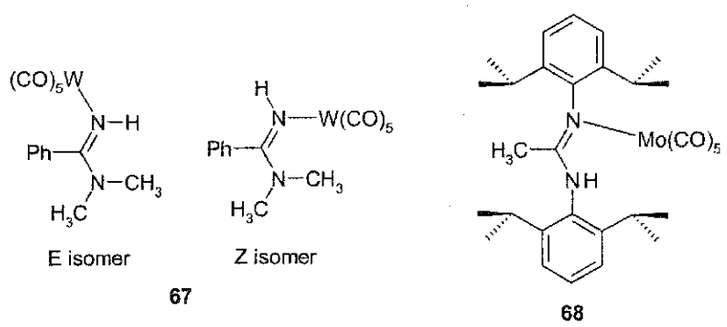

Figure 2.28 Two examples of neutral monodentate amidines

Bridging structure **B** has been used by Cotton and others[39] to investigate multiple bonding between transition metals. The amidine NCN core, isoelectronic with carboxylic acids, has been shown to provide the spacing needed to form metal-metal multiple bonds. Compound **69** shown in Figure 2.29 is formed by the thermal reaction of *N,N'*-diphenylbenzamidine **62** with $Mo(CO)_6$.[39]

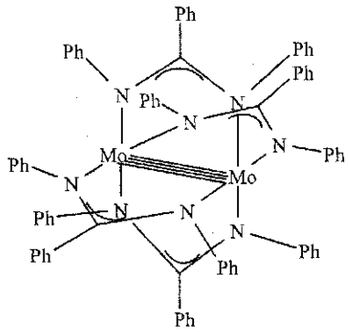

69

Figure 2.29 Example of a bridged Mo complex surrounded by four benzamidinate ligands

When deprotonated, amidines can act as monodentate **C** and chelating ligands **D, E** and **F**. Type **C** coordination complexes are formed through σ-bonded nitrogen-metal bonds and two examples have been characterized by X-ray crystallography, a Pt compound **70**,[40] and a mercury compound **71**[41] (Figure 2.30).

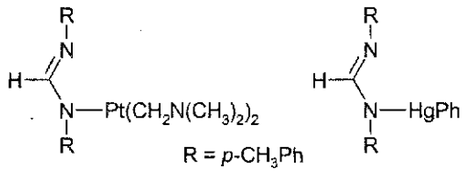

70 **71**

Figure 2.30 Two known amidinates with coordination type C

Coordination types **D, E** and **F** form strained 4-member M(NCN) rings. The most common of the chelates is the σ,σ-symmetrical form, **D**, where the NCN bonding is delocalized. A recent example **72**[42] is shown in Figure 2.31.

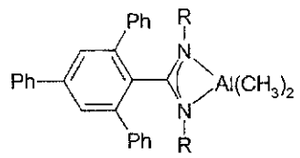

72 R = ^{i}Pr

Figure 2.31 A recent example of coordination type D

The σ,σ-unsymmetrical form, **E**, occurs when both nitrogens bond to the metal, with a formal bond between the imine lone pair electrons and the metal. An example of this is the compound $CH_3TaCl_2\{C_6H_{11}NC(CH_3)NC_6H_{11}\}$ **73** (Figure 2.32).[43]

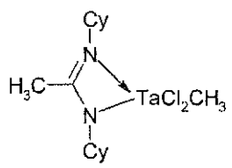

73

Figure 2.32 Example of coordination type E

The third chelate form, **F**, where the amino nitrogen σ bonds to the metal and the C=N double bond interact in an alkene-like manner, has never been observed.[23]

The coordination modes of guanidines are similar to that of amidines, the key difference being the doubly deprotonated *N*,*N*',*N*''-trisubstituted guanidine forming a dianionic species. The guanidinate(2$^-$) is capable of forming four-membered rings with M^{2+} cations **G**, or forming two, four membered rings with M^+ cations **H** (Figure 2.33). Any other coordination modes for guanidines and guanidinates can be thought of as coordination modes **A**-**F** with an amino group attached to the central carbon of the amidine backbone, or combinations of coordination modes **A**-**F** (Figure 1.27).

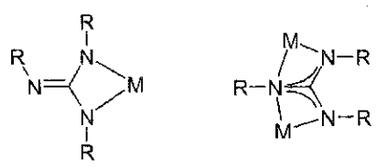

Figure 2.33 Possible dianionic coordination modes for *N,N',N"*-trisubstituted guanidines.

The reaction of *N,N',N"*-triphenylguanidine **74** with $PtCl_2(COD)$ mediated by silver(I) oxide formed the first mononuclear guanidinate(2$^-$) complex **75**, having coordination mode **G** (Figure 2.34).[44] Coordination mode **H** has not been observed for any guanidinate(2$^-$) systems.

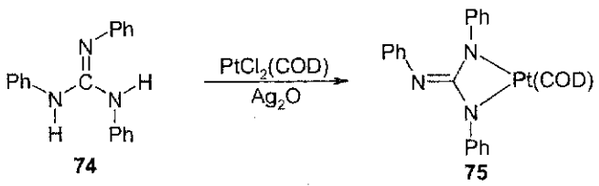

Figure 2.34 Four-membered platinum-guanidinate metal complex

2.7 Sterically bulky amidines and guanidines

As previously mentioned, much work has been done on the use of bulky substituents to kinetically stabilize systems that would not otherwise be isolable. Despite the acknowledged structural distortion of bulky groups, little is known about what effects these bulky substituents have on systems that don't necessarily need the kinetic stabilization, e.g. carbon, oxygen and nitrogen.[38] Our group has isolated a series of sterically bulky amidines, **7-10** and a guanidine **11** that contain the bulky 2,6-diisopropylphenyl (Dip) group on both the amino and imino nitrogens (Figure 2.35).[38,45,46] We have been interested in what way these bulky substituents alter the chemistry of the amidine core.

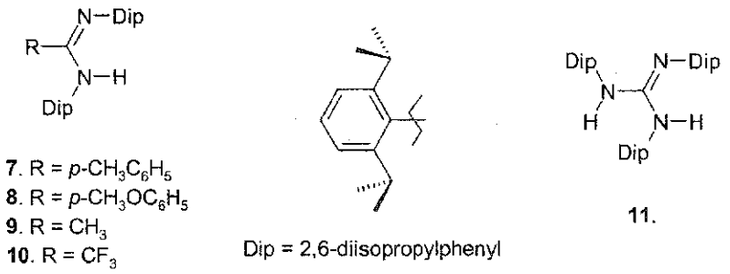

Figure 2.35 Amidines and guanidine with the sterically bulky Dip group on the amino and imino nitrogens.

When reacted with molybdenum hexacarbonyl, the monodentate amidine-$Mo(CO)_5$ complex **68** could be isolated in one case as an intermediate to the more thermally stable arene-η^6-$Mo(CO)_3$ tripod, where the molybdenum does not coordinate to the amidine core, but to the imino Dip ring. When the other bulky amidines (R = *p*-$CH_3C_6H_4$ **7**, *p*-$CH_3OC_6H_4$ **8**, CF_3 **10**) and the bulky guanidine **11** are reacted with $Mo(CO)_6$, the arene-η^6-$Mo(CO)_3$ tripod is isolated directly. Normally amidines form bridging metal structures of type **B** when reacted with Group 6 metal carbonyls. In 1977, Cotton[47] isolated the Mo_2(amidine)$_4$ complex **69** (Figure 2.29) by heating $Mo(CO)_6$ with *N,N'*-bis(diphenyl)benzamidine **62**. It is thought that the steric bulkiness of the Dip groups prevents the bridged structure from forming. These reactions will be discussed in greater detail in Chapter 6.

2.8 C-Amino phosphaalkenes or phosphaamidines

Issleib's group were one of the first to study phosphaamidines, a phosphorous derivative of amidines.[48] There are three possible phosphorus analogues to amidines (Figure 2.36).

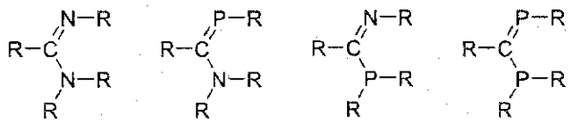

Figure 2.36 Amidine, amino and imino monophosphaamidine and diphosphaamidine

There are numerous examples of *N,N',P*-trisubstituted monophosphaamidines in the literature, but there are few studies on the protonated mono[49] and disubstituted derivatives.[48]

Two examples of the parent *P,P'*-disubstituted diphosphaamidines have been reported, **76** and **77** (Figure 2.37), but they were only characterized by ^{31}P NMR and mass spectroscopy.[50]

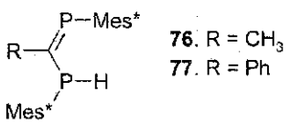

Figure 2.37 Two known protonated *P,P'*-disubstituted diphosphaamidines

The diphosphaformamidine **79** has been isolated as the E-isomer by the reduction of diphosphaallene **78** with sodium bis(methoxyethoxy) aluminum hydride (Figure 2.38).[51]

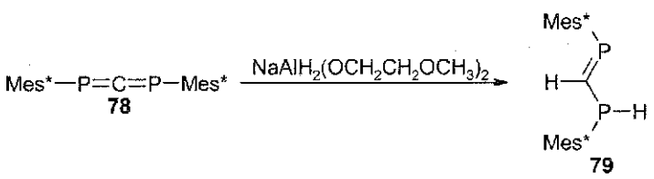

Figure 2.38 Reduction of diphosphaallene to give diphosphaformamidine

2.9 Synthesis of phosphaamidines

Using catalytic amounts of NaOH, the reaction of R-P{Si(CH$_3$)$_3$}$_2$ (R = Ph, ^{t}Bu, Mes) with excess *N,N*-dimethylformamide gives the phosphaamidines **80**, **81** and **82**, with elimination of bis-trimethylsiloxane (Figure 2.39).[52,53] Alternatively, when

$MesPSi(CH_3)_3^-Li^+$ is reacted with *N,N*-dimethylformamide and treated with $ClSi(CH_3)_3$, the phosphaamidine **82** is formed with bis-trimethylsiloxane and LiCl side products (Figure 1.39).[53]

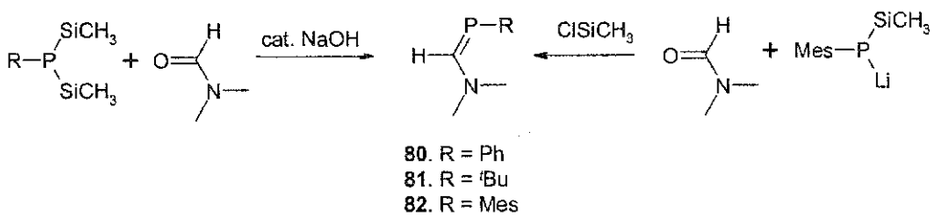

80. R = Ph
81. R = ^{t}Bu
82. R = Mes

Figure 2.39 Two synthetic routes using dimethylformamide to make the dimethylamino phosphaamidine

Another route involves the condensation of carboxylic amide acetates with primary aryl phosphanes (Figure 2.40).[54] It should be noted that this reaction does not occur when primary alkyl phosphanes are used.[55]

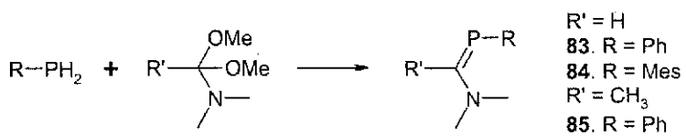

R' = H
83. R = Ph
84. R = Mes
R' = CH_3
85. R = Ph

Figure 2.40 Another route to dimethylamino phosphaamidine using carboxylic amide acetates

The cyclic phosphaamidines, **86**, **87** and **88** were made by the reaction of o-aminophenylphosphane **89** with imidoester-hydrochlorides (Figure 2.41).[56] This heterocyclic ring can also be thought of as a 1-substituted-phosphabenzimidazole.

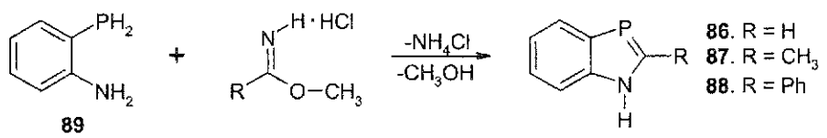

89

86. R = H
87. R = CH_3
88. R = Ph

Figure 2.41 Synthesis of cyclic phosphaamidine

Issleib's work on the silylated *N,P*-disubstituted phosphaamidines followed classic amidine synthesis; the reaction of an imidyl chloride with a disilylated primary phosphane. The initial reaction is thought to form the imino phosphaamidine, followed by 1,3-silyl migration to form the amino phosphaamidine. Upon treatment with MeOH, the protonated phosphaamidine was isolated, but not fully characterized (Figure 2.42). Work in our laboratory has shown the Issleib compounds to be intractable, hard to purify materials that resist all efforts to crystallize them.

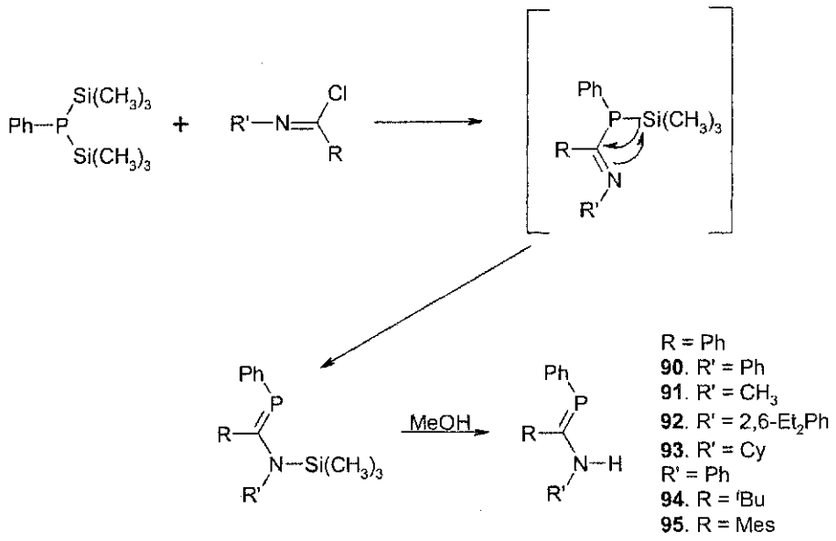

Figure 2.42 Synthesis of silylated and protonated *N,P*-disubstituted monophosphaamidine

Niecke later isolated the first P-substituted monophosphaamidine, **96**, containing an NH_2 group (Figure 2.43).[49]

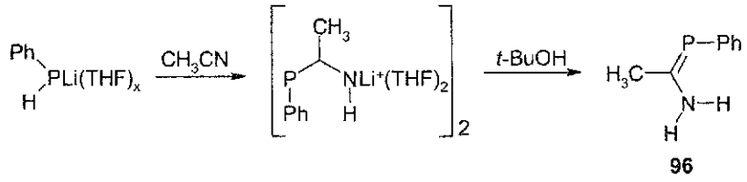

96

Figure 2.43 Synthesis of the first phosphaamidine containing an NH_2 group

2.10 Monophosphaguanidines – protonated/silylated-trisubstituted and tetrasubstituted derivatives

The first phosphaguanidines were published in the early 1980's by Issleib,[57,58] Thewissen,[59] Pudovick[60] and Kolodiazhnyi.[13,61,62] All of these systems are quite sensitive to substituent effects, where in many cases, substitution of a $Si(CH_3)_3$ group with H causes a N=C double bond to be favored over a P=C double bond. The reaction of neat Ph_2PH **97** with di-*p*-tolylcarbodiimide **98** forms the phosphaguanidine **99** straightforwardly (Figure 2.44).[59] In this case, the phosphaguanidine is forced to have a N=C double bond due to disubstitution at the phosphorus atom.[59] Note that the primary alkyl phosphane, $CyPH_2$, does not react with di-*p*-tolylcarbodiimide.

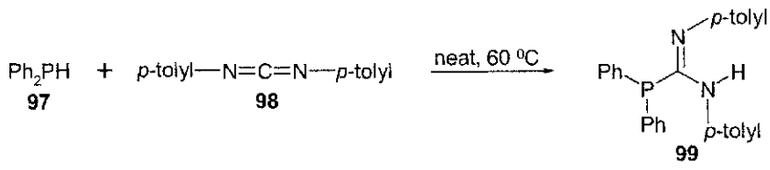

Figure 2.44 Condensation of disubstituted phosphane with carbodiimide

The reaction of the primary aryl phosphane, $PhPH_2$ **100**, with diphenylcarbodiimide **101** does not form the phosphaguanidine, but instead double addition occurs forming formamidinophosphane **102** (Figure 2.45).

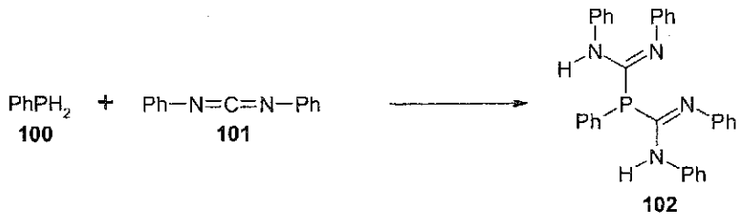

Figure 2.45 Reaction of primary aryl phosphane with diphenylcarbodiimide to give the formamidinophosphane

Yet when $PhPHSi(CH_3)_3$ **103** is reacted with diphenylcarbodiimide **101**, the silylated phosphaguanidine **104** is made (Figure 2.46).[60] In this case the N=C double bond is favored over the P=C double bond, leaving a proton attached to the phosphorus and a $Si(CH_3)_3$ group attached to the amino nitrogen.

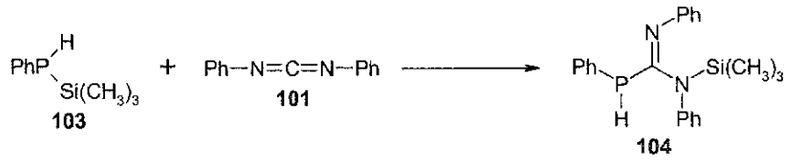

Figure 2.46 Reactions of primary aryl silylated phosphane with diphenylcarbodiimide

Issleib[57] reacted a series of disilylated primary phosphanes with diphenylcarbodiimide **101** to give a series of disilylated phosphaguanidines (Figure 2.47). Here the P=C double bond is favored. However, upon treatment with methanol, the protonated phosphaguanidine is formed and the N=C double bond is favored (Figure 2.48).

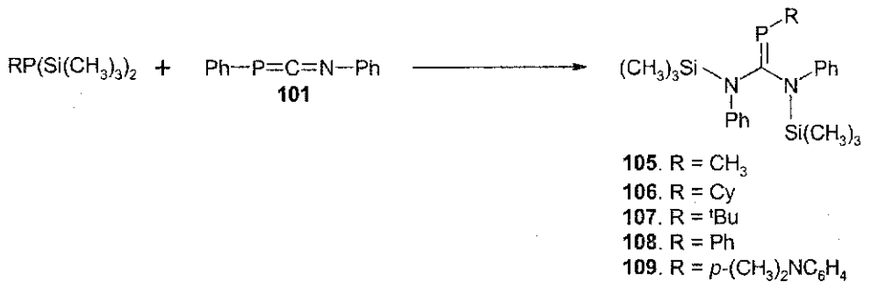

Figure 2.47 Reactions of primary disilylated aryl phosphanes with diphenylcarbodiimide

Similarly, the reaction of a silylated ortho diphosphane **115** with two equivalents of diphenylcarbodiimide **101** gave the expected P=C double bonded compound **116** (Figure 2.49).[63]

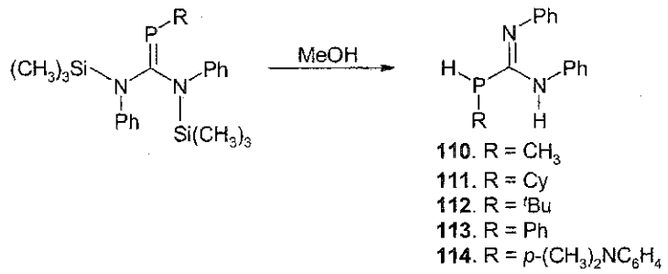

Figure 2.48 Treatment of silylated *N,N',P*-phosphaguanidine with methanol

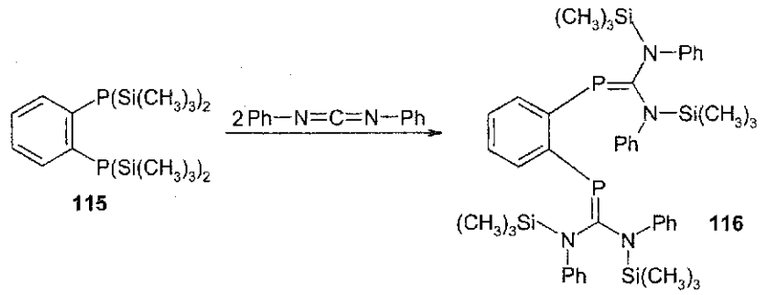

Figure 2.49 Reaction of 1,2-[{$(CH_3)_3Si$}$_2$P]C_6H_4 with diphenylcarbodiimide

When *o-bis*(trimethylsilyl)amino-*bis*(trimethylsilyl)phenylphosphane **117** was reacted with one equivalent of diphenylcarbodiimide **101**, the carbodiimide reacted at the phosphorus center, giving the phosphaguanidine **118** with a P=C double bond (Figure 2.50).[64] Treatment with one equivalent of methanol resulted in the shifting of the double bond from phosphorus to nitrogen **119**. Adding three additional equivalents of methanol caused the remaining $Si(CH_3)_3$ groups to be cleaved off along with the loss of aniline to give the product **120** (Figure 2.51). The final product can be thought of as a phosphaguanidine with a cyclic –C-P=C-N-C- fragment, or as a 2-amino-phosphabenzimidazole.

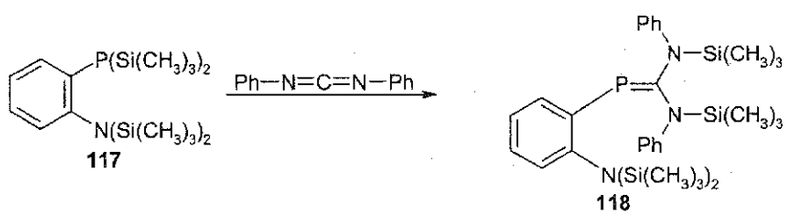

Figure 2.50 Reaction of 1-[N{Si(CH$_3$)$_3$}$_2$]$_2$-2-[P{Si(CH$_3$)$_3$}$_2$]$_2$C$_6$H$_4$ with diphenylcarbodiimide

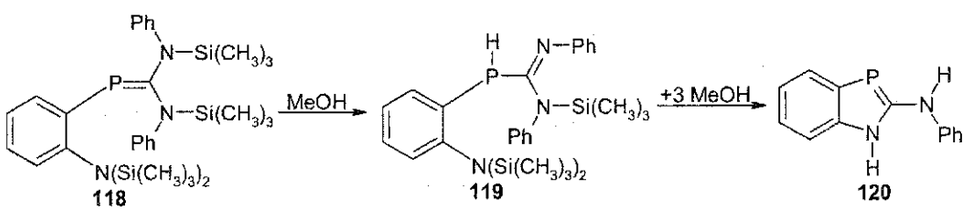

Figure 2.51 Rearrangement of 118 upon N-Si(CH$_3$)$_3$ cleaveage

It is reported that when PhP{Si(CH$_3$)$_3$}$_2$ **121** is added to dicyclohexylcarbodiimide **122** or cyclohexylphenylcarbodiimide **123**, the N=C bond is favored in products **124** and **125** (Figure 2.52), and is retained when the protonated phosphaguanidine is formed by treatment with methanol. However, there is no evidence reported in the paper to substantiate this claim.[48]

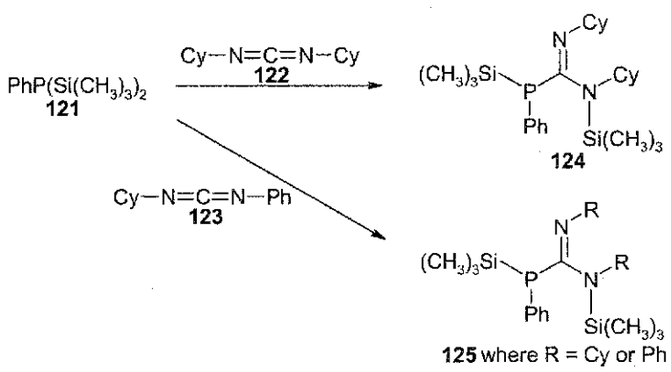

Figure 2.52 Reactions of disilylated phenylphosphane with dicyclohexylcarbodiimide and cyclohexylphenylcarbodiimide

Issleib[58] also reacted both tris(trimethylsilyl) phosphane **126** and bis(trimethylsilyl) phosphane **127** with diphenylcarbodiimide **101**. In these reactions, the P=C double bond is not formed in products **128** and **129**, and the N=C double bond is retained upon treatment with methanol **130** (Figure 2.53).

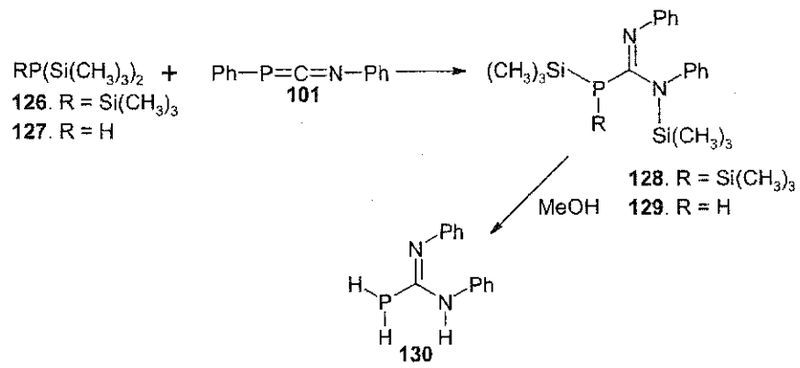

Figure 2.53 Reactions of trisilylated phosphane and disilylated phosphane with diphenylcarbodiimide

Kolodiazhnyi[13,61,62] showed that ^{t}Bu amine **131** readily reacts with phosphaazaallene **42** to form phosphaguanidine **132** with a C=N double bond (Figure 2.54).

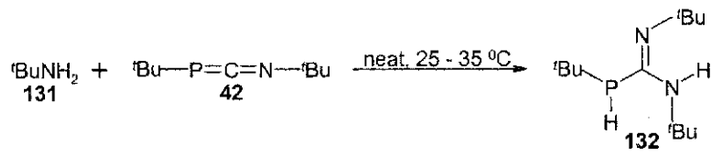

Figure 2.54 Reaction of primary alkyl amine with phosphaazaallene

2.11 Monophosphaguanidines - Pentasubstituted derivatives

Pentasubstituted phosphaguanidines have been made by two routes. The first penta-substitued derivative **133** was made by the treatment of RPH^-Na^+ (R = Ph **134**, Mes **135**) with $EtO\text{-}C^+(N(CH_3)_2)_2\ BF_4^-$ **136** (Figure 2.55).[65]

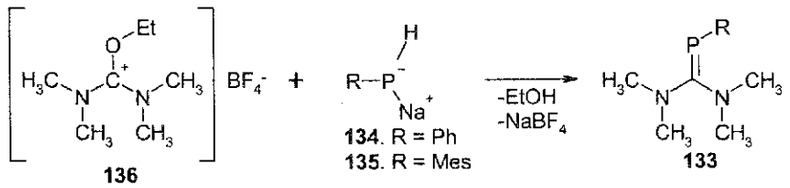

Figure 2.55 Reaction of fluoroborate salt with sodium phosphide to make pentasubstituted phosphaguanidine

A more convenient method involves the reaction between α,α-dihalo amines and silylated phosphanes, with the elimination of trimethylsilyl halides (Figure 2.56).[66,67,68]

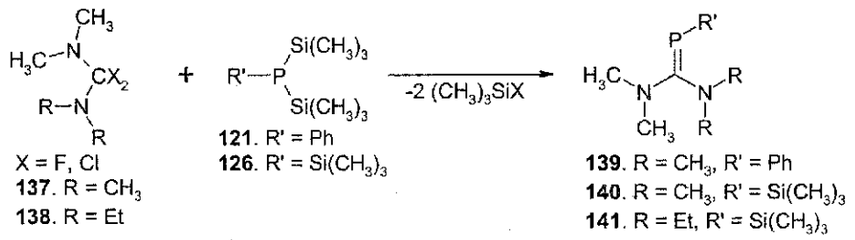

Figure 2.56 Reaction of α,α-dihalo amines with silylated phosphanes

Weber[69] has taken the silylated CH_3 derivative **140** and reacted it with both acyl chlorides **142** and **143** and [Fe]Br **144** to give the phosphaguanidine derivatives **145**, **146** and **147** (Figure 2.57). These phosphaguanidine derivatives have significantly different characteristics than 'normal' phosphaguanidines, due to the effects of the metal center, or conjugation in the C=P-C=O system.

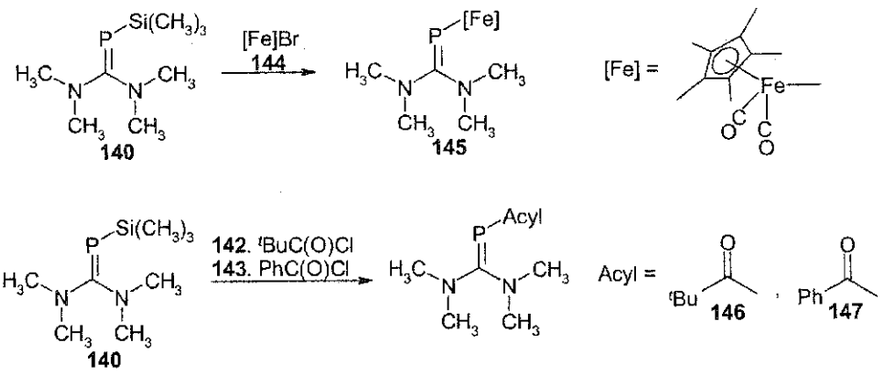

Figure 2.57 [Fe] and Acyl substituted phosphaguanidines

2.12 Metal complexes of phosphaguanidines

η^1-Metal complexes **148** and **149** of phosphaguanidine **99** can be made when reacted with $M(CO)_3(\eta^5\text{-}C_5H_5)Cl$ (M = Mo and W, Figure 2.58).[70]

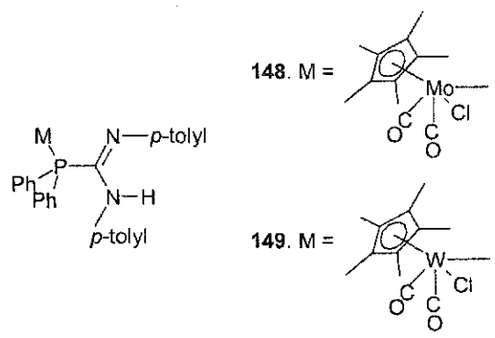

Figure 2.58 Molybdenum and tungsten complexes of phosphaguanidine 99

$Rh(PPh_3)_3Cl$ reacts with phosphaguanidine **99** to give the metal complex **150** shown in Figure 2.59.[71]

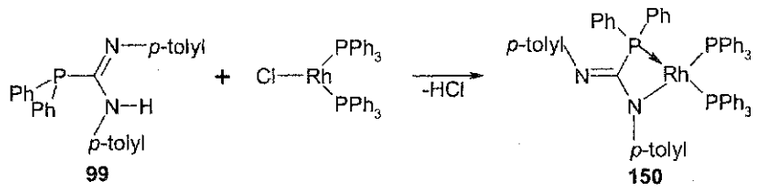

Figure 2.59 Rhodium complex of phosphaguanidine 99

More recently, Stephan[72] isolated and obtained a crystal structure of a phosphaguanidine zirconium complex **151** made from the reaction of zirconium-phosphinidine complex **152** with dicyclohexylcarbodiimide **122** (Figure 2.60).

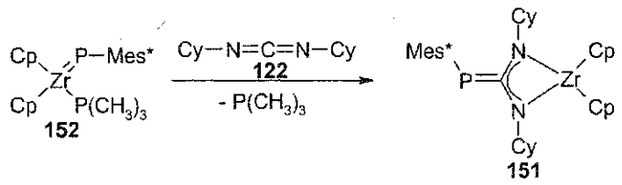

Figure 2.60 Zirconium complex of a phosphaguanidine

2.13 Phosphaamidines, phosphaguanidines and inverse polarization of the P=C bond

In 1989, Regitz discovered that phosphatriafulvenes have inverse polarity at the P=C double bond when compared to normal phosphaalkenes.[73] Normal phosphaalkenes have equal charge distribution between the phosphorus-carbon double bond, whereas inversely polarized phosphaalkenes have a significant negative charge on phosphorus.[55] From the two resonance structures **A** and **B**, it is thought that the ylide structure, **B**, makes a significant contribution to the electronic structure of the molecule (Figure 2.61).

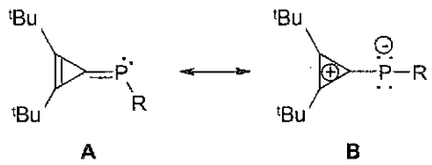

Figure 2.61 Two possible resonance structures for phosphatriafulvenes

Phosphaamidines also are thought to have inverse π-electron density.[74] Resonance structures **C** and **D** show the two resonance structures for phosphaamidines (Figure 2.62). When two amino substituents are attached to the carbon atom, the polarization

is more pronounced because resonance structures F and G *both* contribute to the structure of the phosphaguanidine (Figure 2.62).

Inversely polarized phosphaalkenes are characterized by unusually high field ^{31}P NMR resonances (232.0 ppm for $PhP{=}CPh_2$ **153** [53] vs 28.4 ppm for $PhP{=}C[N\{CH_3\}]_2$ **139** [55]), longer P=C bonds (1.70-1.76 Å vs. 1.65-1.67 Å in normally polarized phosphaalkenes) and are strong nucleophiles via the phosphorus atom.[55]

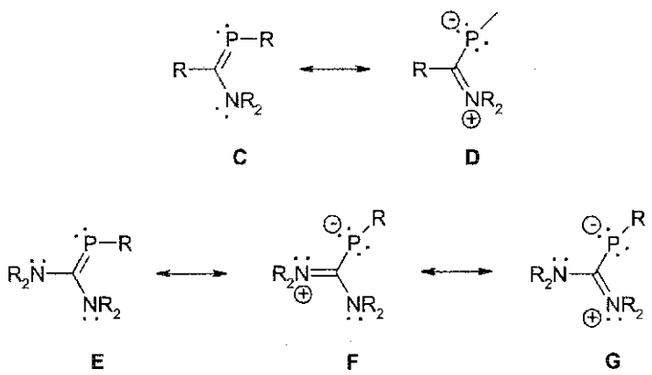

Figure 2.62 The possible resonance structures for phosphaamidines (C and D), and phosphaguanidines (E, F and G).

Reference List

1. Scherer, O. J.; Regitz, M. *Multiple Bonds and Low Coordination in Phosphorus Chemistry,* 1st ed.; Scherer, O. J.; Regitz, M., Editor; Thieme Medical Publishers, Inc.: New York, 1990.

2. Hudson, R. F. *Structure and Mechanism in Organo-Phosphorus Chemistry;* 1 ed. Academic Press: London, 1965.

3. Gier, T. E. *J. Am. Chem. Soc.* **1961**, *83*, 1769-1770.

4. Markl, G. *Angew. Chem., Int. Ed. Engl.* **1966**, *5*(9), 846-847.

5. Ashe, A. J. *J. Am. Chem. Soc.* **1971**, *93*(13), 3293-3295.

6. Hopkinson, M. J.; Kroto, H. W.; Nixon, J. F.; Simmons, N. P. C. *J. Chem. Soc., Chem. Commun.* **1976**, 513-515.

7. Kroto, H. W.; Nixon, J. F. *American Chemical Society Symposium Series* **1981**, *171*, 383-389.

8. Becker, G. *Z. Anorg. Allg. Chem.* **1976**, *423*, 242-254.

9. Yoshifuji, M.; Shima, I.; Inamoto, N. *J. Am. Chem. Soc.* **1981**, *103*, 4587-4589.

10. Yoshifuji, M.; Shima, I.; Inamoto, N.; Hirotsu, K.; Higuchi, S. *J. Am. Chem. Soc.* **1982**, *104*(22).

11. Bertland, G.; Couret, C.; Escudié, J.; Najid, S.; Majoral, J. *Tetrahedron Lett.* **1982**, *23*(35), 3567.

12. Yoshifuji, M. *J. Organomet. Chem.* **2000**, *611*, 210-216.

13. Kolodiazhnyi, O. I. *Tetrahedron Lett.* **1982**, *23*(47), 4933-4936.

14. Escudié, J.; Ranaivonjatovo, H.; Rigon, L. *Chem. Rev.* **2000**, *100*, 3639-3696.

15. Appel, R.; Paulen, W. *Angew. Chem., Int. Ed. Engl.* **1983**, *22*(10), 785-786.

16. Appel, R.; Fölling, P. K. L.; Siray, M.; Knoch, F. *Angew. Chem., Int. Ed. Engl.* **1984**, *23*(12), 970.

17. Appel, R. *Multiple Bonds and Low Coordination in Phosphorus Chemistry,* 1st ed.; Scherer, O. J.; Regitz, M., Editor; Thieme Medical Publishers, Inc.: New York, 1990.

18. Eshtiagh-Hosseini, H.; Kroto, H. W.; Nixon, J. F.; Maah, M. J.; Taylor, M. J. *J. Chem. Soc., Chem. Commun.* **1981**, 199-200.

19. Klebach, T. C.; Lourens, R.; Bickelhaupt, F.; Stam, C. H.; van Herk, A. *J. Organomet. Chem.* **1981**, *210*, 211-221.

20. Cowley, A. H.; Jones, R. A.; Stewart, C. A.; Stuart, A. L.; Atwood, J. L.; Hunter, W. E.; Zhang, H. M. *J. Am. Chem. Soc.* **1983**, *105*, 3737-3738.

21. Davies, J. E.; Mays, M. J.; Raithby, P. R.; Woods, A. D. *J. Chem. Soc., Chem. Commun.* **1999**, 2455-2456.

22. Gerhardt, C. *Annalen* **1858**, *108*, 219.

23. Barker, J.; Kilner, M. *Coord. Chem. Rev.* **1994**, *133*, 219-300.

24. Gautier, J. A.; Miocque, M.; Farnoux, C. C. *The Chemistry Of Amidines And Imidates,* Vol. 1 ed.; Patai, S., Editor; John Wiley & Sons Ltd: London, 1991.

25. Boyd, G. V. *The Chemistry Of Amidines And Imidates,* Vol. 2 ed.; Patai, S.; Rappoport, Z., Editor; John Wiley & Sons Ltd: London, 1991.

26. Perrin, C. L. *The Chemistyr of Amidines and Imidates*; Patai, S.; Rappoport, Z., Ed; Wiley: Chichester, 1991; Vol. 2, pp 147-229.

27. Boeré, R. T.; Hicks, R. G.; Oakley, R. T. *Inorg. Synth.* **1996**, *21*, 94-98.

28. Edelmann, F. T. *Coord. Chem. Rev.* **1994**, *137*, 403-481.

29. Aubrecht, K. B.; Chang, K.; Hillmyer, M. A.; Tolman, W. B. *Journal of Polymer Science: Part A: Polymer Chemistry* **2001**, *39*, 284-293.

30. Jordan, R. F.; Coles, M. P. *J. Am. Chem. Soc.* **1997**, *119*, 8125-8126.

31. Brussee, E. A. C.; Meetsma, A.; Hessen, B.; Teuben, J. H. *Organometallics* **1998**, *17*, 4090-4095.

32. Sita, L. R.; Babcock, J. R. *Organometallics* **1998**, *17*, 5228-5230.

33. Britovsek, G. J. P.; Gibson, V. C.; Wass, D. F. *Angew. Chem. Int. Ed.* **1999**, *38*, 428-447.

34. Decker, J. M.; Geib, S. J.; Meyer, T. Y. *Organometallics* **1999**, *18* , 4417-4420.

35. Foley, S. R.; Zhou, Y.; Yap, G. P. A.; Richeson, D. S. *Inorg. Chem.* **2000**, *39*, 924-929.

36. Patai, S.; Rappoport, Z. *The Chemistry of Amidines and Imidates, Vol. 2*; Wiley: Chichester, 1991.

37. Raubenheimer, H. G.; Kruger, G. J.; Scott, F.; Otte, R. *Organometallics* **1987**, *6*(8), 1789-1795.

38. Boeré, R. T.; Klassen, V.; Wolmershauser, G. *J. Chem. Soc., Dalton Trans.* **1998**, 4147-4154.

39. Cotton, F. A.; Walton, R. A. *Multiple Bonds Between Metal Atoms;* 2nd ed. Clarendon Press: Oxford, 1993.

40. Niemann, L. C.; Stam, C. H. *J. Chem. Soc., Dalton Trans.* **1986**, 717.

41. Kuz'mina, L. G.; Bokii, N. G.; Struchkov, Yu. T.; Minkin, V. I.; Olekhnovich, L. P.; Mikhailov, I. E. *J. Struct. Chem.* **1977**, *18*, 96.

42. Abeysekera, D.; Robertson, K. N.; Cameron, T. S.; Clyburne, J. A. C.

Organometallics , *20* , 5532-5536.

43. Fairlie, D. P.; Jackson, W. G. *Inorg. Chem.* **1990**, *29*, 140.

44. Bailey, P. J.; Pace, S. *Coord. Chem. Rev.* **2001**, *214*, 91-141.

45. Boeré, R. T.; Klassen, V.; Wolmershauser, G. *Can. J. Chem.* **2000**, *78*, 583-589.

46. Boeré, R. E.; Boeré, R. T.; Masuda, J.; Wolmershauser, G. *Can. J. Chem.* **2000**, *78*, 1613-1619.

47. Cotton, F. A.; Inglis, T.; Kilner, M.; Webb, T. R. *Inorg. Chem.* **1975**, *14*(9), 2023-2026.

48. Issleib, K.; Schmidt, H.; Meyer H. *J. Organomet. Chem.* **1978**, *160*, 47-57.

49. Paasch, K.; Nieger, M.; Niecke, E. *Angew. Chem., Int. Ed. Engl.* **1995**, *34*(21), 2369-2371.

50. El-Ouatib, R.; Ballivet-Tkatchenko, D.; Etemad-Moghadam, G.; M. Koening *J. Organomet. Chem.* **1993**, *453*, 77-84.

51. Yoshifuji, M.; Niitsu, T.; Toyota, K.; Inamoto, N. *Tetrahedron Lett.* **1988**, *29*(3), 333-336.

52. Becker, G.; Mundt, O. *Z. Anorg. Allg. Chem.* **1980**, *462*, 130-142.

53. Becker, G.; Uhl, W.; Wessley, H. J. *Z. Anorg. Allg. Chem.* **1981**, *479*, 41-56.

54. Oehme, H.; Leissring, E.; Meyer, H. *Tetrahedron Lett.* **1980**, *21*, 1141-1144.

55. Weber, L. *Eur. J. Inorg. Chem.* **2000**, 2425-2441.

56. Issleib, K.; Vollmer, R.; Meyer, H. *Tetrahedron Lett.* **1978**, *5*, 441-444.

57. Issleib, K.; Schmidt, H.; Meyer H. *J. Organomet. Chem.* **1980**, *192*, 33-39.

58. Issleib, K.; Schmidt, H.; Wirkner, Ch. *Synth. React. Inorg. Met.-Org. Chem.* **1981**, *11*(3), 279-285.

59. Thewissen, D. H. M. W.; Ambrosius, H. P. M. M. *Recl. Trav. Chim. Pays-Bas* **1980**, *99*(11), 344-346.

60. Pudovik, A. N.; Romanov, G. V.; Stepanova, T. Y. *Bulletin of the Academy of Sciences of the U.S.S.R.* **1982**, *6*, 1416-1417.

61. Kolodiazhnyi, O. I. *Phosphorus and Sulfur* **1983**, *18*, 39-42.

62. Kolodyazhnyi, O. I. *Zh. Obshch. Khim.* **1983**, *53*, 1093-1099.

63. Issleib, K.; Schmidt, H.; Bergmann, P. *Z. Anorg. Allg. Chem.* **1985**, *529*, 216-221.

64. Schmidt, H.; LeiBring, E.; Wirkner, C. *Z. Chem.* **1989**, *29*(11), 410-411.

65. Oehme, H.; Leibring, E.; Meyer, H. *Z. Chem.* **1981**, *21*, 407-408.

66. Markovski, L. N.; Romanenko, V. D.; Pidvarko *Zh. Obshch. Khim.* **1982**, *52*(8), 1925-1926.

67. Chernega, A. N.; Antipin, M. Yu.; Struchkov, Yu. T.; Boldescul, I. E.; Sarina, T. V.; Romanenko, V. D. *Ukr. Khim. Zh.* **1985**, *51*, 868-874.

68. Chernega, A. N.; Antipin, M. Y.; Struchov, Y. T.; Bodesu, I. E.; Sarina, T. V.; Romanenko, V. D. *Dokl. AKAD. Nauk SSSR* **1984**, *278*, 365-370.

69. Weber, L.; Uthmann, S.; Bogge, H.; Muller, A.; Stammler, H.; Neumann, B. *Organometallics* **1998**, *17*, 3593-3598.

70. Ambrosius, H. P. M. M.; Van Der Linden, A. H. I. M.; Steggerda, J. J. *J. Organomet. Chem.* **1980**, *204*, 211-220.

71. Thewissen, D. H. M. W.; Ambrosius, H. P. M. M.; Van Gaal, H. L. M.; Steggerda, J. J. *J. Organomet. Chem.* **1980**, *192*, 101-113.

72. Breen, T. L.; Stephan, D. W. *J. Am. Chem. Soc.* **1995**, *117*, 11914-11921.

73. Fuchs, E. P. O.; Heydt, H.; Regitz, M.; Schoeller, W. W.; Busch, T. *Tetrahedron Lett.* **1989**, *30*(38), 5111-5114.

74. Weber, L.; Uthmann, S.; Stammler, H.; Neumann, B.; Schoeller, W. W.; Boese, R.; Blaser, D. *Eur. J. Inorg. Chem* **1999**, 2369-2381.

Chapter 3

Density functional theory study of phosphaamidines

3.1 Introduction

There have been several studies on the electronic structures of the hydrogen substituted model phosphaalkenes, H-P=CH_2[1-6], and model aminophosphaalkenes, E/Z-H-P=C(H)NH_2[2-6], but no work has been done on phosphinoimines, the N=C isomers of aminophosphaalkenes, E/Z-H-N=C(H)PH_2. Much of the earlier, less sophisticated work focused on the optimized geometries, atomic charges and frontier molecular orbitals of the model phosphaalkenes. Later work looked at the model phosphaamidine system, but the authors only looked at the P=C isomers, neglecting to look at the N=C isomers. No previous work has been done to ascertain why the P=C systems are more stable than the N=C isomers. In this work, we look at the model phosphaalkene system, both the optimized geometries and frontier molecular orbitals. Using this information, we can interpret the frontier molecular orbitals of the model phosphaamidine system and see what effects the amino group has on the P=C double bond. In addition, we look at all four possible isomers for the model phosphaamidines, and investigate why the P=C isomers are more stable than the N=C isomers. The full system **20** has also been investigated to determine the stabilities of the eight possible isomers and to have a better understanding of their reactivity.

3.2 Methods and experimental

All structures of the model phosphaamidines and the model phosphaalkene were optimized by DFT methods, using the B3LYP hybrid functional[7] and the 6-31G(d) basis set[8-12], as implemented in Gaussian 98W[13], unless otherwise stated. For the model

systems, stationary points were verified by frequency calculations. For the DFT calculations on **20**, AM1 geometry optimizations were verified by frequency calculations, after which the AM1 geometries were used as starting points for the DFT geometry optimization.

3.3 Model phosphaalkene – Geometry and electronic structure

The staring point of our analysis is the isolated P=C bond. The optimized geometry of the model phosphaalkene (Figure 3.1) is similar to the values found at lower levels of theory (MO LCAO SCF/3-21G*[2], STO-3G and STO 4-31G[1], Table 3.1). All of the bond lengths are slightly longer for the DFT calculations than in the MO LCAO SCF/3-21G* calculations, most notably the P=C bond has lengthened from 1.646 Å to 1.675 Å. The STO-3G calculation gave a much shorter P=C bond length of 1.62 Å, while the STO 4-31G calculation gave a P=C bond length (1.67 Å) more similar to the DFT calculations. However, the STO 4-31G calculation overestimates the P-H bond length, giving 1.47 Å vs 1.433 Å seen in the DFT calculations.

Table 3.1 Optimized bond lengths and angles of the model phosphaalkene

Bond lengths (Å) and angles (°)	B3LYP/6-31G(d) (This work)	B3LYP/6-31G(d)[3]	MO LCAO SCF/3-21G*[2]	STO-3G[1]	STO 4-31G[1]
H-P	1.433		1.408	1.39	1.47
P=C	1.675	1.674	1.646	1.62	1.67
C-H_{cis}	1.087		1.078		
C-H_{trans}	1.088		1.079		
H-P-C	97.64	97.7	98.8	97.0	98.0
P-C-H_{trans}	119.20		120.0		
P-C-H_{cis}	125.56		124.8		

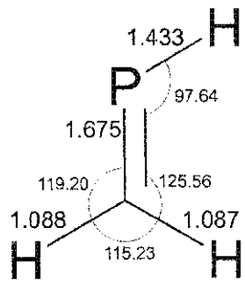

Figure 3.1 Optimized geometry of model phosphaalkene at the B3LYP/6-31G(d) level

Analysis of the computed eigenfunctions of the model phosphaalkene shows the HOMO to be the π(1) orbital, the LUMO as the π(2) orbital, and the HOMO-1 as the phosphorus lone pair, *n*(P) (Figure 3.2). Using STO calculations, Bickelhaupt[6] has shown that upon increasing the H-P-C angle from the geometry optimized value of 97.5° to 120°, the HOMO and HOMO-1 exchange relative position, with the phosphorus lone pair becoming higher in energy and the π(1) orbital essentially being unaffected.

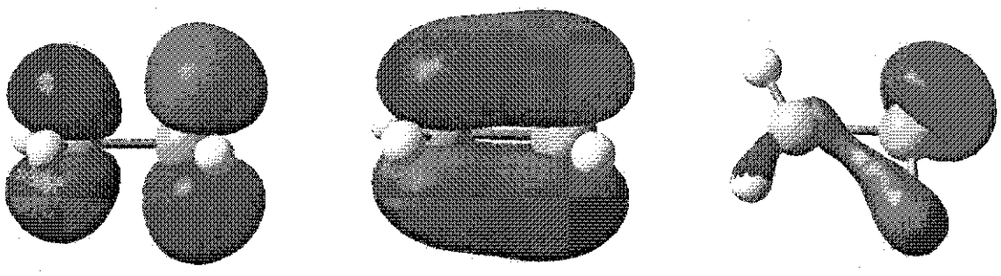

Figure 3.2 Frontier molecular orbitals for the model phosphaalkene

3.4 Model phosphaamidines – Geometries and electronic structures

There are four possible isomers of the model phosphaamidines: Z-(P=C) **A**, E-(P=C) **B**, Z-(N=C) **C** and E-(N=C) **D** and the geometrical parameters of the optimized structures are included in Figure 3.2. Note that even without any symmetry restraints, the aminophosphaalkenes are essentially planar, while the phosphinoimines minimize to a

structure that forces the H-P-H "vee" to be twisted above the plane of the double bond. This geometry allows the phosphorus lone pair to be aligned with the perpendicular *p*-orbitals of the N=C bond.

A recent paper by Schoeller[3] lists the P=C bond length and C-P-C angles of the Z-(P=C) **A** isomer, which are in agreement with our calculations at the same level of theory. An earlier paper calculated the geometry of the E-(P=C) **B** isomer at the MO LCAO SCF/3-21G* level of theory. Our DFT calculations provide longer bond lengths, with the P=C bond being 0.019 Å shorter and the N-C bond length 0.022 Å shorter using the HF method, which ignores electron correlation effects.

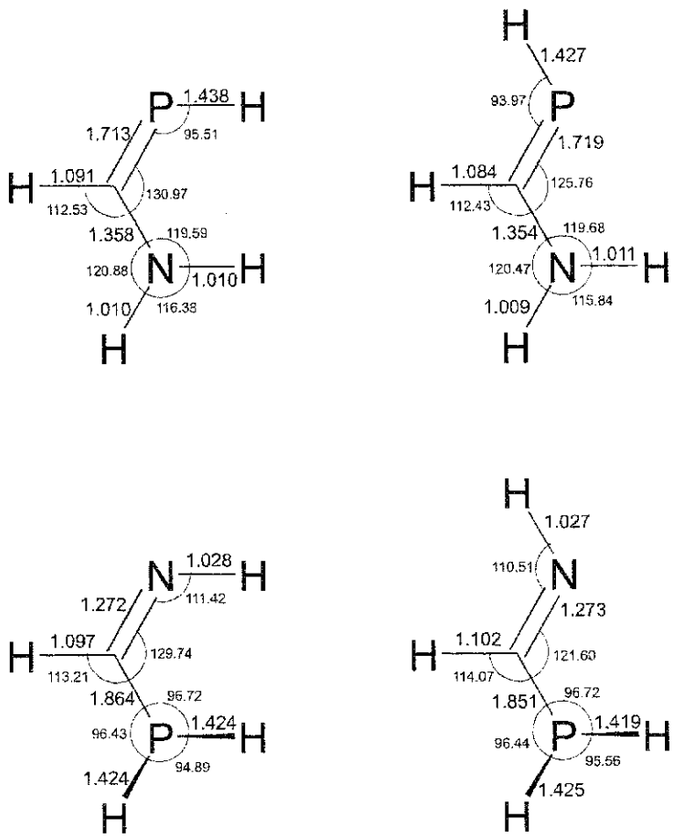

Figure 3.3 Optimized geometries for the four isomers of the model phosphaamidine

In our calculations, the Z-(P=C) isomer is the most stable conformation, followed by the E-(P=C) isomer (Table 3.2). Both the Z-(N=C) and E-(N=C) isomers are approximately 6 kcal/mol less stable than the corresponding P=C isomers, consistent with the observation that compounds of this type normally exist as aminophosphaalkenes rather than phosphinoimines. The Z-anti (P=C) isomer is indeed the major isomer in solution and that found in the solid state for the bulky aryl derivatives described in this work (Chapter 5). However, it bears some careful consideration as to why this should be the case.

Table 3.2 Actual and relative energies calculated for the model phosphaamidines optimized at the B3LYP/6-31G(d) level

	Relative Energies (kcal/mol)	Actual Energies (kcal/mol)
Z-(P=C) **A**	0	-273960.6
E-(P=C) **B**	0.8	-273959.8
Z-(N=C) **C**	5.5	-273954.3
E-(N=C) **D**	5.9	-273953.9

To determine why the aminophosphaalkene isomer is favored over the phosphinoimine form, we turn to the molecular orbital energy diagrams for each of the four isomers (Figure 3.4). This diagram will be referred to throughout the discussion. Note first of all that a consideration of the frontier orbitals would *not* support this stability series; the HOMO in the (N=C) isomers is considerably lower in energy than those in the (P=C) isomers. Aminophosphaalkenes have a very high-lying HOMO, $\pi(2)$, which lies as much as 2 eV higher than the HOMO of a simple phosphaalkene. It is this orbital, along with $\pi(1)$, that is primarily responsible for the inverse polarization of the P=C bond in these compounds and reflects the major contribution of the second canonical resonance form (Figure 3.5).

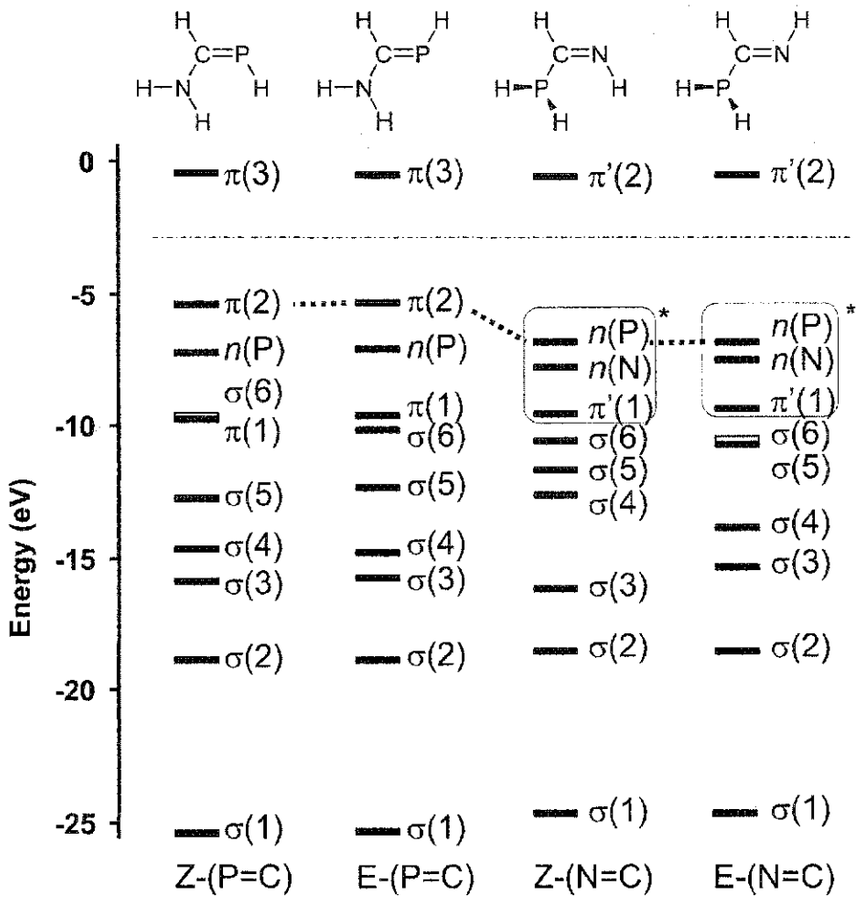

Figure 3.4 Molecular orbital energy diagram of aminophosphaalkene and phosphinoimine isomers

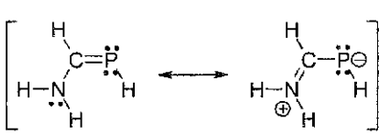

Figure 3.5 Resonance forms of aminophosphaalkenes

A numerical analysis indicates that the energy of filling the highest 5 filled levels in both (P=C) isomers is greater than filling these same orbitals in the (N=C) isomers. It is only with the filling of the sixth level, σ(4), and lower that the energetic preference for the aminophosphaalkenes dominates. Figure 3.4 clearly shows that it is the energetic stabilization of low-lying orbitals, particularly σ(5), σ(4), σ(2) and σ(1), that supports the much higher-lying frontier orbitals of the (P=C) isomers. An analysis of these four low-lying orbitals indicates that they consist of both $p(\sigma)$ and $s(\sigma)$ bonding in the skeleton of the molecule. In contrast, the σ(4) molecular orbital has large contributions from P–H bonding, and this is energetically favored in the (P=C) isomers. This analysis categorically demonstrates that the lower energy of the (P=C) isomers is driven by σ-bond reorganization rather than by the π-system.

3.5 Orbital topology of the Z-(P=C) isomer

Looking at the individual orbital topology of the most stable isomer, Z-(P=C), note the 3π-2π bond overlap between phosphorus and carbon in the π(2) HOMO (Figure 3.6). By far the largest orbital coefficient in this MO is on phosphorus, and this is largely responsible for the overall negative charge density on phosphorus. In contrast, π(1) HOMO-4 is almost entirely localized between the carbon and nitrogen atoms and lies considerably lower in energy. The n(P) HOMO-1 is primarily the phosphorus lone-pair orbital that is the donor atom in coordination complexes of this class of compound.

This description thus fits that of a strongly polarized heteroallylic resonance system. The dative C=N π-bond order is remarkably high, as given by the sum of π(1) and π(2),

and despite the polarization of each molecular orbital, the net bond order comes very close to 1.5 for both C–N and C–P bonds.

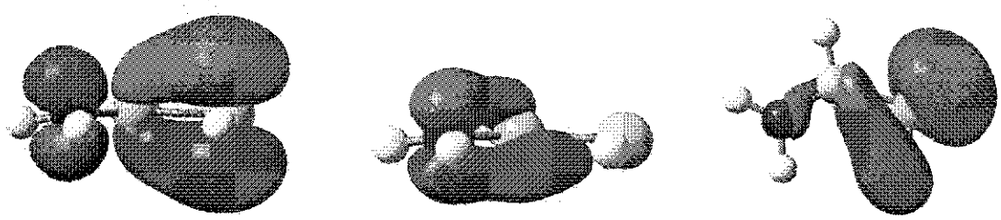

Figure 3.6 Selected individual MO topologies for Z-(P=C) isomer

At our level of theory, almost all the occupied levels in E-(P=C) lie slightly higher than in the Z isomer, with the exception of the main H–C–P–H in-plane σ-bonding molecular orbital σ(6) which is clearly stabilized in the E isomer. The presence of E and Z isomers in aminophosphaalkenes is highly likely, although these have not been commonly observed. There are otherwise no notable differences between these two very similar molecules

3.6 Orbital topology of the Z-(N=C) isomer

The (N=C) isomers are no longer planar molecules, so that there is no clear separation of σ and π orbitals. We have resorted to the use of ' to mark *pseudo* π orbitals in both compounds. First we discuss the three orbitals in the boxed sections of both isomers. It is clear that all three are strongly mixed (Figure 3.7). However, it is possible to describe the HOMO as a mixture of *n*(P) lone pair and N=C π character. Similarly, π'(1) HOMO-2 is an orbital in which the phosphorus lone pair is strongly mixed with the N=C π bond. The HOMO-1 can be described as a combination of the phosphorus lone pair and the nitrogen lone pair. However, we also note that the π'(1) and *n*(P)/π' orbitals essentially

cancel any net contribution of P=C π-bonding in the (N=C) isomer. Consistently, the calculated P–C bond distances (Figure 3.3) in these compounds are quite close to values expected for phosphorus-carbon single bonds (average P-C single bond 1.85 Å[14]).

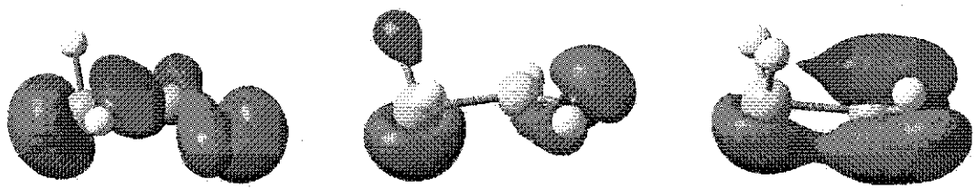

Figure 3.7 Selected individual MO topologies for Z-(N=C) isomer

3.7 Interpretation of the frontier molecular orbitals in model phosphaamidines

Using the frontier molecular orbitals for the model phosphaalkene and model phosphaamidine, we can create an interpretive framework as to why the HOMO of the model phosphaamidine is raised in energy, while maintaining a HOMO-LUMO gap that is essentially the same as the model phosphaalkene. Looking at the molecular orbital diagram of the most stable phosphaamidine isomer, Z-(P=C), one can see that addition of the NH_2 fragment to the model phosphaamidine causes π_1 to be split into the lower lying $\pi_1^{\ddagger}$ orbital and the higher lying $\pi_2^{\ddagger}$ orbital (Figure 3.8). The LUMO, $\pi_3^{\ddagger}$, is also raised in energy, resulting in a similar HOMO-LUMO gap to the model phosphaalkene. Note that the phosphorus lone pair, indicated by n(P), is unaffected by the NH_2 fragment. This frontier orbital picture will be used as a framework for discussion of our experimental results on monophosphaamidines and their metal complexes (Sections 5.4 and 6.5).

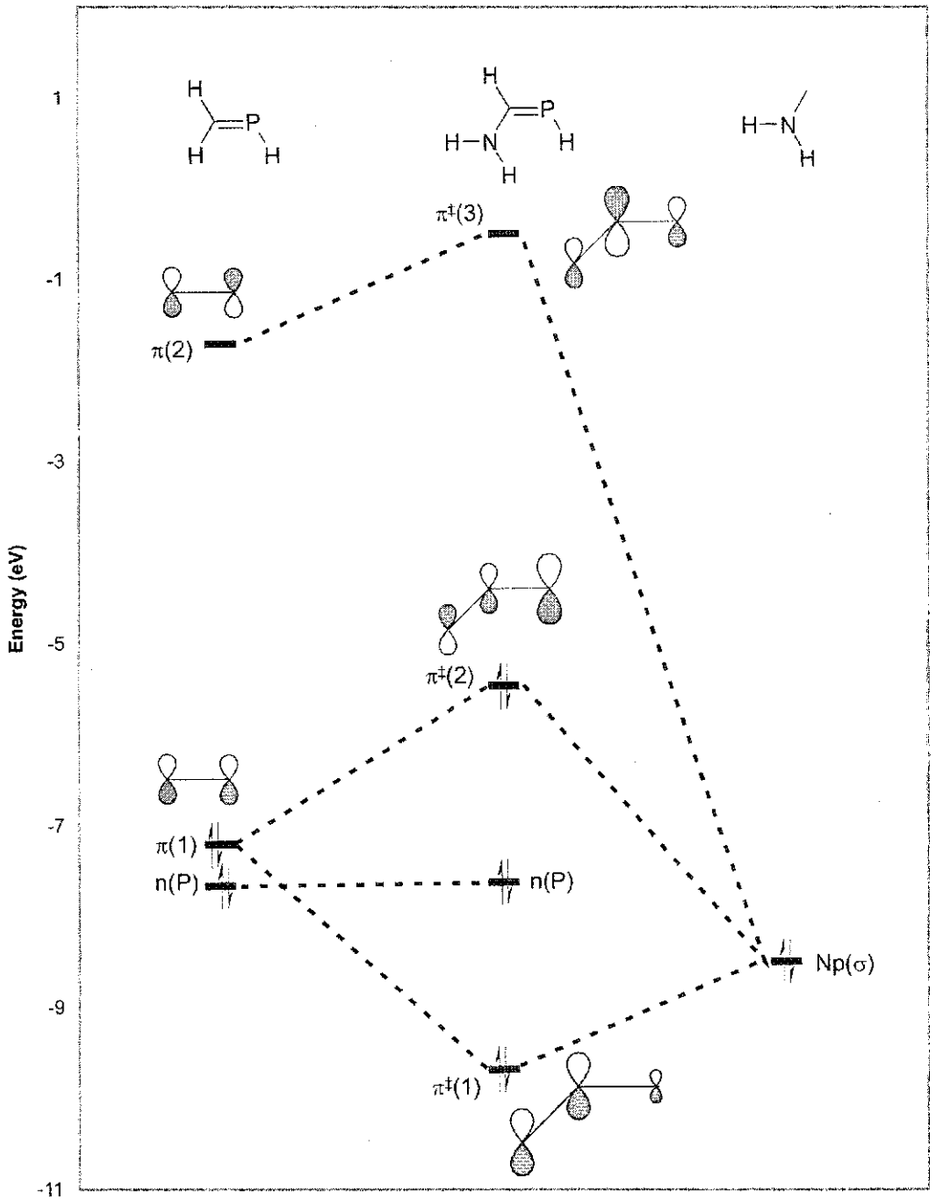

Figure 3.8 Frontier molecular orbital interaction diagram showing the generation of an aminophosphaalkene from a phosphaallene and a nitrogen π-orbital in NH_2

3.8 Extension to the full phosphaamidine structures

We have also performed AM1 and B3LYP/6-31G(d) geometry optimizations of the eight(!) possible isomers and tautomers possible for *N,P*-disubstituted Dipamidines (Figure 3.9). The energies are presented in Tables 3.3 (AM1) and 3.4 (B3LYP), and some key geometric parameters for the B3LYP calculations are presented in Tables 3.5 and 3.6 (NB - Quantum chemical calculations give energies that effectively compare the energy of the molecule to the sum of the energies of the isolated atoms in the molecule, inherently leading to large numbers. In addition, there are no error values to be reported; therefore only relative energies will be discussed. Minor conformational changes can also cause variations in the reported energies, thus these calculations are at best accurate to ± 0.1 kcal/mol). As the AM1 method is poorly parameterized for P(III), the P-C_{aryl} and P=C bond lengths are much shorter than expected (0.15-0.20 Å less than average[14]) and these calculations cannot be viewed as completely accurate, thus little weight should be placed on the relative energies of each isomer.

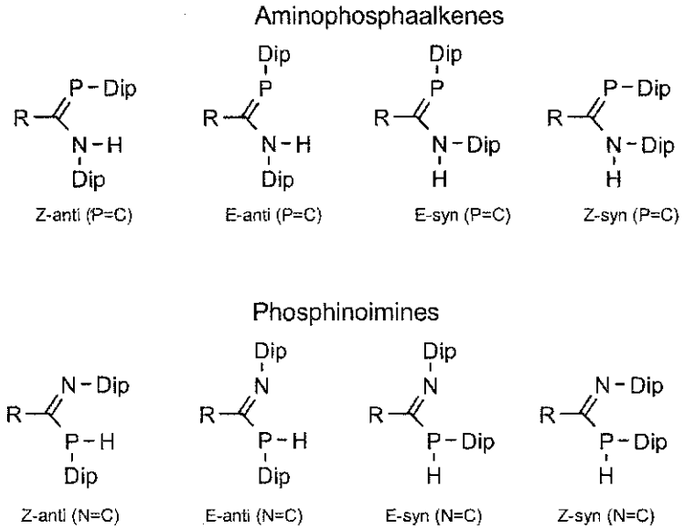

Figure 3.9 Eight isomers and tautomers of *N,P*-disubstituted phosphaamidines. R = *p*-tolyl

Table 3.3 Calculations optimized at the AM1 level

	Relative Energies (kcal/mol)	Actual Energies (kcal/mol)
Z-anti (P=C)	0	-7790.1
E-anti (P=C)	2.3	-7787.8
E-syn (N=C)	3.1	-7787.0
E-anti (N=C)	5.2	-7784.9
E-syn (P=C)	9.0	-7781.1
Z-syn (P=C)	12.3	-7777.8
Z-anti (N=C)	13.4	-7776.7
Z-syn (N=C)	13.6	-7776.5

Table 3.4 Calculations optimized at the B3LYP/6-31G(d) level

	Relative Energies (kcal/mol)	Actual Energies (kcal/mol)	Actual Energies (Hartrees)
Z-anti (P=C)	0	-1029630.5	-1640.82053940
E-syn (P=C)	1.9	-1029628.6	-1640.81388407
Z-anti (N=C)	2.4	-1029628.1	-1640.81679283
E-syn (N=C)	2.7	-1029627.8	-1640.81633034
Z-syn (N=C)	3.3	-1029627.2	-1640.81633047
E-anti (N=C)	4.2	-1029626.3	-1640.81388407
E anti (P=C)	4.3	-1029626.2	-1640.81379209
Z-syn (P=C)	9.9	-1029620.6	-1640.80477944

Table 3.5 Selected bond lengths of aminophosphaalkenes (P=C) optimized at the B3LYP/6-31G(d) level

	P=C	P-C_{aryl}	N-C	N-C_{aryl}	C-C_{aryl}
Z-anti	1.740	1.879	1.371	1.434	1.487
E-anti	1.739	1.867	1.383	1.436	1.483
E-syn	1.736	1.872	1.384	1.438	1.487
Z-syn	1.728	1.871	1.386	1.446	1.499

Table 3.6 Selected bond lengths of phosphinoimines (N=C) optimized at the B3LYP/6-31G(d) level

	P-C	P-C_{aryl}	N=C	N-C_{aryl}	C-C_{aryl}
Z-anti	1.896	1.866	1.283	1.415	1.490
E-anti	1.878	1.865	1.282	1.419	1.493
E-syn	1.877	1.853	1.280	1.419	1.495
Z-syn	1.901	1.869	1.279	1.411	1.498

Full convergence of these extremely expensive calculations was not achieved in all cases. Full convergence was obtained for the experimentally observed Z-anti (P=C) isomer, which is the lowest energy isomer at every level of calculation that we have attempted. The Z-anti (N=C) isomer was also successfully minimized at the DFT level. We will restrict our discussion to a comparison of these two representative (P=C) and (N=C) isomers.

Analysis of the energies of the occupied levels in these two systems produces results very similar to those seen for the simple H-substituted model compounds discussed above. These molecules have 90 occupied valence orbitals. It is necessary to drop down to the 52nd level before the overall energetic preference is for the (P=C) isomer over the (N=C) isomer.

The five highest lying filled orbitals in the (P=C) isomer all lie substantially higher in energy than those in the (N=C) isomer. The $\pi(2)$ HOMO especially, at –4.87 eV in the (P=C) isomer, has the same $\pi(2)$ character as found in the model system. The third-highest filled level in the stack is $\pi(1)$, and the LUMO is $\pi(3)$. These have the same topology as in the model systems, and can be represented by the topological sketches shown in Figure 3.10.

The $\pi(3)$ LUMO is slightly delocalized into the aryl π-system of the tolyl group on C. But the essential picture is the same as in the model compounds. The *n*(P) lone pair orbital, however, is considerably delocalized into the aromatic ring of the Dip group attached to phosphorus. This stabilization may be partly responsible for the 1.25 eV lower energy of this orbital below the HOMO of the system.

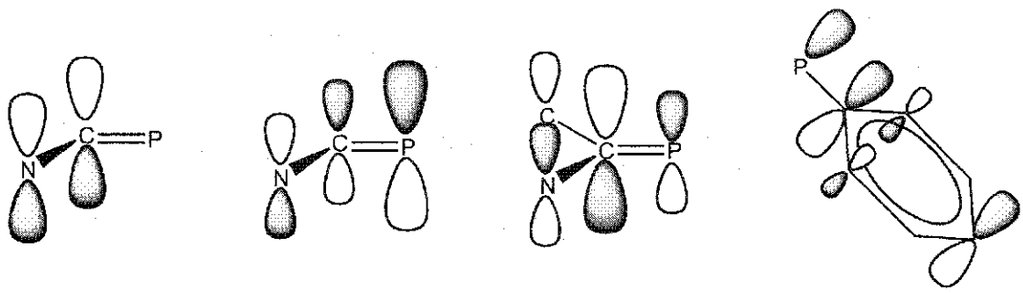

$\pi(1)$ $\pi(2)$ $\pi(3)$ $n(P)$

Figure 3.10 Topological sketches of the molecular orbitals of 20 at the B3LYP/6-31G(d) level

Consequently the Z-anti (P=C) phosphaamidine has two important occupied frontier orbitals: the $\pi(2)$ HOMO, expected to be of significance in electrophilic and cycloaddition reactions, and the *n*(P) HOMO-1, which is of importance in σ-donor reactions, and is in fact utilized in the $LM(CO)_5$ coordination compounds that we have prepared (Chapter 6). The $\pi(3)$ LUMO orbital is of importance for backbonding (See Chapter 6).

Using full B3LYP/6-31G(d), the Z-anti (N=C) isomer is calculated to lie only 2.3 kcal mol^{-1} higher in energy than the Z-anti (P=C) isomer, the major isomer in solution. However, the E-syn (N=C) isomer is almost degenerate with Z-anti (P=C) (approx. 0.3 kcal mol^{-1} difference). To what extent our calculations are affected by conformational effects from the three large substituent groups in these molecules remains unclear. In addition, some of the calculations such as the one for E-anti (N=C) did not fully converge, therefore we hesitate to put any great confidence on the relative energies of the different minority isomers. We *do* see more than one isomer present in all our solution state NMR studies, and find that with polar solvents E-syn (P=C) isomer becomes almost equal in abundance to the main isomer (Chapter 5). Suffice it to say that the energetic

balance for these highly substituted phosphaamidines appears to be very finely tuned, and this is certainly in agreement with our experimental observations.

3.9 Conclusion

In conclusion, we find very good agreement between all calculations that we have performed on the full phosphaamidine structures and the four simple models discussed above. All these results concur that (P=C) isomers are the most stable form, in agreement with our experimental observations. However, other isomers lie close in energy, and the (N=C) isomers may under certain circumstances be expected to occur in equilibrium with the (P=C) isomeric forms, as seen in our NMR studies (Chapter 5).

In all cases, the energetic preference for the (P=C) forms is driven by σ-skeletal orbital reorganization, and cannot be attributed to the π-system. Thus the high-energy delocalized heteroallylic π-orbitals in aminophosphaalkenes are the reactive frontier orbitals, but they are entirely supported by the energenic preference of the low-lying σ-orbitals. In this aspect, aminophosphaamidines resemble other unsaturated main group compounds involving 3rd and higher period elements.[15]

Reference List

1. Thomson, C. *J. Chem. Soc., Chem. Commun.* **1977**, 322-323.

2. Chernega, A. N.; Ruban, A. V.; Romanenko, V. D.; Markovski, L. N.; Korkin, A.

A.; Antipin, M. Yu.; Struchkov, Y. T. *Heteroatom Chemistry* **1991**, *2*(2), 229-241.

3. Schoeller, W. W.; Rozhenko, A. B.; Grigoleit, S. *Eur. J. Inorg. Chem.* **2001**, 2891-2898.

4. Weber, L.; Uthmann, S.; Stammler, H.; Neumann, B.; Schoeller, W. W.; Boese, R.; Blaser, D. *Eur. J. Inorg. Chem* **1999**, 2369-2381.

5. Fuchs, E. P. O.; Heydt, H.; Regitz, M.; Schoeller, W. W.; Busch, T. *Tetrahedron Lett.* **1989** , *30*(38), 5111-5114.

6. van der Knaap, Th. A.; Klebach, Th. C.; Visser, F.; Bickelhaupt, F.; Ros, P.; Baerends, E. J.; Stam, C. H.; Konijn, M. *Tetrahedron* **1984**, *40*(4), 765-776.

7. Becke, A. D. *J. Chem. Phys.* **1993**, *98*, 5648.

8. Ditchfiled, R.; Hehre, W. J.; Pople, J. A. *J. Chem. Phys.* **1971**, *54* , 724.

9. Hehre, W. J.; Ditchfield, R.; Pople, J. A. *J. Chem. Phys.* **1972**, *56* , 2257.

10. Hariharan, P. C.; Pople, J. A. *Mol. Phys.* **1974**, *27*, 209.

11. Gordon, M. S. *Chem. Phys. Lett.* **1980**, *76*, 163.

12. Hariharan, P. C.; Pople, J. A. *Theo. Chim. Acta.* **1973**, *28*, 213.

13. Frisch, M. J.; Trucks, G. W.; Schlegel, H. B.; Scuseria, G. E.; Robb, M. A.; Cheeseman, J. R.; Zakrzewski, V. G. Z.; Montgomery, Jr. J. A.; Stratmann, R. E.; Burant, J. C.; Dapprich, S.; Millam, J. M.; Daniels, A. D.; Kudin, K. N.; Strain, M. C.; Farkas, O.; Tomasi, J.; Barone, V.; Cossi, M.; Cammi, R.; Mennucci, B.; Pomelli, C.; Adamo, C.; Clifford, S.; Ochterski, J.; Petersson, G. A.; Ayala, P. Y.; Cui, Q.; Morokuma, K.; Malick, D. K.; Rabuck, A. D.; Raghavachari, K.; Foresman, J. B.; Cioslowski, J.; Ortiz, J. V.; Baboul, A. G.; Stefanov, B. B.; Liu, G.; Liashenko, A.; Piskorz, P.; Komaromi, I.; Gomperts, R.; Martin, R. L.; Fox, D. J.; Keith, T.; Al-Laham, M. A.; Peng, C. Y.; Nanayakkara, A.; Challacombe, M.; Gill, P. M. W.; Johnson, B.; Chen, W.; Wong, M. W.; Andres, J. L.; Gonzalez, C.; Head-Gordon, M.; Replogle, E. S.; Pople, J. A. *Gaussian 98, Revision A.9* Gaussian, Inc.: Pittsburgh, PA, 1998.

14. Appel, R. *Multiple Bonds and Low Coordination in Phosphorus Chemistry,* 1st ed.; Scherer, O. J.; Regitz, M., Editor; Thieme Medical Publishers, Inc.: New York, 1990.

15. Oakley, R. T. *Progress in Inorganic Chemistry* **1988**, *36*, 299-391.

Chapter 4

Synthesis of 2,6-diisopropylphenyl phosphane and its mono and disilylated derivatives

4.1 Introduction

The chemistry of primary phosphanes has received much attention in recent years. Their utility in both main group chemistry[1-8] and coordination chemistry[9-18] is under active investigation. The primary aryl phosphane, $PhPH_2$ **100**, was first reported in 1877 by Köhler[19] as a clear, pyrophoric, highly toxic liquid made by treating $PhPI_2 \cdot HI$ with ethanol. More recently, the use of bulky *ortho* substituted aryl groups has been particularly popular, imparting considerably greater stability to the phosphanes and more control over their reactions, while lowering their toxicity.[3,4,17] The synthesis of the sterically bulky Mes^*PH_2 **154** has been reported in Inorganic Syntheses.[20] The reaction from the parent hydrocarbon **155** can be performed on a large scale with relatively good yields (44% overall). First, 2,4,6-tri-tert-butyl-benzene **155** is treated with bromine in trimethyl phosphate. The purified aryl bromide **156** is treated with *n*-BuLi in THF, which is then added to a THF solution of PCl_3 to make the phosphonous dichloride **157**. Reduction with $LiAlH_4$ in diethyl ether and recrystalization from ^{i}PrOH produces the phosphine, Mes^*PH_2 **154**, as a white solid (Figure 4.1).

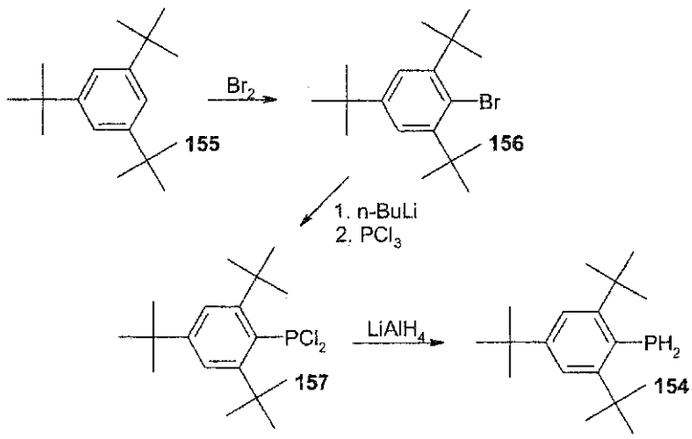

Figure 4.1 Synthetic route to Mes*PH$_2$ 154 via the parent hydrocarbon

The closely related 2,4,6-triisopropylphenylphosphane (TripPH$_2$, **158**) is known, and its chemistry has received some attention (24). While routes to phenyl phosphane **100** and 2,4,6-trisubstituted phenyl phosphanes are well known, there is only one published route to a 2,6-disubstituted phenyl phosphane.[21] 2,6-Di-*tert*-butylbromobenzene **159**[21] is available via the 2,4,6-trisubstituted phenyl bromide **156** (Figure 4.2), which can then be converted to the phosphane following the route outlined for converting Mes*Br **156** to Mes*PH$_2$ **154** (Figure 4.1). This method does not appear to be the optimum method to produce the 2,6-disubstituted derivatives as there are many steps and overall yields are quite low.

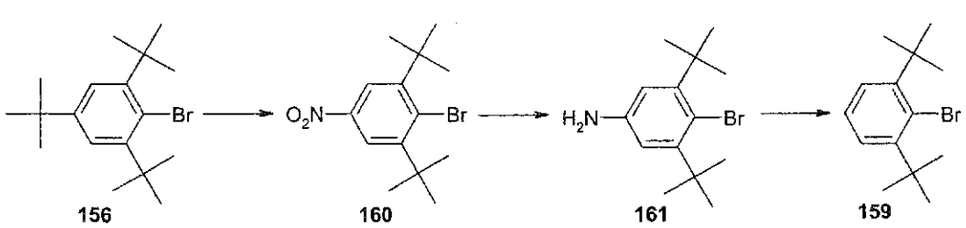

Figure 4.2 Three step process to make the 2,6-disubstituted aryl bromide 159 from the 2,4,6-trisubstituted aryl bromide 156

We have therefore worked out a large scale synthesis of 2,6-diisopropylphenyl phosphane (DipPH$_2$, **15**) for use in the synthesis of the phosphorus analogues to our bulky *N,N'*-amidines[22,23] and *N,N',N''*-guanidine.[24] We have also prepared a series of silyl compounds DipPHSi(CH$_3$)$_3$ **16** , DipPH(TBDMS) **17**, DipP{Si(CH$_3$)$_3$}$_2$ **18** and DipP(TBDMS)$_2$ **19** (Figure 4.3).

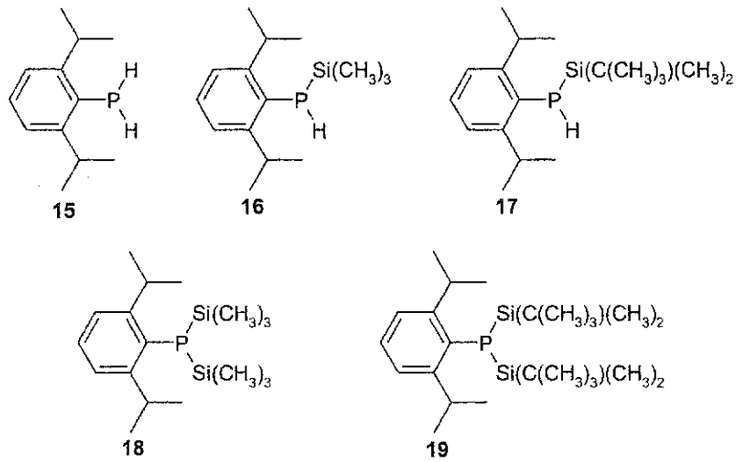

Figure 4.3 DipPH$_2$ and the silylated derivatives described in this work

4.2 2,6-Diisopropylphenylphosphane (DipPH$_2$) and its precursors

4.2.1 Synthesis and characterization of DipBr

To produce DipPH$_2$ **15**, the main challenge was to find an efficient synthesis of DipBr **13**, which we intended to convert to the phosphane **15** following the synthesis outlined for the more bulky Mes*PH$_2$ **154**. After reviewing the literature, a large-scale synthesis of DipBr **13** was found, utilizing the relatively affordable starting material DipNH$_2$ **12**.[25] The published procedure[25] was modified from the original published in 1960[26], and we in turn had to modify the procedure in order to properly purify the material. The procedure, known as the Gattermann reaction, is a modification of the Sandmeyer reaction, using

copper powder rather than copper halide as the catalyst to make the aryl bromide from the diazo compound (Figure 4.4).

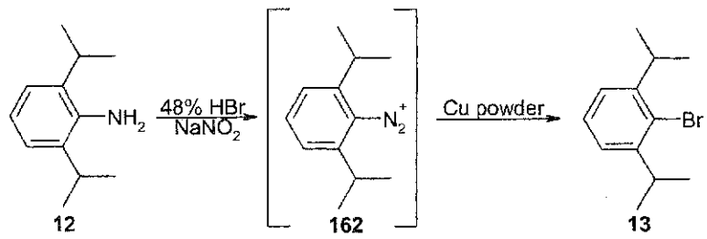

Figure 4.4 Synthesis of DipBr from $DipNH_2$ via Gattermann reaction

The first step involves producing the diazonium ion **162** in situ from the aniline **12**. This was accomplished by cooling a solution of $DipNH_2$ **12**, water and 48% hydrobromic acid between –10 and –15 °C in an ethanol bath. A solution of sodium nitrite in water was then added over a 75 min period. This reaction is highly exothermic and a bath temperature of between –40 and –25 °C was needed. If the internal temperature was allowed to warm above –5 °C, the reaction would foam excessively and overflow the flask. Initially a dry ice/ethanol bath was employed to cool the reaction vessel, but the temperature was hard to control and an excessive amount of dry ice was needed to cool such a large vessel. In later experiments, the ethanol bath was cooled and maintained at low temperature through the periodic addition of liquid nitrogen. After the sodium nitrite solution was completely added, copper powder was added and the contents were allowed to warm to room temperature. Refluxing and extraction with petroleum ether gave over 300 g of a dark oil. ^{1}H NMR showed the oil to be a mixture of DipBr **13** and DipOH **163** in essentially a 1:1 ratio. The literature preparation stated that the dark oil could be purified on a silica gel column, leaving the dark impurities behind and upon distillation, DipBr **13** was isolated in a 50% yield. The silica gel column purification step was

attempted, but the thick oil was extremely slow to pass through the gel due to the low porosity of our silica. Distillation was attempted to separate the two compounds, but after a closer investigation, it was found that the two compounds have similar boiling points (DipOH **163** = 75 °C/5 mm (Aldrich), DipBr **13** = 75-85 °C/5mm). Separation of the two compounds was accomplished by treating the impure DipBr/DipOH oil with an equal volume of saturated methanolic KOH. The resulting green solution was then extracted with hexanes and a dark oil was isolated, which was pure DipBr **13** by ^{1}H NMR. Distillation removed the dark impurities leaving a light yellow oil. If the methanol phase was acidified with concentrated HCl, extracted with hexanes and the extracts distilled, the DipOH **163** could be recovered, with a slight amount of DipBr **13** still present by ^{1}H NMR.

The ^{1}H NMR shows the characteristic peaks for a 2,6-diisopropylphenyl system. The four equivalent ^{i}Pr-C*H*$_3$ groups form a doublet located at 1.24 ppm and the two equivalent ^{i}Pr-C*H* protons form a septet located at 3.50 ppm. The aromatic signals from the protons on the phenyl ring come between 7.10 and 7.27 ppm for the bromide.

4.2.2 Synthesis and characterization of DipPXX, X= Cl_2, Br_2, ClBr

Following work on bulky phosphonous dichlorides by Yoshifuji[21] and Cowley[20], DipBr **13** was reacted with one equivalent of ^{n}BuLi at -78 °C in THF. Complete metallation was confirmed by taking a small aliquot of the Dip$^-$ Li$^+$ mixture, quenching it with wet ether, removing solvent and running a ^{1}H NMR to prove that the parent hydrocarbon had indeed been formed. This solution was then added via cannula to a solution of PCl_3 in THF at -78 °C. After stirring for 30 minutes, the solution was warmed

and volatile components were removed under vacuum, leaving a thick, yellow oil behind. Both ^{31}P and ^{1}H NMR showed a wide mixture of products, with very little $DipPCl_2$ (**44**, XX= Cl_2) present. Increasing the amount of PCl_3 from one to three equivalents did not increase the amount of $DipPCl_2$ (**44**, XX= Cl_2) produced.

Since the Li^+ route did not prove to be effective, we attempted to make the Grignard reagent, DipMgBr, from the bromide **13**. In the same work Schrock[25] published for the synthesis of DipBr **13**, the thiol (DipSH **164**) was produced by the reaction of the Grignard reagent with elemental sulfur in diethyl ether and quenching with water. In the published work, the bromide **13** was combined with Mg turnings and refluxed for several hours in diethyl ether. To speed up the reaction times, we used the higher boiling ether, THF. After 3 hours most of the magnesium had been consumed, and the reaction was cooled in an ice bath. A separate ice/salt bath (< –15 °C) was made to cool a flask containing three equivalents of PCl_3 in THF. The Grignard solution was added via a cannula, and the mixture was allowed to warm to room temperature and refluxed for 2 hours. Analysis of the crude material showed three major products, with very few impurities in the ^{1}H NMR. Only three species (other than PCl_3) were present in the ^{31}P NMR, suggesting the small impurities were not phosphorus containing. The three major products in the ^{1}H NMR had nearly identical chemical shifts, indicating that all three were most likely similar in composition. The three peaks at 151.9, 159.2 and 164.5 ppm ($CDCl_3$) in the ^{31}P NMR spectrum, were similar to the chemical shift found by Cowley[20] for Mes^*PCl_2 **157**, 155 ppm (THF). Distillation proved to remove the impurities to give a clear, viscous oil which consisted of the three phosphorus containing products.

Differences in ^{31}P NMR chemical shifts are thought to originate from a combination of both electronic and steric effects at the phosphorus atom. The trend in the ^{31}P NMR seen in our system is similar to systems such as P(III) alkyl dihalides, where the chemical shifts become more positive as you switch from bromine to chlorine: CH_3PBr_2 **165** (184 ppm), CH_3PClBr **166** (190 ppm) and CH_3PCl_2 **167** (191 ppm).[27] From this knowledge, we postulated that the three products were a mixture of $DipPCl_2$, DipPClBr and $DipPBr_2$ (Figure 4.5). High-resolution mass spectroscopy proved this to be true. With this information, we were able to determine, by carefully integrating the ^{31}P NMR peaks, that the products were present in a 1.6 ($DipPCl_2$) : 2.44 (DipPClBr) : 1.0 ($DipPBr_2$) ratio. This means that virtually all of the bromide contained in the Grignard reagent ends up on phosphorus, remarkable testimony to the higher nucleophilicity of bromide versus chloride. Mixed phosphonous dihalide systems that co-distill have been previously reported in the literature for $Mes_2P(Cl,Br)$ **168**[28] and $TripP(Cl,Br)_2$ **169**.[29]

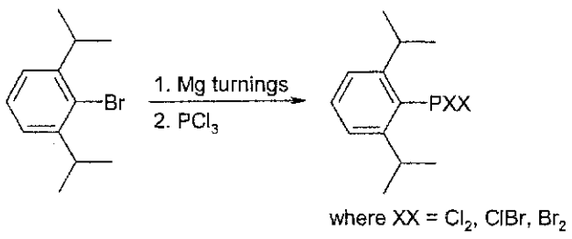

Figure 4.5 Synthesis of the mixed phosphonus dihalide system

To solve the mixed halide problem, we attempted the reaction using PBr_3 following the same procedure. After distillation, distillate from multiple fractions were analyzed by ^{31}P NMR and not only showed the signal corresponding to $DipPBr_2$, but a new signal which appeared at 201 ppm. To investigate the possible origins of this signal, PBr_3 and THF were combined in an NMR tube and ^{31}P NMR showed this mixture produced the same signal in the ^{31}P NMR. From this information we concluded the co-distillate to be a

$THF{\cdot}PBr_3$ adduct. To alleviate the problem of co-distillation between $DipPBr_2$ and the $PBr_3{\cdot}THF$ adduct, we attempted to use diethyl ether as our solvent. Even though Schrock[25] was able to produce the Grignard reagent in diethyl ether, we were unable to reproduce their results, even with prolonged refluxing (overnight), and initial activation of the magnesium turnings with 1,2-dibromoethane. It was decided that the mixed halide system was adequate for our purposes since we were able to work out an "effective molar mass" for the mixture by carefully integrating the peaks in the ^{31}P NMR.

The ^{1}H NMR of DipPXX **14** shows the characteristic peaks formed by the Dip group, but with three separate sets of signals slightly shifted from one another. Again this was caused by the mixed halide system. The $^{i}Pr\text{-}CH_3$ signals appear as three sets of doublets between 1.29-1.34 ppm, the $^{i}Pr\text{-}CH$ signals form three distinct, overlapping septets between 3.23-3.40 ppm and the aromatic signals occur between 7.21-7.44 ppm.

4.2.3 Synthesis and characterization of $DipPH_2$

The synthesis of the primary phosphane was straightforward, following the procedure used for $Mes^{*}PH_2$ **152**[20] with some modifications to the work-up. An ice-cold solution of DipPXX **14** in diethyl ether was added via a cannula to a suspension of lithium aluminum hydride in diethyl ether held at 0 °C (Figure 4.6). The rate of addition did not seem to have an effect on yield. After addition was complete, the mixture was refluxed for 2 hours and allowed to cool. To deactivate any remaining $LiAlH_4$, a hot ammonium chloride/water *paste* was slowly added to the reaction vessel. This is a very important step! Addition of the paste causes the decomposition products to clump, allowing the solvent to be easily removed from the solids. If a hot, *saturated solution* of NH_4Cl is

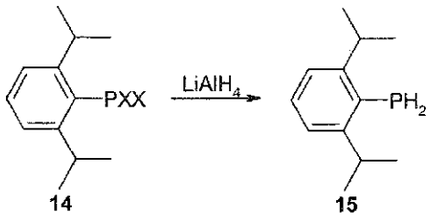

Figure 4.6 Reduction of phosphonus dihalide 14 to produce DipPH$_2$ 15

used, not only are the solids harder to filter off from the solvent, but there is excess H_2O present, making an extra separation step necessary to remove the water layer. Once all of the NH_4Cl paste was added, the precipitates were allowed to settle and then the solution was decanted to another flask under nitrogen. Distillation of the crude material gave a clear, colorless oil, with a distinct phosphane odor. When left open to the atmosphere, the phosphane slowly decomposes over several days to give a white solid.

The ^{1}H NMR shows the characteristic Dip peaks along with a doublet caused by the spin 1/2 ^{31}P coupling with the P-*H* protons. Primary phosphanes tend to have P-H coupling constants between 162 and 226 Hz,[27] and our coupling constant ($^1J_{PH}$ = 208 Hz) is similar to Mes*PH$_2$ **152** ($^1J_{PH}$ = 209 Hz).[20] The equivalent ^{i}Pr-C*H* protons produce the expected septet, but this is further split into a doublet of septets, most likely via a through-space coupling to phosphorus.

The ^{1}H-decoupled ^{31}P NMR shows a singlet at –156 ppm, which turns into a triplet ($^1J_{PH}$ = 208 Hz) in the ^{1}H-coupled spectrum, once again reflecting the P-H coupling. When the crude material is analyzed by ^{1}H-coupled ^{31}P NMR, there is another triplet (δ = -14.6 ppm, $^1J_{PH}$ = 477 Hz) located downfield from the phosphane signal. When the NMR tube is filled with $O_{2(g)}$ and shaken, this signal increases in intensity. When compared to the data for Mes*P(=O)H$_2$ **170** isolated by Yoshifuji (δ = -10.0 ppm, $^1J_{PH}$ = 490.7 Hz)[30],

we determined the signal to be due to the oxidized product $DipP(=O)H_2$ **171**. In the IR spectrum of $DipPH_2$ **15**, the peak located at 2306 cm^{-1} is within the range expected for the P-H stretch in primary phosphanes (ν(P-H) = 2300-2400cm^{-1}).[31]

4.3 Synthesis and characterization of silylated phosphanes

4.3.1 Introduction

A recent review by Fritz and Scheer describes the synthesis and reactions of silylphosphanes.[32] Silylated phosphanes have been used extensively in the synthesis of low coordinate phosphorus compounds,[33-34] including the synthesis of phosphaamidines[35,36] and phosphaguanidines[37-38].

The $-SiR_3$ group is thought of as a synthetic equivalent or 'synthon' to H (Figure 4.7). It often finds uses as a protective group to prevent functional groups such as alcohols from reacting during synthesis.[39] In condensation reactions where HCl is produced, the $-Si(CH_3)_3$ group is often used in place of the disassociating proton. Not only is $ClSi(CH_3)_3$ easily removed from the reaction mixture, but side products, such as HCl salts, are prevented from forming.

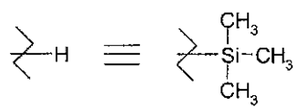

Figure 4.7 SiR_3 is often used as a 'synthon' to H

We initially isolated mono- and disubstituted-trimethylsilyl phosphanes. Repeated attempts to obtain completely pure samples, as monitored by ^1H NMR failed, always with minute amounts of other peaks appearing in the spectra, indicating that there were other $Si(CH_3)_3$ containing compounds present. We attempted to obtain clean high-resolution mass spectra from freshly purified samples of material, but were faced with the

contamination of our samples with phosphane oxides and other silylated derivatives (Figure 4.8). To produce more easily handled materials, the parent phosphane was silylated using the much more bulky *tert*-butyl-dimethylsilyl (TBDMS) group. As the steric bulk of the alkyl groups on silicon increases, the silyl group becomes increasingly inert to reaction conditions.[40] Here the bulky TBDMS group not only slows the rate of oxidation of the phosphane, but reduces the rate of hydrolysis. The effective steric bulk of trialkyl/arylsilyl groups has been outlined in a recent book by Brook[40]:

$Me_2SiH < \mathbf{Me_3Si} < PhMe_2Si < Ph_2MeSi < EtMe_2Si < Ph_3Si < (^{n}Bu)Me_2Si$
$< (^{i}Bu)Me_2Si < (^{n}Bu)Me_2Si < (^{n}Bu)_2MeSi < Et_3Si < (^{i}Pr)Me_2Si <$
$(Cy)Me_2Si < (^{i}Pr)_2MeSi < \mathbf{^{t}BuMe_2Si\ (TBDMS)} < (^{i}PrMe_2C)Me_2Si <$
$(^{i}Pr)_3Si < {}^{t}BuPh_2Si < (^{t}Bu)(^{i}Pr)EtSi < {}^{t}Bu_3Si < (Cy)_3Si$

With the bulkier TBDMS group, clean high-resolution mass spectra, elemental analysis and NMR spectra can be obtained for both the mono- **17** and disubstituted **19** TBDMS phosphanes. The molecular structure of monoTBDMS **17** was confirmed by X-ray crystallographic structure determination.

4.3.2 Preparation of trimethylsilyl phosphanes

4.3.2.1 Monosilylated trimethylsilyl derivative

Silylation of $DipPH_2$ **15** followed the procedure used by Cowley[20] for $Mes^{*}PHSi(CH_3)_3$ **172** and the procedure for $Mes^{*}PH(TBDMS)$ **173**, outlined by Yoshifuji.[34] The phosphine was cooled to 0 °C in THF, whereupon a slight excess of $^{n}BuLi$ was added to give a red solution. The solution was then warmed to room temperature to ensure complete lithiation, cooled again and $(CH_3)_3SiCl$ was added. After

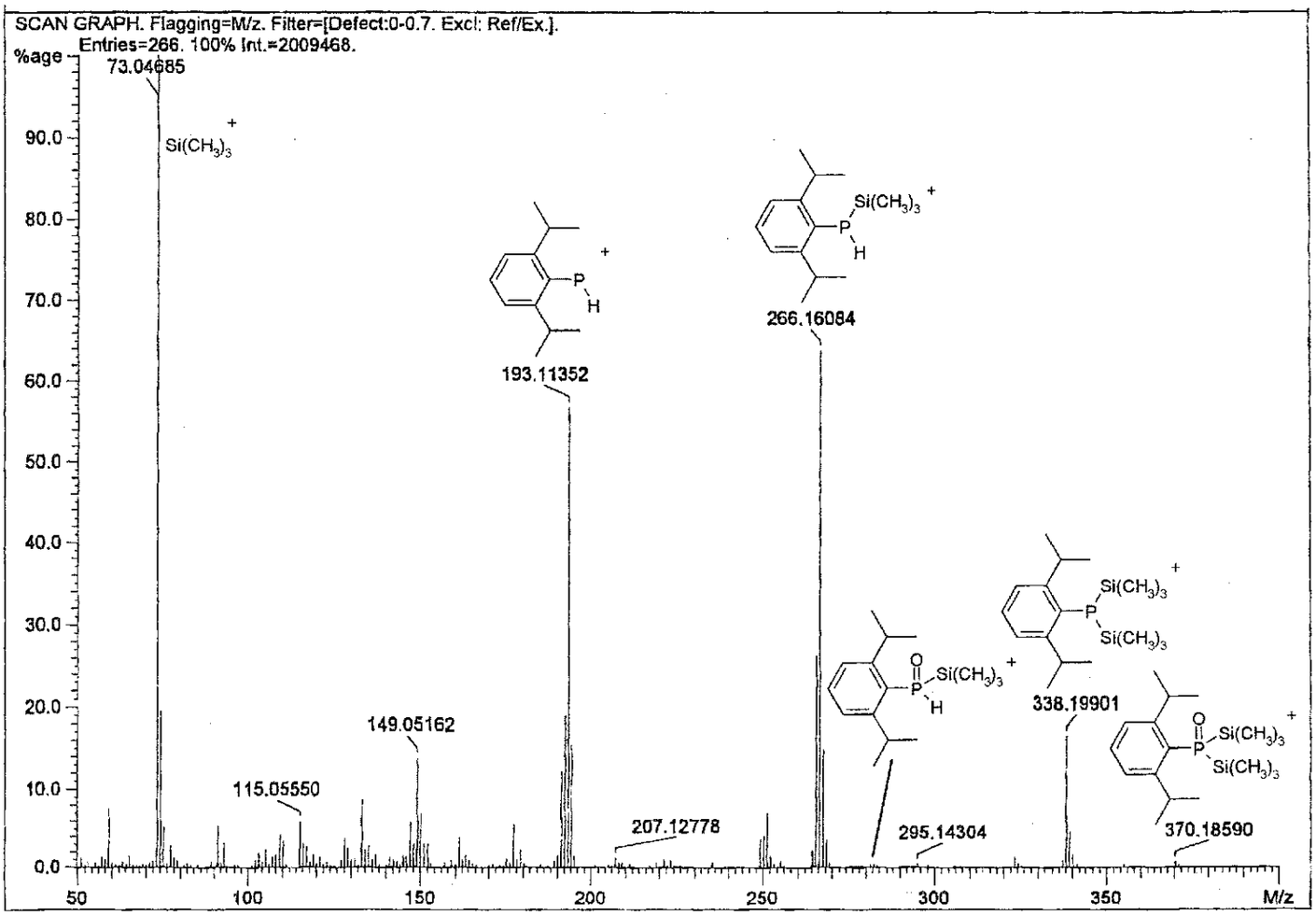

Figure 4.8 Mass spectrum obtained for DipPHSi(CH$_3$)$_3$ **16**. Notice the sample contains DipPSi(CH$_3$)$_3$ **18** and phosphine oxides.

refluxing, filtration, removal of volatile components and distillation, the mono-silylated phosphane **16** was isolated in good yield.

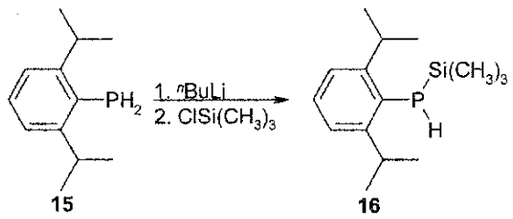

Figure 4.9 Silylation reaction to produce the monosilylated phosphine 16

Often it was found that complete silylation did not occur, therefore it was necessary to approximate the ratio of starting material to product via the ^{31}P NMR and add the appropriate amount of ^{n}BuLi and $ClSi(CH_3)_3$ again. Yoshifuji[34] found that in the case of $Mes^{*}PHSi(CH_3)_3$ **172**, isolation was not only difficult because it was unstable, but the mono-silylated derivative was hard to make due to excess ^{n}BuLi cleaving the $Si(CH_3)_3$ group from the phosphane. It is important to make sure none of the parent phosphane is present before beginning the workup. $DipPH_2$ **15** and $DipPHSi(CH_3)_3$ **16** proved difficult to separate, due to boiling points that are too close to allow proper separation via vacuum distillation in the 18 cm distillation column used.

The ^{1}H NMR spectrum is slightly different than that of $DipPH_2$ **15**. The $Si(CH)_3$ protons are coupled to phosphorus (^{3}J (H-P) 4.3 Hz) and occur at 0.18 ppm. The ^{i}Pr C-*H* signals are still coupled to phosphorus, but slightly shifted downfield from the parent phosphane. The P-*H* doublet is shifted 0.38 ppm upfield, to 3.46 ppm, but the coupling constant is similar to the parent phosphane, $^{1}J_{PH}$ = 211 Hz ($DipPHSi(CH_3)_3$ **16**) vs $^{1}J_{PH}$ = 208 Hz for $DipPH_2$ **15**. The proton coupled ^{31}P NMR shows the expected doublet for the

system, with a slight shift upfield from the parent phosphane. See Table 4.1 for complete spectral details.

4.3.2.2 Bis(trimethylsilyl) derivative

The synthesis of DipP{Si(CH$_3$)$_3$}$_2$ **17** consisted of reacting DipPH$_2$ **15** with one equivalent of ^{n}BuLi, quenching with (CH$_3$)$_3$SiCl, repeating the metallation and quenching step, checking the reaction progress by ^{31}P NMR and on some occasions, repeating the metallation and quenching step with the appropriate amount of material to fully silylate the phosphane. The problem of incomplete silylation due to Si-P bond cleavage[34] that plagues the monosilylated phosphine is more than likely the reason more than two ^{n}BuLi/ClSi(CH$_3$)$_3$ steps are needed.

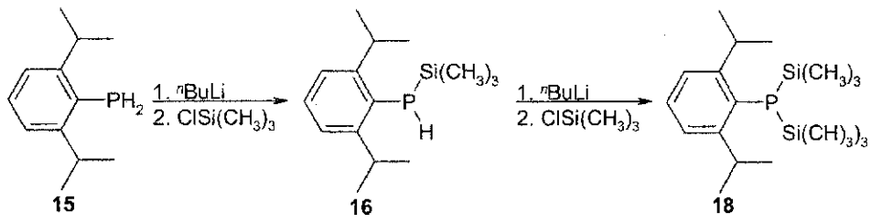

Figure 4.10 Silylation reaction to produce the disilylated phosphane

Purification was attempted by both vacuum distillation and sublimation under dynamic vacuum onto a cold finger. It was found by ^{1}H NMR that sublimed samples tended to have fewer impurities. The ^{1}H NMR shows a doublet from the phosphorus coupled Si*CH*$_3$ groups with a similar chemical shift to the monosilylated derivative **16**. The ^{i}Pr-C*H*$_3$ groups have become equivalent, forming one doublet and the P-*H* doublet has been lost due to full silylation of the phosphane. Interestingly the ^{i}Pr-C*H* groups have lost their coupling to phosphorus and have moved significantly downfield from both the

monosilylated derivative **16** and the parent phosphane **15**. The ^{1}H-coupled ^{31}P NMR spectrum shows only a singlet at –167.1 ppm, reinforcing the fact there are no protons directly connected to the phosphorus center. See Table 4.1 for complete spectral details.

The method outlined by Appel[41] in the reaction of $PhPCl_2$ **173** with four equivalents of lithium metal and two equivalents of $ClSi(CH_3)_3$ is a more straightforward method to the disilylated aryl derivative **121** (Figure 4.11). This reaction has been performed recently in our lab and does not seem to work for the Dip system. Reasons why the reaction does not work are not clear, but one possibility is due to incomplete lithiation of the phosphorus oligimer, or incomplete dilithiation of the phosphonous dichloride.

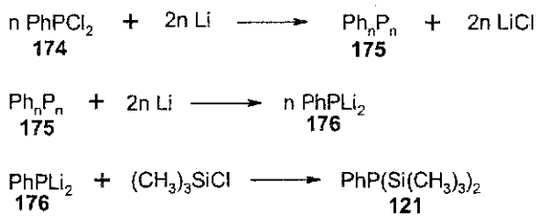

Figure 4.11 Alternative path to the disilylated phosphine

4.3.3 Preparation of TBDMS-silylated phosphanes

4.3.3.1 Monosilylated TBDMS derivative

The procedure used for the $Si(CH_3)_3$ **16** derivative was repeated for the TBDMS derivative **17**. The TBDMS derivative proved to be much easier to handle and purify than the TMS derivative. Purification was achieved by dynamic vacuum sublimation onto a cold finger, which provided much better separation from the parent phosphane **15** than in the $Si(CH_3)_3$ case.

The ^{1}H NMR is quite different from the mono-Si(CH_3)$_3$ derivative **16**. The two methyl groups bonded to the Si atom are diasterotopic, giving two phosphorus coupled doublets at 0.02 and 0.06 ppm, with significantly differing coupling constants, ^{2}J(P-H) = 0.9 Hz and ^{2}J(P-H) = 5.3 Hz, respectively. The ^{t}Bu peak is also coupled to phosphorus, ^{3}J(P-H) = 2.4 Hz, and is located at 1.01 ppm. There are two distinct ^{i}Pr-C*H*$_3$ doublets, resulting from the diastereotopic ^{i}Pr-CH$_3$ groups. The chemical shifts for both the ^{i}Pr-C*H* septet and the P-*H* doublet are essentially identical to the mono-Si(CH_3)$_3$ derivative **16**. When compared to Mes*PH(TBDMS) **173**[34], both the Si-^{t}Bu and *SiCH*$_3$ peaks in the ^{1}H NMR spectrum of **17** are much more shielded. In addition, the SiCH$_3$ groups of **173** appear as one doublet at –0.24 ppm (^{3}J(P-H) = 8.8 Hz) whereas there is a separate signal from each of the diastereotopic Si*CH*$_3$ groups in **17**. See Table 4.1 for full spectral details.

4.3.3.2 Bis-TBDMS derivative

The bis-TBDMS derivative **19** was produced in the same manner as the bis-Si(CH_3)$_3$ derivative **18**. Purification was achieved through sublimation under dynamic vacuum onto a cold finger, with good yields. The ^{1}H NMR spectrum is significantly different from the monosilylated TBDMS derivative **17**, and more similar to the bis-Si(CH_3)$_3$ derivative **18**. The Si*CH*$_3$ protons form a phosphorus-coupled doublet at 0.18 ppm, the same chemical shift as found in the monosilylated Si(CH_3)$_3$ compound **16**. The ^{t}Bu signals are slightly more shielded than in the case of monosilylated TBDMS **17**. The ^{i}Pr-C*H* protons do not couple to phosphorus, similar to the bis-Si(CH_3)$_3$ **18** case, and are shifted even further downfield to 4.29 ppm, nearly 1 ppm downfield from the parent phosphane **15**! See Table 4.1 for complete spectral details.

4.4 Discussion of NMR data

^{1}H NMR data of the phosphane and all four silyl phosphanes have been compiled in Table 4.1. TripPHCH$_3$ **177** and TripPHSiPh$_3$ **178** have also been included to substantiate the assignment and interpretation of our results. The former is of course a secondary phosphane, and hence has a ^{31}P chemical shift that is not comparable to ours. However, there is remarkable agreement between both ^{1}H and ^{13}C parameters of the *ortho* ^{i}Pr groups and of the aromatic ring, for which all the carbon nuclei *except* C_4 (see definition on Table 4.1) are coupled to phosphorus between TripPHCH$_3$ **177** and the more symmetrical of our phosphanes, DipP{Si(CH$_3$)$_3$}$_2$ **18** and DipP(TBDMS)$_2$ **19**. We also find that the silyl methyl and even the ^{t}Bu groups show evidence of coupling to the phosphorus nucleus.

The NMR data show effects that are related to the extent of silylation and to the steric bulkiness of the silyl group. For example, in the ^{1}H NMR spectrum of the parent phosphane, the ^{i}Pr-C*H* signal is located at 3.37 ppm. The signal moves downfield 0.04 ppm in the case of the monosilylated Si(CH$_3$)$_3$ derivative **16** and 0.06 ppm in the case of the monosilylated TBDMS derivative **17**. Where the shift is really apparent is in the disilylated compounds. The bis-Si(CH$_3$)$_3$ **18** septet comes at 4.05 ppm, 0.68 ppm from the parent phosphane **15**, while the bis-TBDMS **19** septet is shifted 0.92 ppm. The ^{31}P NMR shows the opposite trend, in nearly the same order. With silylation the ^{31}P signal moved upfield, from –154 ppm in the parent phosphane, DipPH$_2$ **15**, to –193 ppm in the bulkiest bis-TBDMS **19** derivative.

Table 4.1 Solution NMR data for 15 – 19 as measured in $CDCl_3$ at RT [a]

Compound		**15**	**16**	**17** [b]	**18**	**19** [c]	**177** [d]	**178** [e]
CH_3 (A)	δ (^{1}H)	1.25	1.21	1.21	1.18	1.21	1.2	0.98
	$^3J_{HH}$, Hz	6.7	6.7	6.9	6.9	6.7	6.8	[f]
CH_3 (B)	δ (^{1}H)	= (A)	1.26	1.26	= (A)	= (A)	= (A)	1.09
	$^3J_{HH}$, Hz		6.7	6.7				[f]
CH	δ (^{1}H)	3.36	3.41	3.43	4.06	4.29	3.8	3.52
	$^3J_{HH}$, Hz	6.8	6.7	6.8	6.6	6.7	6.8	[f]
	$^4J_{PH}$, Hz	3.0	3.8	4.0	6.6	6.7	4.8	[f]
PH	δ (^{1}H)	3.84	3.46	3.51			5.6 [g]	4.44
	$^1J_{PH}$, Hz	207.2	210.7	211.0			216.6 [g]	211
$SiCH_3$ (C)	δ (^{1}H)		0.18	0.06	0.22	0.18		
	$^3J_{HH}$, Hz		4.3	5.3	6.1	4.3		
$SiCH_3$ (D)	δ (^{1}H)		= (C)	0.02	= (C)	= (C)		
	$^3J_{HH}$, Hz			0.9				
Si^{t}Bu	δ (^{1}H)			1.01		0.91		
	$^3J_{PH}$, Hz			2.4		0.8		
H–C_4	δ (^{1}H)	7.35-7.25	7.35-7.19	7.26-7.17	7.35-7.23	7.28-7.21		
H–C_3	δ (^{1}H)	7.22-7.10	7.17-7.08	7.12-7.08	7.20-7.07	7.12-7.08		
CH_3 (A)	δ (^{13}C)	23.84	23.97	24.00	25.32	25.67	24.9 s	[f]
CH_3 (B)	δ (^{13}C)		24.18	24.16				[f]
CH	δ (^{13}C)	33.15	33.50	33.53	33.98	33.96	32.7	[f]
	$^3J_{PC}$, Hz	11.7	13.7	13.7	16.1	16.1	14.4	[f]
$SiCH_3$ (C)	δ (^{13}C)		0.67	–4.20	2.55	–1.54		
	$^2J_{CH}$, Hz		10.3	15.6	17.0	7.8		
$SiCH_3$ (D)	δ (^{13}C)			–2.93 s		= (C)		
C_1	δ (^{13}C)	126.04	129.21	129.04	128.29	130.44	130.4	[f]
	$^1J_{PC}$, Hz	13.7	20.5	21.5	14.2	9.3	15.7	[f]
C_2	δ (^{13}C)	152.08	152.03	152.47	156.44	156.57	153.0	[f]
	$^2J_{PC}$, Hz	9.8	9.3	9.3	10.7	11.2	11.1	[f]
C_3	δ (^{13}C)	122.91	122.94	122.97	123.43	128.92	121.6	[f]
	$^3J_{PC}$, Hz	2.4	3.4	3.4	5.4	5.4	3.4	[f]
C_4	δ (^{13}C)	128.53 s	127.44 s	127.52	128.55	128.59	149.7	[f]
	$^4J_{PC}$, Hz				2.0	1.95		[f]
P	δ (^{31}P)	–156.4	–163.8	–175.6	–167.1	–192.9	–113.2	–169
	$^1J_{HP}$, Hz	207.5	210.6	212.1			214.1	211

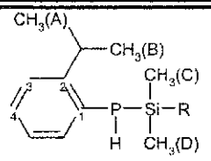

[a] Numbering/Labelling scheme used:

[b] ^{t}Bu signals: ^{1}H 1.01 (d, $^4J_{PH}$ 2.4 Hz, 9H); ^{13}C 27.02 (d, ^{4}J(P-C) 2.9 Hz, C(CH_3)$_3$), 18.70 (d, $^2J_{PC}$ 9.8 Hz, C(CH_3)$_3$)

[c] ^{t}Bu signals: ^{1}H: 25.67 (s, C(CH_3)$_3$); ^{13}C: 27.79 (d, $^4J_{PC}$ 3.9 Hz, C(CH_3)$_3$), 20.18 (d, $^2J_{PC}$ 20.5 Hz, C(CH_3)$_3$)

[d] Measured in C_6D_6 solution at room temperature

[e] Measured in C_6D_6 solution at room temperature

[f] No data provided for this parameter

[g] Data taken for the closely related TripPHPh

4.5 Variable temperature ^{1}H NMR on DipPH(TBDMS)

The asymmetrically substituted phosphanes DipPHSi$(CH_3)_3$ **16** and DipPH(TBDMS) **17** show two distinct ^{i}Pr methyl environments in the room temperature ^{1}H NMR spectrum, but only a *single* resonance from the homotopic ^{i}Pr-C*H* groups. Additionally, DipPH(TBDMS) **17** also displays two distinct silyl methyl peaks, which have *different* degrees of coupling to ^{31}P, i.e. 5.3 and 0.9 Hz. Similar effects are reported in the literature for the *ortho* isopropyl groups of TripPHSiPh$_3$ **178**.[42] The crystal structure of the closely related Mes*PHSiPh$_3$ **179** has been determined, and its ^{1}H NMR spectrum also shows the presence of two distinct *ortho* ^{t}Bu environments, but only below –15°C. In order to probe what is going on in our system, we have conducted a variable temperature NMR study of DipPH(TBDMS) **17** in $C_6D_5CD_3$ solution over the temperature range –95°C to +107°C. We have not done this with DipPHSi$(CH_3)_3$ **16** because of greater difficulty in handling and the lack of completely pure samples. In addition, DipPH(TBDMS) **17** has diastereotopic methyl groups on silicon which are direct probes for the chirality induced by the asymmetric phosphorus atom in the absence of fast pyramidal inversion.

The basic spectral features of the dynamic NMR sample, which was made up in $CD_3C_6D_5$, are very similar to the room temperature spectrum in deuterochloroform as reported in Table 4.1. Figure 4.12 presents several traces selected from the full VT series of spectra which illustrate the key spectral changes. We distinguish three kinetic regimes. At the lowest temperature (processes which are not complete at the lower temperature limit permitted by our solution) there are two distinct isopropyl C-*H* environments

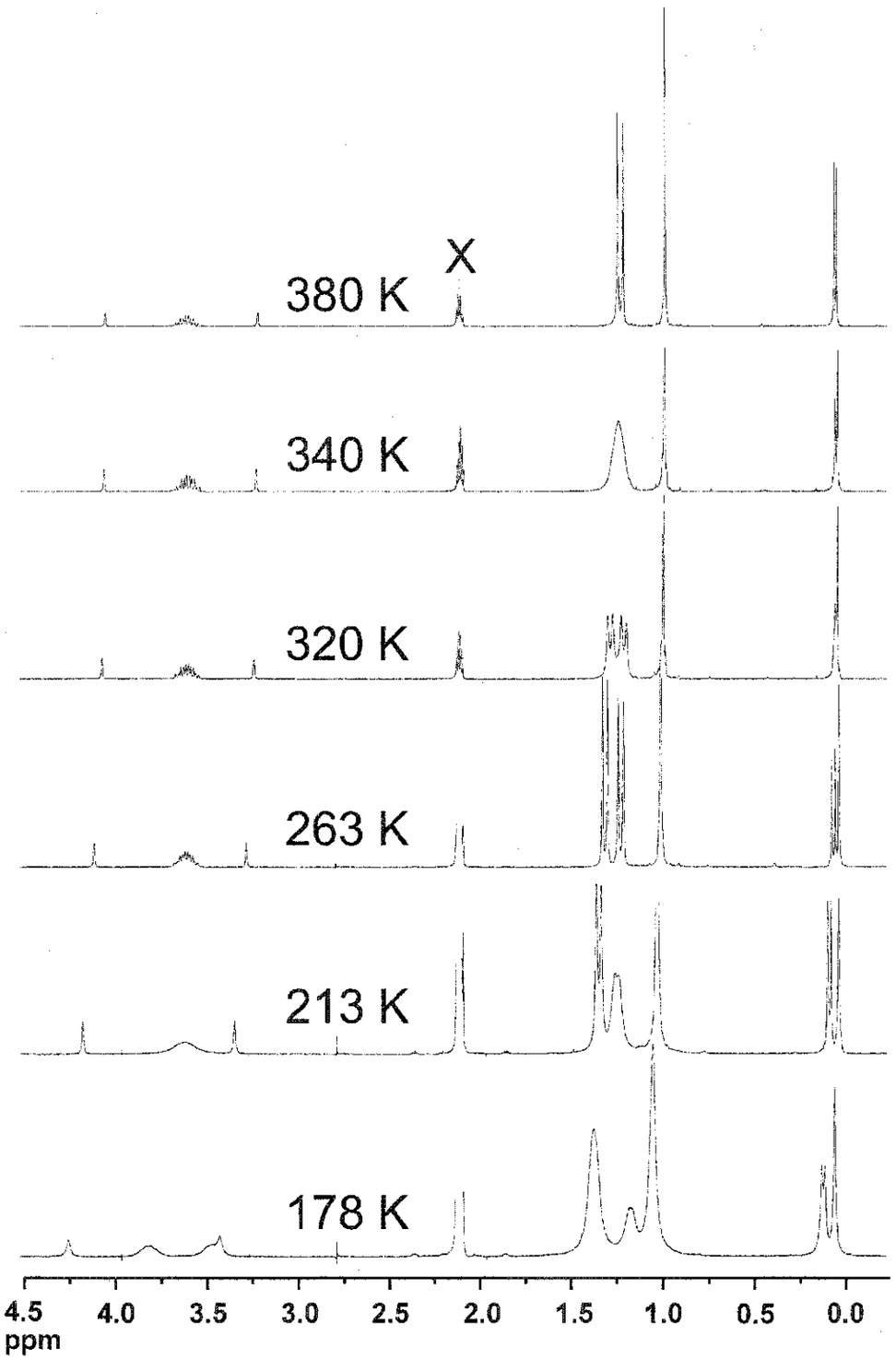

Figure 4.12 Selected traces from VT work on DipPH(TBDMS) 17

($H^{(1,2)}$), and two different isopropyl methyl groups ($CH_3^{(A-D)}$), as well as the two distinct silyl methyl groups ($CH_3^{(E,F)}$) (Figure 4.13).

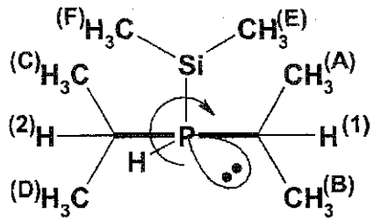

Figure 4.13 Assignment of relevant protons for VT study of DipPH(TBDMS) 17

It is possible to obtain a rough estimate of barrier heights for chemical exchange from variable temperature NMR data.[43] The procedure involves measuring (a) the coalescence temperature T_c and (b) the frequency of separation at the slow exchange limit $\delta\nu$. Using $\delta\nu$, a rate constant k for the exchange process can be determined using Equation (A):

$$k = \frac{\pi\delta\nu}{\sqrt{2}} \qquad \text{Equation (A)}$$

Eyring analysis provides $\Delta G^{\ddagger}$ at temperature T_c using Equation (B):

$$\Delta G^{\ddagger}\ (\text{kJ mol}^{-1}) = 1.194*10^{-2}\, T_c[10.319 + \log(T_c/k)] \qquad \text{Equation (B)}$$

In the case of intramolecular conformational changes, the entropy term, ΔS, is generally negligible, thus the $\Delta G^{\ddagger}$ value provides an estimate of the barrier height for interconversion.

Coalescence of the isopropyl C-*H* signals occurs at –50°C with $\Delta G^{\ddagger} \sim 40$ kJ mol^{-1} and produces the second regime in which $H^{(1)}$ and $H^{(2)}$ are equivalent, and there are two distinct ^{i}Pr methyl environments. In both these regimes and through the coalescence process, the P-*H* signals remain sharp, although they do shift significantly upfield with increasing temperature, and there is no obvious change in the silyl methyl signals

$CH_3^{(E,F)}$. The second coalescence occurs at +63°C and serves to exchange *all* ^{i}Pr methyl groups among themselves and the silyl methyl groups together. The activation energy for this process was measured as ~ 72 kJ mol^{-1} from the isopropyl methyl signals; the changes in the silyl methyl peaks are more complex insofar as they involve exchange between two signals with different coupling constants to phosphorus (5.0 and 0.8 Hz). In the third regime, the fast exchange limit, these in fact average to a single sharp doublet with 3.1 Hz apparent coupling.

Consideration of the symmetry of the system suggests that the lower two regimes can only be averaged by rapid rotation about the aromatic ^{ipso}C–P bond (indicated by circular arrow in Figure 4.13). Such rotation has the effect of mapping the inequivalent methine $H^{(1)}$ on $H^{(2)}$, the $CH_3^{(A)}$ on $CH_3^{(D)}$, and $CH_3^{(B)}$ on $CH_3^{(C)}$. This leaves two symmetry inequivalent sets of methyl groups $CH_3^{(A,D)}$ and $CH_3^{(B,C)}$, as well as $CH_3^{(E,F)}$, consistent with the spectral properties of the room temperature regime. Above room temperature the remaining symmetry inequivalent atoms are averaged by rapid pyramidal inversion at phosphorus. These conclusions were anticipated in a dynamic NMR study reported for TripPHSiPh$_3$ **178**[42], and there is remarkable agreement in the barrier heights measured by these workers (39 and 71 kJ mol^{-1}) and the work reported here. However, in TripPHSiPh$_3$ **178** there are no independent probes of asymmetry at phosphorus as provided by the silyl methyl groups of DipPH(TBDMS) **17**. Thus, it was not possible to prove that the second barrier was in fact that of phosphorus inversion, although this was the favoured hypothesis.[42]

4.6 Crystal structure of tertbutyldimethylsilyl (TBDMS) derivative

X-ray quality crystals were obtained via slow sublimation under dynamic vacuum using a three-zone furnace. The crystals were collected in the glovebox, and sent away to the X-Ray Crystallography Laboratory at the University of Edmonton for collection of intensity data. The structure was solved by direct methods using SHELXS[44], and refined using SHELXL[45] by standard full-matrix least squares methods. Hydrogen atoms were fixed on the aromatic rings so that the coordinates ride on the corresponding aromatic carbon coordinates. ^{i}Pr C-H hydrogen atoms were fixed for idealized tertiary C-H's with all X-C-H angles equal and using a riding model refinement. ^{i}Pr methyl groups were fixed with ideal tetrahedral angles with the C-H distances allowed to vary while allowing the CH_3 group to rotate. The hydrogen on phosphorus was allowed to freely refine. Temperature factors were set to 1.5 (CH_3 groups), 1.2 (CH groups) or 1.2 (Ar-H) times the equivalent isotropic temperature factor of the corresponding carbon atoms. The molecule crystallized in the monoclinic space group P2(1)/c, with four molecules per unit cell. Agreement factors of $R_1 = 0.0518$, $wR_2 = 0.0918$ were found. An ORTEP diagram is shown in Figure 4.14. Crystal data and structure refinement parameters are included in the appendix as Table A.1, as are the crystallographic data (Tables A.2-A.5).

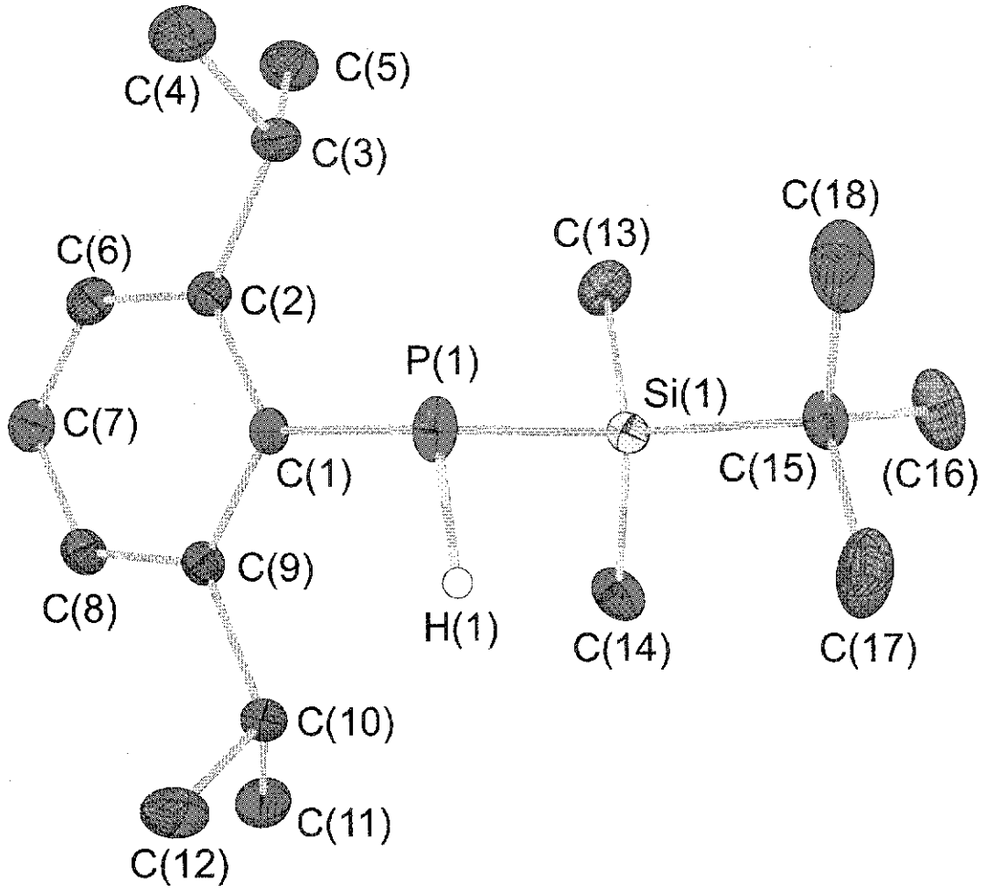

Figure 4.14 An ORTEP diagram (25% probability) of the crystal structure found for DipPH(TBDMS) 17 with atom numbering scheme. Hydrogen atoms on carbon are omitted for clarity.

The crystal structure of DipPH(TBDMS) **17** was determined at –80 °C to minimize the effect of alkyl group thermal motion on the accuracy of the structure. Analysis of the packing diagram shows no evidence of intermolecular contacts other than normal van der Waals' interactions. Noticeable is the essential co-planarity of C(7), C(1), P(1), Si(1), C(15) and C(16). The RMS deviation of these atoms from a least squares plane is 0.05 Å, with Si(1) deviating most. Along the ^{t}Bu–Si–P–aryl vector, the structure adopted is that of the lowest energy staggered conformation about each single bond. This molecular

plane is almost exactly orthogonal to that of the aryl ring (86.38(7)°), with the result that the TBDMS group is located entirely on one side of the aryl ring (Figure 4.15). The two *ortho* ^{i}Pr groups are oriented in the "Vee-back" conformation that we have observed in all solid-state structures determined for Dip groups.[22,23,24] However, these groups are significantly tilted such that C(5) and C(11) avoid contact with the TBDMS group. In the $N\{Si(CH_3)_3\}_2$ substituted Dip group found in the structure of $Cl_3SeC_6H_2{}^{i}Pr_2N\{Si(CH_3)_3\}_2$ **180**, where the symmetrical disilylamino group is co-planar with the aryl ring, such a tilt is not observed.[46] Another noticeable feature of the structure is the large deviation of the phosphorus (0.318(4) Å) and the *ipso* carbon, C(1) (0.038(3) Å) atoms from the mean aryl plane defined by the remaining five carbon atoms. See Figure 4.16 for a graphical view of this deviation. Such a deviation for the phosphorus atom has been observed previously in other "secondary" and "tertiary" phosphane structures with bulky *ortho* groups: $Mes^*P\{Si(CH_3)_3\}_2$ **181**, 0.85 Å[47], $Mes^*P\{OCH_2\}_2$ **182**, 0.82 Å[47] and TripPHPh **183**, 0.48 Å.[48] However, both the structures with *ortho* ^{i}Pr groups have the P atom displaced on the side *opposite* to that of the "R" substituent, while the Mes^*PR_2 structures have the phosphorus pushed out on the *same* side of the ring as the "axial" substituent.

The sum of angles around phosphorus is only 302(2)°, indicative of a highly pyramidal structure at phosphorus. This is commonly observed for secondary phosphanes even with bulky Trip or Mes* substituents (TripPHPh **183**, 304°[48], $Mes^*PHSiPh_3$ **179** 303.9°[42]), values that are statistically indistinguishable from our results. In contrast, when two silyl groups are attached as in $Mes^*P\{Si(CH_3)_3\}_2$ **181**, the sum of angles is greatly increased to 343.2°.[47] There is no known X-ray crystal structure

of a disilylated phosphane where the *ortho* groups are isopropyl. Thus it would be very interesting to have a structure of DipP(TBDMS)$_2$ **19**; to date we have been unable to grow suitable data crystals for this compound.

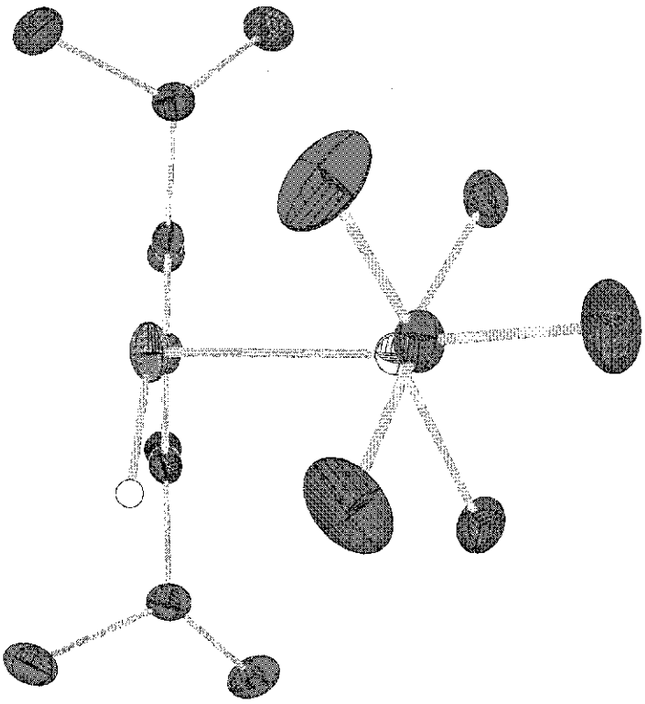

Figure 4.15 ORTEP diagram showing the twist of the phosphorus atom causing the P-Si-^{t}Bu plane to be nearly perpendicular to the aryl ring plane, thus minimizing the interaction between the ^{i}Pr groups and the silyl group. C-H hydrogen atoms omitted for clarity.

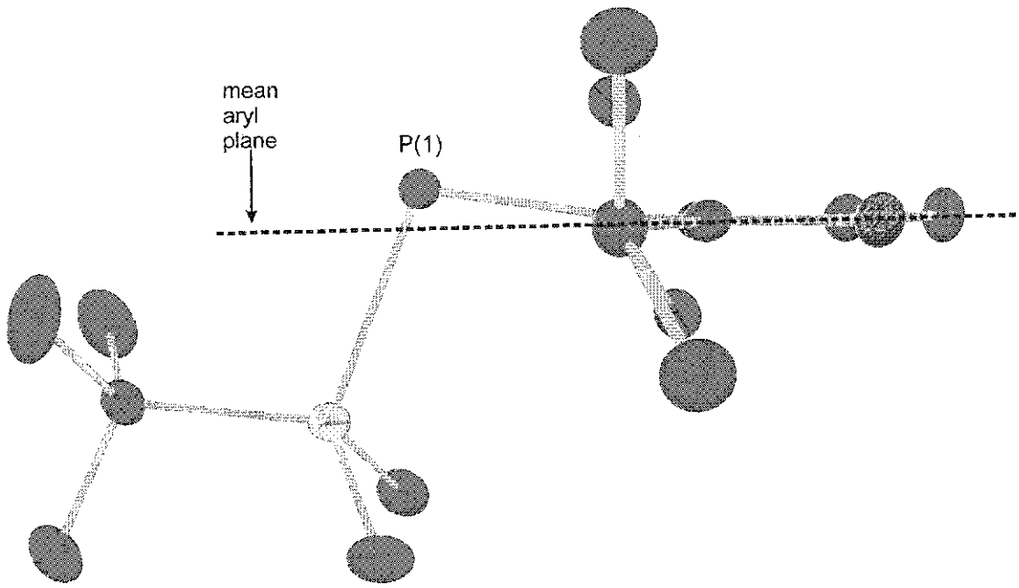

Figure 4.16 ORTEP diagram showing how the phosphorus atom is pushed out-of-plane from the aryl ring, minimizing the interactions between the bulky silyl group and the ortho ^{i}Pr-groups. Hydrogen atoms on carbon are omitted for clarity.

4.7 Synthetically useful bulky silyl phosphanes in the literature

Our investigation of compounds **15-19** has thus been thorough and systematic. This is in stark contrast to the existing literature. Work on the bulky silyl derivatives of Mes^*PH_2 **154** is scattered throughout the literature, often with incomplete work being reported. The Mes*PH(TBDMS) **173** is reported to be an oil[34], thus no crystal structure has been reported, while the disilylated TBDMS derivative has never been reported. The $Mes^*PHSi(CH_3)_3$ **172** is reported to solidify at 0°C and the crystal structure has never been reported, possibly due to the instability of the monosilylated version.[34] As mentioned above, the crystal structure of $Mes^*P\{Si(CH_3)_3\}_2$ **181** has been reported[47], but surprisingly, a full preparation and purification of $Mes^*P\{Si(CH_3)_3\}_2$ **181** has never been reported in a peer-reviewed journal. Cowley's paper[47] on the crystal structure of

Mes*P{Si(CH_3)$_3$}$_2$ **181** does not give details of how the crystals were grown, and only gives two references to Mes*P{Si(CH_3)$_3$}$_2$ **181**. The first is to the preparation of Mes*P=C=O **53** [49], where Mes*P{Si(CH_3)$_3$}$_2$ **181** is only mentioned as a precursor with no references. The second is to a Ph.D. dissertation from Universität Bonn, West Germany[50], which is not easily accessible to the general scientific community. Yoshifuji gives the preparation of Mes*P{Si(CH_3)$_3$}$_2$ **181**, but uses the crude material without further purification.[51] These few examples demonstrate the importance of our work with silyl phosphanes, providing a complete body of work for reference.

4.8 Conclusion

The synthesis of the new compounds, DipPXX **14**, DipPH_2 **15** and some silylated derivatives have been reported. The information presented will fill in many of the gaps present in the published literature on bulky aryl silyl phosphanes and provides a new phosphane that can be used in cases where the more sterically bulky Mes* derivative may not necessarily be desired.

Reference List

1. Berrigan, R. A.; Russell, D. K.; Henderson, W.; Leach, M. T.; Nicholson, B. K.; Woodward, G.; Harris, C. *New. J. Chem.* **2001**, *25*, 322.

2. Frenzel, C.; Somoza, F.; Blaurock, S.; Hey-Hawkins, E. *J. Chem. Soc., Dalton Trans.* **2001**, 3115.

3. Toyota, K.; Matsushita, Y.; Shinohara, N.; Yoshifuji, M. *Heteroatom Chem.* **2001**, 418.

4. Twamley, B.; Hwang, C.-S.; Hardmann, N. J.; Power, P. P. *J. Organomet. Chem.* **2000**, *152*, 609.

5. Dorn, H.; Sinch, R. A.; Massey, J. A.; Nelson, J. M.; Jaska, C. A.; Lough, A. J.; Manners, I. *J. Am. Chem. Soc.* **2000**, *122*, 6669.

6. Driess, M.; Kuntz, S.; Monse, C.; Merz, K. *Eur. J. Chem.* **2000**, *6*, 4343.

7. Rabe, G. W.; Heise, H.; Liable-Sands, L. M.; Guzei, I. A.; Rheingold, A. L. *J. Chem. Soc., Dalton Trans.* **2000**, 1863.

8. Rabe, G. W.; Kheradmandan, S.; Yap, G. P. A. *Inorg. Chem.* **1998**, *37* , 6541.

9. Goodwin, N. J.; Henderson, W.; Nicholson, B. K.; Fawcett, J.; Russell, D. R. *J. Chem. Soc., Dalton Trans.* **1999**, 1785.

10. Pope, S. J. A.; Reid, J. *J. Chem. Soc., Dalton Trans.* **1999**, 1615.

11. Scheper, J. T.; Jayaratne, K. C.; Liable-Sands, L. M.; Yap, G. P. A.; Rheingold, A. L.; Winter, C. H. *Inorg. Chem.* **1999**, *38*, 4354.

12. Campbell, T.; Gibson, A. M.; Hart, R.; Orchard, S. D.; Pope, S. J. A.; Reid, G. *J. Organomet. Chem.* **1999**, *592*, 296.

13. Darensbourg, D. J.; Draper, J. D.; Frost, B. J.; Reibenspies, J. H. *Inorg. Chem.* **1999**, *38*, 4705.

14. Malisch, W.; Thirase, K.; Rehmann, F. J.; Reising, J.; Gunzelmann, N. *Eur. J. Inorg. Chem.* **1998**, 1589.

15. Hadi, G. A. A.; Fromm, K.; Blaurock, S.; Jelonek, S.; Hey-Hawkins, E. *Polyhedron* **1997**, *16*, 721.

16. Felsberg, R.; Blaurock, S.; Jelonek, S.; Gelbrich, T.; Kirmse, R.; Voigt, A.; Hey-Hawkins, E. *Chem. Ber.* **1997**, *130*, 807.

17. Kourkine, I. V.; Maslennikov, S. V.; Ditchfield, R.; Glueck, D. S.; Yap, G. P. A.; Liable-Sands, L. M.; Rheingold, A. L. *Inorg. Chem.* **1996**, *35*, 6708.

18. Ho, J.; Breen, T. L.; Ozarowski, A.; Stephan, D. W. *Inorg. Chem.* **1994**, *33*, 865.

19. Köhler, H.; Michaelis, A. *Ber.* **1877**, *10*, 807-814.

20. Cowley, A. H.; Norman, N. C.; Pakulski, M. *Inorg. Synth.* **1990**, *27* , 235-240.

21. Yoshifuji, M.; Niitsu, T.; Shiomi, D.; Inamoto, N. *Tetrahedron Lett.* **1989**, *30*(40), 5433-5436.

22. Boeré, R. T.; Klassen, V.; Wolmershauser, G. *J. Chem. Soc., Dalton Trans.* **1998**, 4147-4154.

23. Boeré, R. T.; Klassen, V.; Wolmershauser, G. *Can. J. Chem.* **2000**, *78*, 583-589.

24. Boeré, R. E.; Boeré, R. T.; Masuda, J.; Wolmershauser, G. *Can. J. Chem.* **2000**, *78*, 1613-1619.

25. Schrock, R. R.; Wesolek, M.; Liu, A. H.; Wallace, K. C.; Dewan, J. C. *Inorg. Chem.* **1988**, *27*, 2050-2054.

26. Van Zanten, B.; Nauta, W. T. *Recl. Trav. Chim. Pays-Bas* **1960**, *79*, 1211-1222.

27. Crutchfield, M. M.; Dungan, C. H.; Letcher, J. H.; Mark, V.; Van Wazer, J. R. P^{31} *Nuclear Magnetic Resonance*; Interscience Publishers: New York, 1967.

28. Lambert, J. B.; So, J.-H. *J. Org. Chem.* **1991**, *56*, 5960.

29. Komen, C. D. M.; Kanter, d. J. J.; Goede, S. J.; Bickelhaupt, F. *J. Chem. Soc., Perkin Trans. 2* **1993**, 807-812.

30. Yoshifuji, M.; Shibayama, K.; Toyota, K.; Inamoto, N. *Tetrahedron Lett.* **1983**, *24*(39), 4227-4228.

31. Silverstein, R. M.; Webster, F. X. *Spectrometric Identification of Ogranic Compounds;* 6th ed. John Wiley & Sons, Inc.: Toronto, 1998.

32. Fritz, G.; Scheer, P. *Chem. Rev.* **2000**, *100*, 3341-3401.

33. Yoshifuji, M.; Toyota, K.; Inamoto, N. *J. Chem. Soc., Chem. Commun.* **1984**, 689-690.

34. Yoshifuji, M.; Toyota, K.; Shibayama, K.; Inamoto, N. *Chemistry Letters* **1983**, 1653-1656.

35. Issleib, K.; Schmidt, H.; Meyer H. *J. Organomet. Chem.* **1978**, *160*, 47-57.

36. Markovski, L. N.; Romanenko, V. D.; Pidvarko *Zh. Obshch. Khim.* **1982**, *52*(8), 1925-1926.

37. Issleib, K.; Schmidt, H.; Meyer H. *J. Organomet. Chem.* **1980**, *192*, 33-39.

38. Appel, R.; Knoch, F.; Laubach, B.; Sievers, R. *Chem. Ber.* **1983**, *116*, 1873-1879.

39. Colvin, E. W. *Silicon Reagents in Organic Synthesis*; Academic Press: London, 1988.

40. Brook, M. A. *Silicon in Organic, Organometallic, and Polymer Chemistry*; John Wiley & Sons, Incorporated: Toronto, 2000.

41. Appel, R.; Geisler, K. *J. Organomet. Chem.* **1976**, *112*, 61-64.

42. Petrie, M. A.; Power, P. P. *J. Chem. Soc., Dalton Trans.* **1993**, 1737.

43. Sandström, J. *Dynamic NMR Spectroscopy*; Academic Press: Toronto, 1982.

44. Sheldrick, G. *SHELXS-97* University of Gottingen, 1997.

45. Sheldrick, G. *SHELXL-97* University of Gottingen, 1997.

46. Maaninen, A.; Boeré, R. T.; Chivers, T.; Parvez, M. *Z. Naturforsch* **1999**, *54b*, 1170.

47. Cowley, A. H.; Pakulski, M.; Norman, N. C. *Polyhedron* **1987**, *6*(5), 915-919.

48. Brauer, D. J.; Bitterer, F.; Dörrenbach, F.; Heßler, G.; Stelzer, O.; Krüger, C.; Lutz, F. *Z. Naturforsch* **1996**, *51b*, 1183.

49. Appel, R.; Paulen, W. *Angew. Chem., Int. Ed. Engl.* **1983**, *22*(10), 785-786.

50. Paulen, W. Universitat Bonn, West Germany, 1983.

51. Yoshifuji, M.; Shimura, K.; Toyota, K. *Bull. Chem. Soc. Jpn.* **1994**, *67*, 1980-1983.

Chapter 5

N,P-disubstituted monophosphaamidines

5.1 Introduction

The work presented in this chapter is the first study to specifically target the protonated *N,P*-disubstituted phosphaamidine system, which is capable of the kind of *isomerism* and *tautomerism* that *N,N'*-disubstituted amidines exhibit. As discussed in Section 2.7, our group has completed work on a series of bulky *N,N'*-disubstituted amidines, incorporating the sterically bulky Dip group on the amino and imino nitrogen atoms (Figure 5.1).

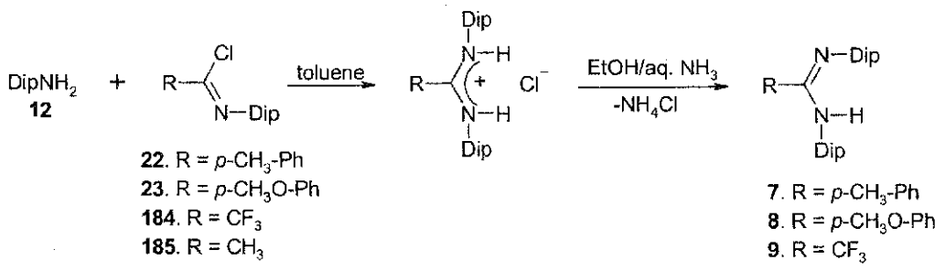

Figure 5.1 Synthesis of bulky *N,N'*-amidines

These amidines exhibit isomerism and tautomerism in solution and are known to adopt three of the four possible conformations in the solid state (Figure 2.21). We have deliberately produced the mono-phosphorus derivatives of our amidines to discover how the monophosphaamidine system differs from their amidine counterparts.

As mentioned in Section 2.9, Issleib performed a preliminary study on silylated *N,P*-disubstituted monophosphaamidines, which were made via the condensation reaction of imidoyl chlorides with primary disilylated phosphines, followed by 1,3-silyl migration (Figure 5.2).[1] Earlier work in our lab with the Issleib compounds showed that they were extremely difficult to purify and resisted any attempts to crystallize them.

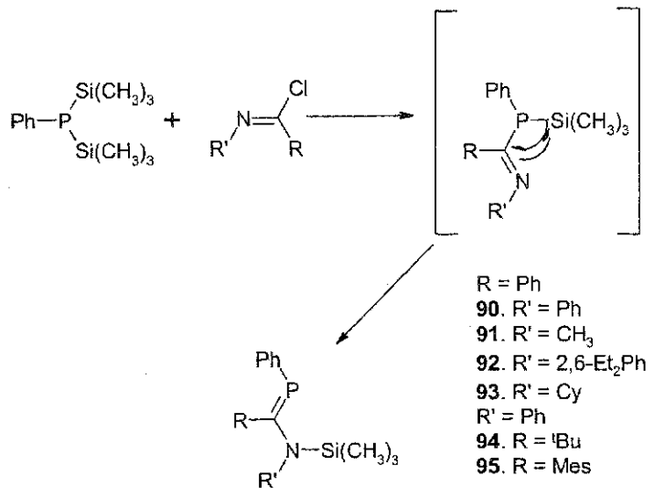

Figure 5.2 Issleib reaction to make silylated phosphaamidine

In addition, these workers briefly mentioned possible protonated phosphaamidines. These were produced by treating the silylated phosphaamidine with MeOH and were only characterized by ^{31}P NMR (Figure 5.3).

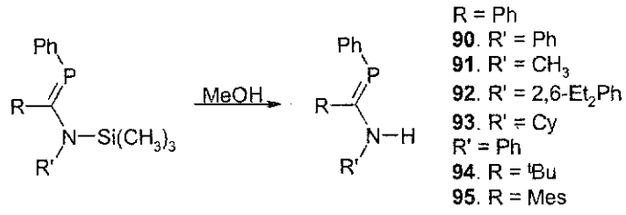

Figure 5.3 Methanolysis of silylated phosphaamidine to give protonated phosphaamidine

We have produced two new phosphorus-substituted amidines **20** and **21**. NMR evidence also shows that these are true 'phosphaamidines', meaning that they exhibit both isomerism and tautomerism in solution..

5.2 Synthesis of phosphaamidines

Reacting $DipPH_2$ **15** with one equivalent of imidoyl chloride[2] in refluxing xylenes produced phosphaamidines **20** and **21** (Figure 5.4). Reaction progress was followed by

^{1}H NMR, and reaction times of up to ten days were needed to complete the reaction. The crude material contained many impurities and quite often the imidoyl chloride starting material.

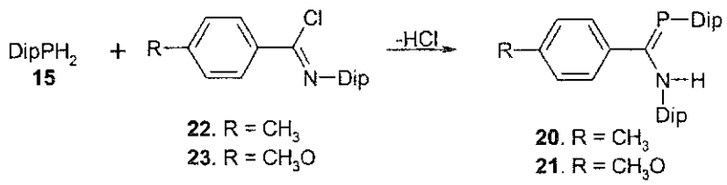

Figure 5.4 Synthesis of protonated phosphaamidines using primary aryl phosphane

In order to decrease reaction times and the amount of side products produced, the silylated phosphine, DipPHSi(CH$_3$)$_3$ **16**, was used (Figure 5.5). It was hoped that the electron donating trimethylsilyl group would enhance the nucleophilicity of the phosphine lone pair and in addition, the HCl in the original reaction would not be available to produce any side products. As a result, reaction times dropped to less than five days and ^{1}H NMR showed there to be fewer side products produced.

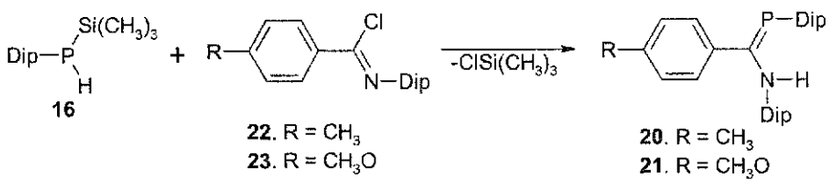

Figure 5.5 Synthesis of protonated phosphaamidines using silylated primary aryl phosphane

Work-up consisted of removal of xylenes from the reaction mixture and crystallization from hot ethanol, producing a yellow amorphous solid. ^{1}H NMR showed this solid to contain trace amounts of impurities. Recrystallization from hot methanol produced beautiful yellow, block-like crystals that were pure by ^{1}H NMR, suitable for analytical and X-ray crystallographic work.

The conversion to the putative product follows the mechanism outlined in Figure 5.6. Initially the (N=C) structure must be formed, and the (P=C) structure determined for **20** and **21** can only be made via a prototopic tautomerism. Further evidence for such a tautomeric process has been deduced from NMR studies (see Section 5.3)

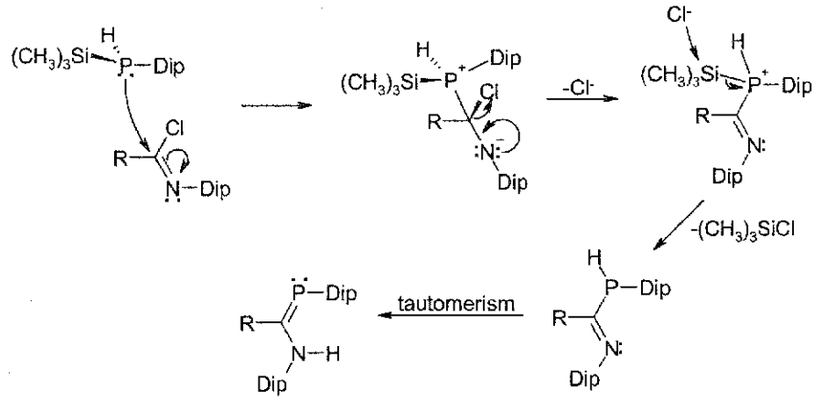

Figure 5.6 Proposed mechanism to the formation of phosphaamidines 20 and 21

When crystalline material is left exposed to the atmosphere for long periods of time, hydrolysis occurs and the amide, **186** or **187,** is the only decomposition product recognizable by ^{1}H NMR (Figure 5.7).

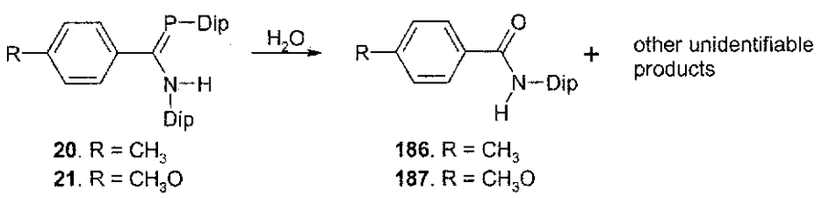

20. R = CH_3
21. R = CH_3O

186. R = CH_3
187. R = CH_3O

Figure 5.7 Hydrolysis of protonated phosphaamidine

5.3 Spectroscopy

5.3.1 Description of the major isomer in solution

We have discovered that there are multiple isomers and tautomers present in solution of phosphaamidines **20** and **21**. Remember that there are 8 possible structures of the *N,P*-disubstituted phosphaamidine system (Figure 3.9). The major isomer in $CDCl_3$ solution will be discussed in this section, while the minor isomers will be discussed in Section 5.3.3. NMR data for the major isomers of both phosphaamidines **20** and **21** have been compiled in Table 5.1, and an annotated spectrum of **20** is included in Figure 5.8.

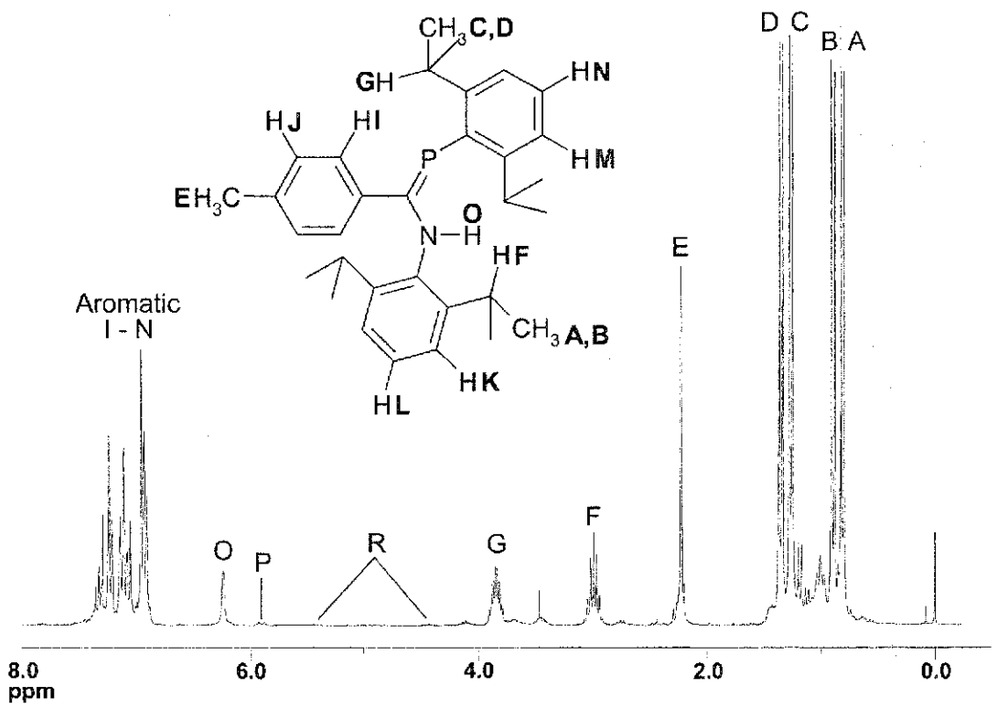

Figure 5.8 Annotated ^{1}H NMR spectrum of 20

Table 5.1 Selected ^{1}H, ^{31}P and ^{15}N NMR data for 20 and 21

^{1}H NMR		**20**	**21**
$^{i}Pr - CH_3$ **A** (amino)	δ (^{1}H)	0.81	0.83
	$^{3}J_{HH}$, Hz	6.7	6.9
$^{i}Pr - CH_3$ **B** (amino)	δ (^{1}H)	0.89	0.92
	$^{3}J_{HH}$, Hz	6.7	6.9
$^{i}Pr - CH_3$ **C** (phosphino)	δ (^{1}H)	1.27	1.27
	$^{3}J_{HH}$, Hz	6.7	6.7
$^{i}Pr - CH_3$ **D** (phosphino)	δ (^{1}H)	1.35	1.36
	$^{3}J_{HH}$, Hz	6.9	6.9
R = *p*-CH_3, *p*-CH_3O **E**	δ (^{1}H)	2.22	3.70
$^{i}Pr - H$ **F** (amino)	δ (^{1}H)	3.00	3.00
	$^{3}J_{HH}$, Hz	6.7	6.7
$^{i}Pr - H$ **G** (phosphino)	δ (^{1}H)	3.84	3.85
	$^{3}J_{HH}$, Hz	6.8	6.7
	$^{4}J_{PH}$, Hz	3.4	3.4
Aromatic signals			
p-R-C_6H_4 **I**	δ (^{1}H)	7.12	7.18
	$^{3}J_{HH}$, Hz	8.1	8.7
	$^{4}J_{PH}$, Hz	1.7	2.1
p-R-C_6H_4 **J**	δ (^{1}H)	6.92	6.62
	$^{3}J_{HH}$, Hz	6.6	8.9
Dip-N **K**	δ (^{1}H)	6.94	6.95
	$^{3}J_{HH}$, Hz	6.9	7.6
Dip-N **L**	δ (^{1}H)	7.08	7.09
	$^{3}J_{HH}$, Hz	7.0	7.0
Dip-P **M**	δ (^{1}H)	7.23	7.23
	$^{3}J_{HH}$, Hz	7.3	7.5
Dip-P **N**	δ (^{1}H)	7.33	7.33
	$^{3}J_{HH}$, Hz	7.6	7.6
	$^{5}J_{PH}$, Hz	2.4	2.4
Major isomer			
N-H **O**	δ (^{1}H)	6.23	6.24
	$^{3}J_{PH}$, Hz	2.4	2.4
Minor isomers			
N-H **P**	δ (^{1}H)	5.90	5.91
	$^{3}J_{PH}$, Hz	11.0	12.8
P-H **R**	δ (^{1}H)	4.92	4.91
	$^{1}J_{PH}$, Hz	242.2	241.4
^{31}P NMR			
Major isomer			
N-H **O**	δ (^{31}P)	53.4	51.4
	$^{3}J_{PH}$, Hz	< linewidth	< linewidth
Minor isomers			
N-H **P**	δ (^{31}P)	79.2 (medium)	79.0 (medium)
	$^{3}J_{PH}$, Hz	9.9	
P-H **R**	δ (^{31}P)	-80.3 (small)	-80.1 (small)
	$^{1}J_{PH}$, Hz	243	241
P-H **S**	δ (^{31}P)	-66.4 (very small)	52.5 (very small)
	$^{1}J_{PH}$, Hz	243	241
^{15}N NMR	δ (^{15}N)	-272.2	
	$^{1}J_{NH}$, Hz	90.7	
^{13}C NMR			
C=P	δ (^{13}C)	186.2	186.1
	$^{1}J_{CP}$, Hz	61.4	62.0

The ^{1}H NMR spectra for both **20** and **21** are markedly similar, with the obvious exception of the *p*-CH_3 and *p*-CH_3O groups located on the aryl ring, where the *p*-CH_3O group of **21** is located approximately 1.5 ppm downfield from the *p*-CH_3 group of **20**. For reasons of clarity and brevity, only the ^{1}H NMR data for **20** will be discussed in detail. ^{1}H NMR of **20** showed there to be one major isomer with similar signals to the previously prepared *N,N'*-Dipamidine **7**.[2] For this discussion, it will be assumed that the major isomer is the Z-anti (P=C) form; arguments as to the assignment of this structure are presented in Section 5.3.2. The ^{i}Pr-C*H*$_3$ groups form 4 doublets, integrating to the expected 24 hydrogens. The ^{i}Pr-C*H* protons form two sets of peaks, one septet corresponding to the amino Dip group, located at 3.00 ppm and one septet that experiences coupling to phosphorus (^{4}J = 3.4 Hz), corresponding to the phosphino Dip group. By looking at the cross peaks between the ^{i}Pr-C*H* peaks and ^{i}Pr-C*H*$_3$ peaks in the 2D-gCOSY spectrum (Figure 5.10), one can assign the two upfield ^{i}Pr-C*H*$_3$ doublets **A** and **B** to the amino Dip group and the downfield pair of doublets **C** and **D** to the phosphino Dip group. The unusually shielded amino ^{i}Pr-C*H*$_3$ peaks can be rationalized through aromatic shielding effects as shown by the solid arrows in Figure 5.9, while the slight shielding experienced by the lower phosphino ^{i}Pr-C*H*$_3$ group is represented by the dotted line.

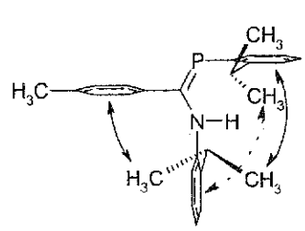

Figure 5. 9 Aromatic shielding effects seen by the amino and phosphino ^{i}Pr-C*H*$_3$ groups. ^{i}Pr groups in the background have been omitted for clarity.

The downfield position of the phosphino ^{i}Pr-C*H* **G** signal relative to the amino ^{i}Pr-C*H* **F** signal is attributed to deshielding effects caused by the proton **G** sitting over the P=C double bond and similar effects are seen in the corresponding *N,N'*-Dipamidine, **7**.

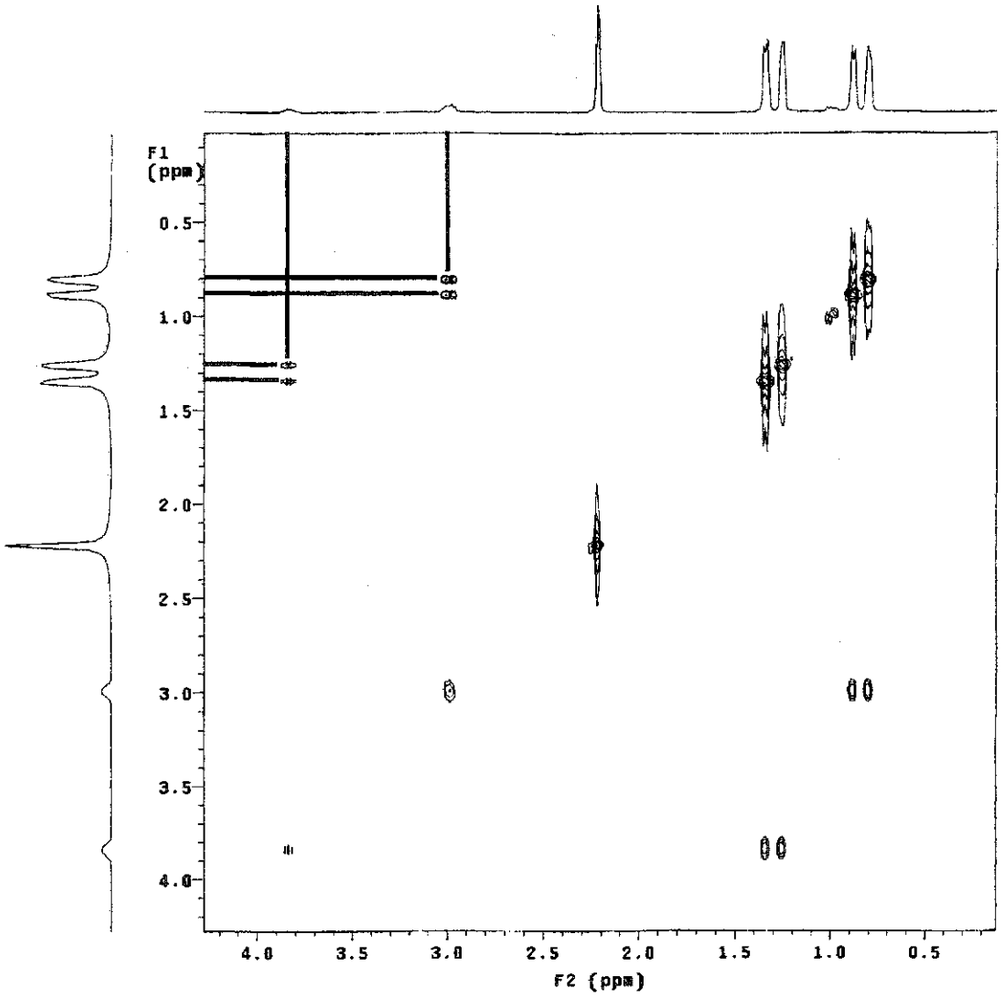

Figure 5.10 g-COSY spectrum showing the cross-peaks between the ^{i}Pr-CH_3 and ^{i}Pr-CH groups

The broad N-*H* peak **O** is located at 6.23 ppm, approximately 0.6 ppm downfield from the corresponding *N,N'*-Dipamidine **7**. ^{3}J coupling to phosphorus is present with a

splitting of 2.4 Hz. The aromatic signals **I-N** are a series of multiplets located between 6.93-7.35 ppm.

The proton-coupled ^{31}P NMR spectrum shows one large singlet located at 53.4 ppm for **20** and 51.4 ppm for **21**. Once again, only the spectrum for **20** will be discussed in detail, as both **20** and **21** have essentially the same spectra. An annotated spectrum has been included in Figure 5.11. In spectra that have a high signal-to-noise ratio, an additional, less intense peak can be seen in the region around the major peak **O**, occurring at 79.2 ppm **P** with a $^{3}J(P\text{-}H) = 9.9$ Hz. We know this species to be an N-H isomer, as it does not exhibit the large coupling constant expected for P-H compounds. In addition, two doublets appear at –66.4 ppm **S** and –80.3 ppm **R**, both with the same coupling constant ($^{1}J(P\text{-}H) = 243$ Hz). When the proton-decoupled spectrum is run, the coupling is lost, confirming that these *are* P-H containing species. Although we cannot prove that these are isomers of our phosphaamidine, we do have evidence that supports our notion that they do belong to our phosphaamidine:

1. These peaks appear in spectra from multiple samples and syntheses, including X-ray grade crystals.
2. The signals do not increase in intensity with time
3. The phosphorus chemical shift and the $^{1}J(P\text{-}H)$ coupling constant is similar to our N=C phosphaguanidine **28**, which contains a P-C single bond (Chapter 7).

This evidence suggests that these P-H signals most likely belong to **20**, and not to other species. These minor isomers will be discussed in Section 5.3.3.

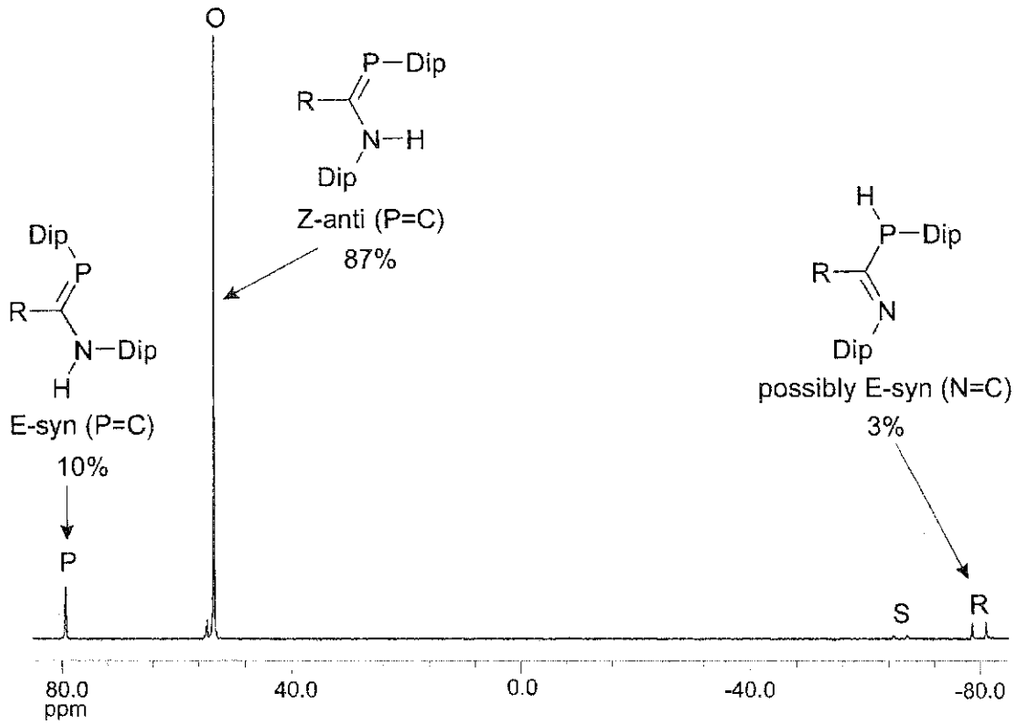

Figure 5.11 Annotated proton coupled-^{31}P NMR spectrum of phosphaamidine 20

Although there is to our knowledge no ^{15}N NMR evidence in the literature for phosphaamidine systems, there is some data on *N,N',N'*-trisubstituted amidines.[3] The ^{15}N NMR shifts for the amino nitrogens are in the range of –169 to -311 ppm and the imino nitrogens are in the range of -135 to –172 ppm. Direct detection ^{15}N NMR performed on **20** shows a doublet at –272.2 ppm (^{1}J(N-H) = 90.7 Hz)), which is within the range of the amino nitrogens in the trisubstituted amidines. The 2-dimensional ^{1}H-^{15}N HSQC experiment shows the ^{15}N signal coupled to the major N-H isomer at 6.23 ppm **O**.

5.3.2 Conformation of the major isomer in solution

As mentioned in Chapter 3, there are eight possible isomers for our phosphaamidine system (Figure 3.9), and DFT calculations have shown the Z-anti (P=C) structure to be

the most stable conformation. We have reason to believe this is also the major isomer in solution (Figure 5.12).

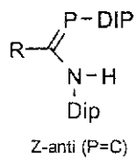

Z-anti (P=C)

Figure 5.12 The major isomer present in solution, Z-anti (P=C)

This is supported by the following evidence:

1. Both phosphaamidines **20** and **21** and all of the metal complexes described in Chapter 6 crystallize in the Z-anti (P=C) form.
2. The ^{1}H NMR spectra of the metal complexes (Chapter 6) are nearly identical to the major isomer of the free ligands, and since the metal complexes are unlikely to isomerize in solution, we can be fairly confident that the free ligand *is* in the Z-anti (P=C) conformation.
3. The ^{1}H NMR spectrum is almost identical to the *N,N'*-Dipamidine **7**, which is known to be in the Z-anti form.

With this information, we have looked at the minor isomers in solution and postulated their structures from among the remaining 7 isomers.

5.3.3 Other isomers detectable in solution

In the 4.4-6.5 ppm region of the ^{1}H NMR spectrum of **20** (Figure 5.13), there are a number of smaller peaks that have been correlated to the minor peaks in the ^{31}P NMR spectrum using a ^{1}H-^{31}P HETCOR experiment.

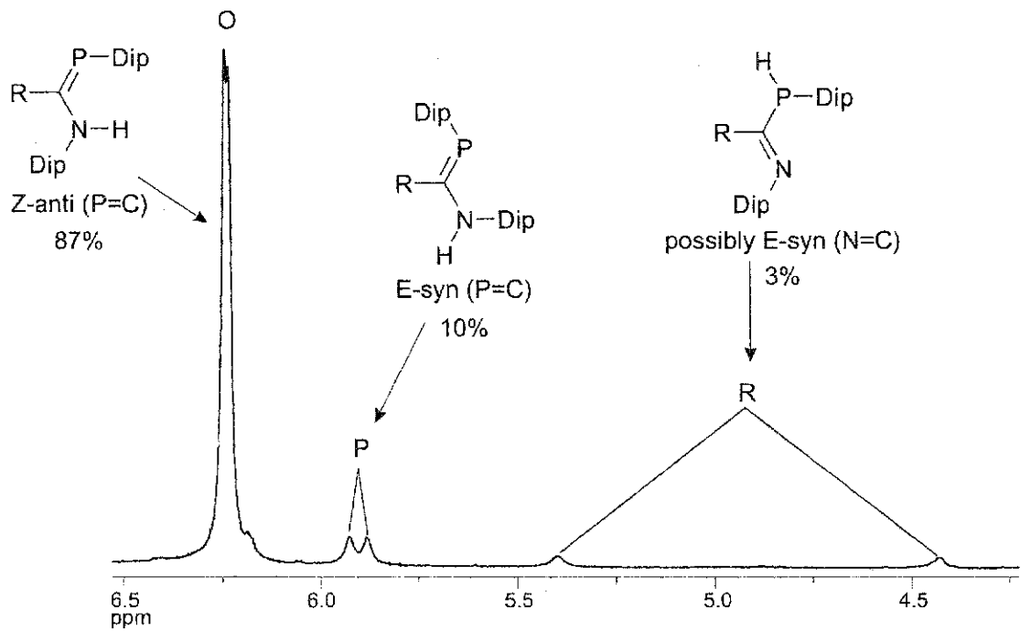

Figure 5.13 Close-up of the 4.0-6.5 ppm region of the ^{1}H NMR of 20

The peak at 5.91 ppm **P** integrates to approximately 10% of the major N-*H* peak **O**. The HETCOR experiment has correlated this signal to the second most intense peak in the ^{31}P NMR spectrum at 79.3 ppm (**P**, Figure 5.10). Analysis of the other minor peaks in the ^{1}H NMR shows that this isomer is most likely the E-syn (P=C) isomer (Figure 5.14).

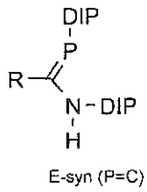

Figure 5.14 The second most common isomer present in solution

We believe this to be the second most abundant isomer in solution for a number of reasons:

1. In general, *trans* coupling constants tend to be larger than *cis* coupling constants. The Z-anti (P=C) isomer has the N-H proton *cis* to the phosphorus center, giving a small 2.4 Hz coupling. The N-H proton of the minor isomer has a ^{3}J coupling constant of 11 Hz, significantly larger than the Z-anti (P=C) isomer, indicating that there is most likely a *trans* interaction with the phosphorus.
2. Our assignment of the E-syn (P=C) isomer is consistent with the ^{13}C NMR data on the electronically similar E/Z-'Becker' phosphaalkenes. Yoshifuji found that the chemical shift and coupling constant for the P=C carbon is smaller and downfield for the E isomer when compared to the Z isomer.[4] Our data is in agreement with this (Table 5.2), substantiating our claim that the other isomer in solution is indeed either the E-syn (P=C) or E-anti (P=C) isomer.
3. Since the only two possible structures with an N-H proton *trans* to the phosphorus are E-syn (P=C) and Z-syn (P=C), we can conclude that the E-syn (P=C) isomer is preferred due to the unfavorable steric interactions in the Z-syn (P=C) isomer.
4. We can exclude the E-anti (P=C) isomer based on the results of our g-COSY spectrum. If the isomer in question was truly E-anti (P=C), we would expect that the chemical shifts for only *one* of the amino $^{i}Pr\text{-}CH_3$ groups to change significantly as it would no longer experience shielding from the phosphino Dip ring (Figure 5.15).

What we do see is the effective inversion of the amino and phosphino ^{i}Pr-CH_3 signals of the minor isomer when compared to the Z-anti (P=C) signals (Table 5.2). This effect could only be seen in the E-syn (P=C) isomer where both phosphino ^{i}Pr-CH_3 groups would experience shielding effects and only one amino ^{i}Pr-CH_3 group would experience shielding (Figure 5.15).

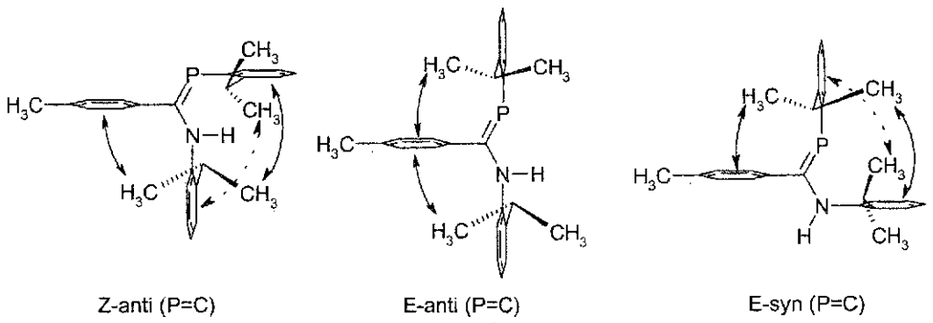

Figure 5.15 Shielding effects present in the two anti (P=C) phosphaamidine structures. Note in the E-anti(P=C) structure how one of the amino ^{i}Pr-C*H*$_3$ groups should no longer be shielded by the phosphino Dip ring. Background ^{i}Pr groups have been omitted for clarity.

The doublet **R** integrating to approximately 3% located at 4.92 ppm (^{3}J(P-H) = 242 Hz) in the ^{1}H NMR spectrum has been correlated to the larger of the two possible P-H isomers at –80.3 ppm (^{3}J(P-H) = 243 Hz). The other P-H isomer in the ^{31}P spectrum is most likely not visible in the ^{1}H NMR because it has less than half of the intensity of the other P-H isomer in the ^{31}P NMR. Although there are peaks of the P-H isomers other than the P-*H* signal in the ^{1}H NMR, these are either buried under the more intense signals, or are so low in intensity that it is difficult, if not impossible, to assign any of these to any certain isomer.

Table 5.2 Selected NMR data for the known major Z-anti (P=C) and minor E-syn (P=C) isomers in $CDCl_3$ solution. Spectrum is shown in Figure 5.16.

^{1}H NMR		**20** Major isomer Z-anti (P=C)		**20** Minor isomer E-syn (P=C)
^{i}Pr – CH_3 **A** (amino)	δ (^{1}H)	0.81	**T**	1.23
	$^3J_{HH}$, Hz	6.7		6.7
^{i}Pr – CH_3 **B** (amino)	δ (^{1}H)	0.89	**U**	1.42
	$^3J_{HH}$, Hz	6.7		6.9
^{i}Pr – CH_3 **C** (phosphino)	δ (^{1}H)	1.27	**V**	0.99
	$^3J_{HH}$, Hz	6.7		6.7
^{i}Pr – CH_3 **D** (phosphino)	δ (^{1}H)	1.35	**W**	1.023
	$^3J_{HH}$, Hz	6.9		6.7
R = *p*-CH_3, *p*-CH_3O **E**	δ (^{1}H)	2.22	**X**	2.25
^{i}Pr – H **F** (amino)	δ (^{1}H)	3.00	**Y**	3.45
	$^3J_{HH}$, Hz	6.7		6.9
^{i}Pr – H **G** (phosphino)	δ (^{1}H)	3.84	**Z**	3.69
	$^3J_{HH}$, Hz	6.8		6.9
	$^4J_{PH}$, Hz	3.4		
N-H **O**	δ (^{1}H)	6.23	**P**	5.90
	$^3J_{PH}$, Hz	2.4		11.0
^{31}P NMR				
N-H **O**	δ (^{31}P)	53.4	**P**	79.2
	$^3J_{PH}$, Hz	< linewidth		9.9
^{13}C NMR				
C=P	δ (^{13}C)	186.2		192.76
	$^1J_{CP}$, Hz	61.4		46.8

Although we already know that prototropic tautomerism occurs during the synthesis of **20**, we have run EXSY experiments to look for other evidence of chemical exchange in the system. Using these results, we can make a reasonable guess as to the conformations of the P-H isomers. Initial EXSY results show that there is a fast interconversion between the major isomer N-H peak at 6.23 ppm and the P-H isomer located at 4.92 ppm. This would indicate a tautomeric process, suggesting that the P-H isomer in question is the E-syn (N=C) isomer. There is slow exchange between the major Z-anti (P=C) isomer at 6.23 ppm and the minor E-syn (P=C) isomer at 5.90 ppm, suggesting that this is structural rearrangement, rather than a tautomeric rearrangement, as would be expected

for these two isomers. Finally, the EXSY experiment shows exchange between the minor E-syn (P=C) isomer at 5.90 ppm and the P-H isomer at 4.92 ppm.

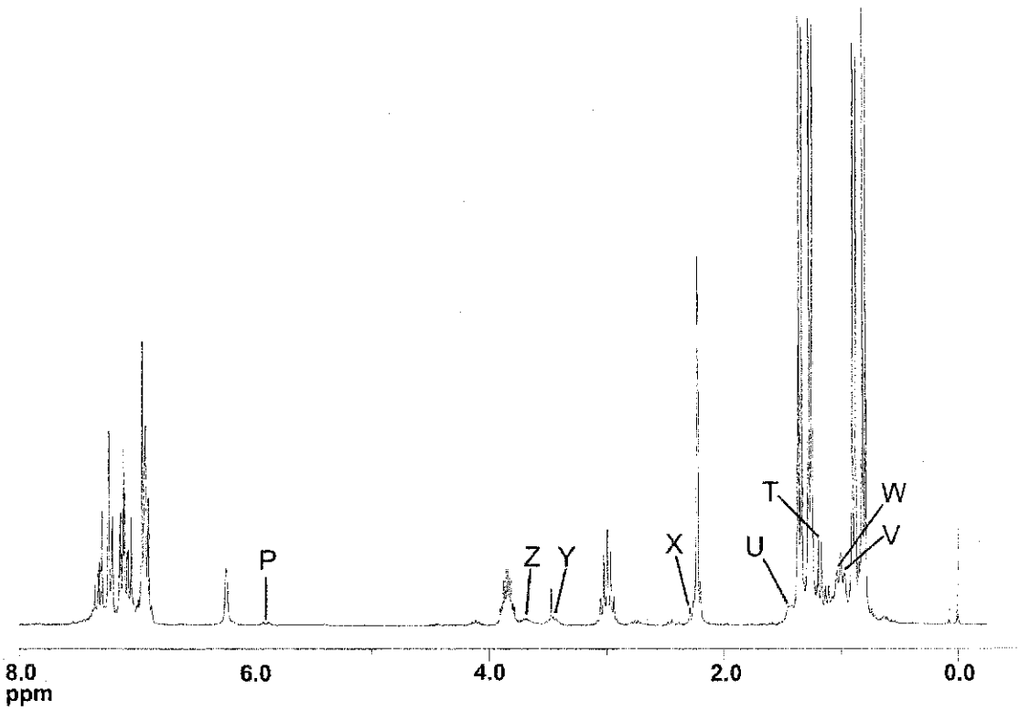

Figure 5.16 Assignment of the signals for the minor E-syn (P=C) isomer

Additional support for exchange has been provided by ^{31}P NMR of aged samples of **20** in acetone-d_6. The weakly acidic acetone-d_6 deuterons exchange with the N-H / P-H proton giving rise to notable changes in the ^{31}P NMR. All of the signals shifted slightly upon deuteration, and in addition, there is also ^{31}P-^{2}D coupling in the P-D isomers, causing the original P-H doublets to become P-D triplets ($^{1}J(^{31}P\text{-}^{2}D) = 37.8$ Hz). This deuteration is fully consistent with the exchange processes present in the phosphaamidine system.

We can interpret these results using an analogy to the base catalyzed tautomerism that is known to exist for enamines[5]. The tautomerism experienced by the enamine functional group is highly comparable to our phosphaamidine system, except the stability of the imine forms are inverted (Figure 5.17)

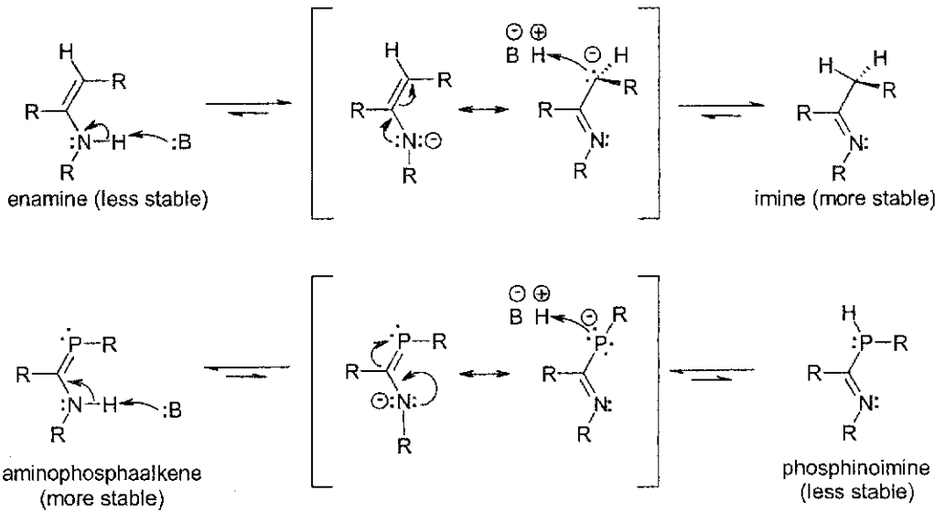

Figure 5.17 Similarities between base catalyzed tautomerism seen in enamine systems and the phosphaamidine system

This tautomerism can be viewed as an autocatalytic process, where the phosphaamidine can act as a base via the phosphorus lone pair (Figure 5.18). This protonated intermediate is also a candidate for E-Z isomerism as there can be rotation around the P-C bond due to delocalization of electron density into the P-C-N system, or there can be rotation about the N-C bond because the partial double bond character in the N-C bond would be less due to the positively charged phosphorus atom withdrawing electron density from the C-N bond.

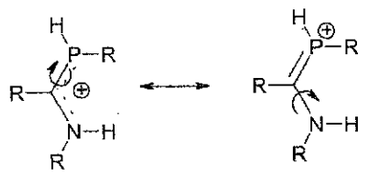

Figure 5.18 The phosphaamidine system acting as a protonated base intermediate allowing rotation about the P-C and N-C bonds

We can now draw a diagram showing the interrelationship of the exchange process as shown by the EXSY experiment (Figure 5.19). This figure outlines the fast exchange between the Z-anti (P=C) and E-Syn (N=C) isomers indicating tautomerism via the tautomeric intermediate shown in Figure 5.19. The slow exchange to the E-syn(P=C) isomer could be viewed as a process that happens via rotation around either the P-C or N-C bond in the protonated base intermediate.

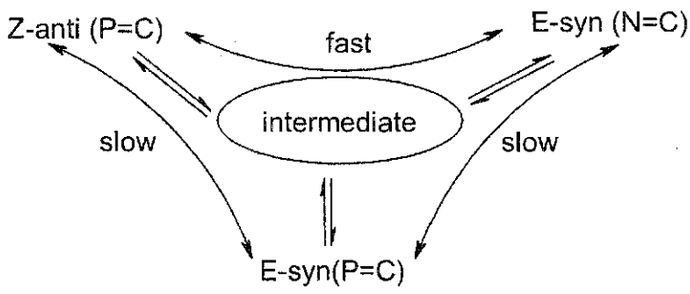

Figure 5.19 Proposed exchange process for phosphaamidine system

5.3.4 NMR spectroscopy in other solvents

We have run ^{1}H, ^{13}C and ^{31}P NMR in the solvents CD_3CN, $(CD_3)_2C=O$, and C_6D_6. The less polar C_6D_6 shows a lower concentration of the minor isomers, while the more polar solvents, CD_3CN and $(CD_3)_2C=O$, show almost equal concentrations of the Z-anti (P=C) and E-syn (P=C) isomers, with little or no change in the relative concentrations of the P-H isomers. The ^{1}H and ^{31}P NMR data for the deuterated acetone solution have

been compiled in Table 5.3. The g-COSY experiment has been used to confirm assignments of ^{i}Pr signals, which are shown in Figure 5.20.

Table 5.3 Selected ^{1}H NMR data for the known Z-anti (P=C) and E-syn (P=C) isomers in $(CD_3)_2C=O$ solution

^{1}H NMR		**20 Z-anti (P=C)**		**20 E-syn (P=C)**
^{i}Pr – CH_3 **A** (amino)	δ (^{1}H)	0.88	**T**	1.25
	$^{3}J_{HH}$, Hz	6.9		6.7
^{i}Pr – CH_3 **B** (amino)	δ (^{1}H)	0.89	**U**	1.46
	$^{3}J_{HH}$, Hz	6.9		6.9
^{i}Pr – CH_3 **C** (phosphino)	δ (^{1}H)	1.24	**V**	1.00
	$^{3}J_{HH}$, Hz	6.7		6.9
^{i}Pr – CH_3 **D** (phosphino)	δ (^{1}H)	1.40	**W**	1.01
	$^{3}J_{HH}$, Hz	6.9		6.9
R = *p*-CH_3, *p*-CH_3O **E**	δ (^{1}H)	2.20	**X**	2.22
^{i}Pr – H **F** (amino)	δ (^{1}H)	3.11	**Y**	3.86
	$^{3}J_{HH}$, Hz	6.7		6.9
^{i}Pr – H **G** (phosphino)	δ (^{1}H)	3.88	**Z**	3.57
	$^{3}J_{HH}$, Hz	6.7		6.9
N-H **O**	δ (^{1}H)	deuterium exchanged	**P**	deuterium exchanged
^{31}P NMR				
N-H **O**	δ (^{31}P)	53.3	**P**	67.6
^{13}C NMR				
C=P	δ (^{13}C)	187.3		195.0
	$^{1}J_{CP}$, Hz	63.5		50.3

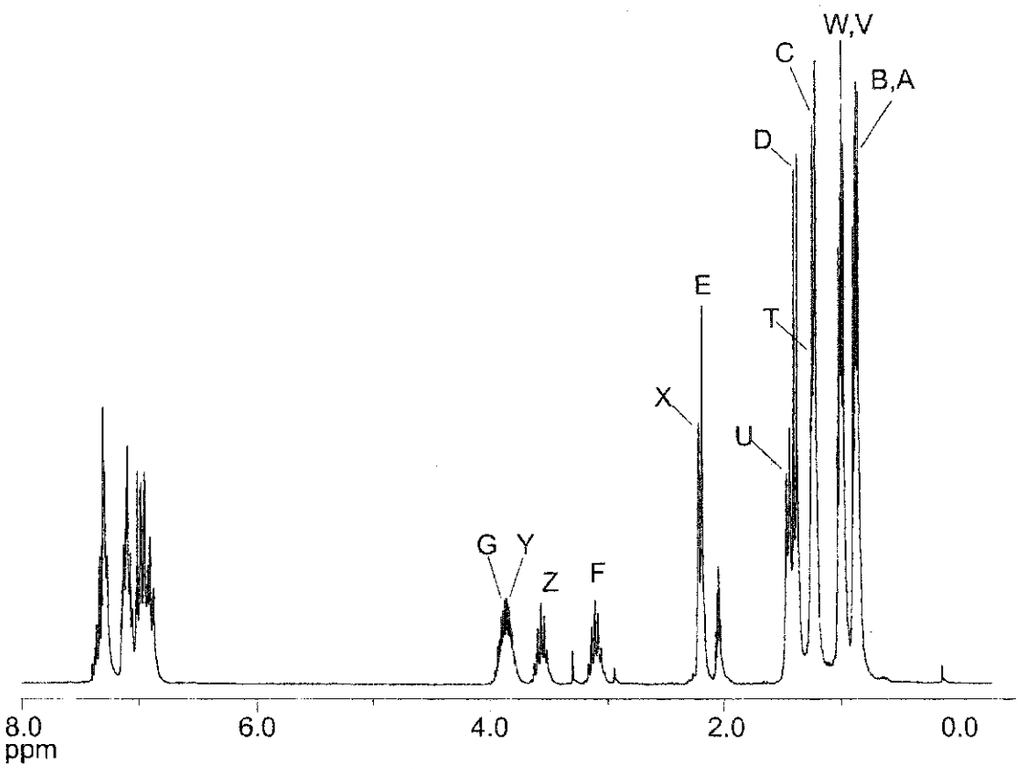

Figure 5.20 Spectrum and peak assignments for phosphaamidine 20 in deuterated acetone.

5.3.5 IR spectroscopy

IR spectroscopy on samples in solution and KBr pellets show that the major isomer in both solution and the solid state is indeed a P=C isomer. The N-H stretches reported in Table 5.4 are in the range for amines, and closely resemble the data for the analogous *N,N'*-Dipamidines **7** and **8**. Since the ν(N-H) values are essentially the same for both **20** and **21** in solution, this suggests that the electronic difference between the *p*-CH_3 and *p*-CH_3O groups have little effect on the N-H bond in solution.

Table 5.4 ν(N-H) stretches of phosphaamidines 20 and 21 and their nitrogen analogues.

	20	**21**	**7**	**8**
ν(N-H)				
Heptane solution	3354	3354	3431, 3366	3431, 3366
$CHCl_3$ solution	3350	3350		
KBr pellet	3351	3357		

5.4 Crystal structures of phosphaamidines **20** and **21**

X-ray quality crystals of **20** and **21** were obtained from a hot methanol solution cooled to –30 °C. Crystals were sent to Dr. Gotthelf Wolmershäuser of the Fachbereich Chemie at the Universität Kaiserslautern, Germany for collection of X-ray intensity data. The structures were solved by direct methods using either SHELXS[6](**20**) or SIR92[7] (**21**), and refined using SHELXL[8] by standard full-matrix squares methods. Hydrogens were fixed on the aromatic rings so that the coordinates ride on the corresponding aromatic carbon atom coordinates. ^{i}Pr C-*H* hydrogens were fixed for idealized tertiary C-H's with all X-C-*H* angles equal with a riding model refinement. ^{i}Pr methyl groups were fixed with ideal tetrahedral angles with the C-H distances allowed to vary, while allowing the CH_3 group to rotate. Temperature factors were set to 1.5 (CH_3 groups)or 1.2 (Ar-H and CH groups) times the equivalent isotropic temperature factor of the corresponding carbon atoms. The amino hydrogens were found on the difference Fourier map, and allowed to freely refine. Both **20** and **21** crystallize in the monoclinic space group P2(1)/c, with four molecules per unit cell. Agreement factors of $R_1 = 0.0490$, $wR_2 = 0.1122$ were found for **20** and $R_1 = 0.0468$, $wR_2 = 0.0986$ for **21**. ORTEP diagrams are shown in Figure 5.21 (**20**) and Figure 5.22 (**21**). Crystal data and structure refinement parameters are included in the appendix as Table A.6 for **20** and Table A.11 for **21**, and crystallographic data are included as Tables A.7-A.10 for **20** and Tables A.12-A.15 for **21**.

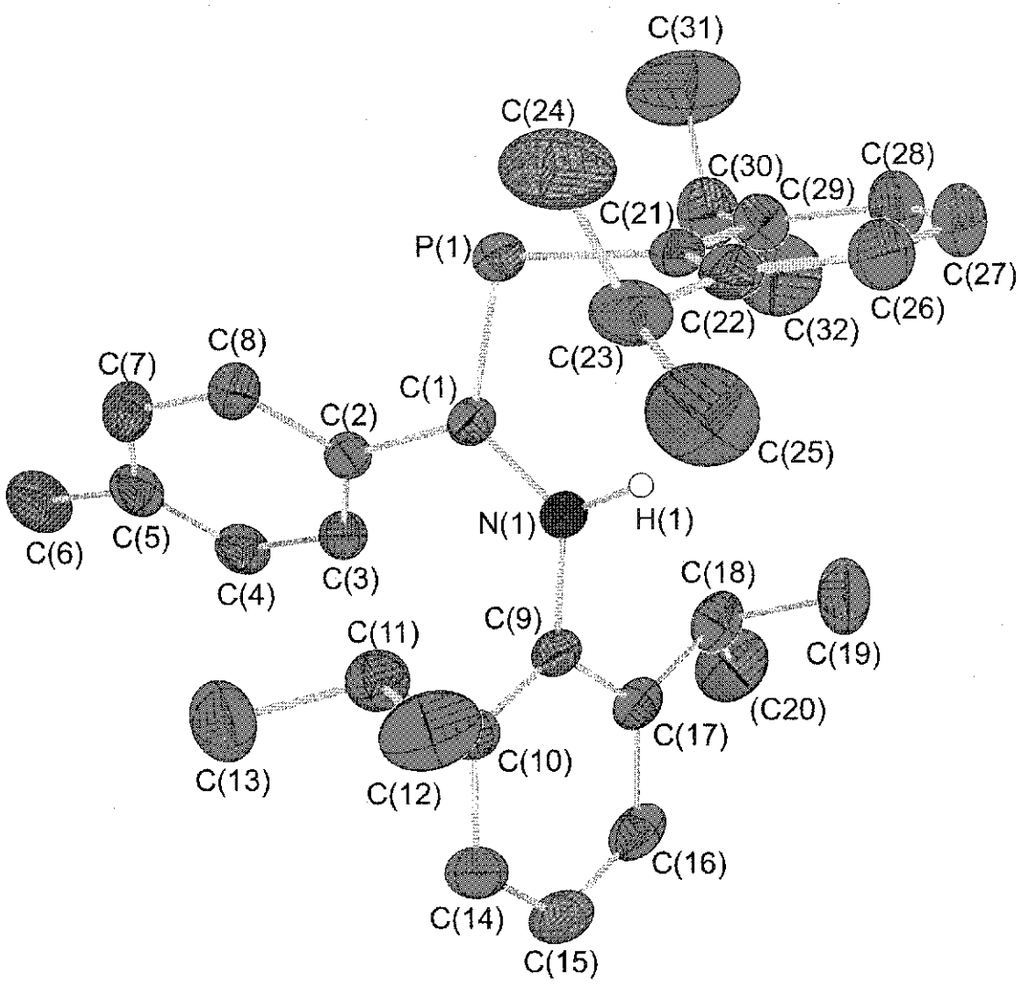

Figure 5.21 An ORTEP diagram (25% probability) of the crystal structure found for 20 with atom numbering scheme. Hydrogen atoms on carbon are omitted for clarity.

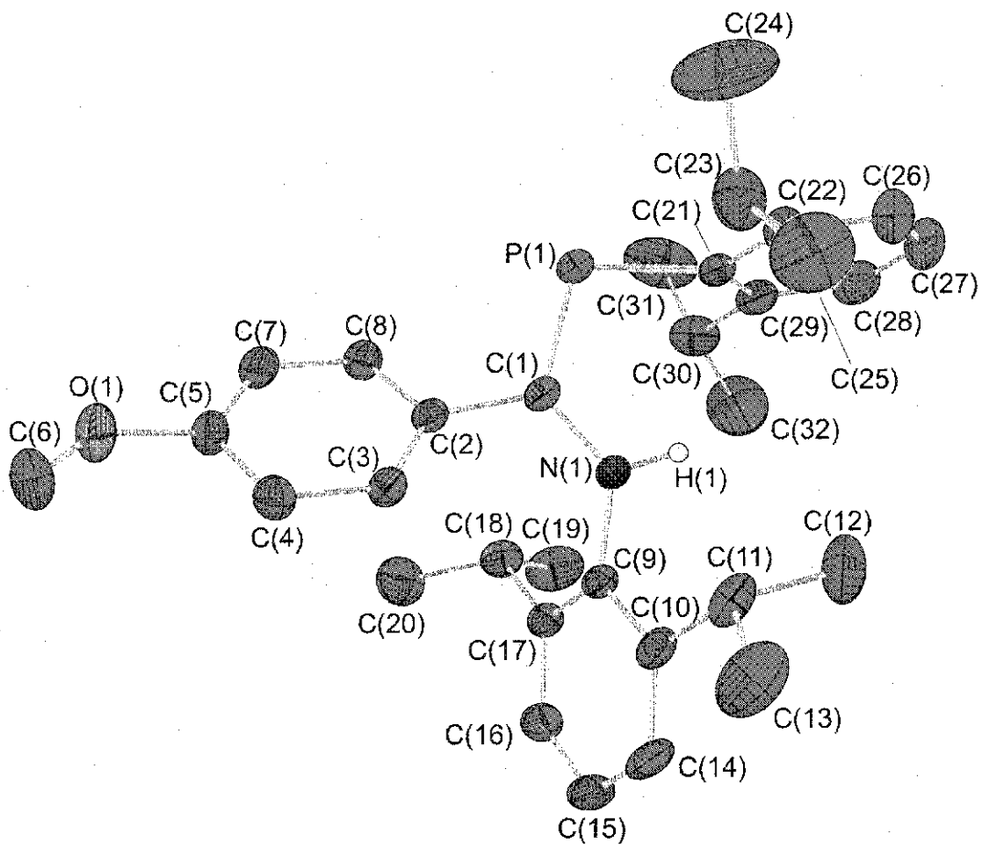

Figure 5.22 An ORTEP diagram (25% probability) of the crystal structure found for 21 with atom numbering scheme. Hydrogen atoms on carbon are omitted for clarity.

Both **20** and **21** crystallize in the Z-anti P=C form, which is the most stable form by AM1 and DFT calculations (Chapter 3). The aryl rings connected to the central phosphaamidine carbon are twisted 39.54° and 41.62° from perpendicular (**20** and **21**, respectively), to minimize interactions with the amino Dip-^{i}Pr groups. Like the silyl phosphane, DipPH(TBDMS) **17**, there is a large deviation from the mean aryl plane by both the phosphorus atom {0.306(6) Å} and the *ipso* carbon C(21) {0.025(4) Å) in **21.** For **20**, the *ipso* carbon C(21) is essentially planar with the five other aryl carbons, and

the phosphorus atom only deviates 0.173(5)Å, significantly less than **21**. Also similar to DipPH(TBDMS) **17**, the phosphorus atom in both phosphaamidines is displaced to one side of the aryl ^{i}Pr groups, while the rest of the molecule is displaced on the opposite side (Figure 5.23). An analysis of the packing diagrams showed no unusual characteristics, and there is no evidence of significant intermolecular contacts beyond normal van der Waals' interactions. Packing diagrams are shown in Figure 5.24 (**20**) and Figure 5.25 (**21**). Selected bond lengths have been compiled in Table 5.5.

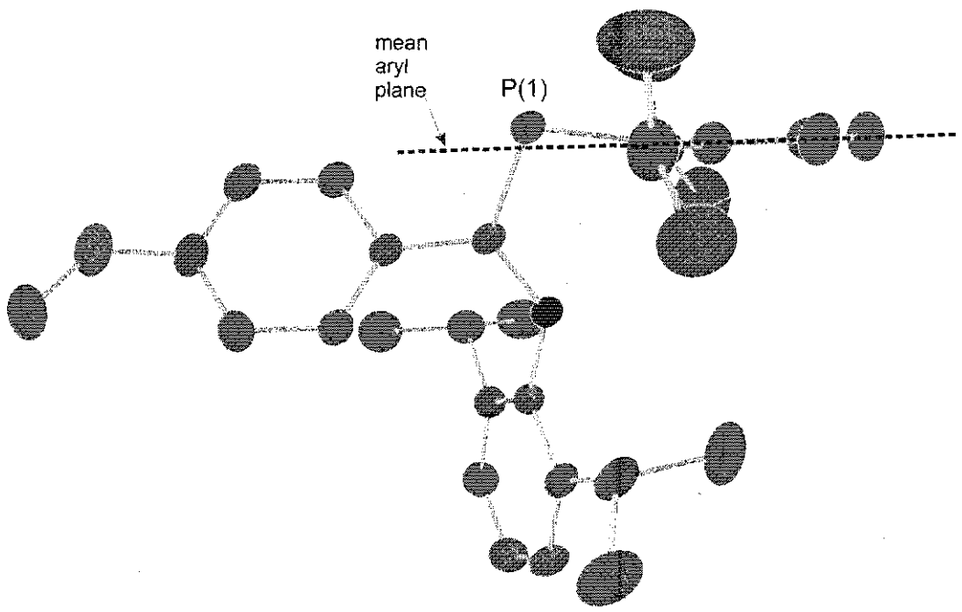

Figure 5.23 Diagram showing the deviation of the phosphorus atom from the mean aryl plane

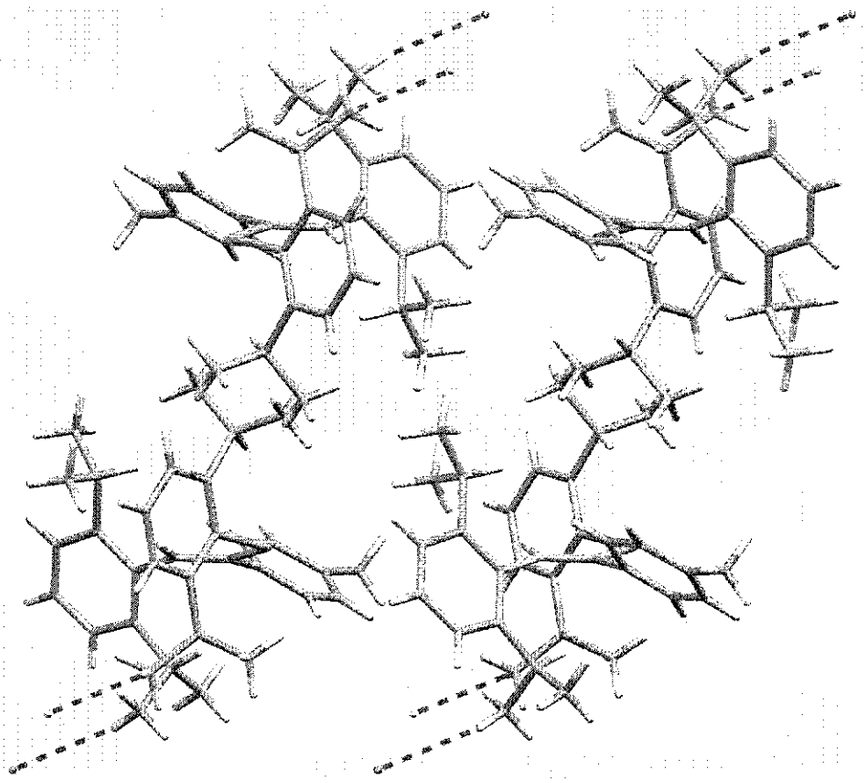

Figure 5.24 Packing diagram of 20. Dashed lines show intermolecular contacts that are equal to the sum of van der Waals radii.

The P=C double bond is 1.709(2) Å for **20** and 1.716(2) Å for **21**, which is in the range (1.70-1.76 Å) of C-amino substituted phosphaalkenes,[9] and quite close to the similar systems MesP=C(Ph)NH_2 **188** (1.704(2) Å)[10] and MesP=C(CH_2C(^{t}Bu)C≡C^{t}Bu)N((CH_2CH_2)$_2$O) **189** (1.711 Å).[11] The P=C bond length of 1.713 Å predicted using DFT methods for the Z-isomer of model phosphaamidine system is essentially the same as both phosphaamidines **20** and **21**, while the calculated structure for the Z-anti (P=C) isomer of **20** shows a slightly longer bond length of 1.740 Å (Chapter 3).

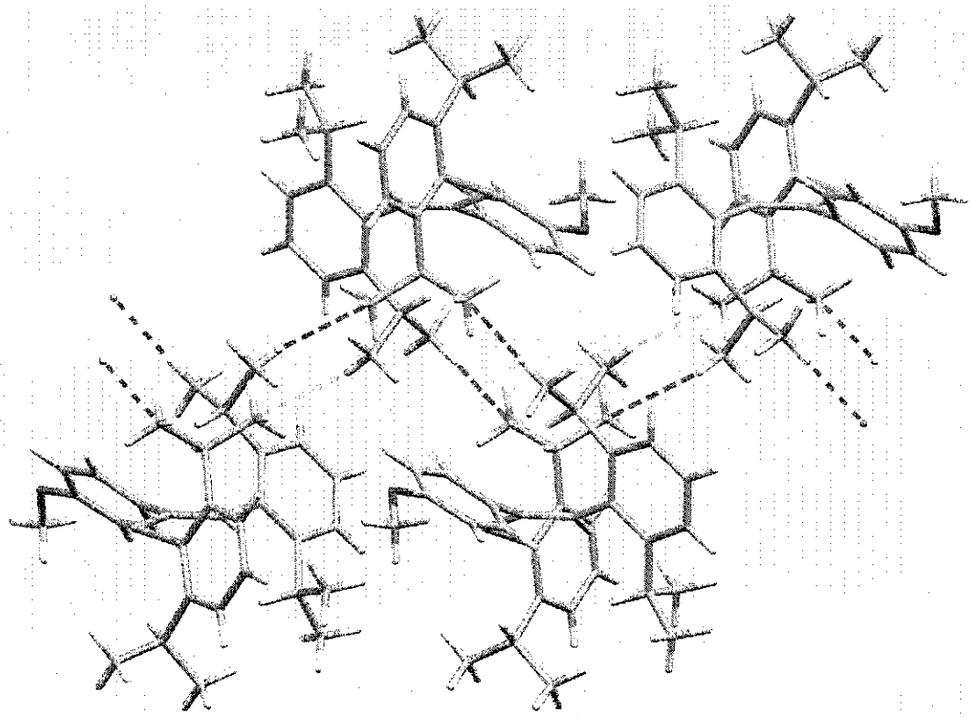

Figure 5.25 Packing diagram of 21. Dashed lines show intermolecular contacts that are equal to the sum of van der Waals radii.

Table 5.5 Selected Bond lengths and angles for 20, 21

	20	21
P=C	1.709(2)	1.716(2)
P-C_{aryl}	1.847(2)	1.849(2)
C-N	1.368(2)	1.366(3)
N-C_{aryl}	1.429(3)	1.435(3)
C-C_{aryl}	1.488(3)	1.479(3)
C-P-C	101.87(10)	103.56(11)
P=C-N	123.38(17)	123.03(18)
C-N-C	131.6(2)	130.9(2)

In contrast, normal phosphaalkenes have a P=C double bond length between 1.65-1.67 Å.[9] The co-planar amino group allows conjugation between the P=C π-bond and the *p*-orbital of the amino group, lengthening the P=C double bond and shortening the N-C

bond, giving the N-C bond significant double bond character. Thus the N-C bond is 1.368(2) Å in length for **20** and 1.366(3) Å for **21**, much shorter than an average C-N single bond (1.45 Å),[9] but close to the lengths found for MesP=C(Ph)NH_2 **188** (1.357(3) Å) and the pentasubstituted phosphaguanidine, $(CH_3)_3SiP{=}CN(CH_3)_2NEt_2$ **141** (1.360(3) and 1.388(3) Å, Average bond length = approx. 1.374 Å).[12,13] Our DFT calculations are in agreement with these lengths; the model phosphaalkene shows a slightly shorter N-C bond of 1.358 Å, while the calculated structure for **20** shows an N-C bond length that is essentially the same as the crystal structure (1.371 Å). The P-C_{Aryl} bond length is 1.847(2) Å for **20** and 1.849(2) Å for **21**, slightly longer than in the phosphaalkene MesP=CPh_2 **41**, 1.828(3) Å) and triphenylphosphine **190** (1.830 Å),[14] but similar to the silylated phosphine **17** described in Chapter 4 (1.854(2) Å). The N-C_{Aryl} bond length is 1.429(3) Å for **20** and 1.435(3) Å for **21**, which is similar to the amino N-C_{Aryl} bond length found in our bulky *N,N'*-amidines **7** and **8** (1.422(3) and 1.427(2) Å respectively),[2] but shorter than the N-C_{Aryl} bond in aniline **191** (1.387(2) Å)[15], where the aromatic ring is co-planar with the NH_2 fragment, allowing conjugation to occur between the nitrogen p-orbital and the aromatic π-system.

The C-P-C angles are 101.87(10)° and 103.56(11) ° for **20** and **21**, respectively. This is slightly smaller than the angle found for MesP=CPh_2 **41** (107.5°), but significantly larger than in the angle calculated by DFT methods for the model phosphaamidine system (95.51°, Chapter 3). These angles are much smaller than the 120° angle expected for an sp^2 hybridized system. The nitrogen analogue MesN=CPh_2 **192** to phosphaalkene **41**, has an angle of 120.8°[16], showing that this angle is achieved for similar nitrogen systems. It can be concluded that the smaller C-P-C bond angles for the phosphorus

systems will impart a higher degree of *s*-character to the phosphorus lone pair. With this in mind, the phosphorus lone pair of phosphaamidines **20** and **21** will have a greater degree of *s*-character than phosphaalkene **41**. Bickelhaupt compared the C-P-C angle for $MesP{=}CPh_2$ **41** and the angle calculated for the parent phosphaalkene system (97.5°), and was unable to attribute the increased bond angle in **41** to steric or electronegativity effects.[17] However, we believe that the increased C-P-C angles can be attributed to the HOMO-1 molecular orbital (Figure 5.26), where the phosphorus lone pair is delocalized into the aryl π-system, as described in Chapter 3.

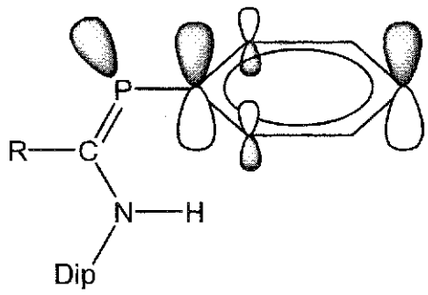

Figure 5.26 HOMO-1 of phosphaamidine 20. The increased C-P-C angles can possibly be attributed to the delocalization of the phosphorus lone pair into the aryl π-system.

5.5 Conclusion

We have produced two new *N,P*-disubstituted phosphaamidines, **20** and **21**, the first well characterized examples of this system to be reported since the preliminary study of the silylated analogues by Issleib over 20 years ago.[1] These compounds are, in our experience, much easier to handle and purify than the original Issleib compounds, thereby allowing us to perform a more detailed study of this system. We have obtained the first crystal structures for this class of compounds, and have been able to prove that the major isomer in solution is the same as the solid state structure, which also agrees with the most

stable isomer calculated by DFT methods. Using both advanced NMR methods along with a simple ^{31}P NMR deuterium-exchange experiment, we have established that there are isomeric and tautomeric processes occuring in solutions of these molecules. Thus the commonly used moniker 'aminophosphaalkenes' seems inappropriate for those structures that are capable of tautomerism. We propose the adoption of 'monophosphaamidines' as a general label for what ought to be recognized as a distinct functional group.

Reference List

1. Issleib, K.; Schmidt, H.; Meyer H. *J. Organomet. Chem.* **1978**, *160*, 47-57.

2. Boeré, R. T.; Klassen, V.; Wolmershauser, G. *J. Chem. Soc., Dalton Trans.* **1998**, 4147-4154.

3. Oszczapowicz, J.; Wawer, I.; Dargatz, M.; Kleinpeter, E. *J. Chem. Soc., Perkin Trans. 2* **1995**, 1127-1131.

4. Yoshifuji, M.; Toyota, K.; Shibayama, K.; Inamoto, N. *Chemistry Letters* **1983**, 1653-1656.

5. Smith, M. B.; March, J. *March's Advanced Organic Chemistry*; Wiley-Interscience: Toronto, 2001.

6. Sheldrick, G. *SHELXS-97* University of Gottingen, 1997.

7. Altomare, A.; Cascarano, G.; Giacovazzo G.; Guagliardi A.; Burla M.C.; Polidori, G.; Camalli, M. *J. Appl. Cryst.* **1994**, *27*, 435.

8. Sheldrick, G. *SHELXL-97* University of Gottingen, 1997.

9. Weber, L. *Eur. J. Inorg. Chem.* **2000**, 2425-2441.

10. Paasch, K.; Nieger, M.; Niecke, E. *Angew. Chem., Int. Ed. Engl.* **1995**, *34*(21), 2369-2371.

11. Fuchs, E.; Krebs, F.; Heydt, H.; Regitz, M. *Tetrahedron* **1994**, *50* , 759.

12. Chernega, A. N.; Antipin, M. Yu.; Struchkov, Yu. T.; Boldescul, I. E.; Sarina, T. V.; Romanenko, V. D. *Ukr. Khim. Zh.* **1985**, *51*, 868-874.

13. Chernega, A. N.; Antipin, M. Y.; Struchov, Y. T.; Bodesu, I. E.; Sarina, T. V.; Romanenko, V. D. *Dokl. AKAD. Nauk SSSR* **1984**, *278*, 365-370.

14. Ziemer, B.; Rabis, A.; Steinberger, H.-U. *Acta Crystallogr., Sect. C (Cr. Str. Comm.)* **2000**, *56*, e58.

15. Ammon, H. L.; Mazzocchi, P. H.; Regan, M. C.; Collicelli, E. *Acta Crystallogr.* **1976**, *B35*(7), 1722-1724.

16. Klebach, T. C.; Lourens, R.; Bickelhaupt, F.; Stam, C. H.; van Herk, A. *J. Organomet. Chem.* **1981**, *210*, 211-221.

17. van der Knaap, Th. A.; Klebach, Th. C.; Visser, F.; Bickelhaupt, F.; Ros, P.; Baerends, E. J.; Stam, C. H.; Konijn, M. *Tetrahedron* **1984**, *40*(4), 765-776.

Chapter 6

Group 6 metal carbonyl complexes of monophosphaamidines

6.1 Introduction

As mentioned in Chapter 2, there are numerous coordination modes for both amidines and phosphaalkenes. In reactions with group 6 metal carbonyls, simple phosphaalkenes form σ-bonded metal complexes that are coordinated to the phosphorus lone pair. Generally, these ligand displacement reactions take place under mild conditions, via the metal carbonyl, $LM(CO)_5$ (L = THF, η^2-cyclooctene, Figure 6.1).

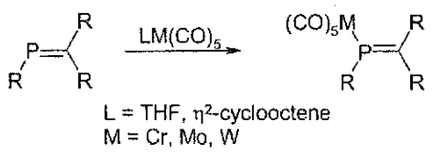

Figure 6.1 Ligand displacement reactions to form phosphaalkene metal complex

Under forcing conditions, amidines react with group 6 metal carbonyls in a different fashion. When *N,N'*-diphenylbenzamidine **62** is refluxed with $Mo(CO)_6$ in light petroleum (bp 100-120 °C) the quadruply-bonded $Mo_2(C_6H_5C(NC_6H_5)_2)_4$ complex **69** is formed (Figure 6.2).[1]

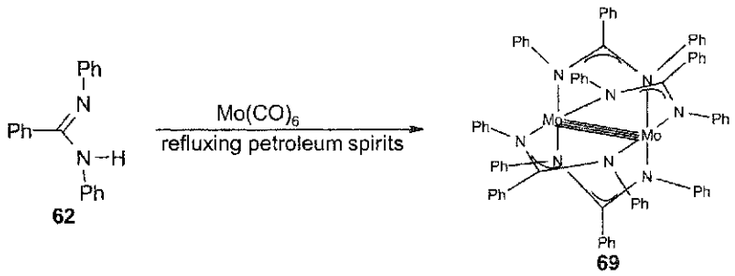

Figure 6.2 Reaction of *N,N'*-diphenylbenzamidine with $Mo(CO)_6$

However, reaction of our bulky amidines, **7**, **8**, **9**, **10**, with $Mo(CO)_6$ in refluxing *n*-heptane gave two products (Figure 6.3): (1.) An η^6-half sandwich, "piano-stool"

$LMo(CO)_3$ complex, coordinated to the aromatic ring attached to the imino nitrogen A, R = *p*-$CH_3C_6H_4$ **193**, *p*-$CH_3OC_6H_4$ **194**, CH_3 **195** and CF_3 **196**, or (2.) An $LMo(CO)_5$ complex **68** σ-bonded to the lone pair on the imino nitrogen (coordination type **A**, Figure 2.27), isolated as an intermediate on the way to the more thermodynamically stable $LMo(CO)_3$ complex **195**.

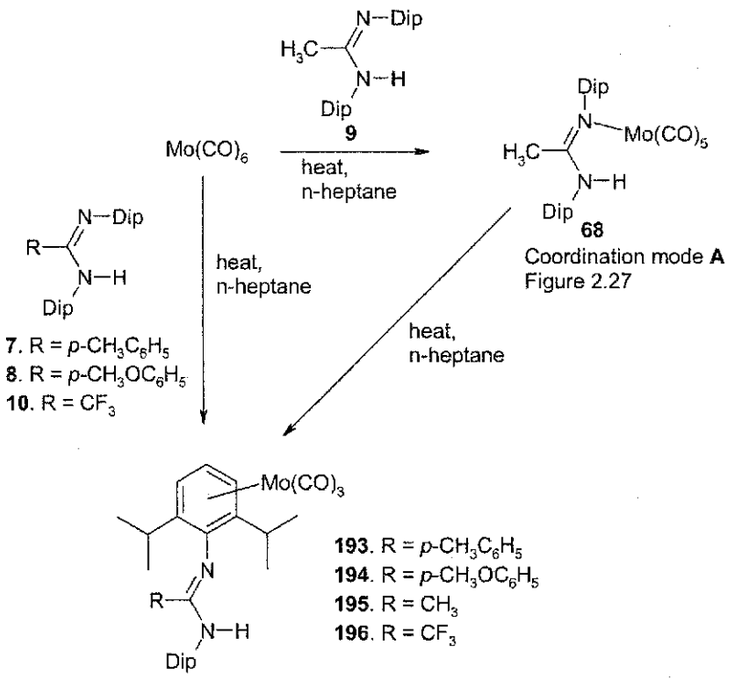

Figure 6.3 Thermal reaction of bulky *N,N'*-amidines with $Mo(CO)_6$

To determine the effects that the phosphorus atom would have on the coordination chemistry of the amidine core, we repeated the reactions performed with the *N,N'*-Dipamidines by reacting the *N,P*-phosphaamidines with molybdenum, chromium and tungsten hexacarbonyls.

6.2 Synthesis of $(CO)_5$Mo-*N,P*-phosphaamidines

We deliberately chose to react our phosphaamidines under identical conditions to the bulky *N,N'*-Dipamidine complexes.[2,3] Whereas the latter formed η^6-arene 'piano stool' complexes as the thermodynamically favored product, our phosphaamidines form σ-bonded η^1-metal pentacarbonyls. Following the reaction conditions outlined for the synthesis of the *N,N'*-Dipamidines,[2,3,4] one equivalent of molybdenum hexacarbonyl was combined with the phosphaamidine **20** or **21** in refluxing *n*-heptane (Figure 6.4).

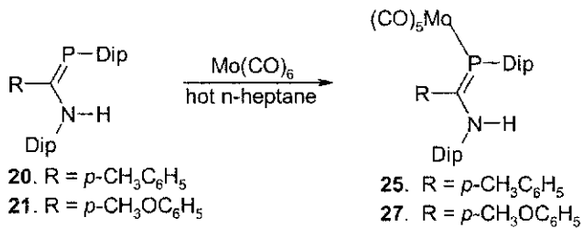

20. R = *p*-$CH_3C_6H_5$
21. R = *p*-$CH_3OC_6H_5$

25. R = *p*-$CH_3C_6H_5$
27. R = *p*-$CH_3OC_6H_5$

Figure 6.4 Thermal reaction of $Mo(CO)_6$ with phosphaamidines 20 and 21

The reaction progress could be followed by solution IR. As the single $Mo(CO)_6$ band decreased in intensity (approx. 1989 cm^{-1}), the four peaks related to a pentacarbonyl complex with an unsymmetrical ligand increased in integrated intensity (Figure 6.5).

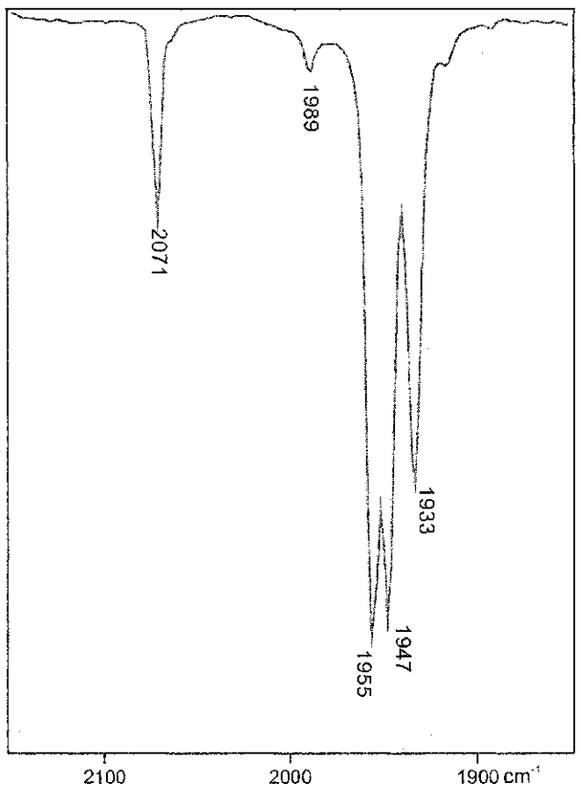

Figure 6.5 Four-peak IR spectrum seen for 27. Peak at 1989 cm^{-1} is a small amount of $Mo(CO)_6$ impurity.

The reaction was stopped once the $Mo(CO)_6$ peak was no longer present by solution IR. Filtration of the crude product solution through a bed of celite removed dark impurities to give a bright yellow solution. Cooling to –30 °C gave very small yellow crystals that were pure by solution IR and ^1H NMR. X-ray quality crystals were produced by dissolving the crystals in a minimum of room temperature *n*-heptane and cooling to –30 °C. This gave larger, more uniform yellow blocks. Attempts to see if the $Mo(CO)_5$-L product could be thermally driven to $Mo(CO)_3$-L, as seen in the *N,N'*-Dipamidine case, were performed by further heating the pentacarbonyl complex in refluxing *n*-heptane. This resulted in the complete loss of carbonyl peaks in the solution IR after 6 hours of

reflux. In addition, the solution appeared to darken with the appearance of solids (Mo metal). Loss of $Mo(CO)_5$ was confirmed by filtering off the solids and running a ^1H NMR on the filtrate after removal of solvent and dissolving in $CDCl_3$. Only the free ligand 7 and some hydrolysis products were apparent in the spectrum (Figure 6.6).

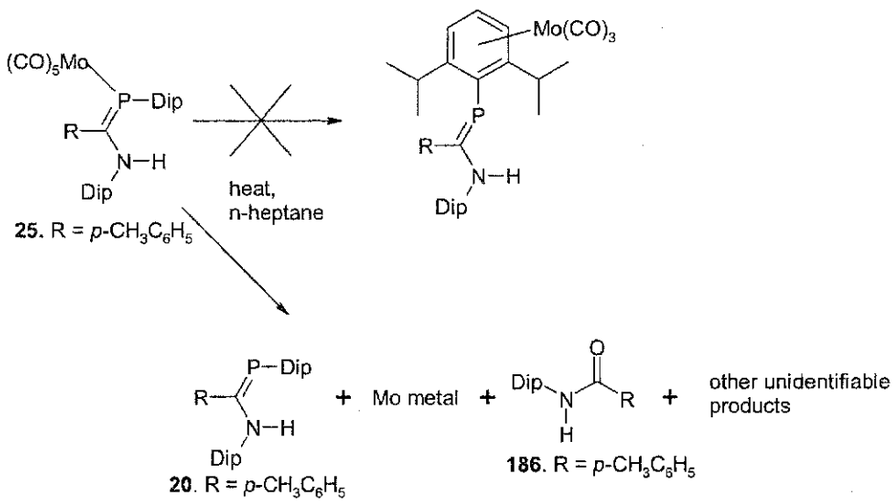

Figure 6.6 Thermal decomposition of phosphaamidine-Mo(CO)$_6$ complex

6.3 Synthesis of $(CO)_5$M-*N,P*-phosphaamidines, M= Cr, W

The reaction of molybdenum hexacarbonyl with phosphaamidine 7 was repeated with both chromium hexacarbonyl and tungsten hexacarbonyl. Unfortunately these reactions were much slower, taking over 5 days for most of the $Cr(CO)_6$ to be consumed and over 15 days for most of the $W(CO)_6$ to be consumed. Attempts to isolate material from these reactions were fruitless due to the lack of product remaining, most likely due to the decomposition of the pentacarbonyl complex over the long reaction times.

Much work has been done using $M(CO)_5$·THF (M = Cr, Mo, W) as a more reactive metal precursor to $Mo(CO)_5$-L phosphine complexes.[5] THF is a considerably more labile

ligand than C≡O, allowing displacement by the phosphine ligand to happen much more readily. Thus these reactions usually take place at room temperature, making thermal decomposition less of a problem.

The $M(CO)_5$·THF (M = Cr, W) complex is easily made by dissolving the metal hexacarbonyl in dry THF under an inert atmosphere and irradiating the solution with UV light. Almost immediately the solution takes on a light brown color, and by following the reaction by solution IR, the reaction can be stopped at the point of mono-substitution. This solution can then be added directly to the ligand and after stirring overnight, solution IR shows complete conversion to the $M(CO)_5$-*N*,*P*-phosphaamidine complex (Figure 6.7).

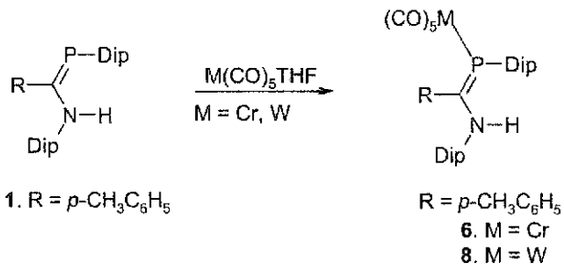

1. R = *p*-$CH_3C_6H_5$

R = *p*-$CH_3C_6H_5$
6. M = Cr
8. M = W

Figure 6.7 Ligand displacement reaction to form chromium and tungsten pentacarbonyl complexes

After removal of THF, the $W(CO)_5$-phosphaamidine complex **8** was taken up in a minimum of hot *n*-heptane and cooled to –30 °C. Yellow crystals formed which were pure by ^{1}H NMR and solution IR. Analytically pure crystals were grown from a room temperature saturated *n*-heptane solution slowly cooled to –30 °C. *n*-Heptane solutions of the $Cr(CO)_5$-phsosphaamidine complex **6** tended to grow feather-like crystals, pure by ^{1}H NMR and solution IR, but were unsuitable for X-ray crystallography. Recrystallization from a concentrated diethyl ether solution cooled to –30 °C gave yellow blocks suitable for crystallographic work.

6.4 NMR Spectroscopy

Selected ^{1}H, ^{31}P NMR and IR data have been compiled in Table 6.1 below.

Table 6.1 Selected ^{1}H and ^{31}P NMR data for the major isomers of 20 and 21 and their metal complexes

		20	**24**	**25**	**26**	**21**	**27**
^{1}H NMR							
$^{i}Pr - CH_3$ **A** (amino)	δ (^{1}H)	0.81	0.79	0.87	0.88	0.83	0.88
	$^{3}J_{HH}$, Hz	6.7	6.7	6.6	6.7	6.9	6.7
$^{i}Pr - CH_3$ **B** (amino)	δ (^{1}H)	0.89	0.92	0.97	0.97	0.92	0.98
	$^{3}J_{HH}$, Hz	6.7	6.9	6.7	6.7	6.9	6.9
$^{i}Pr - CH_3$ **C** (phosphino)	δ (^{1}H)	1.27	1.29	1.36	1.36	1.27	1.36
	$^{3}J_{HH}$, Hz	6.7	6.7	6.7	6.7	6.7	6.7
$^{i}Pr - CH_3$ **D** (phosphino)	δ (^{1}H)	1.35	1.40	1.45	1.47	1.36	1.45
	$^{3}J_{HH}$, Hz	6.9	6.7	6.7	6.7	6.9	6.7
R = *p*-CH_3, *p*-CH_3O **E**	δ (^{1}H)	2.22	2.15	2.23	2.23	3.70	3.71
	$^{7}J_{PH}$, Hz		1.8	1.8	1.8		
$^{i}Pr - H$ **F** (amino)	δ (^{1}H)	3.00	2.96	3.02	3.02	3.00	3.01
	$^{3}J_{HH}$, Hz	6.7	6.6	6.7	6.8	6.8	6.6
$^{i}Pr - H$ **G** (phosphino)	δ (^{1}H)	3.84	3.91	4.01	3.99	3.85	4.0
	$^{3}J_{HH}$, Hz	6.8	6.7	6.7	6.7	6.7	6.7
	$^{4}J_{PH}$, Hz	3.4				3.4	
N-H **O**	δ (^{1}H)	6.23	6.43	6.45	6.45	6.24	6.45
	$^{3}J_{PH}$, Hz	2.4				2.4	
^{31}P NMR	δ (^{31}P)	53.4	45.0	30.2	6.0	51.4	29.6
	$^{1}J(^{183}W\text{-}^{31}P)$				255		

All four metal complexes have ^{1}H NMR spectra that are extremely similar to the major isomers of their respective free ligands. This indicates that the metal selectively reacts with the Z-anti isomer of the free ligand, and not with the other minor isomers in solution. There are only slight shifts of the ^{i}Pr-C*H* and CH_3 signals and chemical shifts for the *p*-CH_3 and *p*-CH_3O protons are virtually unchanged. The N-*H* proton exhibited the largest change in the ^{1}H NMR, shifting approximately 0.2 ppm downfield from the parent ligand, in all of the metal complexes. Also, the ^{4}J(P-H) coupling the phosphino ^{i}Pr-C*H* septet experiences is larger. Since all of the metal complexes crystallize in the Z-anti (P=C) geometry (Chapter 5) and isomerization of the metal complexes in solution is

highly unlikely, we can assume that the major isomer present in the ^{1}H NMR of the parent ligand is indeed the Z-anti (P=C).

2-D ^{1}H-^{1}H correlation NMR spectroscopy confirms that the CH_3 bear the same relationship to the CH signals in the metal complexes as observed in the free ligand. Therefore the correspondence in the ^{1}H NMR spectra is not simply accidental, but implies the same stereochemistry of the ^{i}Pr groups in both sets of compounds.

However, there were noticeable changes in the ^{31}P NMR spectra. The ^{31}P chemical shift for **21** is 51.4 ppm and upon coordination to molybdenum pentacarbonyl the phosphorus signal is shifted over 20 ppm upfield to 29.6 ppm. In the case of **20**, the ^{31}P chemical shift of the parent ligand is 53.6 ppm, and when coordinated to molybdenum pentacarbonyl, the phosphorus signal is also shifted up-field to 30.2 ppm. When **20** is coordinated to chromium pentacarbonyl the phosphorus signal is only slightly shifted upfield to 45.0 ppm. When **20** is coordinated to tungsten pentacarbonyl, the ^{31}P NMR signal shifts nearly 50 ppm from the free ligand, to 6.0 ppm. The phosphorus is also coupled to the spin-1/2 ^{183}W ($J(P\text{-}^{183}W) = 255$ Hz), giving a less intense doublet, due to ^{183}W being only 14.3% abundant, in addition to the main signal. This coupling constant is similar to other low-coordinate P=C systems and the tungsten pentacarbonyl complex of the primary phosphane, Mes^*PH_2 **158** (Figure 6.8, Table 6.2).[6]

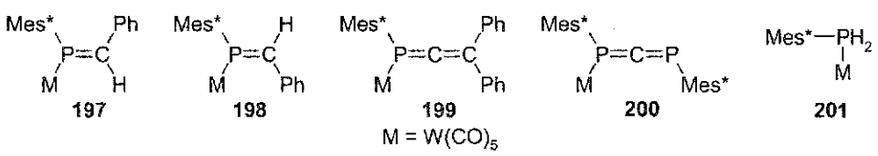

Figure 6.8 Various P=C systems and primary phosphane 201 coordinated to $W(CO)_5$

Table 6.2 Observed ^{1}J(W-P) coupling for 26 vs other W(CO)$_5$ complexes

	26	**197**	**198**	**199**	**200**	**201**
^{1}J(W-P) (Hz)	255	273.4	271.0	268.6	238.0	227.1

A trend can also be noted from the signals of **24**, **25** and **26** (Figure 6.9). As the metal is changed from Cr to Mo to W, the ^{31}P NMR signal moves significantly upfield. While it is not entirely clear what contributes to the change in the ^{31}P NMR signals, such trends have been well established for tertiary phosphanes.[7] More recently, Yoshifuji has correlated the ^{31}P NMR chemical shifts of several low-coordinate, P=C and P=P, phosphorus complexes (CO)$_5$M-L (M = Cr, Mo, W) complexes.[6] The Yoshifuji data has been ignored, as the exact chemical shifts were not reported in the paper, nor were many of the references reported for the compounds used. Although the PR$_3$ compounds below are not phosphaalkene-type systems, our results fit reasonably well with the data.

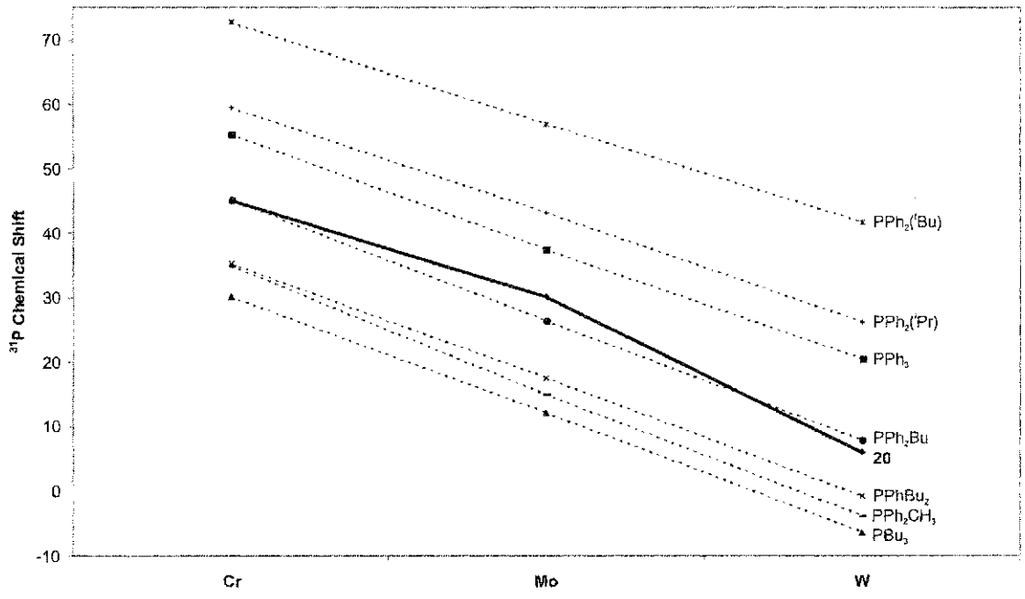

Figure 6.9 Trends seen in the ^{31}P NMR chemical shifts of group 6 metal pentacarbonyl complexes. Bold line represents trend for phosphaamidine ligand 20

As can be seen in Figure 6.9, **24**, **25** and **26** follow the trends of the tertiary phosphane metal complexes. Slight deviations can be noted, which could possibly be attributed to the slight changes in the pyramidalization of the phosphorus center (See Chapter 5).

6.5 IR spectroscopy

Selected IR data for metal complexes **24**, **25**, **26** and **27** are presented in Table 6.3, along with the phosphaamidine ligands **20** and **21** for comparison purposes. Note that ν(N-H) is unchanged between the ligands and the metal complexes, indicating that there is little or no perturbation of the N-H bond upon coordination.

The IR spectra of the metal complexes are dominated by C≡O stretches from the metal carbonyl. With this data, the relative *trans*-influence of phosphaamidines **20** and **21** can be qualitatively ranked with respect to other ligands. This ranking can be accomplished by analyzing the low-energy band of the four νC≡O stretches in the IR spectrum. This low-energy band is caused by the A_1 stretching normal mode of vibration, which is dominated by the contribution of the stretch of the carbonyl group that is *trans* to the ligand (Figure 6.10).

Table 6.3 Selected IR data: ν(N-H) and ν(C≡O) stretches

IR	**20**	**21**	**24**	**25**	**26**	**27**
v(CO) (*n*-heptane)			2063, 1949, 1934, 1912	2071, 1955, 1948, 1933	2070, 1948, 1939, 1929	2071, 1955, 1947, 1933
v(CO) ($CHCl_3$)				2071, 1949, 1939, 1914	2069, 1944, 1938, 1915	2071, 1949, 1940, 1915
v(N-H) (*n*-heptane)	3354	3354	3351	*	*	*
v(N-H) ($CHCl_3$)	3350	3350		3349	3349	3350

* Unable to obtain data due to low solubility in *n*-heptane

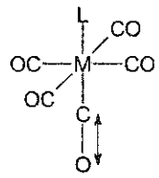

Figure 6.10 The A_1 stretch of the carbonyl group *trans* to ligand L.

In Table 6.4, **20** and **21** have been ranked with respect to their *trans*-influence vs other group 15 ligands. *Trans*-influence effects are caused by a combination of σ-donation and *dπ-pπ**-backbonding of the ligand (Figure 2.12). To what extent σ-donation and *dπ-pπ**-backbonding each contribute to the *trans*-influence varies with each ligand. If the ligand is a strong σ-donor, the *trans* C≡O stretch will become lower in energy because there is more electron density on the metal, which allows more effective π-backbonding to the carbonyl ligand. But, if the *dπ-pπ**-backbonding is stronger for the ligand, the *trans* C≡O stretch will become higher in energy.

Table 6.4 *ν*(C≡O) of Group 15 $Mo(CO)_5L$ compounds, listed in decreasing *trans*-influence

$Mo(CO)_5L$	A1(1)	B2	E	A1(2)	Comments	Reference
PCl_3	2095		1985	1999		8
$P(OPh)_3$	2083		1963	1975		8
$P(OCH_3)_3$	2080	1993	1952	1965		8
2,4,6-triphenylphosphabenzene	2079		1962	1962	overlap of E and A_1	9
$BiPh_3$	2078		1960	1960	overlap of E and A_1	8
PPh_3	2073	1984	1952	1952	overlap of E and A_1	8
PEt_3	2069		1941	1947		8
$AsEt_3$	2070	1983	1943	1943	overlap of E and A_1	8
PH_3	2081		1956	1925		9
Phosphaamidine **21**	2071	1949	1940	1915		this work
Phosphaamidine **20**	2071	1949	1939	1914		this work
N,N'-Dipamidine **9**	2072	1942	1931	1908		4
$P(t\text{-}Bu)_3$	2073		1944	1907		9
NCS-	2105	2073	1941	1876		8

For example, PCl_3 is a poor σ-donor due to the electronegative Cl atoms pulling electron density from the phosphorus lone pair. But at the same time, the electronegative

Cl atoms enhance the $d\pi$-$p\sigma^*$-backbonding by withdrawing electron density from the filled, metal *d*-orbitals to the empty *p*-orbitals of the ligand. In contrast, $P(^tBu)_3$ is a weaker π-acid than PEt_3, which can be attributed to steric effects, since electronic effects can be ruled out as Et and ^{t}Bu are very similar electronically. The bulky ^{t}Bu groups force the metal to be farther away from the ligand, weakening its σ-donation, which should give rise to a higher energy *trans* νC≡O stretch, thus the lower energy *trans* νC≡O stretch can only be attributed to the poorer $d\pi$-$p\pi^*$-backbonding capabilities. According to DFT calculations on the Z-anti structure of phosphaamidine **20** (Chapter 3), the σ-bonding capabilities of the phosphorus lone pair have been reduced due to delocalization of electron density from the phosphorus lone pair into the π-system of the P-Dip ring (Figure 6.11). With only this in mind, one would expect the electron density located on the metal center to be less than expected, giving rise to higher energy *trans* νC≡O stretches.

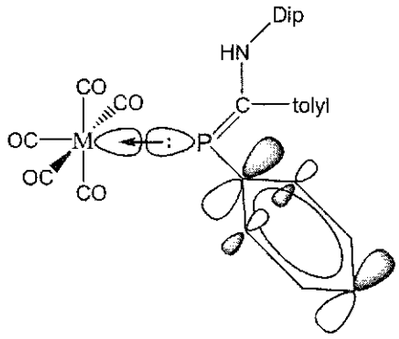

Figure 6.11 Decreased σ-donation by the phosphorus lone pair due to delocalization of electron density to the aryl π-system. Ortho ^{i}Pr groups have been omitted for clarity.

Since the *trans* νC≡O stretches of our phosphaamidines are quite low in energy, we must look at the $d\pi$-$p\pi^*$-backbonding capabilities of the ligand to explain why this happens.

Generally, there is a greater degree of $d\pi$-$p\pi^*$-backbonding character in simple phosphaalkene complexes than in tertiary phosphanes.[5]

In simple phosphaalkenes, the π^*-orbital shows essentially equal distribution between both phosphorus and carbon, allowing the metal *d*-orbitals to efficiently overlap with the π^*-orbital on phosphorus, giving rise to higher energy *trans* νC≡O stretches (Figure 6.12). However, DFT calculations on the Z-anti form of **20** show that the larger coefficient of the π^*-orbital is on carbon and *not* on phosphorus, thus decreasing the overlap between the filled metal *d*-orditals and the π^*-orbital on phosphorus, which gives rise to lower energy *trans* νC≡O stretches (Figure 6.13).

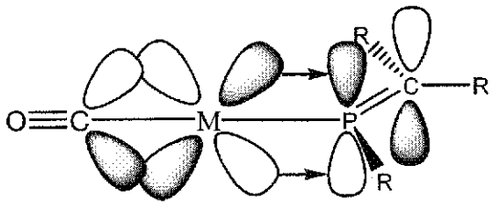

Figure 6.12 Efficient $d\pi$-$p\pi^*$-backbonding in simple phosphaalkenes due to equal distribution of the π^*-orbital on both phosphorus and carbon

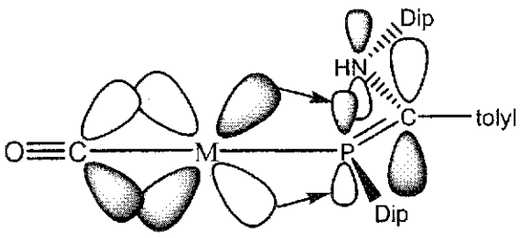

Figure 6.13 Poor $d\pi$-$p\pi^*$-backbonding in phosphaamidines due to the small coefficient on phosphorus in the π^*-orbital

In summary, we can conclude that our phosphaamidines are poor σ-donors via the phosphorus lone pair, and have poor $d\pi$-$p\pi^*$-backbonding properties when compared to simple phosphaalkenes. We are currently in the process of making group 6 metal

carbonyl complexes of a Dip-P-substituted phosphaalkene in order to obtain futher evidence for this effect.

6.6 X-ray crystallography

Dissolving the pure crystals of **25**, **26** and **27** in a minimum of room temperature *n*-heptane and cooling to –30 °C gave beautiful yellow blocks that were appropriate for crystallographic work. X-ray quality crystals of **24** were grown from a cooled (-30 °C), saturated solution in diethyl ether. Crystals were sent to Dr. Gotthelf Wolmershäuser of the Fachbereich Chemie at the Universität Kaiserslautern, Germany for collection of X-ray intensity data. The structure was solved by Patterson methods using SHELXS[10], and refined using SHELXL[11] by standard full-matrix least squares methods. Hydrogen atoms were fixed on the aromatic rings so that the coordinates ride on the corresponding aromatic carbon coordinates. ^{i}Pr C-H hydrogen atoms were fixed for idealized tertiary C-H's with all X-C-H angles equal with a riding model refinement. ^{i}Pr methyl groups were fixed with ideal tetrahedral angles with the C-H distances allowed to vary while allowing the CH_3 group to rotate. Temperature factors were set to 1.5 (CH_3 groups), 1.2 (CH groups) or 1.2 (Ar-H) times the equivalent isotropic temperature factor of the corresponding carbon atoms. The amino hydrogen on all of the metal derivatives were found on the difference Fourier map, and allowed to freely refine. Compounds **24**, **25**, **26** and **27** all crystallize in the triclinic space group P-1, with two molecules per unit cell. Complexes **24**, **25** and **26** are isostructural, meaning that the atoms are in the same position of the unit cell for each molecule. Agreement factors of $R_1 = 0.0292$, $wR_2 = 0.0674$ were found for **25**, $R_1 = 0.0406$, $wR_2 = 0.0920$ for **27**, $R_1 = 0.0402$, $wR_2 = 0.0931$ for **24** and $R_1 = 0.0540$, $wR_2 = 0.1300$ for **26**. ORTEP diagrams are shown in Figure 6.14

(**25**), Figure 6.15 (**24**), Figure 6.16 (**26**) and Figure 6.17 (**27**). Crystal data and structure refinement parameters are included in the appendix as Table A.16 (**25**), Table A.21 (**26**), Table A.26 (**27**) and Table A.31 (**24**). Crystallographic data are also included in the appendix as Tables A.17-A.20 (**25**), A.22-A.25 (**26**), A.27-A.30 (**27**) and A.32-A.36 (**24**).

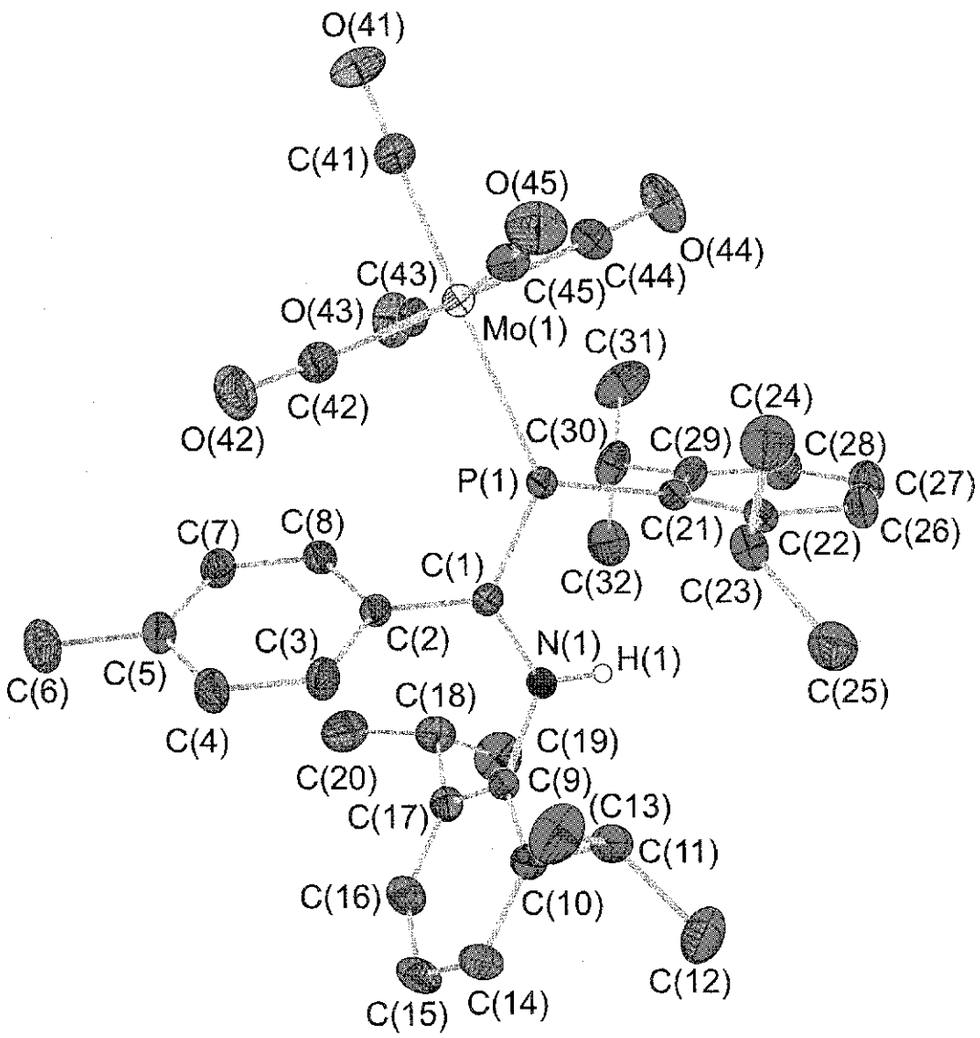

Figure 6.14 An ORTEP diagram (25% probability) of the crystal structure found for 25 with the atom numbering scheme. Hydrogen atoms on carbon are omitted for clarity.

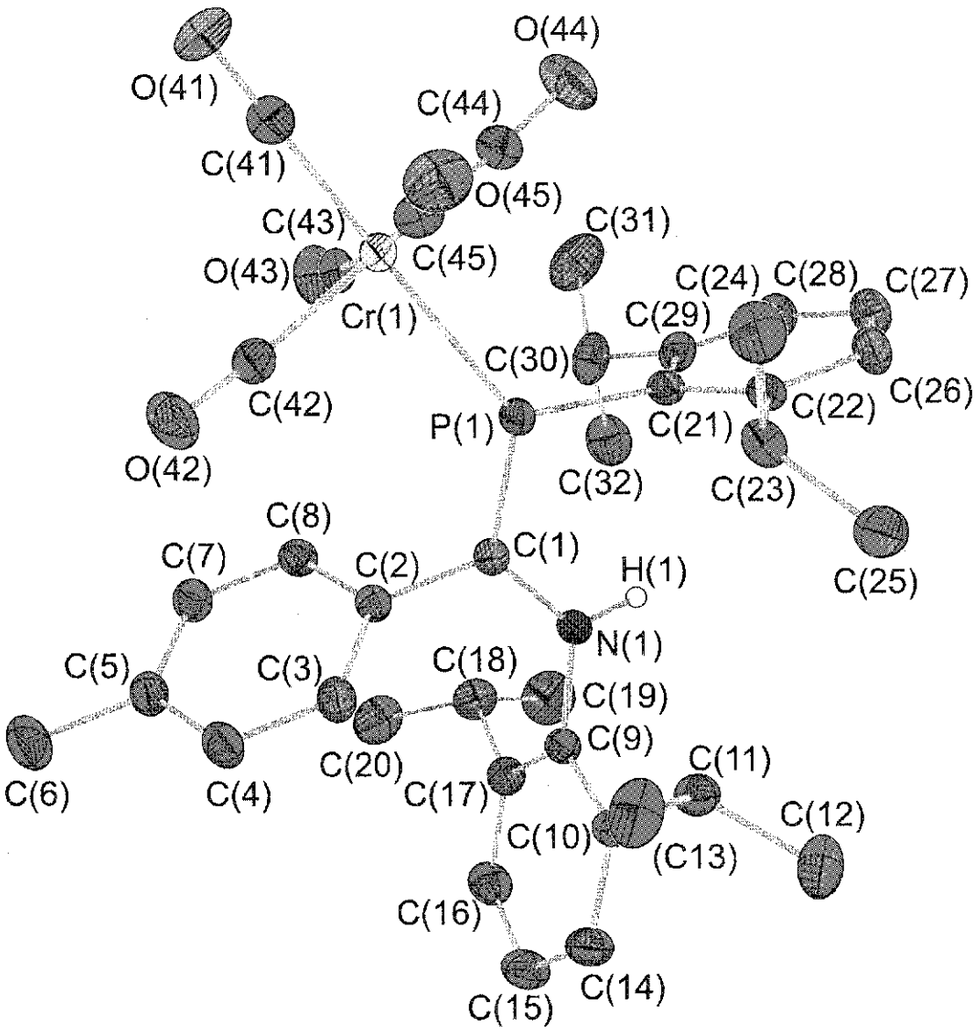

Figure 6.15 An ORTEP diagram (25% probability) of the crystal structure found for 24 with the atom numbering scheme. Hydrogen atoms on carbon are omitted for clarity.

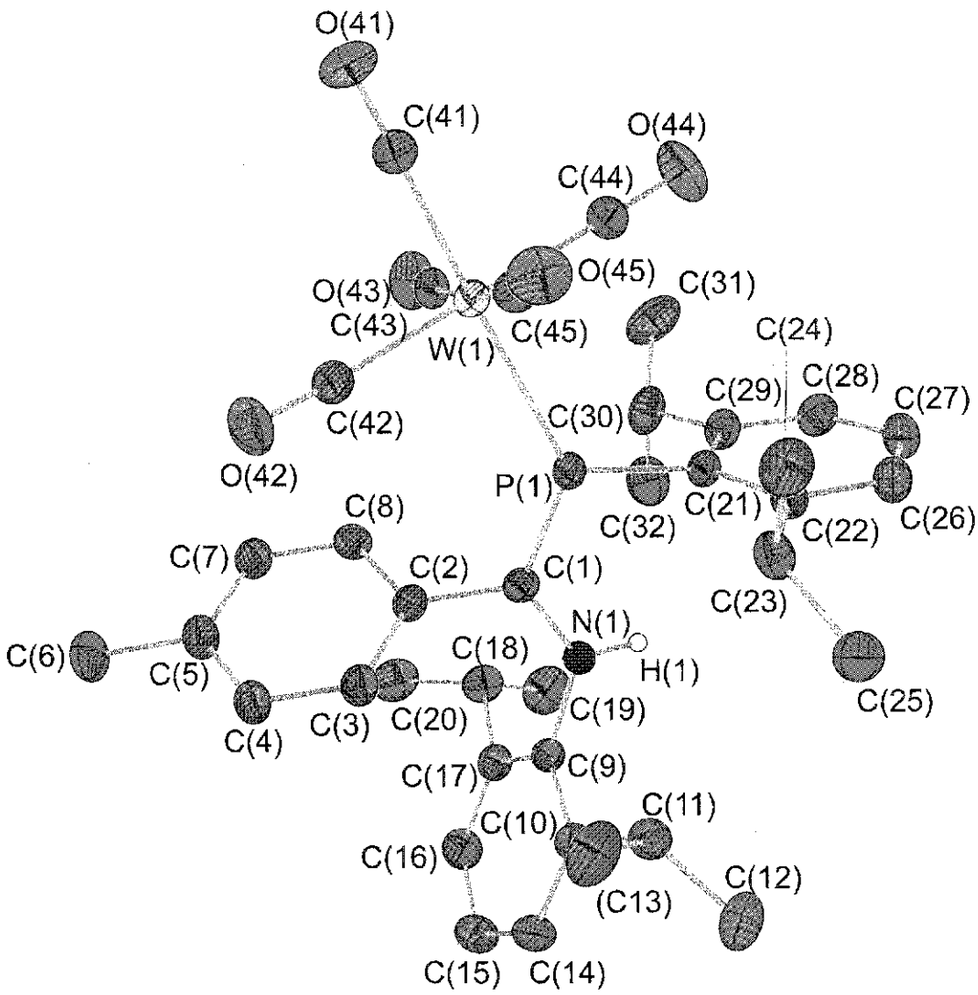

Figure 6.16 An ORTEP diagram (25% probability) of the crystal structure found for 26 with the atom numbering scheme. Hydrogen atoms on carbon are omitted for clarity.

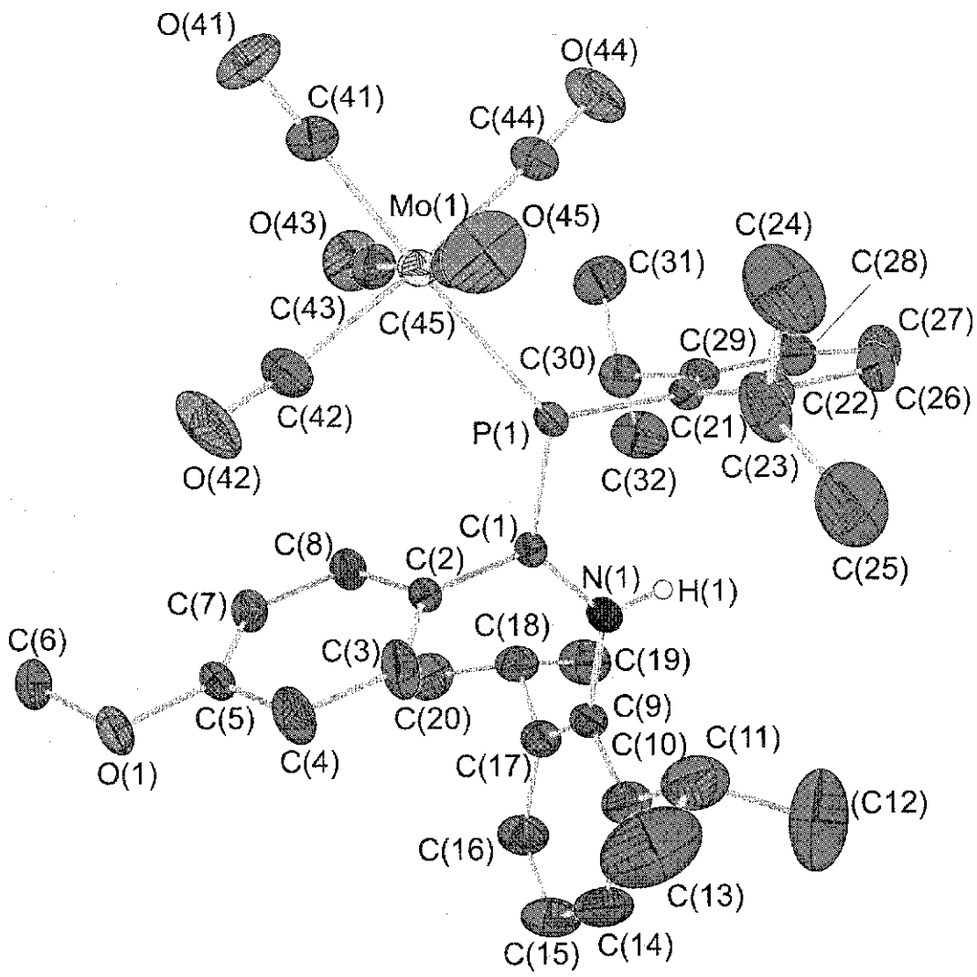

Figure 6.17 An ORTEP diagram (25% probability) of the crystal structure found for 27 with the atom numbering scheme. Hydrogen atoms on carbon are omitted for clarity.

In the solid state, all metal complexes retain the same Z-anti (P=C) geometry of their respective parent ligands, with the metal pentacarbonyl coordinated to the phosphorus lone pair. A table of selected bond lengths has been included below (Table 6.5). What is remarkable is how similar the structures of the coordinated ligands are to those found in the X-ray structures of the free ligands (Chapter 5). Upon coordination, the P=C double bond is slightly shortened (1.10 % or less), indicating that there is electron donation to the metal center. The N-C single bond is also shortened, especially in the case of **26** (1.86 %), indicating that there is enhanced conjugation in the P=C-N system due to the lowered electron density in the P=C bond. The P-C_{Ar} bond is correspondingly shortened in the solid state, possibly due to the electron donation to the phosphorus-metal bond.

Table 6.5 Selected Bond lengths (Å) and angles (°) for phosphaamidines 20 and 21, and their metal carbonyl complexes

	20	**24**	**25**	**26**	**21**	**27**
P=C	1.709(2)	1.700(2)	1.706(2)	1.705(5)	1.716(2)	1.697(3)
% shortening of P=C bond		0.53	*	*		1.10
P-C_{Ar}	1.847(2)	1.836(2)	1.841(2)	1.836(6)	1.849(2)	1.837(3)
C-N	1.368(2)	1.363(3)	1.364(3)	1.343(8)	1.366(3)	1.360(4)
% shortening of C-N bond		*	*	1.86		*
P-M		2.4260(7)	2.561(1)	2.538(2)		2.5561(8)
C-P-C angles	101.9(1)	106.8(1)	106.8(1)	107.0(3)	103.6(1)	106.3(1)
Sum of angles around P		358.19(8)	358.75(8)	358.4(3)		360.0(1)

*Within experimental error.

Similar to the silyl phosphane, DipP(TBDMS) **17** and both phosphaamidines **20** and **21**, the phosphorus atom and the *ipso* carbon are bent out of the mean aryl plane, but now the phosphorus atom of the phosphaamidine ligand **20** in metal complexes **24**, **25** and **26** have a large deviation, whereas the phosphorus atom in the phosphaamidine ligand **21** in the metal complex **27** is only slightly out of the mean aryl plane. These deviations have

been compiled in Table 6.6. Packing diagrams show no contacts shorter than normal van der Walls' radii.

Table 6.6 Least squares plane deviations (Å) of phosphorus atom P(1) and *ipso* carbon atom C(21)

	20	**24**	**25**	**26**	**21**	**27**
deviation of P(1) from: mean aryl plane C(22)-C(26)-C(27)-C(28)-C(29)	-0.1729 (53)	0.3416 (48)	-0.3242 (48)	-0.3209 (139)	0.3035 (59)	-0.0621 (68)
deviation of ipso carbon C(21) from: Mean aryl plane C(22)-C(26)-C(27)-C(28)-C(29)	-0.0053 (34)	0.0397 (32)	-0.0320 (32)	-0.0319 (92)	0.0246 (38)	0.0093 (41)
C(1)-M(1)-C(21) plane M = Cr, Mo, W		0.1512 (13)	0.1274 (12)	0.1411 (31)		0.0253 (16)

When the simple phosphaalkene MesP=CPh_2 **41** is coordinated to $Cr(CO)_5$, the P=C bond is also shortened slightly (0.77%) to 1.679(4) Å, from 1.692(3) Å in the parent phosphaalkene. The P-Cr bond is slightly longer for **24** than for $(CO)_5$-MesP=CPh_2 **56**, indicating that the phosphorus-chromium bond is weaker for **24**. This result is complemented by the well known '*trans* effect'. The Cr-C_{trans} bond length is shorter for **24** than $(CO)_5$-MesP=CPh_2 **56**, while the C_{trans}-O_{trans} bond length is longer for **24**. This implies that the overall electron density on the metal should be higher for **24**, caused by a combination of σ-donation and $d\pi$-$p\pi^*$-backbonding effects, which is in agreement with our IR data (Section 6.5). In agreement with the free ligands, the C-P-C bond angle is smaller for **24** (106.75(10) °) than $(CO)_5$Cr-MesP=CPh_2 **56**, where the C-P-C angle is 109.8°.

A recent DFT study on the parent phosphaamidines coordinated to group 6 metal carbonyls predicts that the phosphorus center becomes slightly pyramidalized upon coordination.[12] The sum of angles around phosphorus were calculated to be: Cr 348.9°, Mo 353.9°, W 350.9°. In our phosphaamidine systems, the phosphorus centers are not nearly as pyramidal, with the sum of angles between 358.19(25) for **24** and 359.95(32) for **27**. As expected, these values correspond to the deviations of the phosphorus atom from the C(21)-C(1)-M(1) (M = Cr, Mo, W) plane; the larger the deviation, the more pyramidal the phosphorus center is (Table 6.6).

6.7 Conclusion

The first systematic series of Cr, Mo and W coordinated phosphaamidines have been produced. The metal complexes are easily made and purified, and have been characterized by a full spectroscopic and structural investigation. Solution IR data show that these phosphaamidines have a weak ligand field strength when compared to other group 15 ligands. X-ray crystallography shows that both the metal complexes are remarkably similar to the parent ligands, indicating that the metals only slightly perturb the overall structure. The crystallographic data also shows that our phosphaamidines are weaker π-acceptors than simple phosphaalkenes, which is supported by their molecular orbital diagrams. Also important, is that the ^{1}H NMR data supports our assumption that the major isomer in solution of the parent ligand is indeed the Z-anti (P=C) structure, since all of the metal complexes crystallize in the Z-anti (P=C) form and isomerization of these metal complexes in solution is highly unlikely. We are currently in the process of producing a series of group 6 metal carbonyl complexes of a Dip-P-substituted

phosphaalkene so we have a *full* series of simple phosphaalkene molecules to directly compare to our phosphaamidine complexes.

Reference List

1. Cotton, F. A.; Inglis, T.; Kilner, M.; Webb, T. R. *Inorg. Chem.* **1975**, *14*(9), 2023-2026.

2. Boeré, R. T.; Klassen, V.; Wolmershauser, G. *J. Chem. Soc., Dalton Trans.* **1998**, 4147-4154.

3. Boeré, R. T.; Klassen, V.; Wolmershauser, G. *Can. J. Chem.* **2000**, *78*, 583-589.

4. Boeré, R. E.; Boeré, R. T.; Masuda, J.; Wolmershauser, G. *Can. J. Chem.* **2000**, *78*, 1613-1619.

5. Wilkinson, G.; Gillard, R. D.; McCleverty, J. A. *Comprehensive Coordination Chemistry ;* 1st ed. Pergamon Press: New York , 1987.

6. Yoshifuji, M.; Shibayama, K.; Hashida, T.; Toyota, K.; Niitsu, T.; Matsuda, I.; Sato, T.; Inamoto, N. *J. Organomet. Chem.* **1986**, *311*, C63-C67.

7. Nixon, J. F.; Pidcock, A. *Annual Review of NMR Spectroscopy*; Mooney, E. F., Editor; Academic Press Inc.: New York, 1969; Vol. 2.

8. Braterman, D. S. *Metal Carbonyl Spectra*; Academic Press: New York, 1975.

9. Deberitz, J.; Noth, H. *J. Organomet. Chem.* **1973**, *49*, 453-467.

10. Sheldrick, G. *SHELXS-97* University of Gottingen, 1997.

11. Sheldrick, G. *SHELXL-97* University of Gottingen, 1997.

12. Schoeller, W. W.; Rozhenko, A. B.; Grigoleit, S. *Eur. J. Inorg. Chem.* **2001**, 2891-2898.

Chapter 7

Synthesis of bulky *N,N',P* phosphaguanidine

7.1 Introduction

Since we had successfully isolated the bulky monophosphaamidine homologues to our bulky *N,N'*-amidines, we thought that the next logical step would be to isolate the monophosphorus analogue of our bulky *N,N',N''*-triarylguanidine **11**.

A common route to making guanidines is by the reaction of carbodiimides with amines. *N,N',N''*-triphenylguanidine **202** is made by combining aniline **191** and diphenylcarbodiimide **101** in refluxing toluene (Figure 7.1).[1]

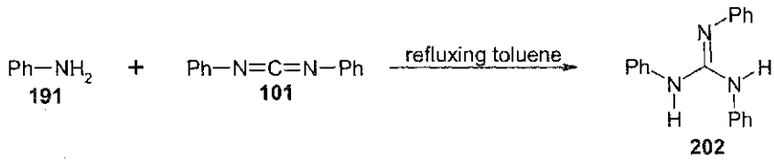

Figure 7.1 Synthesis of *N,N',N''*-triphenylguanidine

However, in attempting to synthesize *N,N',N''*-tris(2,6-diisopropylphenyl)guanidine **11**, thermal condensation did not work in refluxing toluene or xylenes.[2] We came up with two factors that could be hindering this reaction. First, the ortho alkyl groups cause the aryl rings to be slightly electron donating, making the central –N=C=N- carbon a poorer electrophile. Second, and more significantly, the ortho alkyl groups on both the aniline **12** and carbodiimide **204** sterically hinder the reaction. Both diphenylcarbodiimide **101** and bis(2,6-diisopropylphenyl)carbodiimide **204** have been structurally optimized using AM1 parameters, as implemented in Gaussian 98W[3], and pictures of these structures are shown below to substantiate this claim (Figure 7.2).

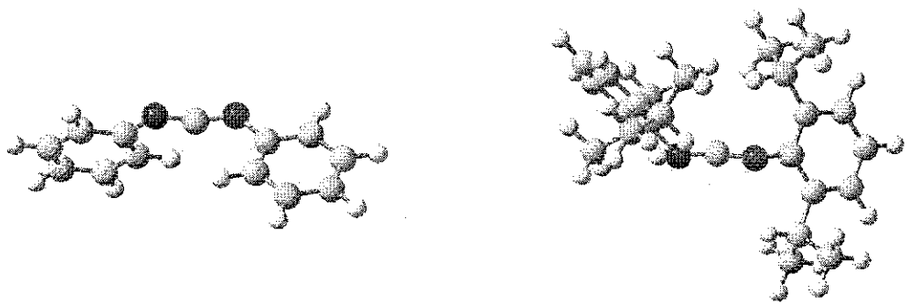

Figure 7.2 AM1 optimized structures of diphenylcarbodiimide 101 and bis(2,6-diisopropylphenyl)carbodiimide 204. Notice the increased steric bulk of the Dip groups

Instead we reacted the lithium anilide **203** with the Dipcarbodiimide **204** in refluxing THF. After quenching the reaction with water, the bulky guanidine **11** was produced (Figure 7.3).

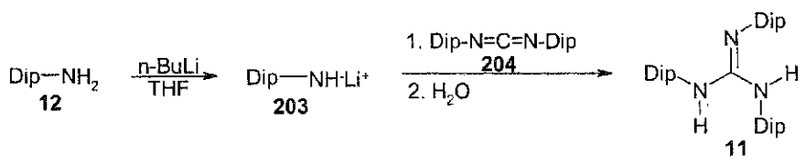

Figure 7.3 Synthesis of *N,N',N"*-tris(2,6diisopropylphenyl)guanidine 11 via lithium anilide route

7.2 Synthesis of *N,N',P*-tris(2,6-diisopropylphenyl)phosphaguanidine **28**

Following the synthetic route that we used for the synthesis of **11**,[2] we attempted the reaction of DipPH$^-$Li$^+$ with Dipcarbodiimide **203**. There are two possible isomers that can be formed: **A**, the phosphaguanidine with a P=C double bond, and **B**, the phosphaguanidine with an N=C double bond (Figure 7.4). Generally, P=C containing compounds are yellow/orange in color, whereas secondary phosphanes are typically colorless. Therefore, it would be expected that if isomer **A** was made the molecule would be colored, while isomer **B** should be colorless.

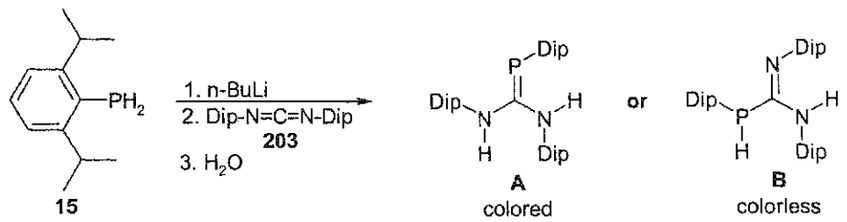

Figure 7.4 Two possible phosphaguanidine products

We reacted $DipPH_2$ **15** with a slight excess (5%) of *n*-BuLi in THF at 0 °C. The solution was allowed to warm to room temperature to ensure complete lithiation and cooled again. Then one equivalent of Dipcarbodiimide[4] **203** in THF was added dropwise to the lithium phosphide and the mixture was refluxed for two hours. Quenching with H_2O and removal of volatile components left an off-white solid. Recrystalization from hot ethanol gave the phosphaguanidine as colorless crystals. The colorless product provided the first evidence that we had produced the N=C isomer **B**.

7.3 Spectroscopy

7.3.1 NMR spectroscopy

The ^1H NMR spectrum (Figure 7.5) shows a singlet **F** occurring at 5.35 ppm corresponding to the N-*H* proton, and a doublet **E** occurring at 4.87 ppm (J(P-H) = 237 Hz), with one half of the doublet hidden under the N-*H* signal. A doublet with such a large coupling constant indicates that there *is* a hydrogen atom located on phosphorus. By implication, the molecule must have a P-C single bond, thus requiring a C=N double bond to be present and reinforcing the fact that isomer **B** was produced. The ^{i}Pr-C*H* peaks occur as two separate exchange broadened singlets, **C** and **D**, that each integrate to 2 protons, and one septet, **B**, integrating to two protons, that is partially overlapping the upfield exchange broadened singlet. The ^{i}Pr-CH_3 groups form a complex mixture of

broad singlets and sharp doublets **A** that integrate to the expected 24 protons. We have seen similar dynamic processes in our *N,N',N''*-Dipguanidine **11**, where one of the amino Dip groups undergoes slow exchange at room temperature, where the related ^{i}Pr-CH_3 groups become an exchange-broadened singlet, while the ^{i}Pr-CH_3 signals of the remaining imino and amino Dip groups appear as four sharp doublets. A similar process is occurring in our phosphaguanidine system, where we see five sharp doublets and one exchange broadened singlet with the same relative positioning as in **11**. However, it is unclear if it is the amino or phosphino Dip group that is exchanging at room temperature. Variable temperature NMR and 2-D NMR techniques are needed to sort out the complex signals of the ^{i}Pr groups.

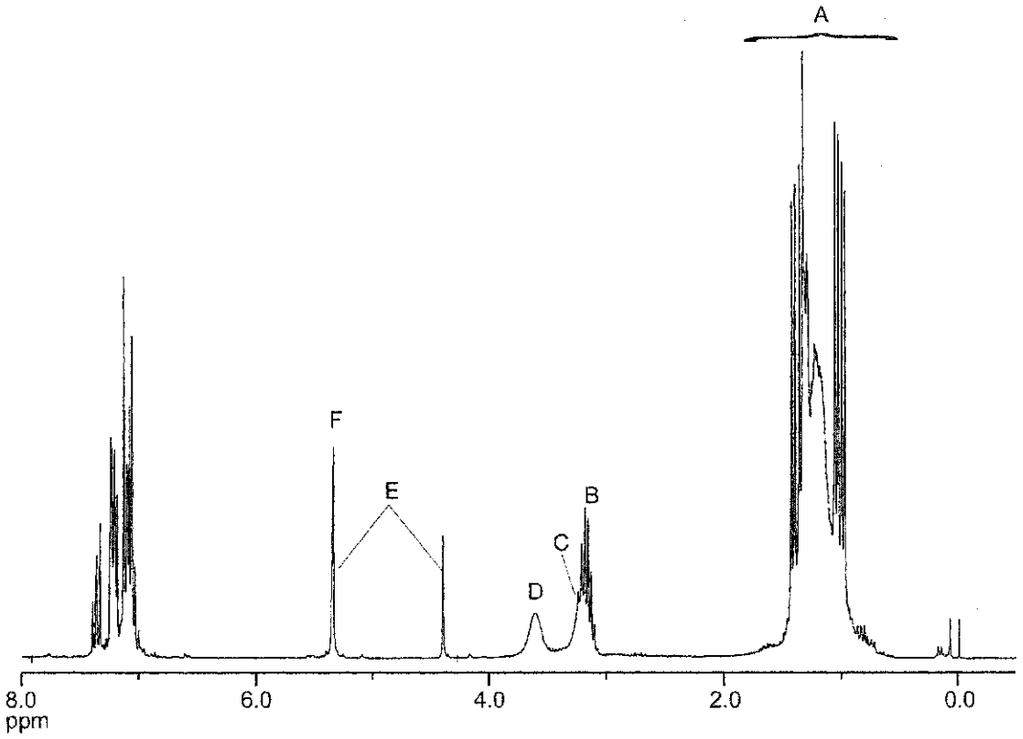

Figure 7.5 ^{1}H NMR spectrum of phosphaguanidine 28

There are also other small singlets and doublets with $^{1}J(P\text{-}H) = 237$ Hz in the 4.0-6.75 ppm range of the spectrum, indicating the possibility that there are very small amounts of other isomers present in solution. This cannot be said for certain, and additional experiments are needed to prove if the signals can be attributed to other isomers.

The proton coupled ^{31}P NMR shows one large doublet ($^{1}J(P\text{-}H) = 237$ Hz) at –94.8 ppm, confirming that the major species in solution is indeed the C=N form, **B**. The P-H coupling constant is within the range of known P-H phosphaguanidines (179 to 240 Hz) and the ^{31}P chemical shift is also within the range of secondary P-H phosphaguanidines (-29 to –85.9 ppm).[5,6,7,8,9] Furthermore, the chemical shift and coupling constant for **28** are similar to the values found for the P-H isomers of phosphaamidine **20** (δ ^{31}P NMR = -66 ppm and –80 ppm, $^{1}J(P\text{-}H) = 243$ Hz). There are several other small doublets present, reinforcing the fact that there are possibly other isomers in solution. There are also series of singlets between 10 and -10 ppm, indicating that there may also be P=C isomers in solution.

7.3.2 IR spectroscopy

IR spectroscopy shows that in the solid phase and in solution that there are both the P-H (2374 cm^{-1} KBr and 2373 cm^{-1} $CHCl_3$) and N-H (3385 cm^{-1} KBr and 3392 cm^{-1} $CHCl_3$) stretching bands, indicating that the P-H form, **B**, is not only isolated to the solution phase. The P-H stretch is slightly higher in energy than the *N*-monosilylated *N,N',P*-triphenylphosphaguanidine **104** (2350 cm^{-1})[5] and *N,N',P*-tri-^{t}Bu-phosphaguanidine **132** (2280 cm^{-1}),[6,7] while the N-H stretch is slightly lower in energy

than *N,N'*-di(*p*-tolyl)-*P,P*-diphenylphosphaguanidine **99** (3407 cm^{-1})[10] and *N,N',P*-tri-^{t}Bu-phosphaguanidine **132** (3400 cm^{-1})[6,7].

7.4 Crystal structure of *N,N',P*-phosphaguanidine **28**

X-ray quality crystals were obtained from a slowly cooled ethanol solution. Crystals were sent to Dr. Gotthelf Wolmershäuser of the Fachbereich Chemie at the Universität Kaiserslautern, Germany for collection of X-ray intensity data. The structure was solved by direct methods using SHELXS[11] and refined using SHELXL[12] by standard full-matrix least squares methods. Hydrogen atoms were fixed on the aromatic rings so that the coordinates ride on the corresponding aromatic carbon coordinates. ^{i}Pr-CH hydrogen atoms were fixed for idealized tertiary C-H's with all X-C-H angles equal, with a riding model refinement. ^{i}Pr methyl groups were fixed with ideal tetrahedral angles, with the C-H distances allowed to vary while allowing the CH_3 group to rotate. Temperature factors were set to 1.5 (CH_3 groups) or 1.2 (CH groups, Ar-H) times the equivalent isotropic temperature factor of the corresponding carbon atoms. Both the N-H and P-H hydrogens were found on the difference Fourier map, and were allowed to freely refine. **28** crystallizes in the monoclinic space group P2(1)/n, with four molecules per unit cell. Agreement factors of $R_1 = 0.0434$, $wR_2 = 0.0952$ were found. A numbered ORTEP diagram is shown in Figure 7.6, a packing diagram is shown in Figure 7.7 and crystallographic data are included in the appendix as Tables A.37-A.40.

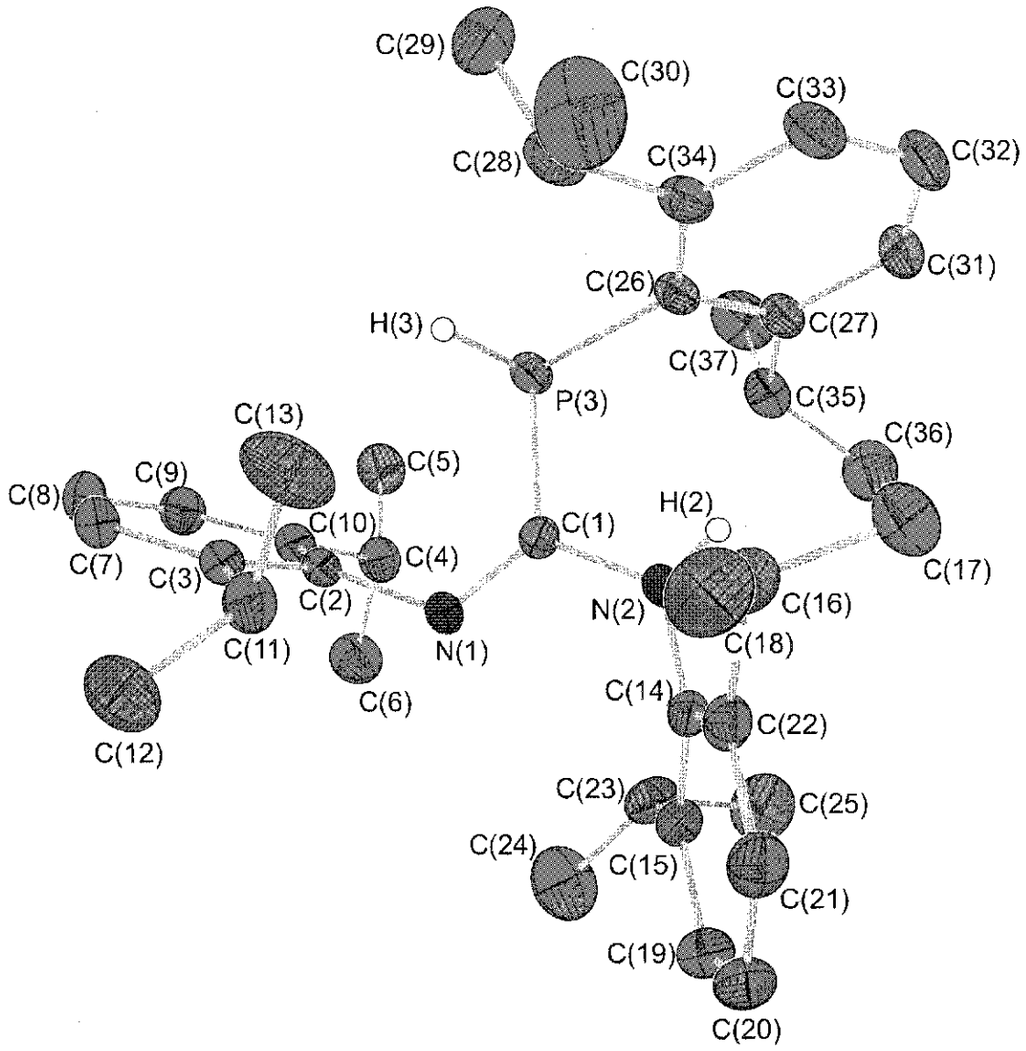

Figure 7.6 A numbered ORTEP diagram (25% probability) of the crystal structure found for 28. Hydrogen atoms on carbon are omitted for clarity.

Phosphaguandine **28** has the same overall 'paddle wheel' structure as the nitrogen analogue **11**, where the Dip rings are nearly orthogonal with the phosphaguanidine core, precluding any major steric interactions between the rings, but allowing ony one possible geometry. The N=C double bond is 1.280(2) Å, basically the same length as

the representative N=C double bond distance.[13] The N-C single bond (1.280(2) Å) is in the expected range and the length of the P-C bond (1.8733(19) Å) is close to that of the average phosphorus-carbon single bond (1.85 Å).[14] The guanidine core is essentially planar (sum of angles at C = 359.79(15)°). Selected bond lengths and angles for phosphaguanidine **28** and the nitrogen homologue **11** are included in Table 7.1.

Table 7.1 Selected bond Lengths (Å) and angles (°) for *N,N',P*-phosphaguanidine 28 and *N,N',N"*-guanidine 11. Figure 7.7 shows the atom numbering scheme used for 28. Numbering scheme for 11 is the same, except P(3) = N(3)

28		**11**	
N(1) – C(1)	1.280(2)	N(1) – C(1)	1.316(2)
N(2) – C(1)	1.380(2)	N(2) – C(1)	1.348(2)
P(3) – C(1)	1.873(2)	N(3) – C(1)	1.357(2)
N(1) – C(2)	1.423(2)	N(1) – C(2)	1.430(2)
N(2) – C(14)	1.441(2)	N(2) – C(14)	1.421(2)
P(3) – C(26)	1.845(2)		
N(1) – C(1) – N(2)	119.4(2)	N(1) – C(1) – N(2)	122.0(1)
N(1) – C(1) – P(3)	124.8(1)	N(1) – C(1) – N(3)	119.5(1)
N(2) – C(1) – P(3)	115.6(2)	N(2) – C(1) – N(3)	118.5(1)
C(26) – P(3) – C(1)	103.20(8)	C(26) – N(3) – C(1)	122.8(1)
C(1) – N(2) – C(14)	121.8(2)	C(1) – N(2) – C(14)	124.3(1)
C(1) – N(1) – C(2)	121.4(2)	C(1) – N(1) – C(2)	120.2(1)

A least squares calculation on P(3) and *ipso*-C(26) show that the deviations of both the carbon (0.0171(27) Å) and phosphorus (0.0675(40) Å) from the mean aryl plane, defined by C(27)-C(31)-C(32)-C(33)-C(34), are very small when compared to the other Dip systems studied in this work. The phosphorus is only slightly bent to the opposite side of the aryl ring from the guanidine core. Analysis of the packing diagram showed no unusual characteristics, and there is no evidence of significant intermolecular contacts other then normal van der Waals' interactions (Figure 7.8).

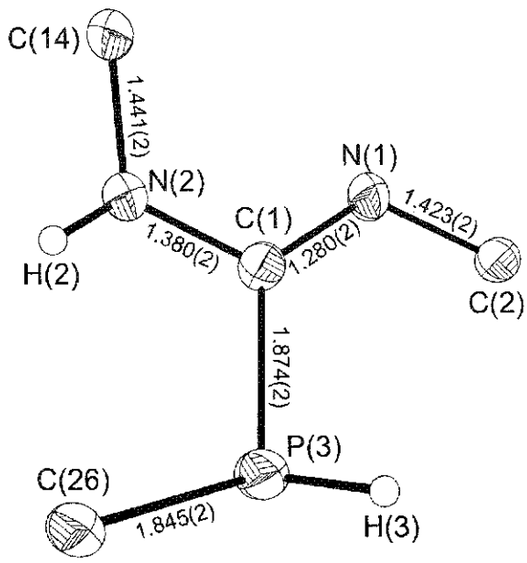

Figure 7.7 ORTEP diagram showing the central diazaphosphamethane fragment for 28.

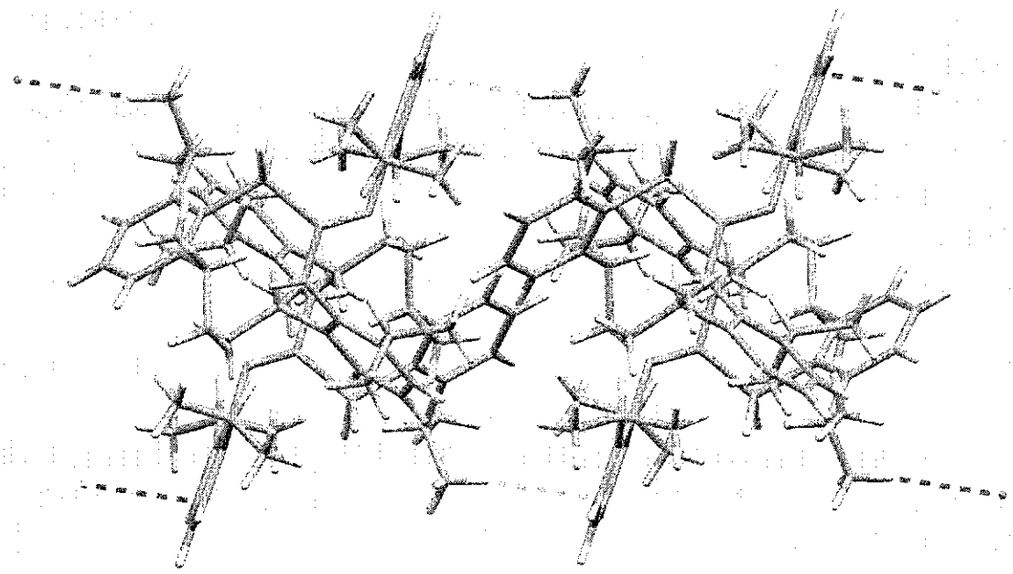

Figure 7.8 Packing diagram of 28. Dashed lines show intermolecular contacts that are equal to the sum of van der Waals radii.

When looking at the phosphaguanidine core, the structure can be thought of as a phosphaamidine in the Z-anti (N=C) form with an additional amino group attached to the carbon core (Figure 7.9). Additionally, with respect to the N=C-N fragment, the

phosphaguanidine can be thought of as an amidine in the E-syn form with an additional phosphino group attached to the central carbon.

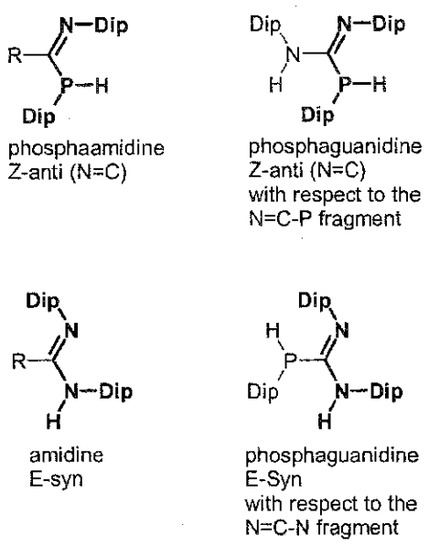

Figure 7.9 Conformation of the phosphaguanidine in terms of phosphaamidine and amidine geometry.

Häfelinger and Kuske[15] have defined the parameter $\Delta_{CN} = d(\text{C-N}) - d(\text{C=N})$ for the central N-C=N linkage in amidines and guanidines. The parameter (Δ_{CN}) was found by the authors to range from 0 to 0.178 Å. When the difference (Δ_{CN}) between the single and double carbon-nitrogen bonds is high, the structure is unlikely to be experiencing hydrogen bonding or disorder. When Δ_{CN} is low, the structure is more likely to be hydrogen bonded or disordered. In previous studies on our bulky amidines, **7** was found to have a $\Delta_{CN} = 0.027(6)$ and **8** had a $\Delta_{CN} = 0.057(3)$. The former was found to have disorder with two N-H positions in the solid state, corresponding to the Z-anti (72%) and E-syn forms (28%). The crystal structure of the latter did not show similar disorder. Δ_{CN} for *N,N',N''*-guanidine **11** was found to be 0.032(6), and the single crystal structure was found to have positional disorder with respect to one of the two N-H protons. As with **7**,

the positional disorder in **11** offers both the Z-anti (70%) and E-syn (30%) conformations with respect to the disordered N=C-N fragment. In the case of phosphaguanidine **28**, Δ_{CN} = (1.380(2)) – (1.280(2)) = 0.100(4). From the measured parameters, positional disorder of the amino proton with respect to the amidine fragment is clearly not observed.

7.5 Conclusion

In conclusion, the first in a series of bulky phosphaguanidines have been made. The ^{1}H NMR shows that that there are multiple dynamic processes occurring at room temperature, as well as the possibility of isomerism and tautomerism similar to the phosphaamidine systems (Chapter 5), both warranting further investigations. The solid-state 'paddle wheel' structure is essentially the same as the nitrogen analogue **11**. In addition, the structure favors an N=C double bond over a P=C double bond in both solution and the solid state. Reasons as to why the N=C double bond are favored over the P=C double bond need further investigations. A DFT study similar to the one completed on the phosphaamidine system (Chapter 3) may be able to help explain this preference.

Reference List

1. Bailey, P. J.; Mitchell, L. A.; Parsons, S. *J. Chem. Soc., Dalton Trans.* **1996**, 2839.

2. Boeré, R. E.; Boeré, R. T.; Masuda, J.; Wolmershauser, G. *Can. J. Chem.* **2000**, *78*, 1613-1619.

3. Frisch, M. J.; Trucks, G. W.; Schlegel, H. B.; Scuseria, G. E.; Robb, M. A.; Cheeseman, J. R.; Zakrzewski, V. G. Z.; Montgomery, Jr. J. A.; Stratmann, R. E.; Burant, J. C.; Dapprich, S.; Millam, J. M.; Daniels, A. D.; Kudin, K. N.; Strain, M. C.; Farkas, O.; Tomasi, J.; Barone, V.; Cossi, M.; Cammi, R.; Mennucci, B.; Pomelli, C.; Adamo, C.; Clifford, S.; Ochterski, J.; Petersson, G. A.; Ayala, P. Y.; Cui, Q.; Morokuma, K.; Malick, D. K.; Rabuck, A. D.; Raghavachari, K.; Foresman, J. B.; Cioslowski, J.; Ortiz, J. V.; Baboul, A. G.; Stefanov, B. B.; Liu, G.; Liashenko, A.; Piskorz, P.; Komaromi, I.; Gomperts, R.; Martin, R. L.; Fox, D. J.; Keith, T.; Al-Laham, M. A.; Peng, C. Y.; Nanayakkara, A.; Challacombe, M.; Gill, P. M. W.; Johnson, B.; Chen, W.; Wong, M. W.; Andres, J. L.; Gonzalez, C.; Head-Gordon, M.; Replogle, E. S.; Pople, J. A. *Gaussian 98, Revision A.9* Gaussian, Inc.: Pittsburgh, PA, 1998.

4. Himbert, G.; Schwickerath, W. *Liebigs. Ann. Chem.* **1984**, 85.

5. Pudovik, A. N.; Romanov, G. V.; Stepanova, T. Y. *Bulletin of the Academy of Sciences of the U.S.S.R.* **1982**, *6*, 1416-1417.

6. Kolodiazhnyi, O. I. *Tetrahedron Lett.* **1982**, *23*(47), 4933-4936.

7. Kolodyazhnyi, O. I. *Zh. Obshch. Khim.* **1983**, *53*, 1093-1099.

8. Issleib, K.; Schmidt, H.; Meyer H. *J. Organomet. Chem.* **1980**, *192*, 33-39.

9. Schmidt, H.; LeiBring, E.; Wirkner, C. *Z. Chem.* **1989**, *29*(11), 410-411.

10. Thewissen, D. H. M. W.; Ambrosius, H. P. M. M. *Recl. Trav. Chim. Pays-Bas* **1980**, *99*(11), 344-346.

11. Sheldrick, G. *SHELXS-97* University of Gottingen, 1997.

12. Sheldrick, G. *SHELXL-97* University of Gottingen, 1997.

13. Argay, G.; Kalman, A.; Karpor, A.; Ribar, B. *Acta Crystallogr. Sect. B (Struct. Crystallogr. Cryst. Chem.)* **1980**, *B36*, 363.

14. Appel, R. *Multiple Bonds and Low Coordination in Phosphorus Chemistry,* 1st ed.; Scherer, O. J.; Regitz, M., Editor; Thieme Medical Publishers, Inc.: New York, 1990.

15. Häfelinger, G.; Kuske, K. H. *The Chemistry of the Amidines and Imidates*; Patai, S.; Rappoport, Z., Editors; Wiley: Chichester, 1991; Vol. 2.

Chapter 8

Future Work

8.1 Introduction

As mentioned in Chapter 1, there are two phosphorus homologues to our bulky amidines and three homologues to our bulky guanidine. The circled molecules in Figure 8.1 still have to be made to complete the series.

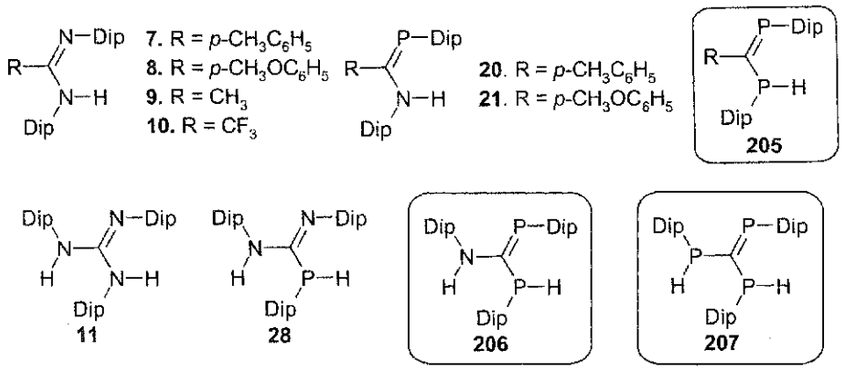

Figure 8.1 ***N,N'*-amidine, *N,N',N"*-guanidine and their phosphorus homologues. Circled molecules are still needed to complete the series.**

Currently, we are not completely sure that the Dip substituent will be sufficiently bulky to stabilize the phosphorus centers in the higher homologues. If attempts fail to produce these systems, or if the target molecules are too reactive to be handled during work-up, the bulkier Mes* substituent may have to be employed to prevent oligimerization or other side reactions.

8.2 Synthesis of *P,P'*-diphosphaamidines **205**

8.2.1 'Becker' phopshaalkene route

There are several approaches that could be taken for the synthesis of the diphospha-analogues to our bulky amidines and monophosphaamidines. The first route involves the

synthesis of 'Becker" phosphaalkene **208**, from the corresponding acid chloride and DipP{$Si(CH_3)_3$}$_2$ **18** (Figure 8.2). Yoshifuji has done work on a similar system, where the bulky Mes* substituent is located on phosphorus.[1]

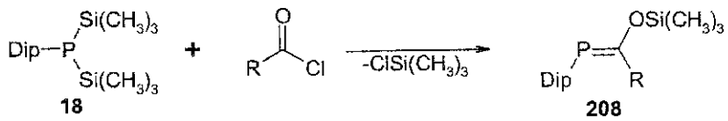

Figure 8.2 Synthesis of 'Becker' phosphaalkene 208

The 'Becker' phopshaalkene **208** can be then reacted with one equivalent of lithium phosphide **209**, producing the diphosphaamidine **205** (Figure 8.3). If needed, the work-up can be simplified by treating the reaction with $ClSi(CH_3)_3$, eliminating problems caused by the Li^+ $^-OSi(CH_3)_3$ side product, by producing LiCl and $O(Si(CH_3)_3)_2$.

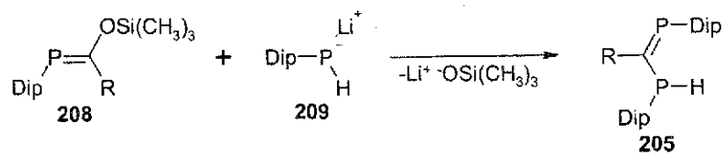

Figure 8.3 Synthesis of diphosphaamidine 205 from 'Becker' phosphaalkene

8.2.2 Phosphaamide route

The phosphorus analogues to the amides reported in the original *N,N'*-Dipamidine papers[2,3] could be made in a number of ways. All three methods start from the acid chloride, but each differs in the method of attachment of the DipPH fragment (Figure 8.4). The first and least aggressive method utilizes the monosilyl phosphane **16**, producing the phosphaamide **210** and the easily removable side product $ClSi(CH_3)_3$. The second route would involve reacting $DipPH_2$ **15** with the acid chloride in the presence of a base such as DBU to remove any HCl produced. Several of the nitrogen analogues have been made in this way, but use a second equivalent of $DipNH_2$ **12** as the acid 'sponge'. The third method involves using the more reactive lithium phosphide **209**.

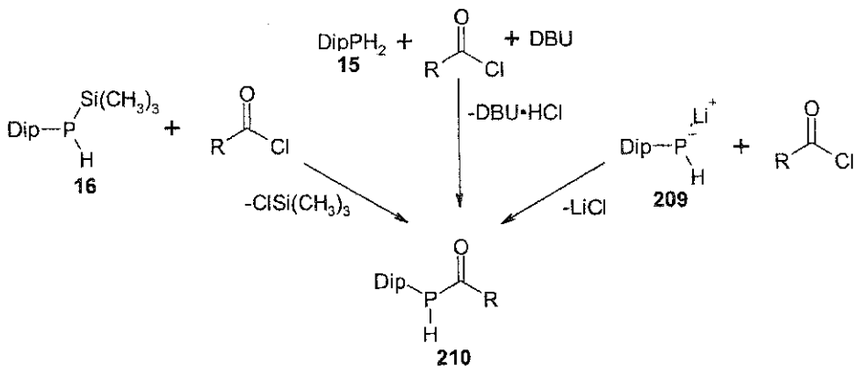

Figure 8.4 Three possible routes to phosphaamide

The phosphaamide **210** could be then reacted with DipP{Si(CH$_3$)$_3$}$_2$ **18** in the presence of a small amount of NaOH to act as a catalyst (Figure 8.5). This method has been used to make phosphaalkenes from benzophenones,[4] as well as trisubstituted phosphaamidines from dimethylformamide.[5,4]

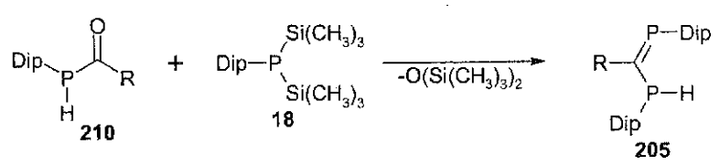

Figure 8.5 Synthesis of diphosphaamidine 205 via the phosphaamide 210

8.2.3 Phospha-imidoyl chloride route

The phosphorus analogues to imidoyl chlorides could be made in a similar manner to that used to produce the nitrogen analogues. Reacting the phosphaamide **210** with thionyl chloride or phosphorus pentachloride may produce the phospha-imidoyl chloride **211** (Figure 8.6). One would have to be careful in the choice of dehydrating and halogenating agent. An incorrect choice could result in oxidation of the phosphorus center, from P(III) to P(V).

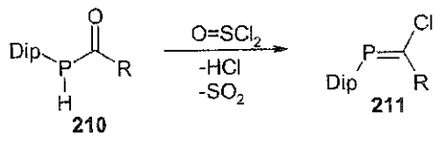

Figure 8.6 Possible synthesis of phospha-imidoyl chloride

If the phospha-imidoyl chloride can be isolated, it could be then be used in a similar fashion to the nitrogen analogues in the synthesis of our phosphaamidines **20** and **21** (Figure 8.7).

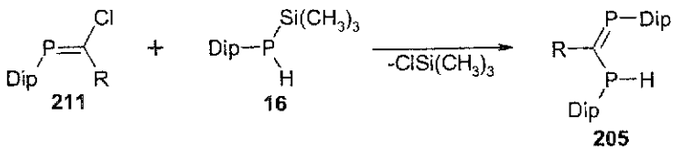

Figure 8.7 Synthesis of diphosphaamidine 205 via phospha-imidoyl chloride 211 route

8.3 Synthesis of diphosphaguanidine

8.3.1 Isocyanide dichloride route

The unpublished isocyanide dichloride **212** made in our lab could be reacted with two equivalents of $DipPHSi(CH_3)_3$ **16** to give the diphospaguanidine **206**. This route is analogous to the route used to make the phosphaamidines in Chapter 5 (Figure 8.8), and has been used to make other diphosphaguanidines.[6]

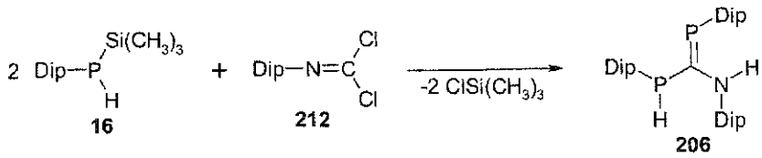

Figure 8.8 Isocyanide dichloride route to diphoshaguanidine

8.3.2 Azaphosphaallene route

The azaphosphaallene, Dip-P=C=N-Dip **213**, has never been reported in the literature, but should be isolable since the less bulky ^{t}Bu analogue has been made. There are

multiple routes to azaphosphaallenes[7], but there are three that utilize materials that have been made in our lab, or are commercially available (Figure 8.9). The first route used to make azaphosphaallenes, utilizes either the isocyanate **214** or the isothiocyanate **215**. The second route involves reacting the isocyanide dichloride **212** with $DipP\{Si(CH_3)_3\}_2$ **18**. The third and most promising route, because it was used to make the bulkier Mes*-P=C=N-Mes* **52**, involves reacting DipPH(TBDMS) **17** with ^{n}BuLi to produce the lithium phosphide **216**, then reacting with isocyanate **214**.

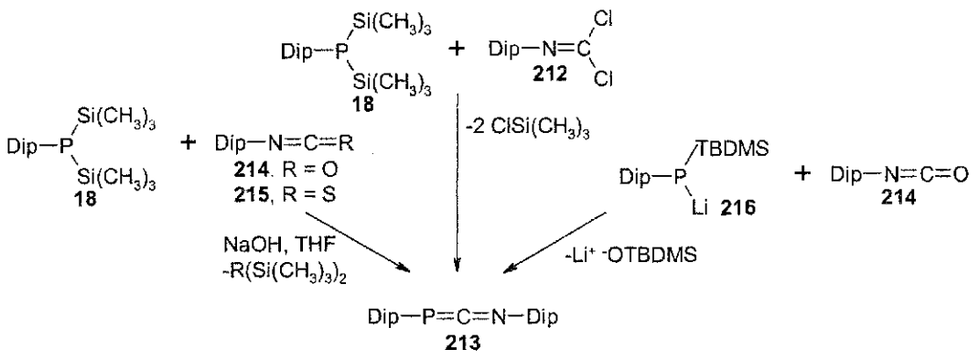

Figure 8.9 Three routes to azaphosphaallene Dip-P=C=N-Dip 213

In a similar manner as phosphaguanidine **28** was produced in Chapter 7, the azaphosphaallene **213** can then be reacted with lithium phosphide **209**, to produce the diphosphaguanidine **206**.

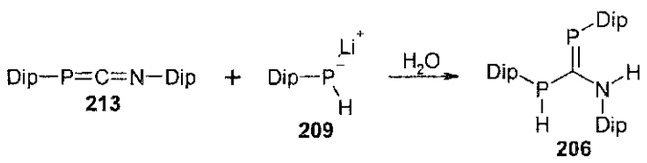

Figure 8.10 Possible synthesis of diphosphaguanidine

8.4 Synthesis of triphosphaguanidine

The phosphorus analogue to an isocyanide dichloride has been made using the bulky Mes* group.[8] Although it has not been attempted using less bulky substituents, it may be

possible to produce DipP=CCl_2 **217**, which then could be reacted with two equivalents of DipPHSi$(CH_3)_3$ **16** to give the triphosphaguanidine **207** (Figure 8.11).

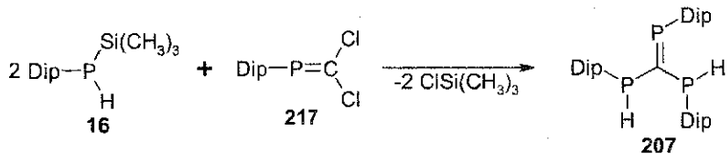

Figure 8.11 Possible route to triphosphaguanidine 207

8.5 Conclusion

There are several possible routes to the higher phosphorus homologues to our amidines and monophosphaguanidines. The main hindrance to the synthesis of these molecules is whether the Dip group is sufficiently bulky to allow isolation of these compounds and their precursors; if not, the sterically bulkier Mes* substituent may be utilized in some cases. With these molecules we will be able to continue the systematic study of the changes substitution of nitrogen by phosphorus will have on the versatile amidine system.

Reference List

1. Yoshifuji, M.; Toyota, K.; Shibayama, K.; Inamoto, N. *Chemistry Letters* **1983**, 1653-1656.

2. Boeré, R. T.; Klassen, V.; Wolmershauser, G. *J. Chem. Soc., Dalton Trans.* **1998**, 4147-4154.

3. Boeré, R. T.; Klassen, V.; Wolmershauser, G. *Can. J. Chem.* **2000**, *78*, 583-589.

4. Becker, G.; Uhl, W.; Wessley, H. J. *Z. Anorg. Allg. Chem.* **1981**, *479*, 41-56.

5. Becker, G.; Mundt, O. *Z. Anorg. Allg. Chem.* **1980**, *462*, 130-142.

6. Appel, R.; Knoch, F.; Laubach, B.; Sievers, R. *Chem. Ber.* **1983**, *116*, 1873-1879.

7. Escudié, J.; Ranaivonjatovo, H.; Rigon, L. *Chem. Rev.* **2000**, *100*, 3639-3696.

8. Goede, S. J.; Bickelhaupt, F. *Chem. Ber.* **1991**, *124*, 2677-2684.

Chapter 9

Experimental

9.1 General

All experimental procedures were performed under a nitrogen atmosphere using modified Schlenk techniques, unless otherwise noted. 2,6-Diisopropylaniline **12** (Aldrich) was distilled from KOH and stored under nitrogen prior to use while PCl_3, $ClSi(CH_3)_3$, ClSiTBDMS, 1.6M ^nBuLi in hexanes (Aldrich) and metal carbonyls (Strem) were used as received. Solvents were reagent grade, or better, and used as received (petroleum ether, methanol, ethanol, hexanes), distilled from sodium/benzophenone (tetrahydrofuran, diethyl ether), distilled over $LiAlH_4$ (*n*-heptane) or distilled over sodium (xylenes). Infared spectra were recorded on Bomem MB-100 or Nicolet Avatar 360 spectrometers as liquid smears on CsI plates, KBr pellets or in a 0.1 mm NaCl solution cell. ^1H, ^{13}C and ^{31}P NMR spectra were recorded on a Bruker AC250 / Tecmag Macspect spectrometer operating at 250.13, 101.26 and 62.90 MHz, respectively, or a Varian Inova 500 operating at 499.3 (^1H), 202.1 (^{31}P), 125.6 (^{13}C), and 50.6 (^{15}N) MHz. ^1H NMR were referenced to tetramethylsilane or residual acetone, ^{13}C NMR were referenced to $CDCl_3$ or $(CD_3)_2C{=}O$, ^{13}P NMR were referenced to an external H_3PO_4 sample and ^{14}N NMR were referenced to an external CH_3NO_2 sample. Mass spectra were obtained from the Mass Spectrometry Centre, Department of Chemistry, University of Alberta, except for DipBr **13**, which was obtained in the Dept. of Biology, University of Lethbridge. Elemental analyses were run by MHW Laboratories, Phoenix, Az.

9.2 Preparation of 1-bromo-2,6-diisopropylphenylbenzene **13**

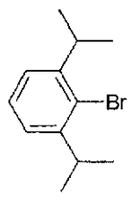

13

298 g (1.68mol) of 2,6-diisopropylaniline **12** and 600 ml of water were placed in a 5-liter three-necked round bottomed flask equipped with a mechanical stirrer and cooled with an ethanol/dry ice bath to approximately -10°C. 750ml of 48% HBr was then slowly added while maintaining the reaction temperature below -5°C. 173g (2.49 mol) of $NaNO_2$ in 400ml of water was added dropwise over a 75 min period, maintaining a reaction temperature between -10 and -15°C. Upon complete addition of the $NaNO_2$, the reaction mixture was cooled to the point at which the solution began to solidify (approx. -16 to -18°C) and 11g (0.17 mol) of copper powder was added. The mixture was allowed to slowly warm in the ethanol/dry ice bath to room temperature and then brought to reflux for 2 hours and left to cool. The resulting dark brown solution was then washed 4x with 400ml of petroleum ether and the organic layers combined. The organic portion was then washed with 3x 400 ml 1M HCl, 1x 400 ml water and 3x 400 ml NaOH, dried with anhydrous $MgSO_4$, filtered and volatiles removed under reduced pressure producing 318.7 g of a dark red solution. This was then combined with an equal volume of concentrated methanolic KOH solution. The resulting dark green solution was then extracted with 4x 200ml of hexanes. The solution was dried over anhydrous $MgSO_4$, filtered and concentrated.

Distillation of the residue (75-85°C, 0.5 mbar) yielded 155.17g (38.2%) of a bright yellow oil.

^{1}H NMR ($CDCl_3$): δ 1.24 (d, J(H-H) 6.7 Hz, 12 H), 3.50 (sept, J(H-H) 7.0 Hz, 2H), 7.10-7.27 (m, 3H).

^{13}C NMR ($CDCl_3$): δ 23.29 (^{i}Pr-CH_3), 33.80 (^{i}Pr-CH_3), 124.36 (*meta*-C), 126.78 (*ipso*-C), 127.58 (*para*-C), 147.99 (*ortho*-C).

MS(HPLC/GC): Dip^{81}Br - *m/z* 242 (M^+); 227 ($M\text{-}CH_3^+$), Dip^{79}Br - *m/z* 240 (M^+); 225 ($M\text{-}CH_3^+$).

9.3 Preparation of 2,6-diisopropylphenylphosphonus mixed halide **14**

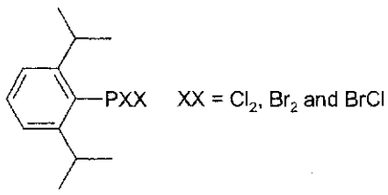

14

In a three liter, 3-necked flask, 6 g (0.247 mol) of freshly ground Mg turnings were stirred under vacuum at 80°C for 1 hour. 250 ml of THF and 1.0 ml of 1,2-dibromoethane were added, and the mixture brought to reflux with stirring for 30 min and subsequently cooled to room temperature. A solution of 60g (0.247 mol) 1-bromo-2,6-diisopropylphenylbenzene **13** in 900 ml THF was added. The reaction was refluxed for 3 hours, at which point most of the magnesium had been consumed. In another three liter, 3-necked flask, a solution of (67.0g, 0.488 mol) PCl_3 in THF (200 ml) was made and cooled to ice-salt bath temperature. The Grignard was cooled to 0°C and added via a cannula to the stirring PCl_3 mixture over a 15 min period. The mixture was allowed to slowly warm overnight in the bath, then refluxed for 2 hours. The resulting orange solution was concentrated, taken up in 500ml of diethyl ether and filtered. Removal of the ether yielded an orange oil that was purified by distillation (106-111°C/0.5 mbar) to produce a viscous clear oil. Yield: 14.2 g of mixed product in a 1.6 : 2.44 : 1.0 $DipPCl_2$:DipPClBr:$DipPBr_2$ ratio from integration of ^{31}P NMR. Yield: $DipPCl_2$ = 4.5 g, DipPClBr = 6.9 g, $DipPBr_2$ = 2.8 g. Total % yield = 38.1%

^1H NMR ($CDCl_3$): δ 1.29-1.34 (three doublets), 3.23-3.40 (three septets), 7.21-7.44 (multiplet).

^{31}P NMR ($CDCl_3$): δ 151.9 ($DipPBr_2$), 159.2 (DipPClBr), 164.5 ($DipPCl_2$).

MS(70 eV): $DipP^{81}Br_2$ - *m/z* 354 (M^+, 5.52%); 271 (M-$^{81}Br^+$, 10%), $DipP^{79}Br^{81}Br$ - *m/z* 352 (M^+, 5.52%); 273 (M-$^{79}Br^+$, 9.83%); 271 (M-$^{81}Br^+$, 10.00%), $DipP^{79}Br_2$ - *m/z* 352 (M^+, 5.52%); 271 (M-$^{79}Br^-$, 9.83%), $DipP^{81}BrCl$ - *m/z* 308 (M^+, 26.5%); 273 (M-$^{81}Br^+$, 9.8%); 227 (M-Cl^+, 100%), $DipP^{79}BrCl$ - *m/z* 306 (M^+, 21.4%); 271 (M-$^{79}Br^+$, 10%); 227 (M-Cl^+, 100%), $DipPCl_2$ - *m/z* 262 (M^-, 44.9%); 227 (M-Cl^+, 100%).

9.4 Preparation of 2,6-diisopropylphenylphosphane **15**

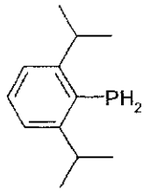

15

10.0 g (32.7 mmol) of DipPXX **14** was combined with 150 ml diethyl ether in a 250 ml side arm flask. This was added via cannula to another flask containing 2.78 g (73.2 mmol) of $LiAlH_4$ in 150 ml diethyl ether at -5°C. After warming to room temperature, the solution was refluxed for 22 hours. After cooling the solution in an ice bath, 53 ml of a saturated NH_4Cl solution was slowly added causing the remaining $LiAlH_4$ to clump. The organic layer was decanted off and the solids washed 3x 100 ml with degassed diethyl ether. The extracts were combined, dried with $MgSO_4$, filtered and the volatiles removed under vacuum leaving a slightly milky oil. Distillation (73 - 85°C, 0.5 mbar) produced 4.76 g (24.6 mmol) of a clear oil. Yield = 75.3%.

^{1}H NMR ($CDCl_3$): δ 1.25 (d, J(H-H) 6.7 Hz, 12 H), 3.37 (d of sept., ^{4}J (H-P) 3.0 Hz, J(H-H) 6.7 Hz, 2H), 3.84 (d, J(P-H) 208 Hz, 2H), 7.11-7.29 (m, 3H).

^{13}C NMR ($CDCl_3$): δ 23.84 (s, ^{i}Pr-CH_3), 33.15 (d, ^{3}J(P-C) 11.7 Hz, ^{i}Pr-CH), 122.91 (d, ^{3}J(P-C) 2.4 Hz, *meta-C*), 126.04 (d, J(P-C) 13.7 Hz, *ipso-C*), 128.53 (s, *para-C*), 152.10 (d, ^{2}J(P-C) 9.8 Hz, *ortho-C*).

^{31}P NMR ($CDCl_3$): δ -156.4 (triplet, J(P-H) 208 Hz).

IR (neat oil) cm^{-1}: 3056 (w), 2961 (vs), 2868 (m), 2627 (s), 2306 (m), 1572 (w), 1461 (s), 1423 (w), 1383 (m), 1362 (m), 1247 (w), 1181 (w), 1162 (w), 1106 (w), 1086 (m), 1054 (m), 1037 (w), 923 (w), 831 (m), 792 (s), 720 (s), 499 (w).

MS(70eV): *m/z* 194.12306 (M^+, 100%), 193 ($DipPH^+$, 44%), 179 ($C_{11}H_{16}P^+$, 30%), 161 ($C_{12}H_{17}^+$, 54%), 152 ($C_9H_{13}P^+$, 44%), 151 ($C_9H_{12}P^+$, 26%), 137 ($C_8H_{10}P^+$, 25%), 110 ($C_6H_7P^+$, 52%), 91 ($C_7H_7^+$, 26%).

Elemental Analysis : Calc. for $C_{12}H_{19}P$: C, 74.20, H, 9.86%. Found: C, 74.43, H, 9.74%.

9.5 Preparation of *N,P*-bis(2,6-diisopropylphenyl)-*p*-methyl-benzphosphaamidine **20**

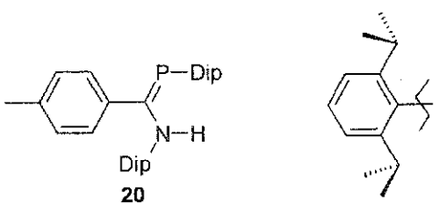

20

Dip = 2,6-diisopropylphenyl

38 ml of dry xylenes were freeze-thaw degassed (5X) in a 250ml side arm flask. Then 5.00 g (15.9 mmol) of tolyl imidoyl chloride **22** and 3.10 g (15.9 mmol) $DipPH_2$ **15** were added. The flask was fitted with a reflux condenser and heated in a 200-215°C oil bath. The reaction was monitored by ^1H NMR over four days, after which time all starting materials were consumed. Xylenes were removed under high vacuum. The remaining orange solid was dissolved in a minimum of hot 99% ethanol and cooled to –30°C . After four days bright yellow crystals were filtered off and the filtrate was reduced to half the original volume. After harvesting a second crop, a total of 3.06 g (6.49 mmol) of crystals were obtained. Analytically pure crystals were obtained by recrystallization from hot methanol. Yield: 41% Melting Point: 115-119°C.

^1H NMR ($CDCl_3$): δ 0.81 (d, J(H-H) 6.7 Hz, 6H), 0.89 (d, J(H-H) 6.7 Hz, 6H), 1.26 (d, J(H-H) 6.7 Hz, 6H), 1.35 (d, J(H-H) 6.9 Hz, 6H), 2.22 (s, 3H), 3.00 (sept., J(H-H) 6.7 Hz, 2H), 3.84 (doublet of septets, J(H-H) 6.8 Hz, ^{4}J(P-H) 3.4 Hz, 2H), 6.23 (d, J(P-H) 2.4 Hz, 1H), 6.93-7.35 (mult., 10H).

^{13}C NMR ($CDCl_3$): δ 21.12 (s, *p*-CH_3-C_6H_4), 22.30 (s, amino-Dip-^{i}Pr-CH_3), 23.05 (s, phosphino-Dip-^{i}Pr-CH_3), 25.17 (s, amino-Dip-^{i}Pr-CH_3), 26.01 (d, ^{4}J(P-C) 2.0 Hz, phosphine-Dip-^{i}Pr-CH_3), 28.23 (s, amino-Dip-^{i}Pr-CH), 33.03 (d, ^{3}J(P-C) 7.5 Hz,

phosphino-Dip-^{i}Pr-*C*H), 123.00 (s, phosphino-Dip-*m*-*C*), 123.43 (s, amino-Dip-*m*-*C*), 126.80 (s, amino-Dip-*p*-*C*), 127.24 (d, ^{3}J(P-C) 15.7 Hz, *o*-*C*-C_6H_4), 128.35 (s, *m*-*C*-C_6H_4), 129.50 (s, phosphino-Dip-*p*-*C*), 134.38 (d, ^{5}J(P-C) 29.5, *p*-*C*-C_6H_4), 135.14 (s, *ipso*-*C*-C_6H_4), 138.31 (d, ^{3}J(P-C) 3.0 Hz, *ipso*-*C*-N) 144.53 (d, ^{4}J(P-C) 2.1 Hz, amino-Dip-*o*-*C*), 153.79 (d, ^{2}J(P-C) 4.8 Hz, phosphino-Dip-*o*-*C*), 186.21 (d, ^{1}J(P-C) 61.4 Hz, P=*C*)

^{31}P NMR ($CDCl_3$): δ 53.60 (major isomer, s)

IR (CH_2Cl_2) cm^{-1}: 3385(w), 3349(m), 3025(w), 2907(s), 2806(w), 2726(w), 2590(w), 2069(vs), 1942(w), 1905(w), 1873(w), 1803(w), 1709(w), 1666(m), 1659(w), 1641(w), 1607(s), 1586(s), 1565(s), 1510(m), 1501(m), 1493(s), 1484(s), 1468(m), 1383(m), 1345(s), 1203(m), 1180(m), 1111(m), 1056(s), 1007(w), 932(w), 820(w).

IR ($CHCl_3$) cm^{-1}: 3350 (w), 2955 (m), 2928 (m), 2866 (m), 1939 (w), 1870 (w), 1666 (w), 1606 (m), 1587 (m), 1565 (m), 1485 (m), 1462 (vs), 1454 (s), 1383 (m), 1345 (vs), 1310 (m), 1264 (w), 1101 (vs), 1002 (s), 889 (w), 866 (w), 833 (w).

IR (*n*-heptane) cm^{-1}: 3354(vs), 1932(m), 1955(w), 1947(w), 1896(w), 1888(s), 1863(m), 1795(w), 1692(m), 1642(m), 1608(s), 1566(s), 1324(m), 1255(m), 1203(s), 1179(vs), 1111(s), 1055(m), 1038(m), 1007(m), 814(vs), 800(vs), 755(w).

IR (KBr) cm^{-1}: 3351(m), 3055(w), 3020(w), 2961(vs), 2925(s), 2867(s), 1588(w), 1563(w), 1492(s), 1466(s), 1385(m), 1349(s), 1308(m), 1278(w), 1254(w), 1204(w), 1183(w), 1110(w), 1056(w), 931(w), 816(m), 802(m), 795(m), 755(m), 746(m), 712(w).

UV (methanol): λ_{max} 203 (ε 74 000), 232 (ε 24 000), 267 (ε 13 000), 347 (ε 9600).

UV (*n*-hexane): λ_{max} 231 (ε 20 000), 272 (ε 11 000), 356 (ε 14 000).

MS(70eV): *m/z* 471 (M^+, 23%); 428 (M – ^iPr, 100%); 278 (M – $C_6H_3{}^iPr_2H^+$, 81%); 176 ($C_6H_3{}^iPr_2NH^+$); 105 ($C_8H_9^+$, 20); 91 ($C_6H_5N^+$, 16).

Elemental Analysis: Calc. for $C_{32}H_{42}NP$: C, 81.49; H, 8.98; N, 2.97. Found: C, 81.57; H, 8.48; N, 3.02%.

9.6 Preparation of *N,P*-bis(2,6-diisopropylphenyl)-*p*-methoxy-benzphosphaamidine **21**

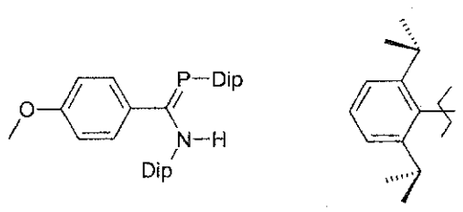

Dip = 2,6-diisopropylphenyl

In a Schlenk tube, 1.00 g (3.75 mmol) DipPHTMS **16** and 1.24 g (3.75 mmol) methoxy imidoyl chloride **23** were combined with 7 ml xylenes. After refluxing overnight the volatiles were removed under vacuum to leave a yellow solid. This was dissolved in a minimum of hot 99% EtOH and cooled to –30 °C. Yellow globular crystals formed. Yield: 0.724 g, 39.6%. Analytically pure and X-ray grade crystals were grown by the slow cooling of a hot MeOH solution to offer yellow block-like crystals. mp: 133-136 °C

^{1}H NMR ($CDCl_3$): δ 0.83 (d, J(H-H) 6.9Hz, 6H), 0.92 (d, J(H-H) 6.9Hz, 6H) , 1.27 (d, J(H-H) 6.7Hz, 6H), 1.36 (d, J(H-H) 6.9Hz, 6H), 3.00 (sept., J(H-H) 6.7 Hz, 2H), 3.70 (s, 3H), 3.85 (doublet of septets, J(H-H) 6.7Hz, ^{4}J(P-H) 3.4Hz, 2H), 6.24 (d, J(P-H) 2.4Hz, 1H), 6.63-7.35 (mult., 10H)

^{13}C NMR ($CDCl_3$): δ 22.53, 23.30, 25.43, 26.21, 26.24, 28.54, 33.23, 33.35, 55.44, 113.44, 123.24, 123.70, 127.12, 128.90, 129.16, 129.73,130.16, 130.58, 135.34, 135.46, 135.53, 136.11, 144.95, 144.98, 154.10, 154.18, 160.28, 160.33, 185.65, 186.64.

^{31}P NMR ($CDCl_3$, ^{1}H coupled): δ 51.38 (major isomer, s)

IR (KBr) cm^{-1}: 3357 (m), 3052 (w), 2960 (vs), 2868 (w), 1603 (m), 1572 (w), 1506 (s), 1494 (s), 1465 (vs), 1387 (m), 1354 (s), 1293 (m), 1249 (vs), 1207 (m), 1174 (s), 1109 (w), 1035 (m), 1055 (w), 999 (w), 931 (w), 830 (s), 803 (m), 756 (s), 748 (m), 724 (w).

IR ($CHCl_3$) cm^{-1}: 3350 (w), 2955 (m), 2928 (m), 2859 (m), 1604 (vs), 1573 (m), 1485 (m), 1462 (vs), 1454 (s), 1383 (m), 1344 (vs), 1306 (m), 1294 (s), 1172 (w), 1111 (w), 1000 (w), 833 (w).

IR (*n*-heptane) cm^{-1}: 3354 (w), 1604 (vs), 1574 (m), 1511 (w), 1326 (w), 1291 (w), 1250 (vs), 1216 (vs), 1175 (vs), 1110 (m), 1042 (m), 1000 (w), 82 (m), 800 (m), 758 (m).

UV(methanol): λ_{max} 204 (ε 303 847); 275nm (ε 28 603); 327nm (ε 33 761).

MS(70eV): *m/z* 487 (M^+, 12%); 444 (M – ^iPr, 69); 294 (M – $C_6H_3{}^iPr_2H^+$, 100); 176 ($C_6H_3{}^iPr_2NH^+$,11); 135 (C_8H_9NO, 34); 121 ($C_8H_9O^+$, 21); 91 ($C_6H_5N^+$, 11); 77 ($C_6H_5^+$, 6.8).

Elemental Analysis: Calc. for $C_{32}H_{42}NOP$: C, 78.81; H, 8.68; N, 2.87. Found: C, 76.07; H, 7.58; N, 2.80%.

9.7 Preparation of η^1-(*N*,*P*-bis(2,6-diisopropylphenyl)-*p*-methyl-benzphosphaamidine)-molybdenum pentacarbonyl **25**

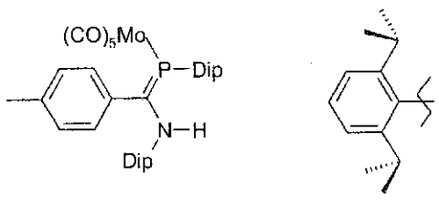

Dip = 2,6-diisopropylphenyl

In a Schlenk tube, 0.500g (1.06 mmol) of phosphaamidine **20**, 0.280g (1.06 mmol) $Mo(CO)_6$ and 26 ml of dry heptane were combined. This was brought to reflux and monitored via solution IR to monitor the consumption of metal carbonyl. After 8 hours heating was ceased and the solution was slowly cooled to -30°C. After 6 days, the solution was filtered offering 0.284 g of fine yellow/brown crystals. Yield: 41%. Analytical crystals were grown by dissolving the crude crystals in room temperature heptane and cooling to –30 °C. Melting Point: 155°C (decomp.).

^{1}H NMR ($CDCl_3$): δ 0.87(d, J(H-H) 6.6 Hz, 6H), 0.97 (d, J(H-H) 6.7 Hz, 6H), 1.36 (d, J(H-H) 6.7 Hz, 6H), 1.45 (d, J(H-H) 6.7 Hz, 6H), 2.23 (d, J(H-P) 1.8 Hz, 3H), 3.02 (sept., J(H-H) 6.7 Hz, 2H), 4.00 (sept., J(H-H) 6.7 Hz, 2H), 4.02 (sept., J(H-H) 6.7 Hz, 2H), 6.45 (s, 1H), 6.89-7.48 (mult., 10H).

^{31}P NMR (Proton Coupled, $CDCl_3$): δ 30.17 ppm

IR (KBr pellet) cm^{-1}: 3358 (w), 3054 (w), 2966 (w), 2927 (w), 2870 (w), 2069 (s), 1955(vs), 1929 (vs), 1907 (vs), 1607 (w), 1480 (w), 1465 (m), 1383 (w), 1361 (w), 1323 (m), 1264 (w), 1202 (w), 1178 (w), 815 (w), 804 (w), 759 (w), 748 (w) 607 (m), 587 (m).

IR ($CHCl_3$) cm^{-1}: 3349 (w), 2962 (w), 2928 (w), 2872 (w), 2071 (s), 1949 (vs), 1939 (vs), 1914 (s), 1607 (w), 1484 (w), 1462 (m), 1453 (w), 1385 (w), 1365 (w), 1343 (w), 1326 (w), 1105 (w), 1059 (w).

IR (*n*-heptane) cm^{-1}: 2071(m), 1955(vs), 1948(vs), 1933(s).

MS(70eV): *m/z* 709.18640 (ML^+ based on ^{98}Mo, 0.05%); 653 ($ML - 2(CO)^+$, 0.22); 625 ($ML - 3(CO)^+$, 1.1); 569 ($ML - 5(CO)^+$, 3.1); 471 (L^+, 15); 428 ($L - {}^iPr^+$, 100); 278 ($L - C_6H_3{}^iPr_2PH^+$, 67); 105 ($C_8H_9^+$, 18).

Elemental Analysis: Calc. for $C_{37}H_{42}MoNO_6P$: C, 62.79; H, 6.00; N, 1.98. Found: C, 62.93; H, 6.15; N, 2.07%.

9.8 Preparation of η^1-(*N*,*P*-bis(2,6-diisopropylphenyl)-*p*-methyl-benzphosphaamidine)-chromium pentacarbonyl **24**

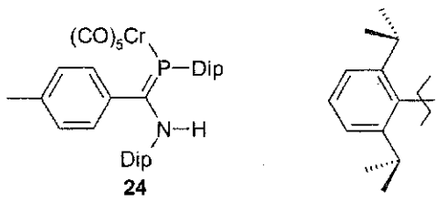

24

Dip = 2,6-diisopropylphenyl

In a 250 ml side arm flask, 0.500g (1.06 mmol) phosphaamidine **20** was combined with 125 ml of a 8.482 x 10^{-3} M $Cr(CO)_5$·THF solution in THF. The reaction was stirred for 1.5 hours and monitored by solution IR. No noticeable color change was noticed. When the reaction was completed, THF was removed, leaving yellow solids. The solids were taken up in 90 ml of room temperature *n*-heptane, filtered through celite and placed in a –15 °C freezer. Isolation of multiple crops gave 215 mg (0.324 mmol) of long needle-like yellow crystals. Yield: 30.6% X-ray data crystals were grown from a concentrated Et_2O solution cooled to –15 °C.

^{1}H NMR ($CDCl_3$): δ 0.79(d, J(H-H) 6.7 Hz, 6H), 0.92(d, J(H-H) 6.9 Hz, 6H), 1.29 (d, J(H-H) 6.7 Hz, 6H), 1.40 (d, J(H-H) 6.7 Hz, 6H), 2.15 (d, ^{7}J(H-P) 1.8 Hz, 3H), 2.96 (sept., J(H-H) 6.6 Hz, 2H), 3.90 (septet, J(H-H) 6.7 Hz, 1H), 3.92 (septet, J(H-H) 6.7 Hz, 1H), 6.43 (s, 1H), 6.80-7.40(mult., 10H).

^{31}P NMR (Proton Coupled, $CDCl_3$): δ 45.03 ppm (s)

IR (KBr pellet) cm^{-1}: 3362(w), 2963(w), 2927(w), 2869(w), 2061(s), 1994(m), 1986(m), 1946(vs), 1926(vs), 1913(vs), 1906(vs), 1461(w), 1384(w), 1363(w), 1321(w), 1204(w), 1108(w), 1056(w), 804(w)759(w), 748(w), 670(m), 656(m), 455(w).

IR (*n*-heptane) cm^{-1}: 3351 (w), 2063 (s), 1949 (vs), 1934 (vs), 1912 (m), 1216 (s), 1104 (w), 803 (w), 758 (w).

UV (*n*-hexane) λ_{max} 246 (ε 28 600), 375 (ε 6 800).

MS(70eV): *m/z* 663.21879 (ML^+ based on ^{52}Cr, 0.31%); 607 ($ML - 2(CO)^+$, 1.6); 579 ($ML - 3(CO)^+$, 0.79); 523 ($ML - 5(CO)^+$, 67); 471 (L^+, 17); 428 ($L - {}^iPr^+$, 100); 278 ($L - C_6H_3{}^iPr_2PH^+$, 80); 105 ($C_8H_9^+$, 25); 91 ($C_7H_7^+$, 11).

9.9 Preparation of η^1-(*N*,*P*-bis(2,6-diisopropylphenyl)-*p*-methyl-benzphosphaamidine)-tungsten pentacarbonyl **26**

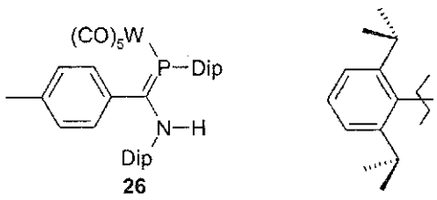

26

Dip = 2,6-diisopropylphenyl

In a 250 ml side arm flask, 0.500g (1.06 mmol) phosphaamidine **20** was combined with 125 ml of a 8.482 x 10^{-3} M $W(CO)_5$·THF solution in THF. A red solution formed which was allowed to stir overnight. Removal of THF left brown-yellow solids which were taken up in 65 ml of slightly warm *n*-heptane, filtered through celite and placed in a –15 °C freezer. Isolation of multiple crops gave 208 mg (0.261 mmol) of yellow crystals. Yield: 24.7%

^{1}H NMR ($CDCl_3$): δ 0.88 (d, J(H-H) 6.7 Hz, 6H), 0.97 (d, J(H-H) 6.7 Hz, 6H), 1.36 (d, J(H-H) 6.7 Hz, 6H), 1.47 (d, J(H-H) 6.7 Hz, 6H), 2.23 (d, J^7(P-H) 1.8 Hz, 3H), 3.02 (sept., J(H-H) 6.8 Hz, 2H), 3.98 (sept., J(H-H) 6.7 Hz, 1H), 4.00 sept., J(H-H) 6.6 Hz, 1H), 6.45 (s, 1H), 6.89-7.48 (mult., 10H).

^{31}P NMR ($CDCl_3$, ^{1}H coupled): δ 6.01 (d, J(P-^{183}W) = 255 Hz).

IR ($CHCl_3$) cm^{-1}: 3349 (w), 2963 (w), 2869 (w), 2069 (m), 1983 (w), 1944 (vs), 1938 (vs), 1915 (s), 1606 (w), 1462 (w), 1385 (w), 1365 (w), 1343 (w), 1325 (w).

IR (KBr) cm^{-1}: 3357 (w), 3055 (w), 2966 (m), 2927 (w), 2871 (w), 2067 (s), 1979 (s), 1946 (vs), 1923 (vs), 1901 (vs), 1607 (w), 1481 (w), 1465 (m), 1384 (w), 1362 (w), 1324 (m), 1265 (w), 1202 (m), 1177 (w), 816 (w), 803 (m), 759 (w), 748 (w), 597 (m), 579 (m), 512 (w).

IR (*n*-heptane) cm^{-1}: 2070 (w), 1948 (vs), 1939 (vs), 1929 (m). Due to low solubility in heptane, only CO peaks were noticeably visible.

UV (*n*-hexane) λ_{max} 239 (ε 35 900), 280 (ε 12 000), 401 (ε 9 700).

MS(70eV): *m/z* 739.23915 (ML - $2(CO)^+$ based on ^{184}W, 3.6%); 711 (ML - $3(CO)^+$, 44); 683 (ML - $4(CO)^+$, 2.1); 655 (ML – $5(CO)^+$, 11); 471 (L^+, 12); 278 (L - $C_6H_3{}^iPr_2PH^+$, 100); 236 (L - $C_6H_3{}^iPr_2PH$ $^iPr^+$, 5.5); 222 ($C_8H_9NCC_6H_4CH_3^+$, 6); 105 ($C_8H_9^+$, 19); 91 ($CH_3C_6H_4^+$, 10).

Elemental Analysis: Calc. for $C_{37}H_{42}WNO_6P$: C, 55.85; H, 5.33; N, 1.76. Found: C, 56.03; H, 5.30; N, 1.79%.

9.10 Preparation of η^1-(*N*,*P*-bis(2,6-diisopropylphenyl)-*p*-methoxy-benzphosphaamidine)-molybdenum pentacarbonyl **27**

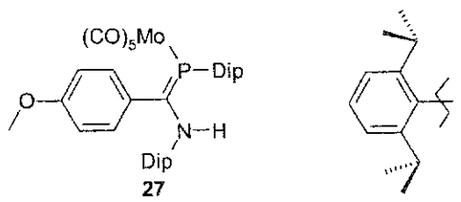

27

Dip = 2,6-diisopropylphenyl

In a schlenk tube, 0.140g (0.530 mmol) $Mo(CO)_6$ and 0.258g (0.530 mmol) phospaamidine **21** were combined with 13mL *n*-heptane. This was brought to reflux and followed by solution IR. After 4hrs all $Mo(CO)_6$ was consumed leaving a dark green/yellow solution. Cooling to –30 °C yielded fine green/yellow needles. The crystals were then dissolved in 55 ml of room temperature heptane, filtered though celite and cooled to –30 °C, giving small yellow blocks. Yield: 60 mg, 13.9%. mp: 150-160 °C decomp.

^{1}H NMR ($CDCl_3$): δ 0.88(d, J(H-H) 6.7 Hz, 6H), 0.98(d, J(H-H) 6.9 Hz, 6H), 1.36 (d, J(H-H) 6.7 Hz, 6H), 1.45 (d, J(H-H) 6.7 Hz, 6H), 3.01 (sept., J(H-H) 6.6 Hz, 2H), 3.71 (s, 3H), 3.99 (septet, J(H-H) 6.7 Hz, 1H), 4.01 (septet, J(H-H) 6.6 Hz, 1H), 6.45 (s, 1H), 6.690-7.47(mult., 10H).

^{13}C NMR ($CDCl_3$): Reliable spectrum could not be obtained due to rapid decomposition

^{31}P NMR (Proton Coupled, $CDCl_3$): δ 29.55 ppm (s)

IR (KBr) cm^{-1}: 3362 (w), 3065 (w), 2964 (m), 2929 (w), 2869 (w), 2070 (s), 1991 (m), 1953 (vs), 1933 (vs), 1908 (vs), 1606 (w), 1575 (w), 1511 (w), 1459 (m), 1384

(w), 1363 (w), 1324 (w), 1296 (w), 1253 (m), 1207 (w), 1174 (w), 1107 (w), 1040 (w), 829 (w), 804 (w), 759 (w), 606 (m), 587 (m).

IR (heptane) cm^{-1}: 2071 (m), 1955 (vs), 1947 (vs), 1933 (s).

IR ($CHCl_3$) cm^{-1}: 3350 (w), 2987 (w), 2941 (m), 2911 (m), 2850 (s), 2731 (w), 2669 (w), 2071 (s), 1991 (w), 1949 (vs), 1940 (vs), 1915 (s), 1605 (w), 1484 (w), 1467 (s), 1462 (s), 1454 (m), 1378 (m), 1343 (m), 1325 (w).

MS(70eV): *m/z* 741.19643 ($M - 3(CO)^+$ based on ^{98}Mo, 0.43%); 487 (L^+, 19); 444 L - $^iPr^+$, 100); 326 (L - $C_6H_3{}^iPr_2^+$, 6); 294 (L - $C_6H_3{}^iPr_2PH^+$, 89); 121 ($C_8H_9O^+$, 22); 91 ($C_6H_5N^+$, 7).

Elemental Analysis: Calc. for $C_{37}H_{42}MoNO_6P$: C, 61.41; H, 5.85; N, 1.94. Found: C, 61.60; H, 5.93; N, 2.03%.

9.11 Preparation of *N*,N',*P*-tris(2,6-diisopropylphenyl)phosphaguanidine **28**

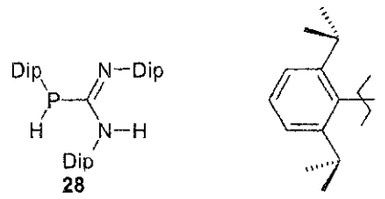

28

Dip = 2,6-diisopropylphenyl

In a 250 ml side arm flask, 3.22 g (16.6mmol) of $DipPH_2$ **15** and 60 ml dry THF were combined and cooled in an ice bath. 8.36ml (2.5% excess) of 2M *n*-BuLi was then added, resulting in a dark orange solution. This was stirred for another 10 min, removed from the ice bath and allowed to warm to room temperature. Upon cooling in an ice bath, 6.0 g (16.6 mmol) of Dip-N=C=N-Dip **204** in 35 ml dry THF were added drop-wise via a dropping funnel. The solution changed to a deep red color. After refluxing for 2 hr, the reaction was cooled, quenched with 2 ml H_2O, dried with anhydrous $MgSO_4$, filtered and all volatiles were removed under vacuum. The resulting red solid was taken up in a minimum of hot 99% ethanol and cooled to -30°C. First harvest of crystals offered colorless crystals while the second, significantly smaller crop produced crystals with orange impurities to give a total of 3.508 g. Analytical crystals were obtained by a second recrystallization. Yield: 38% Melting Point: 135-139°C.

^1H NMR ($CDCl_3$): δ 1.00(d, J(H-H) 6.7 Hz, 6H), 1.06(d, J(H-H) 6.7 Hz, 6H), approx. 1.21(s, 12H), 1.36(d, J(H-H) 6.9 Hz, 6H), 1.42(d, J(H-H) 6.9 Hz, 6H), 3.17(sept., J(H-H) 6.9 Hz, 2H), approx. 3.20(hidden under other septet)(s, 2H), 3.61(broad s, 2H), 4.87(d, J(P-H) 237 Hz, 1H), 5.35(s, 1H), 7.04-7.41(m, 9H).

^{13}C NMR ($CDCl_3$): δ 22.97, 23.28, 23.47, 23.59, 23.79, 23.91, 24.08, 24.38, 24.65, 24.94, 25.22, 27.88, 27.99, 28.35, 28.45, 28.73, 29.20, 33.30, 33.50, 33.79, 33.99, 122.42, 122.88, 123.03, 123.32, 123.81, 124.27, 126.77, 127.12, 127.34, 128.31, 130.76, 131.74, 134.37, 139.33, 139.62, 146.01, 146.18, 146.67, 154.36, 156.52, 157.09.

^{31}P NMR ($CDCl_3$): δ -94.82 ppm (d, J(H-P) 237 Hz)

IR (KBr) cm^{-1}: 3385(s), 3057(w), 2961(vs), 2929(s), 2867(s), 2374 (w), 2074(w), 1609(vs), 1582(vs), 1483(m), 1456(vs), 1434(s), 1419(m), 1384(m), 1361(m), 1345(w), 1324(m), 1302(w), 1272(m), 1255(w), 1216(w), 1189(m), 1160(w), 1138(m), 1107(m), 1055(w), 1040(w), 958(w), 935(w), 921(w), 880(w), 805(m), 799(m), 777(m), 758(s), 747(m), 729(w).

IR (CH_2Cl_2) cm^{-1}: 3392(m), 3019(w), 2867(s), 2728(w), 2669(w), 2591(w), 2373(w), 2306(w), 2165(w), 1949(w), 1925(w), 1875(w), 1804(w), 1708(w), 1665(w), 1620(m), 1612(vs), 1605(vs), 1581(vs), 1573(vs), 1480(m), 1382(m), 1363(m), 1343(w), 1327(w), 1219(w), 1185(w), 1141(w), 1106(w), 1058(m), 1042(w), 959(W), 935(w), 877(w), 805(w).

IR ($CHCl_3$) cm^{-1}: 3395 (w), 2958 (m), 2867 (m), 2376 (w, is this co2?), 1606 (vs), 1580 (vs), 1574 (s), 1462 (vs), 1454 (s), 1384(m), 1363 (m), 1343 (w), 1324 (m), 1141 (m), 1103 (m), 959 (w), 888 (w).

IR (heptane) cm^{-1}: 3401(s), 3327(broad), 3070(w), 2552(w), 2376(w), 2171(w), 1620(vs), 1612(vs), 1584(vs), 1574(s), 1324(w), 1255(w), 1220(m), 1187(m), 1108(m), 1056(w), 1042(w), 800(m), 757(w).

Mass Spectrum: *m/z* 556.39424 (M^+, 13%); 513 (M - $^iPr^+$, 9); 363 (M – $C_6H_3{}^iPr_2PH^+$, 100); 186($C_{13}H_{16}N^+$, 26); 177 ($C_6H_3{}^iPr_2NH_2^+$, 45); 162 ($C_{11}H_{16}N^+$, 22.81); 146 ($C_{10}H_{12}N^+$, 19.94); 69 ($C_5H_9^+$, 84.23).

Elemental Analysis: Calc. for $C_{37}H_{53}N_2P$: C, 79.81; H, 9.59; N, 5.03. Found: C, 79.51; H, 8.91; N, 5.05%.

9.12 Preparation of 2,6-diisopropylphenyl-trimethylsilylphosphane **16**

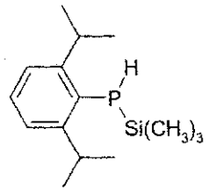

16

In a 250 ml side arm flask, 8.412g (43.29 mmol) $DipPH_2$ **15** and 80 ml THF were combined and stirred in an ice bath. Then 28.4 ml of 1.6M *n*-BuLi was added. The clear solution turned yellow initially and upon complete addition of *n*-BuLi the solution became red. The flask was then removed from the ice bath and allowed to stir for 20 minutes and returned to the ice bath. To the rapidly stirring solution, 5.77 ml (45.46 mmol, 5% excess) $ClSiMe_3$ was added via syringe. The solution was then refluxed for 2hr. Volatiles were removed under vacuum to leave a red paste, to which 100 ml hexanes were added. Removal of hexanes and vacuum distillation (110-115°C, 0.5 mbar) gave a clear oil. Yield: 7.39 g, 64%

^{1}H NMR ($CDCl_3$): δ 0.18 (d, J^3(H-P) 4.3 Hz, 9H), 1.21 (d, J(H-H) 6.7 Hz, 6H), 1.26 (d, J(H-H) 6.7 Hz, 6H), 3.41 (septet of doublets, J^4(H-P) 3.8 Hz, J(H-H) 6.7 Hz, 2H), 3.46 (d, J(H-P) 211 Hz, 1H), 7.09-7.25 (mult., 3H).

^{13}C NMR ($CDCl_3$): δ 0.67 (d, ^{2}J(P-C) 10.3 Hz, $SiCH_3$), 23.97 (s, ^{i}Pr-CH_3), 24.18 (s, ^{i}Pr-CH_3), 33.50 (d, ^{3}J(P-C) 13.7 Hz, ^{i}Pr-CH), 122.94 (d, ^{3}J(P-C) 3.4 Hz, *meta-C*), 127.44 (s, *para-C*), 129.21 (d, ^{1}J(P-C) 20.5 Hz, *ipso-C*), 152.03, (d, ^{2}J(P-C) 20.5 Hz, *ortho-C*).

^{31}P NMR (Proton Coupled, $CDCl_3$): δ -163.8 (d, J(H-P) 211 Hz).

Mass Spectrum: *m/z* 266.16084 (M^+, 64%); 193 ($C_6H_3{}^iPr_2PH^+$, 57); 149 ($C_9H_{10}P$, 14); 73 (C_3H_9Si, 100). The oxide, dioxide, disilylated and disilylatedoxide are also present in small quantities.

9.13 Preparation of 2,6-diisopropylphenyl-bis(trimethylsilyl)phosphane **18**

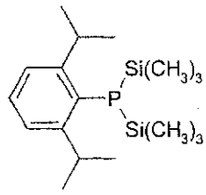

In a Schlenk tube, 2.00 g (10.3mmol) of $DipPH_2$ **15** and 20 ml THF were combined and cooled in an ice bath. 6.76ml (10.8 mmol, 5% excess) of 1.6M BuLi was added to the stirring solution to give an orange colored solution. After 20 minutes, 1.37 ml (10.8 mmol) of TMSCl was added giving a clear solution with a white ppt. Analysis by ^{31}P NMR spectroscopy showed some starting material present. Another 5.07 ml (8.11mmol) of 1.6M *n*-BuLi and 1.03ml (8.11mmol) TMSCl were added following the same procedure as before. NMR analysis showed 75% DipPTMS2 and 25% DipPHTMS. Again 5.07 ml (8.11mmol) of 1.6M BuLi and 1.03ml (8.11mmol) TMSCl were added following the same procedure and NMR analysis showed complete conversion to desired product. Volatiles were removed under vacuum and 100 ml hexanes were added to the remaining solids. Filtration of LiCl solids and removal of hexanes left a off-white oily solid. Distillation yielded 2.20 g of a white paste. (b.p. 120-130°C, full vacuum) Yield: 63%.

^{1}H NMR ($CDCl_3$): δ 0.22 (d, J^{3}(H-P) 6.1 Hz, 18H), 1.18 (d, J(H-H) 6.9 Hz, 12H), 4.05 (sept., J(H-H) 6.4, 2H), 7.08-7.26(m, 3H).

^{13}C NMR ($CDCl_3$): δ 2.55 (d, ^{2}J(P-C) 17.0 Hz, $Si(CH_3)_3$), 25.32 (s, ^{i}Pr-CH_3), 33.98 (d, ^{3}J(H-P) 16.1 Hz, ^{i}Pr-CH), 123.43 (d, ^{3}J(P-C) 5.4 Hz, *meta-C*), 128.29 (d, ^{1}J(P-C) 14.2 Hz, *ipso-C*), 128.55 (d, ^{4}J(P-C) 2.0 Hz, *para-C*), 156.44 (d, ^{2}J(P-C) 10.7 Hz, *ortho-C*).

^{31}P NMR (Proton Coupled, $CDCl_3$): δ -167.1 (s) ppm

IR (neat oil) cm^{-1}: 3050(m), 2957 (vs), 2867 (s), (CO2?? 2360 and 2340), 1935 (w), 1861 (w), 1695 (w), 1651 (w), 1633 (w), 1589 (w), 1569 (m), 1557 (w), 1463 (s), 1381 (m), 1361 (m), 1304 (m), 1246 (s), 1177 (m), 1048 (m), 992 (m), 835 (s), 801 (m), 748 (m), 684 (m), 625 (m), 509 (w), 402 (w).

MS(70eV): *m/z* 338.20229 (M^+, 49%); 266 ($C_6H_3{}^iPr_2PH(Si(CH_3)_2{}^+$, 15); 193 ($C_6H_3{}^iPr_2PH^+$, 16); 73 ($Si(CH_3)_3$, 100).

9.14 Preparation of 2.6-diisopropylphenyl-(tert-butyl-dimethylsilyl)phosphane **17**

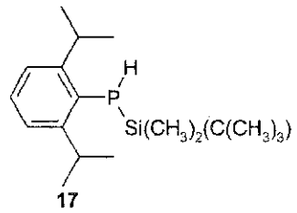

17

In a Schlenk tube, 4.00 g (20.59 mmol) of $DipPH_2$ **15** was combined with 40 ml THF and placed in an ice bath. Then 13.5 ml (21.62 mmol, 5% excess) of a 1.6M *n*-BuLi solution was added to form a yellow solution. After stirring at room temperature for 30 mins the solution was cooled again in an ice bath. Then 3.104 g (20.59 mmol) $ClSi\{CH_3)_2{}^tBu\}$ was added. Upon refluxing for 1 hour, ^{31}P NMR showed 70% conversion. The reaction sequence was then repeated using 4.5 ml *n*-BuLi and 1.05 g $ClSi\{CH_3)_2{}^tBu\}$, where ^{31}P NMR showed complete conversion. Volatiles were removed under vacuum leaving a white solid. Addition of 20 ml hexanes, filtration and removal of solvent left a white solid. Static vacuum sublimation onto a cold finger gave a white crystalline solid. Yield: 3.60 g, 56.7 %. mp: 45-51°C. X-ray quality crystals were obtained by sublimation in a three zone tube furnace under dynamic vacuum.

^1H NMR ($CDCl_3$): δ 0.02 (d, ^2J(P-H) 0.9 Hz, 3H), 0.06 (d, ^2J(P-H) 5.3 Hz, 3H), 1.01 (d, ^3J(P-H) 2.4 Hz, 9H), 1.21 (d, J(H-H) 6.9Hz, 6H), 1.26 (d, J(H-H) 6.7 Hz, 6H), 3.43 (doublet of septets, ^{4}(P-H) 4.0 Hz, J(H-H) 6.8 Hz, 2H), 3.51 (d, J(P-H) 211 Hz, 1H), 7.08-7.26 (m, 3H).

^{13}C NMR ($CDCl_3$): δ -4.20 (d, ^2J(P-C) 15.6 Hz, $SiCH_3$), -2.93 (s, $SiCH_3$), 18.70 (d, ^2J(P-C) 9.8 Hz, $C(CH_3)_3$), 24.00 (s, ^iPr-CH_3), 24.16 (s, ^iPr-CH_3), 27.02 (d, ^4J(P-C) 2.9 Hz, $C(CH_3)_3$), 33.53 (d, ^3J(P-C) 13.7 Hz, ^iPr-CH), 122.97 (d, ^4J(P-C) 3.4 Hz, *meta-C*),

127.52 (s, *para-C*), 129.04 (d, ^{1}J(P-C) 21.4 Hz, *ipso-C*), 152.47 (d, ^{2}J(P-C) 9.3 Hz, *ortho-C*).

^{31}P NMR ($CDCl_3$): δ -175.6 ppm (d, J(H-P) 212.1 Hz).

IR (KBr) cm^{-1}: 3050(w), 2958(vs), 2925(vs), 2856(s), 2330(m), 1567(w), 1463(s), 1417(w), 1381(w), 1362(s), 1246(m), 1176(w), 1050(w), 1006(w), 938(w), 839(s), 821(s), 804(vs), 773(w), 737(vs), 680(w), 601(w), 578(w), 444(w), 430(w).

MS(70eV): *m/z* 308.20866 (M^+, 53%); 251 ($C_6H_3{}^{i}Pr_2PH(Si(CH_3)_2{}^-$, 11); 193 ($C_6H_3{}^{i}Pr_2PH^-$, 15); 115 ($(CH_3)_3CSi(CH_3)_2{}^+$, 13.7); 73 ($Si(CH_3)_3$, 100).

Elemental Analysis: Calc. for $C_{18}H_{33}PSi$: C, 70.08; H, 10.78. Found: C, 69.84; H, 10.62%.

9.15 Preparation of 2,6-diisopropylphenyl-bis(tert-butyl-dimethylsilyl)phosphane **19**

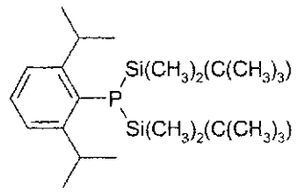

19

A solution of 2.00 g (10.3 mmol) $DipPH_2$ **15** in 20 ml THF held at 0°C was treated with 6.43 ml (10.29 mmol) of 1.6 M *n*-BuLi. After warming to RT, the yellow solution was cooled again and treated with 1.55 g (10.29 mmol) $ClSi\{(CH_3)_2{}^tBu\}$. The faint yellow solution was allowed to warm to room temperature over 30 mins. Cooling again in an ice bath and treatment with another 6.43 ml of 1.6 M *n*BuLi gave an orange solution. Again 1.55 g $ClSi\{CH_3)_2{}^tBu\}$ was added after warming the reaction mixture to room temperature and cooling to 0°C. The faint yellow solution was then heated to reflux for 12 hours and NMR analysis showed complete conversion to product. Evaporation of solvent, extraction into 30 ml pentane, filtering, and evaporation yielded a white solid, which was purified by sublimation under dynamic vacuum onto a water-cooled cold finger to give 2.934 g of a white crystalline solid (7.7 mmol, 75% yield, mp. 57-62 °C).

^1H NMR ($CDCl_3$): δ 0.182 (d, J(P-H) 4.3 Hz, 12H) 0.869 (d, J(H-P) 0.76 Hz, 18H) 1.21 (d, J(H-H) 6.7 Hz, 12H), 4.29 (sept., J(H-H) 6.7 Hz, 2H), 7.08-7.26 (m, 3H).

^{13}C NMR ($CDCl_3$): δ –1.54 (d, ^2J(P-C) 7.8 Hz, $SiCH_3$), 20.18 (d, ^2J(P-C) 20.5 Hz, $C(CH_3)_3$), 25.67 (s, ^iPr-CH_3), 27.79 (d, ^4J(P-C) 3.9 Hz, $C(CH_3)_3$), 33.96 (d, ^3J(P-C) 16.1 Hz, ^iPr-CH), 128.59 (d, ^4J(P-C) 1.95 Hz, *para-C*), 128.92 (d, ^3J(P-C) 5.4 Hz, *meta-C*), 130.44 (d, ^1J(P-C) 9.3 Hz, *ipso-C*), 156.57 (d, ^2J(P-C) 11.2 Hz, *ortho-C*).

^{31}P NMR ($CDCl_3$): δ -193.25 (s).

IR (KBr) cm^{-1}: 3047(w), 2958(vs), 2929(vs), 2894(s), 2857(s), 2569(w), 1471(m), 1460(m), 1403(w), 1388(m), 1380(m), 1360(m), 1251(s), 1245(s), 1177(w), 1048(w), 1024(w), 1005(w), 834(vs), 820(s), 794(vs), 760(s), 742(m), 681(w), 670(m), 660(w), 575(w), 470(w), 408(w).

MS(70eV): *m/z* 422.29533 (M^+, 30%); 251 (M - $^tBu^+$, 11); 73 ($Si(CH_3)_3$, 100).

Elemental Analysis: Calc. for $C_{24}H_{47}PSi_2$: C, 68.18; H, 11.21. Found: C, 67.99; H, 10.94%.

Appendix

Table A.1 Crystal data and structure refinement for **17**.

Identification code	**17**	
Empirical formula	C18 H33 P Si	
Formula weight	308.50	
Temperature	193(2) K	
Wavelength	0.71073 Å	
Crystal system	Monoclinic	
Space group	P2(1)/c	
Unit cell dimensions	a = 8.5768(10) Å	α= 90°.
	b = 28.104(3) Å	β= 93.341(3)°.
	c = 8.1102(9) Å	γ = 90°.
Volume	1951.6(4) $Å^3$	
Z	4	
Density (calculated)	1.050 Mg/m^3	
Absorption coefficient	0.194 mm^{-1}	
F(000)	680	
Crystal size	0.14 x 0.19 x 0.20 mm^3	
Theta range for data collection	2.38 to 26.41°.	
Index ranges	-10<=h<=10, -29<=k<=35, -8<=l<=10	
Reflections collected	11570	
Independent reflections	4009 [R(int) = 0.0618]	
Completeness to theta = 26.41°	99.8 %	
Absorption correction	None	
Refinement method	Full-matrix least-squares on F^2	
Data / restraints / parameters	4009 / 0 / 194	
Goodness-of-fit on F^2	0.953	
Final R indices [I>2sigma(I)]	R1 = 0.0518, wR2 = 0.1141	
R indices (all data)	R1 = 0.0918, wR2 = 0.1308	
Largest diff. peak and hole	0.338 and -0.196 $e.Å^{-3}$	

Table A.2 Atomic coordinates (x 10^4) and equivalent isotropic displacement parameters ($Å^2$x 10^3) for **17**. U(eq) is defined as one third of the trace of the orthogonalized U^{ij} tensor.

	x	y	z	U(eq)
Si(1)	2847(1)	6292(1)	2962(1)	29(1)
P(1)	5366(1)	6439(1)	2418(1)	38(1)
C(1)	6514(2)	6085(1)	3987(3)	27(1)
C(2)	7018(3)	6307(1)	5489(3)	30(1)
C(9)	7022(3)	5620(1)	3641(3)	31(1)
C(3)	6485(3)	6800(1)	5989(3)	36(1)
C(10)	6485(3)	5350(1)	2086(3)	38(1)
C(8)	8085(3)	5400(1)	4765(3)	37(1)
C(6)	8068(3)	6066(1)	6569(3)	39(1)
C(7)	8614(3)	5621(1)	6202(3)	42(1)
C(11)	6129(3)	4824(1)	2405(4)	56(1)
C(12)	7672(3)	5398(1)	764(3)	57(1)
C(4)	7728(3)	7175(1)	5712(4)	55(1)
C(5)	6007(3)	6819(1)	7769(3)	54(1)
C(15)	1600(3)	6670(1)	1468(3)	39(1)
C(13)	2482(3)	6443(1)	5140(3)	51(1)
C(14)	2351(3)	5652(1)	2646(4)	52(1)
C(16)	-112(3)	6620(1)	1861(5)	73(1)
C(17)	1752(4)	6504(2)	-294(4)	86(1)
C(18)	2066(4)	7193(1)	1616(5)	95(1)

Table A.3 Bond lengths [Å] and angles [°] for **17**.

Si(1)-C(13)	1.861(3)
Si(1)-C(14)	1.864(3)
Si(1)-C(15)	1.894(3)
Si(1)-P(1)	2.2681(9)
P(1)-C(1)	1.854(2)
C(1)-C(9)	1.410(3)
C(1)-C(2)	1.415(3)
C(2)-C(6)	1.396(3)
C(2)-C(3)	1.521(3)
C(9)-C(8)	1.396(3)
C(9)-C(10)	1.521(3)
C(3)-C(5)	1.524(3)
C(3)-C(4)	1.523(3)
C(10)-C(12)	1.527(4)
C(10)-C(11)	1.533(4)
C(8)-C(7)	1.374(3)
C(6)-C(7)	1.375(4)
C(15)-C(17)	1.516(4)
C(15)-C(18)	1.527(4)
C(15)-C(16)	1.526(4)
C(13)-Si(1)-C(14)	107.49(14)
C(13)-Si(1)-C(15)	111.09(13)
C(14)-Si(1)-C(15)	109.72(13)
C(13)-Si(1)-P(1)	110.97(9)
C(14)-Si(1)-P(1)	111.20(9)
C(15)-Si(1)-P(1)	106.42(8)
C(1)-P(1)-Si(1)	104.03(7)
C(9)-C(1)-C(2)	119.9(2)
C(9)-C(1)-P(1)	121.26(17)
C(2)-C(1)-P(1)	118.49(17)
C(6)-C(2)-C(1)	118.6(2)
C(6)-C(2)-C(3)	118.0(2)
C(1)-C(2)-C(3)	123.4(2)

C(8)-C(9)-C(1)	118.6(2)
C(8)-C(9)-C(10)	118.3(2)
C(1)-C(9)-C(10)	123.1(2)
C(2)-C(3)-C(5)	112.6(2)
C(2)-C(3)-C(4)	111.5(2)
C(5)-C(3)-C(4)	110.2(2)
C(9)-C(10)-C(12)	110.9(2)
C(9)-C(10)-C(11)	113.3(2)
C(12)-C(10)-C(11)	110.6(2)
C(7)-C(8)-C(9)	121.7(2)
C(7)-C(6)-C(2)	121.5(2)
C(8)-C(7)-C(6)	119.7(2)
C(17)-C(15)-C(18)	109.4(3)
C(17)-C(15)-C(16)	107.8(3)
C(18)-C(15)-C(16)	108.8(3)
C(17)-C(15)-Si(1)	110.8(2)
C(18)-C(15)-Si(1)	110.73(19)
C(16)-C(15)-Si(1)	109.25(19)

Table A.4 Anisotropic displacement parameters ($Å^2 x\ 10^3$) for **17**. The anisotropic displacement factor exponent takes the form: $-2\pi^2[\ h^2\ a^{*2}U^{11} + ...\ + 2\ h\ k\ a^*\ b^*\ U^{12}\ ]$

	U^{11}	U^{22}	U^{33}	U^{23}	U^{13}	U^{12}
Si(1)	29(1)	27(1)	31(1)	0(1)	5(1)	-1(1)
P(1)	28(1)	52(1)	35(1)	16(1)	2(1)	-1(1)
C(1)	21(1)	31(1)	29(1)	5(1)	5(1)	-3(1)
C(2)	30(1)	30(1)	31(1)	3(1)	5(1)	-4(1)
C(9)	28(1)	32(1)	32(1)	1(1)	6(1)	0(1)
C(3)	39(2)	33(1)	36(1)	-4(1)	0(1)	-1(1)
C(10)	36(1)	39(2)	38(1)	-9(1)	0(1)	5(1)
C(8)	38(2)	32(1)	42(1)	3(1)	2(1)	6(1)
C(6)	41(2)	42(2)	32(1)	2(1)	-4(1)	-4(1)
C(7)	40(2)	45(2)	41(2)	10(1)	-7(1)	4(1)
C(11)	60(2)	38(2)	70(2)	-14(1)	-4(2)	-1(1)
C(12)	61(2)	70(2)	42(2)	-18(1)	12(1)	2(2)
C(4)	57(2)	38(2)	69(2)	-3(1)	6(2)	-10(1)
C(5)	63(2)	58(2)	43(2)	-14(1)	7(1)	1(2)
C(15)	28(1)	43(2)	47(2)	6(1)	1(1)	3(1)
C(13)	43(2)	72(2)	40(2)	-4(1)	12(1)	-10(1)
C(14)	44(2)	31(2)	82(2)	0(1)	11(2)	-5(1)
C(16)	35(2)	81(3)	103(3)	22(2)	9(2)	14(2)
C(17)	69(2)	146(4)	43(2)	10(2)	-7(2)	36(2)
C(18)	82(3)	52(2)	146(4)	38(2)	-38(2)	-7(2)

Table A.5 Hydrogen coordinates (x 10^4) and isotropic displacement parameters ($Å^2$x 10^3) for **17**.

	x	y	z	U(eq)
H(3)	5544	6883	5260	43
H(10)	5493	5501	1640	45
H(8)	8453	5090	4530	45
H(6)	8415	6212	7581	46
H(7)	9352	5466	6939	51
H(11A)	5670	4679	1390	84
H(11B)	5391	4800	3279	84
H(11C)	7098	4658	2749	84
H(12A)	7278	5234	-244	86
H(12B)	8664	5254	1163	86
H(12C)	7835	5735	524	86
H(4A)	7344	7488	6032	82
H(4B)	7957	7179	4543	82
H(4C)	8680	7098	6385	82
H(5A)	5254	6564	7949	82
H(5B)	5527	7127	7979	82
H(5C)	6931	6775	8522	82
H(13A)	2624	6786	5313	77
H(13B)	3220	6268	5885	77
H(13C)	1412	6354	5369	77
H(14A)	2440	5568	1482	78
H(14B)	1279	5594	2954	78
H(14C)	3073	5455	3336	78
H(16A)	-410	6283	1819	109
H(16B)	-767	6799	1047	109
H(16C)	-257	6746	2968	109
H(17A)	2833	6547	-596	130
H(17B)	1054	6692	-1040	130
H(17C)	1468	6167	-387	130
H(18A)	3130	7234	1260	142

H(18B)	2024	7295	2768	142
H(18C)	1342	7386	915	142
H(1)	5270(50)	6171(16)	1090(50)	140(15)

Table A.6 Crystal data and structure refinement for **20**.

Identification code	**20**	
Empirical formula	C32 H42 N P	
Formula weight	471.64	
Temperature	293(2) K	
Wavelength	0.71073 Å	
Crystal system	Monoclinic	
Space group	P2(1)/c	
Unit cell dimensions	a = 18.2859(15) Å	α= 90°.
	b = 10.0468(5) Å	β= 117.175(9)°.
	c = 18.1513(14) Å	γ = 90°.
Volume	2966.6(4) $Å^3$	
Z	4	
Density (calculated)	1.056 Mg/m^3	
Absorption coefficient	0.111 mm^{-1}	
F(000)	1024	
Crystal size	0.12 x 0.06 x 0.20 mm^3	
Theta range for data collection	2.25 to 26.16°.	
Index ranges	-22<=h<=22, -12<=k<=12, -22<=l<=22	
Reflections collected	25282	
Independent reflections	5769 [R(int) = 0.0722]	
Completeness to theta = 26.16°	97.1 %	
Absorption correction	None	
Refinement method	Full-matrix least-squares on F^2	
Data / restraints / parameters	5769 / 0 / 320	
Goodness-of-fit on F^2	0.820	
Final R indices [I>2sigma(I)]	R1 = 0.0490, wR2 = 0.1122	
R indices (all data)	R1 = 0.1017, wR2 = 0.1301	
Largest diff. peak and hole	0.219 and -0.160 $e.Å^{-3}$	

Table A.7 Atomic coordinates (x 10^4) and equivalent isotropic displacement parameters ($Å^2$x 10^3) for **20**. U(eq) is defined as one third of the trace of the orthogonalized U^{ij} tensor.

	x	y	z	U(eq)
P(1)	2646(1)	4509(1)	6169(1)	68(1)
C(1)	2465(1)	3129(2)	6611(1)	53(1)
C(2)	2351(1)	1854(2)	6154(1)	54(1)
N(1)	2493(1)	3132(2)	7377(1)	57(1)
C(21)	2852(2)	5786(2)	6973(1)	64(1)
C(17)	2890(2)	1841(2)	8623(1)	62(1)
C(9)	2288(1)	2135(2)	7814(1)	54(1)
C(8)	1907(2)	1842(3)	5292(1)	71(1)
C(10)	1508(2)	1554(2)	7475(1)	60(1)
C(29)	3674(2)	6175(3)	7477(2)	78(1)
C(3)	2730(2)	687(2)	6546(1)	62(1)
C(23)	1320(2)	6071(3)	6507(2)	89(1)
C(30)	4391(2)	5466(4)	7435(2)	107(1)
C(22)	2208(2)	6445(3)	7041(2)	73(1)
C(4)	2692(2)	-445(3)	6094(2)	73(1)
C(5)	2282(2)	-453(3)	5240(2)	76(1)
C(18)	3720(2)	2524(3)	8991(2)	80(1)
C(14)	1355(2)	628(3)	7961(2)	76(1)
C(26)	2405(3)	7484(3)	7611(2)	99(1)
C(6)	2291(2)	-1670(3)	4752(2)	115(1)
C(11)	812(2)	1950(3)	6644(1)	71(1)
C(15)	1931(2)	333(3)	8752(2)	85(1)
C(7)	1880(2)	701(3)	4849(2)	83(1)
C(16)	2683(2)	930(3)	9077(2)	79(1)
C(13)	446(2)	759(4)	6065(2)	113(1)
C(20)	4417(2)	1678(5)	9622(2)	135(2)
C(12)	160(2)	2733(4)	6771(2)	117(1)
C(27)	3193(3)	7860(3)	8089(2)	116(1)
C(28)	3825(3)	7229(3)	8028(2)	106(1)
C(24)	960(2)	6773(5)	5658(3)	146(2)
C(25)	751(3)	6302(5)	6901(3)	171(2)

C(19)	3676(2)	3877(4)	9371(2)	113(1)
C(32)	5107(3)	5194(6)	8278(3)	173(2)
C(31)	4656(4)	6173(7)	6878(4)	220(3)

Table A.8 Bond lengths [Å] and angles [°] for **20**.

P(1)-C(1)	1.709(2)
P(1)-C(21)	1.847(2)
C(1)-N(1)	1.368(2)
C(1)-C(2)	1.488(3)
C(2)-C(3)	1.383(3)
C(2)-C(8)	1.395(3)
N(1)-C(9)	1.429(3)
C(21)-C(22)	1.404(4)
C(21)-C(29)	1.411(4)
C(17)-C(16)	1.395(3)
C(17)-C(9)	1.407(3)
C(17)-C(18)	1.515(4)
C(9)-C(10)	1.397(3)
C(8)-C(7)	1.388(3)
C(10)-C(14)	1.396(3)
C(10)-C(11)	1.516(3)
C(29)-C(28)	1.395(4)
C(29)-C(30)	1.525(4)
C(3)-C(4)	1.385(3)
C(23)-C(22)	1.511(4)
C(23)-C(25)	1.525(4)
C(23)-C(24)	1.543(4)
C(30)-C(31)	1.486(5)
C(30)-C(32)	1.516(5)
C(22)-C(26)	1.396(4)
C(4)-C(5)	1.380(4)
C(5)-C(7)	1.382(4)
C(5)-C(6)	1.514(4)
C(18)-C(20)	1.525(4)
C(18)-C(19)	1.544(4)
C(14)-C(15)	1.370(4)
C(26)-C(27)	1.353(5)
C(11)-C(13)	1.530(4)
C(11)-C(12)	1.532(4)

C(15)-C(16)	1.362(4)
C(27)-C(28)	1.366(5)

C(1)-P(1)-C(21)	101.87(10)
N(1)-C(1)-C(2)	119.98(19)
N(1)-C(1)-P(1)	123.38(17)
C(2)-C(1)-P(1)	116.39(14)
C(3)-C(2)-C(8)	117.8(2)
C(3)-C(2)-C(1)	122.27(18)
C(8)-C(2)-C(1)	119.6(2)
C(1)-N(1)-C(9)	131.6(2)
C(22)-C(21)-C(29)	119.9(2)
C(22)-C(21)-P(1)	121.4(2)
C(29)-C(21)-P(1)	118.44(19)
C(16)-C(17)-C(9)	117.4(2)
C(16)-C(17)-C(18)	121.7(2)
C(9)-C(17)-C(18)	120.9(2)
C(10)-C(9)-C(17)	121.7(2)
C(10)-C(9)-N(1)	121.49(19)
C(17)-C(9)-N(1)	116.6(2)
C(7)-C(8)-C(2)	120.4(2)
C(14)-C(10)-C(9)	117.4(2)
C(14)-C(10)-C(11)	119.0(2)
C(9)-C(10)-C(11)	123.5(2)
C(28)-C(29)-C(21)	118.6(3)
C(28)-C(29)-C(30)	119.8(3)
C(21)-C(29)-C(30)	121.6(2)
C(2)-C(3)-C(4)	120.9(2)
C(22)-C(23)-C(25)	115.2(3)
C(22)-C(23)-C(24)	111.7(3)
C(25)-C(23)-C(24)	109.2(3)
C(31)-C(30)-C(32)	111.9(4)
C(31)-C(30)-C(29)	111.4(3)
C(32)-C(30)-C(29)	113.6(3)
C(26)-C(22)-C(21)	118.4(3)
C(26)-C(22)-C(23)	119.9(3)

C(21)-C(22)-C(23)	121.7(2)
C(5)-C(4)-C(3)	121.6(3)
C(4)-C(5)-C(7)	117.4(2)
C(4)-C(5)-C(6)	121.0(3)
C(7)-C(5)-C(6)	121.5(3)
C(17)-C(18)-C(20)	113.8(3)
C(17)-C(18)-C(19)	110.4(2)
C(20)-C(18)-C(19)	110.6(3)
C(15)-C(14)-C(10)	121.7(3)
C(27)-C(26)-C(22)	121.5(3)
C(10)-C(11)-C(13)	112.5(2)
C(10)-C(11)-C(12)	110.0(2)
C(13)-C(11)-C(12)	112.2(3)
C(16)-C(15)-C(14)	120.0(2)
C(5)-C(7)-C(8)	121.7(2)
C(15)-C(16)-C(17)	121.7(2)
C(26)-C(27)-C(28)	120.8(3)
C(27)-C(28)-C(29)	120.8(4)

Table A.9 Anisotropic displacement parameters ($Å^2 x\ 10^3$) for **20**. The anisotropic displacement factor exponent takes the form: $-2\pi^2[\ h^2\ a^{*2}U^{11} + ... + 2\ h\ k\ a^*\ b^*\ U^{12}\ ]$

	U^{11}	U^{22}	U^{33}	U^{23}	U^{13}	U^{12}
P(1)	98(1)	58(1)	62(1)	-1(1)	50(1)	-6(1)
C(1)	57(1)	55(1)	48(1)	0(1)	26(1)	2(1)
C(2)	58(1)	55(1)	57(1)	-5(1)	32(1)	-6(1)
N(1)	79(1)	50(1)	48(1)	-1(1)	33(1)	-5(1)
C(21)	93(2)	49(2)	63(1)	5(1)	46(1)	2(1)
C(17)	77(2)	64(2)	51(1)	3(1)	33(1)	11(1)
C(9)	72(2)	48(1)	50(1)	5(1)	34(1)	6(1)
C(8)	81(2)	73(2)	58(1)	-7(1)	31(1)	-6(1)
C(10)	72(2)	56(2)	61(1)	2(1)	38(1)	1(1)
C(29)	98(2)	61(2)	74(2)	-3(1)	39(2)	-3(2)
C(3)	70(2)	57(2)	65(1)	-3(1)	36(1)	2(1)
C(23)	106(2)	70(2)	115(2)	17(2)	72(2)	19(2)
C(30)	86(2)	113(3)	114(2)	-18(2)	38(2)	-10(2)
C(22)	104(2)	56(2)	78(2)	7(1)	57(2)	8(1)
C(4)	84(2)	56(2)	92(2)	-8(1)	52(2)	-4(1)
C(5)	91(2)	64(2)	91(2)	-23(1)	58(2)	-17(2)
C(18)	77(2)	98(2)	57(1)	-3(1)	25(1)	8(2)
C(14)	95(2)	66(2)	86(2)	2(1)	58(2)	-7(1)
C(26)	155(3)	62(2)	107(2)	-5(2)	83(3)	15(2)
C(6)	158(3)	86(2)	136(3)	-48(2)	98(3)	-32(2)
C(11)	63(2)	79(2)	72(2)	5(1)	32(1)	1(1)
C(15)	126(3)	70(2)	79(2)	17(1)	64(2)	4(2)
C(7)	97(2)	94(2)	64(1)	-25(1)	41(2)	-22(2)
C(16)	112(2)	77(2)	55(1)	15(1)	45(2)	18(2)
C(13)	109(3)	105(3)	95(2)	-8(2)	20(2)	-24(2)
C(20)	98(3)	185(4)	93(2)	27(2)	19(2)	36(3)
C(12)	94(2)	145(3)	129(3)	36(2)	68(2)	38(2)
C(27)	195(4)	70(2)	94(2)	-21(2)	75(3)	-5(3)
C(28)	137(3)	80(2)	83(2)	-20(2)	35(2)	-20(2)
C(24)	110(3)	147(4)	160(3)	69(3)	43(3)	16(3)
C(25)	175(4)	167(5)	254(5)	-26(4)	171(4)	-5(3)

C(19)	111(3)	124(3)	102(2)	-48(2)	46(2)	-26(2)
C(32)	109(3)	202(6)	179(4)	18(4)	42(3)	19(3)
C(31)	245(7)	235(7)	288(7)	85(6)	216(6)	59(5)

Table A.10 Hydrogen coordinates (x 10^4) and isotropic displacement parameters ($Å^2$x 10^3) for **20**.

	x	y	z	U(eq)
H(8)	1627	2602	5013	85
H(3)	3016	661	7121	74
H(23)	1310	5114	6400	107
H(30)	4184	4595	7182	128
H(4)	2948	-1220	6373	88
H(18)	3852	2706	8534	95
H(14)	848	201	7743	91
H(26)	1985	7928	7663	119
H(6A)	2300	-2458	5055	172
H(6B)	2771	-1650	4666	172
H(6C)	1808	-1674	4226	172
H(11)	1043	2552	6379	86
H(15)	1809	-275	9066	102
H(7)	1584	713	4275	100
H(16)	3068	724	9615	95
H(13A)	29	1064	5539	170
H(13B)	208	152	6304	170
H(13C)	872	315	5990	170
H(20A)	4933	2112	9769	203
H(20B)	4416	822	9386	203
H(20C)	4340	1567	10108	203
H(12A)	-240	3080	6249	175
H(12B)	417	3455	7148	175
H(12C)	-106	2154	6996	175
H(27)	3306	8556	8463	140
H(28)	4363	7505	8358	127
H(24A)	402	6490	5329	219
H(24B)	1281	6547	5380	219
H(24C)	974	7719	5737	219
H(25A)	216	5950	6546	256

H(25B)	709	7240	6977	256
H(25C)	971	5862	7429	256
H(19A)	4179	4358	9523	170
H(19B)	3600	3732	9854	170
H(19C)	3223	4384	8972	170
H(32A)	4906	4810	8635	259
H(32B)	5386	6014	8513	259
H(32C)	5482	4587	8219	259
H(31A)	5073	5662	6825	329
H(31B)	4872	7031	7106	329
H(31C)	4193	6282	6342	329
H(1)	2680(15)	3870(30)	7652(15)	72(8)

Table A.11 Crystal data and structure refinement for **21**.

Identification code	**21**	
Empirical formula	C32 H42 N O P	
Formula weight	487.64	
Temperature	293(2) K	
Wavelength	0.71073 Å	
Crystal system	Monoclinic	
Space group	P2(1)/c	
Unit cell dimensions	a = 18.1914(16) Å	α= 90°.
	b = 10.1898(5) Å	β= 117.319(9)°.
	c = 18.1080(12) Å	γ = 90°.
Volume	2982.2(4) $Å^3$	
Z	4	
Density (calculated)	1.086 Mg/m^3	
Absorption coefficient	0.115 mm^{-1}	
F(000)	1056	
Crystal size	0.43 x 0.30 x 0.16 mm^3	
Theta range for data collection	2.94 to 25.35°.	
Index ranges	-21<=h<=21, -12<=k<=12, -20<=l<=20	
Reflections collected	30557	
Independent reflections	5133 [R(int) = 0.0962]	
Completeness to theta = 25.35°	94.2 %	
Absorption correction	None	
Max. and min. transmission	0.9819 and 0.9523	
Refinement method	Full-matrix least-squares on F^2	
Data / restraints / parameters	5133 / 0 / 328	
Goodness-of-fit on F^2	0.844	
Final R indices [I>2sigma(I)]	R1 = 0.0468, wR2 = 0.0986	
R indices (all data)	R1 = 0.1090, wR2 = 0.1164	
Largest diff. peak and hole	0.157 and -0.134 $e.Å^{-3}$	

Table A.12 Atomic coordinates (x 10^4) and equivalent isotropic displacement parameters ($Å^2$x 10^3) for **21**. U(eq) is defined as one third of the trace of the orthogonalized U^{ij} tensor.

	x	y	z	U(eq)
P(1)	2336(1)	358(1)	3820(1)	58(1)
O(1)	2945(2)	6118(2)	5430(2)	101(1)
N(1)	2517(1)	1735(2)	2631(1)	52(1)
C(1)	2554(1)	1724(2)	3402(2)	43(1)
C(2)	2717(1)	2942(2)	3897(2)	45(1)
C(8)	3201(2)	2891(3)	4761(2)	62(1)
C(7)	3270(2)	3964(3)	5247(2)	71(1)
C(5)	2865(2)	5117(3)	4890(2)	67(1)
C(6)	2373(3)	7160(3)	5132(3)	124(2)
C(4)	2417(2)	5214(3)	4041(2)	63(1)
C(3)	2344(2)	4119(2)	3550(2)	53(1)
C(9)	2741(2)	2732(2)	2211(2)	47(1)
C(10)	2148(2)	3060(2)	1405(2)	55(1)
C(11)	1308(2)	2404(3)	1015(2)	74(1)
C(13)	617(2)	3249(4)	366(2)	126(2)
C(12)	1348(2)	1065(4)	636(2)	107(1)
C(14)	2366(2)	3967(3)	963(2)	72(1)
C(15)	3134(2)	4524(3)	1304(2)	76(1)
C(16)	3703(2)	4200(3)	2089(2)	68(1)
C(17)	3537(2)	3278(2)	2566(2)	53(1)
C(18)	4230(2)	2877(3)	3402(2)	64(1)
C(19)	4897(2)	2108(4)	3284(3)	113(1)
C(20)	4598(2)	4061(3)	3981(2)	103(1)
C(21)	2077(2)	-900(2)	3003(2)	51(1)
C(29)	2695(2)	-1613(2)	2911(2)	64(1)
C(30)	3597(2)	-1248(3)	3393(2)	84(1)
C(31)	4009(3)	-1992(5)	4218(3)	168(2)
C(32)	4085(3)	-1415(5)	2907(4)	178(2)
C(28)	2452(3)	-2688(3)	2370(2)	87(1)
C(27)	1640(3)	-3034(3)	1930(2)	100(1)
C(26)	1044(2)	-2326(3)	2007(2)	93(1)

C(22)	1239(2)	-1256(3)	2531(2)	67(1)
C(23)	546(2)	-478(3)	2578(2)	91(1)
C(24)	216(3)	-1142(5)	3093(4)	184(3)
C(25)	-152(2)	-128(5)	1726(3)	148(2)

Table A.13 Bond lengths [Å] and angles [°] for **21**.

P(1)-C(1)	1.716(2)
P(1)-C(21)	1.849(2)
O(1)-C(5)	1.374(3)
O(1)-C(6)	1.409(4)
N(1)-C(1)	1.366(3)
N(1)-C(9)	1.435(3)
C(1)-C(2)	1.479(3)
C(2)-C(3)	1.379(3)
C(2)-C(8)	1.400(3)
C(8)-C(7)	1.373(4)
C(7)-C(5)	1.379(4)
C(5)-C(4)	1.374(4)
C(4)-C(3)	1.395(3)
C(9)-C(10)	1.401(3)
C(9)-C(17)	1.402(3)
C(10)-C(14)	1.395(4)
C(10)-C(11)	1.514(4)
C(11)-C(13)	1.532(4)
C(11)-C(12)	1.544(4)
C(14)-C(15)	1.366(4)
C(15)-C(16)	1.360(4)
C(16)-C(17)	1.399(3)
C(17)-C(18)	1.515(4)
C(18)-C(20)	1.536(4)
C(18)-C(19)	1.540(4)
C(21)-C(29)	1.411(3)
C(21)-C(22)	1.412(4)
C(29)-C(28)	1.399(4)
C(29)-C(30)	1.509(4)
C(30)-C(32)	1.519(5)
C(30)-C(31)	1.530(5)
C(28)-C(27)	1.364(5)
C(27)-C(26)	1.361(5)
C(26)-C(22)	1.381(4)

C(22)-C(23)	1.524(4)
C(23)-C(24)	1.483(5)
C(23)-C(25)	1.524(5)

C(1)-P(1)-C(21)	103.56(11)
C(5)-O(1)-C(6)	118.0(3)
C(1)-N(1)-C(9)	130.9(2)
N(1)-C(1)-C(2)	121.0(2)
N(1)-C(1)-P(1)	123.03(18)
C(2)-C(1)-P(1)	115.80(17)
C(3)-C(2)-C(8)	117.8(2)
C(3)-C(2)-C(1)	122.2(2)
C(8)-C(2)-C(1)	119.7(2)
C(7)-C(8)-C(2)	120.8(3)
C(8)-C(7)-C(5)	120.4(3)
O(1)-C(5)-C(4)	123.8(3)
O(1)-C(5)-C(7)	116.0(3)
C(4)-C(5)-C(7)	120.1(2)
C(5)-C(4)-C(3)	119.3(3)
C(2)-C(3)-C(4)	121.5(3)
C(10)-C(9)-C(17)	121.5(2)
C(10)-C(9)-N(1)	116.8(2)
C(17)-C(9)-N(1)	121.5(2)
C(14)-C(10)-C(9)	118.1(3)
C(14)-C(10)-C(11)	121.2(3)
C(9)-C(10)-C(11)	120.7(2)
C(10)-C(11)-C(13)	114.0(3)
C(10)-C(11)-C(12)	110.7(2)
C(13)-C(11)-C(12)	110.2(3)
C(15)-C(14)-C(10)	121.2(3)
C(16)-C(15)-C(14)	120.1(3)
C(15)-C(16)-C(17)	122.2(3)
C(16)-C(17)-C(9)	117.0(3)
C(16)-C(17)-C(18)	118.8(2)
C(9)-C(17)-C(18)	124.1(2)
C(17)-C(18)-C(20)	111.9(2)

C(17)-C(18)-C(19)	110.2(2)
C(20)-C(18)-C(19)	111.7(3)
C(29)-C(21)-C(22)	119.7(2)
C(29)-C(21)-P(1)	121.9(2)
C(22)-C(21)-P(1)	117.99(19)
C(28)-C(29)-C(21)	118.2(3)
C(28)-C(29)-C(30)	120.6(3)
C(21)-C(29)-C(30)	121.2(3)
C(29)-C(30)-C(32)	114.0(3)
C(29)-C(30)-C(31)	111.0(3)
C(32)-C(30)-C(31)	110.8(4)
C(27)-C(28)-C(29)	121.4(3)
C(26)-C(27)-C(28)	120.2(3)
C(27)-C(26)-C(22)	121.6(3)
C(26)-C(22)-C(21)	118.9(3)
C(26)-C(22)-C(23)	119.5(3)
C(21)-C(22)-C(23)	121.6(2)
C(24)-C(23)-C(25)	110.7(4)
C(24)-C(23)-C(22)	112.4(3)
C(25)-C(23)-C(22)	113.0(3)

Table A.14 Anisotropic displacement parameters ($Å^2 x\ 10^3$) for **21**. The anisotropic displacement factor exponent takes the form: $-2\pi^2[\ h^2\ a^{*2}U^{11} + ...\ + 2\ h\ k\ a^*\ b^*\ U^{12}\ ]$

	U^{11}	U^{22}	U^{33}	U^{23}	U^{13}	U^{12}
P(1)	82(1)	55(1)	48(1)	-3(1)	41(1)	-10(1)
O(1)	141(2)	85(2)	86(2)	-41(1)	60(2)	-26(2)
N(1)	70(1)	49(1)	41(1)	-2(1)	30(1)	-9(1)
C(1)	42(1)	55(1)	36(2)	1(1)	20(1)	1(1)
C(2)	46(1)	53(2)	42(2)	-2(1)	25(1)	-6(1)
C(8)	70(2)	65(2)	48(2)	-4(1)	25(1)	-10(1)
C(7)	90(2)	78(2)	45(2)	-15(2)	31(2)	-23(2)
C(5)	83(2)	65(2)	67(2)	-25(2)	46(2)	-26(2)
C(6)	210(5)	64(2)	135(4)	-25(2)	111(4)	-4(3)
C(4)	75(2)	54(2)	73(2)	-6(1)	44(2)	-2(1)
C(3)	60(2)	57(2)	47(2)	-3(1)	29(1)	-2(1)
C(9)	63(2)	45(1)	44(2)	2(1)	33(1)	4(1)
C(10)	70(2)	62(2)	42(2)	0(1)	31(1)	11(1)
C(11)	74(2)	102(2)	43(2)	-4(2)	24(2)	11(2)
C(13)	87(3)	184(4)	75(3)	15(3)	9(2)	30(3)
C(12)	98(3)	126(3)	92(3)	-48(2)	40(2)	-25(2)
C(14)	107(3)	79(2)	42(2)	16(2)	43(2)	23(2)
C(15)	114(3)	66(2)	71(2)	14(2)	63(2)	3(2)
C(16)	86(2)	64(2)	74(2)	1(2)	53(2)	-8(1)
C(17)	64(2)	52(1)	55(2)	1(1)	38(1)	2(1)
C(18)	53(2)	75(2)	67(2)	9(1)	30(1)	1(1)
C(19)	89(2)	143(3)	131(4)	39(3)	72(2)	40(2)
C(20)	92(2)	102(2)	83(3)	-8(2)	12(2)	-27(2)
C(21)	73(2)	44(1)	45(2)	2(1)	36(1)	-3(1)
C(29)	87(2)	56(2)	64(2)	7(1)	49(2)	7(1)
C(30)	85(2)	76(2)	110(3)	17(2)	61(2)	20(2)
C(31)	99(3)	178(5)	183(5)	88(4)	27(3)	7(3)
C(32)	167(4)	207(5)	249(7)	-50(5)	171(5)	-24(4)
C(28)	132(3)	67(2)	90(3)	-3(2)	75(2)	12(2)
C(27)	161(4)	69(2)	83(3)	-28(2)	67(3)	-18(2)
C(26)	114(3)	87(2)	73(3)	-24(2)	40(2)	-26(2)

C(22)	83(2)	63(2)	58(2)	-8(1)	34(2)	-9(2)
C(23)	66(2)	104(2)	97(3)	-19(2)	32(2)	-8(2)
C(24)	203(5)	203(5)	240(7)	89(5)	182(5)	73(4)
C(25)	97(3)	187(5)	142(4)	21(3)	40(3)	24(3)

Table A.15 Hydrogen coordinates (x 10^4) and isotropic displacement parameters ($Å^2$x 10^3) for **21**.

	x	y	z	U(eq)
H(1)	2299(15)	1040(20)	2327(16)	62
H(8)	3479	2120	5009	74
H(7)	3591	3914	5820	85
H(6A)	2469	7664	4737	186
H(6B)	2439	7712	5588	186
H(6C)	1820	6813	4869	186
H(4)	2164	6002	3796	76
H(3)	2037	4184	2976	63
H(11)	1159	2231	1463	89
H(13A)	589	4070	611	189
H(13B)	98	2798	173	189
H(13C)	731	3408	-94	189
H(12A)	1483	1199	187	160
H(12B)	822	634	431	160
H(12C)	1766	529	1055	160
H(14)	1982	4196	425	87
H(15)	3269	5127	999	91
H(16)	4219	4604	2316	82
H(18)	3994	2286	3665	77
H(19A)	4641	1412	2891	170
H(19B)	5288	1745	3807	170
H(19C)	5178	2689	3079	170
H(20A)	4860	4636	3753	155
H(20B)	5000	3761	4519	155
H(20C)	4165	4525	4034	155
H(30)	3617	-314	3529	101
H(31A)	3696	-1865	4518	251
H(31B)	4561	-1668	4542	251
H(31C)	4029	-2911	4111	251
H(32A)	4094	-2325	2775	268

H(32B)	4641	-1110	3236	268
H(32C)	3827	-915	2402	268
H(28)	2852	-3178	2309	104
H(27)	1493	-3754	1575	120
H(26)	493	-2570	1700	111
H(23)	789	352	2856	109
H(24A)	-54	-1943	2827	277
H(24B)	-175	-577	3154	277
H(24C)	663	-1336	3631	277
H(25A)	-476	-897	1476	221
H(25B)	78	200	1380	221
H(25C)	-497	532	1786	221

Table A.16 Crystal data and structure refinement for **25**.

Identification code	**25**	
Empirical formula	C37 H42 Mo N O5 P	
Formula weight	707.63	
Temperature	293(2) K	
Wavelength	0.71073 Å	
Crystal system	Triclinic	
Space group	P-1	
Unit cell dimensions	a = 10.594(2) Å	α= 84.58(3)°.
	b = 12.270(3) Å	β= 79.00(3)°.
	c = 14.862(3) Å	γ = 71.67(3)°.
Volume	1798.9(6) $Å^3$	
Z	2	
Density (calculated)	1.306 Mg/m^3	
Absorption coefficient	0.450 mm^{-1}	
F(000)	736	
Crystal size	0.56 x 0.21 x 0.08 mm^3	
Theta range for data collection	2.06 to 25.97°.	
Index ranges	-12<=h<=12, -15<=k<=15, -18<=l<=18	
Reflections collected	25690	
Independent reflections	6562 [R(int) = 0.0698]	
Completeness to theta = 25.97°	93.1 %	
Refinement method	Full-matrix least-squares on F^2	
Data / restraints / parameters	6562 / 0 / 449	
Goodness-of-fit on F^2	0.913	
Final R indices [I>2sigma(I)]	R1 = 0.0292, wR2 = 0.0674	
R indices (all data)	R1 = 0.0420, wR2 = 0.0711	
Largest diff. peak and hole	0.240 and -0.459 $e.Å^{-3}$	

Table A.17 Atomic coordinates (x 10^4) and equivalent isotropic displacement parameters ($Å^2$x 10^3) for **25**. U(eq) is defined as one third of the trace of the orthogonalized U^{ij} tensor.

	x	y	z	U(eq)
Mo(1)	9423(1)	8427(1)	7086(1)	40(1)
P(1)	11447(1)	7266(1)	7835(1)	42(1)
N(1)	13483(2)	5371(1)	8161(1)	39(1)
C(21)	12397(2)	7982(2)	8363(2)	40(1)
C(2)	11923(2)	5085(2)	7253(1)	35(1)
C(41)	7900(3)	9374(2)	6481(2)	57(1)
O(45)	7195(2)	8914(2)	8878(1)	76(1)
O(42)	8532(2)	6223(2)	6884(2)	82(1)
C(1)	12364(2)	5849(2)	7764(1)	33(1)
C(42)	8906(3)	6977(2)	6938(2)	54(1)
C(45)	8060(3)	8689(2)	8265(2)	51(1)
O(43)	11218(2)	8365(2)	5095(1)	88(1)
C(43)	10626(3)	8337(2)	5810(2)	54(1)
C(8)	11913(2)	5287(2)	6321(1)	42(1)
C(9)	14146(2)	4155(2)	8265(1)	37(1)
C(7)	11562(3)	4562(2)	5820(2)	50(1)
C(3)	11545(3)	4152(2)	7665(2)	48(1)
C(26)	12705(3)	8833(2)	9671(2)	57(1)
C(5)	11199(3)	3626(2)	6227(2)	51(1)
C(22)	12127(2)	8130(2)	9319(2)	44(1)
C(10)	13926(2)	3612(2)	9124(2)	43(1)
C(23)	11214(3)	7564(2)	9980(2)	53(1)
C(29)	13283(3)	8507(2)	7790(2)	50(1)
C(17)	14972(2)	3550(2)	7508(2)	45(1)
O(41)	7019(2)	9922(2)	6142(2)	89(1)
C(28)	13826(3)	9200(2)	8187(2)	61(1)
C(4)	11186(3)	3437(2)	7162(2)	55(1)
C(11)	13139(3)	4262(2)	9978(2)	51(1)
O(44)	9971(3)	10727(2)	7448(2)	100(1)
C(16)	15495(3)	2364(2)	7621(2)	58(1)
C(14)	14470(3)	2424(2)	9187(2)	56(1)

C(15)	15227(3)	1809(2)	8445(2)	63(1)
C(44)	9812(3)	9893(2)	7316(2)	58(1)
C(27)	13531(3)	9370(2)	9114(2)	64(1)
C(18)	15370(3)	4128(2)	6604(2)	60(1)
C(25)	11778(3)	7083(2)	10864(2)	70(1)
C(12)	13933(3)	3951(3)	10766(2)	77(1)
C(24)	9800(3)	8406(3)	10219(2)	74(1)
C(6)	10834(4)	2835(3)	5675(2)	81(1)
C(13)	11762(3)	4088(3)	10272(2)	80(1)
C(20)	15326(4)	3507(3)	5776(2)	86(1)
C(32)	15161(4)	7540(3)	6559(2)	94(1)
C(19)	16789(4)	4230(4)	6577(3)	102(1)
C(31)	13519(4)	9434(4)	6195(2)	110(1)
C(30)	13708(3)	8315(3)	6765(2)	68(1)

Table A.18 Bond lengths [Å] and angles [°] for **25**.

Mo(1)-C(41)	1.984(3)
Mo(1)-C(45)	2.027(3)
Mo(1)-C(44)	2.038(3)
Mo(1)-C(42)	2.061(3)
Mo(1)-C(43)	2.064(3)
Mo(1)-P(1)	2.5609(11)
P(1)-C(1)	1.706(2)
P(1)-C(21)	1.841(2)
N(1)-C(1)	1.364(3)
N(1)-C(9)	1.443(3)
C(21)-C(29)	1.411(3)
C(21)-C(22)	1.413(3)
C(2)-C(3)	1.381(3)
C(2)-C(8)	1.386(3)
C(2)-C(1)	1.489(3)
C(41)-O(41)	1.140(3)
O(45)-C(45)	1.148(3)
O(42)-C(42)	1.129(3)
O(43)-C(43)	1.130(3)
C(8)-C(7)	1.385(3)
C(9)-C(10)	1.397(3)
C(9)-C(17)	1.399(3)
C(7)-C(5)	1.375(3)
C(3)-C(4)	1.385(3)
C(26)-C(27)	1.367(4)
C(26)-C(22)	1.390(3)
C(5)-C(4)	1.386(3)
C(5)-C(6)	1.507(3)
C(22)-C(23)	1.522(3)
C(10)-C(14)	1.391(3)
C(10)-C(11)	1.519(3)
C(23)-C(24)	1.527(4)
C(23)-C(25)	1.537(4)
C(29)-C(28)	1.390(3)

C(29)-C(30)	1.522(4)
C(17)-C(16)	1.391(3)
C(17)-C(18)	1.509(3)
C(28)-C(27)	1.374(4)
C(11)-C(13)	1.517(4)
C(11)-C(12)	1.521(4)
O(44)-C(44)	1.128(3)
C(16)-C(15)	1.370(4)
C(14)-C(15)	1.367(4)
C(18)-C(20)	1.523(4)
C(18)-C(19)	1.540(5)
C(32)-C(30)	1.524(5)
C(31)-C(30)	1.521(5)

C(41)-Mo(1)-C(45)	85.54(11)
C(41)-Mo(1)-C(44)	89.10(11)
C(45)-Mo(1)-C(44)	87.79(10)
C(41)-Mo(1)-C(42)	89.92(11)
C(45)-Mo(1)-C(42)	87.77(10)
C(44)-Mo(1)-C(42)	175.51(10)
C(41)-Mo(1)-C(43)	87.11(11)
C(45)-Mo(1)-C(43)	172.39(10)
C(44)-Mo(1)-C(43)	90.14(10)
C(42)-Mo(1)-C(43)	94.19(10)
C(41)-Mo(1)-P(1)	177.49(8)
C(45)-Mo(1)-P(1)	95.90(7)
C(44)-Mo(1)-P(1)	88.90(8)
C(42)-Mo(1)-P(1)	92.19(7)
C(43)-Mo(1)-P(1)	91.38(8)
C(1)-P(1)-C(21)	107.19(10)
C(1)-P(1)-Mo(1)	130.37(8)
C(21)-P(1)-Mo(1)	121.19(7)
C(1)-N(1)-C(9)	125.21(18)
C(29)-C(21)-C(22)	119.8(2)
C(29)-C(21)-P(1)	119.03(16)
C(22)-C(21)-P(1)	120.68(17)

C(3)-C(2)-C(8)	117.6(2)
C(3)-C(2)-C(1)	122.71(18)
C(8)-C(2)-C(1)	119.70(18)
O(41)-C(41)-Mo(1)	179.4(3)
N(1)-C(1)-C(2)	117.87(17)
N(1)-C(1)-P(1)	123.23(15)
C(2)-C(1)-P(1)	118.89(15)
O(42)-C(42)-Mo(1)	175.1(2)
O(45)-C(45)-Mo(1)	172.8(2)
O(43)-C(43)-Mo(1)	174.8(2)
C(7)-C(8)-C(2)	121.0(2)
C(10)-C(9)-C(17)	121.86(19)
C(10)-C(9)-N(1)	118.58(18)
C(17)-C(9)-N(1)	119.55(18)
C(5)-C(7)-C(8)	121.6(2)
C(2)-C(3)-C(4)	121.1(2)
C(27)-C(26)-C(22)	121.4(2)
C(7)-C(5)-C(4)	117.4(2)
C(7)-C(5)-C(6)	121.3(2)
C(4)-C(5)-C(6)	121.3(2)
C(26)-C(22)-C(21)	118.8(2)
C(26)-C(22)-C(23)	118.5(2)
C(21)-C(22)-C(23)	122.7(2)
C(14)-C(10)-C(9)	117.5(2)
C(14)-C(10)-C(11)	119.5(2)
C(9)-C(10)-C(11)	123.01(18)
C(22)-C(23)-C(24)	110.7(2)
C(22)-C(23)-C(25)	112.6(2)
C(24)-C(23)-C(25)	109.7(2)
C(28)-C(29)-C(21)	118.4(2)
C(28)-C(29)-C(30)	118.6(2)
C(21)-C(29)-C(30)	123.0(2)
C(16)-C(17)-C(9)	117.5(2)
C(16)-C(17)-C(18)	119.3(2)
C(9)-C(17)-C(18)	123.2(2)
C(27)-C(28)-C(29)	121.7(3)

C(3)-C(4)-C(5)	121.3(2)
C(13)-C(11)-C(10)	112.3(2)
C(13)-C(11)-C(12)	110.6(2)
C(10)-C(11)-C(12)	111.6(2)
C(15)-C(16)-C(17)	121.4(2)
C(15)-C(14)-C(10)	121.5(2)
C(14)-C(15)-C(16)	120.1(2)
O(44)-C(44)-Mo(1)	177.1(3)
C(26)-C(27)-C(28)	119.9(2)
C(17)-C(18)-C(20)	113.3(2)
C(17)-C(18)-C(19)	108.1(2)
C(20)-C(18)-C(19)	111.0(3)
C(31)-C(30)-C(29)	112.7(3)
C(31)-C(30)-C(32)	111.0(3)
C(29)-C(30)-C(32)	110.4(2)

Table A.19 Anisotropic displacement parameters ($Å^2 x\ 10^3$) for **25**. The anisotropic displacement factor exponent takes the form: $-2\pi^2[\ h^2\ a^{*2}U^{11} + ...\ + 2\ h\ k\ a^*\ b^*\ U^{12}\ ]$

	U^{11}	U^{22}	U^{33}	U^{23}	U^{13}	U^{12}
Mo(1)	37(1)	37(1)	46(1)	-4(1)	-13(1)	-8(1)
P(1)	37(1)	36(1)	55(1)	-9(1)	-18(1)	-7(1)
N(1)	40(1)	32(1)	48(1)	-3(1)	-16(1)	-10(1)
C(21)	38(1)	34(1)	51(1)	-5(1)	-17(1)	-7(1)
C(2)	33(1)	37(1)	37(1)	-4(1)	-7(1)	-10(1)
C(41)	55(2)	53(1)	62(2)	-1(1)	-17(1)	-13(1)
O(45)	59(1)	81(1)	72(1)	-5(1)	8(1)	-10(1)
O(42)	64(1)	64(1)	131(2)	-22(1)	-17(1)	-33(1)
C(1)	31(1)	39(1)	31(1)	0(1)	-4(1)	-13(1)
C(42)	41(2)	55(1)	66(2)	-10(1)	-14(1)	-10(1)
C(45)	47(2)	46(1)	58(1)	2(1)	-16(1)	-8(1)
O(43)	91(2)	124(2)	57(1)	-19(1)	10(1)	-50(1)
C(43)	51(2)	58(1)	60(2)	-9(1)	-17(1)	-20(1)
C(8)	49(1)	40(1)	38(1)	0(1)	-6(1)	-15(1)
C(9)	35(1)	33(1)	45(1)	-2(1)	-12(1)	-9(1)
C(7)	61(2)	58(1)	35(1)	-6(1)	-11(1)	-21(1)
C(3)	62(2)	56(1)	36(1)	2(1)	-12(1)	-32(1)
C(26)	64(2)	54(1)	58(2)	-16(1)	-16(1)	-18(1)
C(5)	58(2)	53(1)	49(1)	-9(1)	-13(1)	-23(1)
C(22)	44(1)	36(1)	53(1)	-10(1)	-12(1)	-7(1)
C(10)	42(1)	40(1)	47(1)	-1(1)	-10(1)	-11(1)
C(23)	61(2)	49(1)	51(1)	-13(1)	-7(1)	-19(1)
C(29)	47(2)	56(1)	54(1)	1(1)	-18(1)	-21(1)
C(17)	39(1)	45(1)	48(1)	-6(1)	-6(1)	-11(1)
O(41)	74(2)	87(2)	99(2)	14(1)	-50(1)	0(1)
C(28)	61(2)	66(2)	70(2)	-1(1)	-17(1)	-35(1)
C(4)	72(2)	55(1)	53(1)	3(1)	-17(1)	-38(1)
C(11)	57(2)	45(1)	45(1)	-1(1)	-9(1)	-10(1)
O(44)	137(2)	58(1)	118(2)	-26(1)	-9(2)	-49(1)
C(16)	54(2)	44(1)	68(2)	-15(1)	-4(1)	-4(1)
C(14)	64(2)	41(1)	60(2)	7(1)	-12(1)	-11(1)

C(15)	68(2)	32(1)	81(2)	-3(1)	-14(1)	-3(1)
C(44)	62(2)	50(1)	60(2)	-6(1)	-7(1)	-14(1)
C(27)	67(2)	61(2)	78(2)	-13(1)	-24(2)	-31(1)
C(18)	59(2)	63(2)	50(1)	-3(1)	4(1)	-13(1)
C(25)	88(2)	61(2)	56(2)	-4(1)	-10(1)	-17(1)
C(12)	73(2)	100(2)	61(2)	-15(2)	-24(2)	-19(2)
C(24)	54(2)	89(2)	77(2)	-12(2)	-5(1)	-20(2)
C(6)	116(3)	75(2)	74(2)	-15(2)	-30(2)	-48(2)
C(13)	52(2)	113(3)	65(2)	-20(2)	-6(1)	-8(2)
C(20)	96(3)	90(2)	55(2)	-14(2)	-5(2)	-4(2)
C(32)	93(3)	106(3)	77(2)	-20(2)	6(2)	-31(2)
C(19)	77(3)	137(3)	95(3)	9(2)	7(2)	-54(2)
C(31)	101(3)	150(4)	77(2)	43(2)	-25(2)	-43(3)
C(30)	66(2)	103(2)	54(2)	4(1)	-15(1)	-50(2)

Table A.20 Hydrogen coordinates (x 10^4) and isotropic displacement parameters ($Å^2$x 10^3) for **25**.

	x	y	z	U(eq)
H(8)	12140(20)	5920(20)	6027(16)	51
H(7)	11570(30)	4710(20)	5194(19)	60
H(3)	11530(30)	4000(20)	8292(18)	57
H(26)	12530(30)	8940(20)	10300(20)	68
H(23)	11139	6921	9671	63
H(28)	14400(30)	9560(20)	7816(19)	73
H(4)	10930(30)	2820(20)	7458(18)	66
H(11)	12993	5082	9826	61
H(16)	16040(30)	1940(20)	7127(19)	70
H(14)	14310(30)	2040(20)	9747(19)	67
H(15)	15560(30)	1010(30)	8500(19)	76
H(27)	13890(30)	9850(20)	9360(20)	76
H(18)	14738	4905	6583	73
H(25A)	11292	6584	11189	105
H(25B)	11678	7706	11244	105
H(25C)	12716	6659	10711	105
H(12A)	13469	4454	11261	116
H(12B)	14815	4033	10560	116
H(12C)	14016	3171	10972	116
H(24A)	9221	8018	10599	111
H(24B)	9447	8698	9666	111
H(24C)	9841	9031	10544	111
H(6A)	10388	3271	5192	121
H(6B)	10241	2470	6067	121
H(6C)	11639	2261	5415	121
H(13A)	11329	4467	10836	120
H(13B)	11865	3281	10361	120
H(13C)	11220	4405	9805	120
H(20A)	15464	3966	5228	130
H(20B)	14463	3381	5841	130

H(20C)	16024	2781	5736	130
H(32A)	15410	7414	5913	140
H(32B)	15240	6817	6889	140
H(32C)	15749	7901	6745	140
H(19A)	17038	4641	6024	153
H(19B)	17427	3476	6591	153
H(19C)	16786	4637	7098	153
H(31A)	13739	9269	5555	165
H(31B)	14101	9833	6335	165
H(31C)	12597	9905	6334	165
H(30)	13132	7913	6588	82
H(1)	13690(20)	5810(20)	8458(16)	44(6)

Table A.21 Crystal data and structure refinement for **26**.

Identification code	**26**	
Empirical formula	C37 H42 N O5 P W	
Formula weight	795.54	
Temperature	293(2) K	
Wavelength	0.71073 Å	
Crystal system	Triclinic	
Space group	P-1	
Unit cell dimensions	a = 10.5413(9) Å	α= 84.662(11)°.
	b = 12.2130(11) Å	β= 79.167(11)°.
	c = 14.8135(14) Å	γ = 71.661(10)°.
Volume	1776.8(3) $Å^3$	
Z	2	
Density (calculated)	1.487 Mg/m^3	
Absorption coefficient	3.337 mm^{-1}	
F(000)	800	
Crystal size	0.50 x 0.35 x 0.10 mm^3	
Theta range for data collection	2.21 to 26.03°.	
Index ranges	-12<=h<=12, -15<=k<=15, -18<=l<=18	
Reflections collected	25702	
Independent reflections	6536 [R(int) = 0.1371]	
Completeness to theta = 26.03°	93.3 %	
Absorption correction	None	
Refinement method	Full-matrix least-squares on F^2	
Data / restraints / parameters	6536 / 0 / 419	
Goodness-of-fit on F^2	1.031	
Final R indices [I>2sigma(I)]	R1 = 0.0540, wR2 = 0.1300	
R indices (all data)	R1 = 0.0578, wR2 = 0.1325	
Largest diff. peak and hole	2.460 and -2.950 $e.Å^{-3}$	

Table A.22 Atomic coordinates (x 10^4) and equivalent isotropic displacement parameters ($Å^2$x 10^3) for **26**. U(eq) is defined as one third of the trace of the orthogonalized U^{ij} tensor.

	x	y	z	U(eq)
W(1)	9423(1)	8425(1)	7093(1)	46(1)
P(1)	11434(2)	7266(1)	7843(1)	48(1)
N(1)	13479(6)	5369(4)	8148(4)	47(1)
O(42)	8541(7)	6212(5)	6892(5)	84(2)
O(45)	7182(6)	8906(5)	8886(4)	78(2)
C(9)	14152(6)	4153(4)	8265(4)	43(1)
C(2)	11921(6)	5087(4)	7251(4)	43(1)
C(21)	12392(6)	7985(4)	8367(4)	46(1)
C(1)	12368(6)	5847(4)	7760(3)	43(1)
O(43)	11236(7)	8351(6)	5110(4)	92(2)
C(45)	8031(8)	8686(5)	8272(5)	59(2)
C(42)	8917(7)	6982(5)	6951(5)	57(2)
C(17)	14978(7)	3535(5)	7508(4)	51(1)
C(10)	13927(7)	3597(5)	9124(4)	51(1)
C(44)	9816(8)	9873(6)	7329(5)	62(2)
O(44)	10017(9)	10708(5)	7468(6)	100(2)
C(43)	10650(8)	8338(6)	5821(5)	62(2)
C(7)	11556(8)	4572(6)	5807(4)	57(2)
C(8)	11912(7)	5296(5)	6308(4)	50(1)
C(22)	12110(7)	8132(5)	9325(4)	50(1)
C(11)	13141(7)	4259(5)	9981(4)	56(2)
C(3)	11527(7)	4147(5)	7664(4)	53(1)
O(41)	7021(8)	9916(5)	6127(5)	92(2)
C(29)	13286(8)	8505(6)	7783(5)	58(2)
C(14)	14476(8)	2427(5)	9188(5)	61(2)
C(26)	12711(8)	8833(6)	9679(5)	64(2)
C(23)	11208(8)	7569(5)	9985(4)	59(2)
C(41)	7900(8)	9384(6)	6482(5)	61(2)
C(5)	11191(8)	3619(6)	6225(5)	59(2)
C(15)	15226(9)	1790(5)	8447(6)	68(2)
C(28)	13832(9)	9197(6)	8191(5)	66(2)

C(4)	11176(8)	3424(6)	7156(5)	61(2)
C(16)	15499(8)	2349(6)	7626(5)	66(2)
C(27)	13531(9)	9378(6)	9109(6)	68(2)
C(18)	15374(8)	4127(6)	6600(5)	66(2)
C(25)	11778(10)	7078(7)	10868(5)	75(2)
C(24)	9797(9)	8414(8)	10231(6)	77(2)
C(30)	13703(9)	8313(8)	6772(5)	72(2)
C(12)	13938(10)	3949(9)	10763(6)	82(2)
C(6)	10838(11)	2823(7)	5666(6)	83(3)
C(13)	11760(9)	4105(9)	10267(6)	85(2)
C(20)	15334(12)	3501(8)	5772(6)	92(3)
C(19)	16785(12)	4239(11)	6567(8)	105(3)
C(32)	15156(12)	7556(10)	6572(7)	99(3)
C(31)	13519(13)	9413(11)	6195(7)	112(4)

Table A.23 Bond lengths [Å] and angles [°] for **26**.

W(1)-C(41)	1.983(7)
W(1)-C(44)	2.013(7)
W(1)-C(42)	2.034(7)
W(1)-C(45)	2.038(8)
W(1)-C(43)	2.066(8)
W(1)-P(1)	2.5375(16)
P(1)-C(1)	1.705(5)
P(1)-C(21)	1.836(6)
N(1)-C(1)	1.343(8)
N(1)-C(9)	1.440(7)
O(42)-C(42)	1.145(9)
O(45)-C(45)	1.135(10)
C(9)-C(17)	1.401(8)
C(9)-C(10)	1.402(8)
C(2)-C(3)	1.393(8)
C(2)-C(8)	1.398(8)
C(2)-C(1)	1.481(8)
C(21)-C(22)	1.410(8)
C(21)-C(29)	1.418(9)
O(43)-C(43)	1.117(10)
C(17)-C(16)	1.385(9)
C(17)-C(18)	1.517(9)
C(10)-C(14)	1.365(8)
C(10)-C(11)	1.525(8)
C(44)-O(44)	1.148(9)
C(7)-C(8)	1.380(9)
C(7)-C(5)	1.395(9)
C(22)-C(26)	1.400(9)
C(22)-C(23)	1.506(9)
C(11)-C(13)	1.504(12)
C(11)-C(12)	1.508(11)
C(3)-C(4)	1.384(9)
O(41)-C(41)	1.140(9)
C(29)-C(28)	1.393(10)

C(29)-C(30)	1.498(10)
C(14)-C(15)	1.371(10)
C(26)-C(27)	1.374(11)
C(23)-C(24)	1.520(11)
C(23)-C(25)	1.535(11)
C(5)-C(4)	1.376(9)
C(5)-C(6)	1.503(9)
C(15)-C(16)	1.366(11)
C(28)-C(27)	1.360(11)
C(18)-C(20)	1.519(12)
C(18)-C(19)	1.528(14)
C(30)-C(31)	1.502(12)
C(30)-C(32)	1.509(14)

C(41)-W(1)-C(44)	89.1(3)
C(41)-W(1)-C(42)	90.6(3)
C(44)-W(1)-C(42)	175.3(3)
C(41)-W(1)-C(45)	85.3(3)
C(44)-W(1)-C(45)	88.2(3)
C(42)-W(1)-C(45)	87.2(3)
C(41)-W(1)-C(43)	87.4(3)
C(44)-W(1)-C(43)	89.8(3)
C(42)-W(1)-C(43)	94.9(3)
C(45)-W(1)-C(43)	172.4(3)
C(41)-W(1)-P(1)	177.2(2)
C(44)-W(1)-P(1)	88.6(2)
C(42)-W(1)-P(1)	91.8(2)
C(45)-W(1)-P(1)	96.2(2)
C(43)-W(1)-P(1)	91.0(2)
C(1)-P(1)-C(21)	107.0(3)
C(1)-P(1)-W(1)	130.3(2)
C(21)-P(1)-W(1)	121.08(18)
C(1)-N(1)-C(9)	126.4(5)
C(17)-C(9)-C(10)	121.0(5)
C(17)-C(9)-N(1)	119.4(5)
C(10)-C(9)-N(1)	119.5(5)

C(3)-C(2)-C(8)	117.6(5)
C(3)-C(2)-C(1)	123.0(5)
C(8)-C(2)-C(1)	119.4(5)
C(22)-C(21)-C(29)	121.1(5)
C(22)-C(21)-P(1)	119.8(4)
C(29)-C(21)-P(1)	118.6(4)
N(1)-C(1)-C(2)	117.7(5)
N(1)-C(1)-P(1)	123.6(4)
C(2)-C(1)-P(1)	118.7(4)
O(45)-C(45)-W(1)	173.9(6)
O(42)-C(42)-W(1)	175.3(7)
C(16)-C(17)-C(9)	117.6(6)
C(16)-C(17)-C(18)	120.0(6)
C(9)-C(17)-C(18)	122.3(5)
C(14)-C(10)-C(9)	117.9(6)
C(14)-C(10)-C(11)	119.8(6)
C(9)-C(10)-C(11)	122.3(5)
O(44)-C(44)-W(1)	178.9(8)
O(43)-C(43)-W(1)	174.9(8)
C(8)-C(7)-C(5)	121.3(6)
C(7)-C(8)-C(2)	120.6(5)
C(26)-C(22)-C(21)	118.0(6)
C(26)-C(22)-C(23)	118.4(6)
C(21)-C(22)-C(23)	123.6(5)
C(13)-C(11)-C(12)	111.3(7)
C(13)-C(11)-C(10)	112.2(6)
C(12)-C(11)-C(10)	111.5(6)
C(4)-C(3)-C(2)	121.3(5)
C(28)-C(29)-C(21)	117.2(6)
C(28)-C(29)-C(30)	119.2(6)
C(21)-C(29)-C(30)	123.6(6)
C(10)-C(14)-C(15)	122.4(6)
C(27)-C(26)-C(22)	121.0(7)
C(22)-C(23)-C(24)	110.6(6)
C(22)-C(23)-C(25)	113.1(7)
C(24)-C(23)-C(25)	109.5(6)

O(41)-C(41)-W(1)	178.6(7)
C(4)-C(5)-C(7)	118.2(6)
C(4)-C(5)-C(6)	121.2(6)
C(7)-C(5)-C(6)	120.6(6)
C(16)-C(15)-C(14)	119.1(6)
C(27)-C(28)-C(29)	122.3(7)
C(5)-C(4)-C(3)	121.0(5)
C(15)-C(16)-C(17)	121.8(6)
C(28)-C(27)-C(26)	120.3(6)
C(17)-C(18)-C(20)	112.9(7)
C(17)-C(18)-C(19)	108.6(7)
C(20)-C(18)-C(19)	110.8(8)
C(29)-C(30)-C(31)	113.4(8)
C(29)-C(30)-C(32)	110.0(8)
C(31)-C(30)-C(32)	110.2(8)

Table A.24 Anisotropic displacement parameters ($Å^2 x\ 10^3$) for **26**. The anisotropic displacement factor exponent takes the form: $-2\pi^2[\ h^2\ a^{*2}U^{11} + ...\ + 2\ h\ k\ a^*\ b^*\ U^{12}\ ]$

	U^{11}	U^{22}	U^{33}	U^{23}	U^{13}	U^{12}
W(1)	43(1)	47(1)	47(1)	-3(1)	-13(1)	-11(1)
P(1)	45(1)	45(1)	57(1)	-8(1)	-19(1)	-10(1)
N(1)	50(3)	42(2)	53(3)	-2(2)	-19(2)	-14(2)
O(42)	64(4)	77(3)	124(5)	-20(3)	-15(3)	-34(3)
O(45)	60(4)	91(3)	68(3)	-4(3)	6(3)	-13(3)
C(9)	40(3)	44(2)	48(3)	0(2)	-14(2)	-13(2)
C(2)	42(3)	50(2)	38(2)	-5(2)	-6(2)	-14(2)
C(21)	41(3)	50(3)	50(3)	-3(2)	-16(2)	-14(2)
C(1)	46(3)	50(2)	31(2)	3(2)	-2(2)	-16(2)
O(43)	91(5)	126(5)	62(3)	-22(3)	14(3)	-49(4)
C(45)	52(4)	52(3)	71(4)	0(3)	-19(3)	-8(2)
C(42)	41(4)	59(3)	71(4)	-6(3)	-17(3)	-9(3)
C(17)	48(4)	56(3)	48(3)	-5(2)	-8(2)	-14(2)
C(10)	52(4)	50(3)	51(3)	-1(2)	-13(3)	-11(2)
C(44)	62(5)	56(3)	63(4)	-6(3)	-12(3)	-10(3)
O(44)	121(6)	71(3)	118(6)	-25(3)	-7(5)	-46(4)
C(43)	61(5)	62(3)	68(4)	-8(3)	-13(3)	-23(3)
C(7)	68(5)	65(3)	38(3)	-5(2)	-7(3)	-23(3)
C(8)	54(4)	52(3)	42(3)	2(2)	-3(2)	-18(2)
C(22)	47(4)	50(3)	56(3)	-9(2)	-11(3)	-12(2)
C(11)	63(4)	51(3)	50(3)	-2(2)	-7(3)	-12(3)
C(3)	65(4)	65(3)	38(3)	4(2)	-11(2)	-33(3)
O(41)	85(5)	89(4)	104(5)	14(3)	-54(4)	-10(3)
C(29)	56(4)	67(3)	61(4)	-1(3)	-19(3)	-27(3)
C(14)	67(5)	52(3)	61(4)	7(3)	-11(3)	-17(3)
C(26)	67(5)	67(4)	61(4)	-11(3)	-16(3)	-21(3)
C(23)	65(4)	62(3)	51(3)	-13(3)	-1(3)	-23(3)
C(41)	48(4)	66(3)	71(4)	-3(3)	-21(3)	-14(3)
C(5)	66(5)	65(3)	53(3)	-8(3)	-9(3)	-30(3)
C(15)	76(5)	44(3)	78(5)	0(3)	-17(4)	-9(3)
C(28)	67(5)	73(4)	69(4)	5(3)	-19(3)	-34(3)

C(4)	79(5)	66(3)	52(3)	5(3)	-18(3)	-41(3)
C(16)	59(4)	57(3)	70(4)	-15(3)	-4(3)	-4(3)
C(27)	73(5)	66(4)	80(5)	-13(3)	-25(4)	-31(3)
C(18)	66(5)	74(4)	50(3)	-1(3)	3(3)	-17(3)
C(25)	85(6)	74(4)	59(4)	-8(3)	-8(4)	-15(4)
C(24)	62(5)	96(5)	70(5)	-8(4)	-7(4)	-20(4)
C(30)	70(5)	106(5)	56(4)	-2(4)	-10(3)	-48(4)
C(12)	73(6)	112(6)	62(4)	-18(4)	-17(4)	-22(5)
C(6)	117(8)	82(5)	69(5)	-16(4)	-31(5)	-46(5)
C(13)	54(5)	126(7)	67(5)	-23(4)	-3(4)	-14(4)
C(20)	106(8)	99(6)	56(4)	-13(4)	-1(4)	-11(5)
C(19)	83(7)	155(9)	84(6)	11(6)	6(5)	-59(7)
C(32)	98(8)	113(7)	79(6)	-29(5)	10(5)	-31(6)
C(31)	106(9)	156(10)	75(6)	39(6)	-30(6)	-45(7)

Table A.25 Hydrogen coordinates (x 10^4) and isotropic displacement parameters ($Å^2$x 10^3) for **26**.

	x	y	z	U(eq)
H(7)	11560	4724	5180	68
H(8)	12148	5928	6014	60
H(11)	13006	5081	9825	67
H(3)	11500	4002	8294	63
H(14)	14336	2047	9754	73
H(26)	12552	8931	10310	76
H(23)	11124	6927	9674	71
H(15)	15544	990	8502	82
H(28)	14423	9547	7822	79
H(4)	10926	2798	7449	73
H(16)	16049	1922	7132	79
H(27)	13883	9873	9352	81
H(18)	14732	4906	6581	79
H(25A)	11341	6527	11165	113
H(25B)	11612	7694	11275	113
H(25C)	12736	6706	10718	113
H(24A)	9211	8020	10598	116
H(24B)	9446	8729	9678	116
H(24C)	9844	9027	10572	116
H(30)	13133	7900	6594	87
H(12A)	14824	4031	10556	123
H(12B)	14022	3164	10970	123
H(12C)	13475	4453	11261	123
H(6A)	10192	3270	5292	124
H(6B)	10455	2306	6071	124
H(6C)	11643	2387	5279	124
H(13A)	11211	4455	9806	128
H(13B)	11340	4466	10842	128
H(13C)	11846	3297	10335	128
H(20A)	15398	3988	5228	139

H(20B)	14497	3317	5858	139
H(20C)	16081	2802	5705	139
H(19A)	17021	4662	6016	158
H(19B)	17434	3484	6572	158
H(19C)	16788	4641	7094	158
H(32A)	15394	7389	5930	148
H(32B)	15257	6848	6933	148
H(32C)	15741	7949	6725	148
H(31A)	13729	9237	5556	167
H(31B)	14113	9812	6325	167
H(31C)	12596	9894	6336	167
H(1)	13790(80)	5700(60)	8340(50)	43(18)

Table A.26 Crystal data and structure refinement for **27**.

Identification code	**27**	
Empirical formula	C37 H42 Mo N O6 P	
Formula weight	723.63	
Temperature	293(2) K	
Wavelength	0.71073 Å	
Crystal system	Triclinic	
Space group	P-1	
Unit cell dimensions	a = 10.7566(8) Å	α= 104.733(10)°.
	b = 13.4617(11) Å	β= 108.862(9)°.
	c = 14.2564(12) Å	γ = 92.700(9)°.
Volume	1870.3(3) $Å^3$	
Z	2	
Density (calculated)	1.285 Mg/m^3	
Absorption coefficient	0.436 mm^{-1}	
F(000)	752	
Crystal size	0.40 x 0.22 x 0.14 mm^3	
Theta range for data collection	2.02 to 25.93°.	
Index ranges	-12<=h<=12, -16<=k<=16, -17<=l<=17	
Reflections collected	26419	
Independent reflections	6736 [R(int) = 0.0549]	
Completeness to theta = 25.93°	92.2 %	
Absorption correction	None	
Refinement method	Full-matrix least-squares on F^2	
Data / restraints / parameters	6736 / 0 / 428	
Goodness-of-fit on F^2	0.945	
Final R indices [I>2sigma(I)]	R1 = 0.0406, wR2 = 0.0920	
R indices (all data)	R1 = 0.0618, wR2 = 0.0986	
Largest diff. peak and hole	0.428 and -0.293 $e.Å^{-3}$	

Table A.27 Atomic coordinates (x 10^4) and equivalent isotropic displacement parameters ($Å^2$x 10^3) for **27**. U(eq) is defined as one third of the trace of the orthogonalized U^{ij} tensor.

	x	y	z	U(eq)
Mo(1)	8343(1)	5413(1)	7331(1)	48(1)
P(1)	6948(1)	6744(1)	7945(1)	45(1)
N(1)	5861(3)	8529(2)	8045(2)	61(1)
C(21)	6010(3)	6579(2)	8781(2)	48(1)
O(5)	9038(3)	9181(2)	5136(2)	82(1)
C(1)	6624(3)	7877(2)	7665(2)	37(1)
C(7)	7395(3)	8023(2)	5296(2)	55(1)
C(2)	7240(3)	8206(2)	6978(2)	39(1)
C(8)	6817(3)	7713(2)	5938(2)	52(1)
C(45)	9963(4)	5992(3)	8628(3)	75(1)
C(44)	7668(4)	4464(3)	8003(3)	65(1)
O(44)	7305(4)	3893(3)	8357(3)	111(1)
C(5)	8403(4)	8813(2)	5692(2)	54(1)
C(22)	6633(4)	6906(2)	9858(3)	67(1)
O(45)	10915(3)	6262(3)	9332(3)	127(1)
C(3)	8235(4)	9026(3)	7358(3)	78(1)
O(43)	5998(4)	4295(3)	5231(3)	119(1)
O(41)	9944(4)	3707(3)	6585(3)	122(1)
C(43)	6822(4)	4740(3)	5987(3)	71(1)
C(9)	5613(4)	9509(2)	7839(3)	59(1)
C(29)	4695(4)	6076(2)	8335(3)	59(1)
C(41)	9355(4)	4333(3)	6862(3)	74(1)
O(42)	9626(5)	6730(4)	6232(5)	182(3)
C(10)	6340(4)	10426(3)	8596(3)	77(1)
C(42)	9115(5)	6297(4)	6618(4)	98(2)
C(18)	3780(4)	8578(3)	6126(3)	76(1)
C(6)	8890(5)	8566(3)	4140(3)	79(1)
C(23)	8074(6)	7381(4)	10392(3)	104(2)
C(17)	4683(4)	9524(3)	6902(3)	66(1)
C(30)	3982(4)	5672(3)	7186(3)	72(1)
C(28)	4022(5)	5918(3)	8983(4)	84(1)

C(16)	4559(5)	10493(3)	6711(4)	87(1)
C(14)	6136(5)	11362(3)	8342(4)	98(2)
C(26)	5903(7)	6732(4)	10469(3)	94(2)
C(15)	5273(5)	11383(3)	7415(4)	101(2)
C(31)	3833(6)	4490(4)	6824(4)	109(2)
C(4)	8799(5)	9338(3)	6717(3)	89(1)
C(20)	3630(6)	8516(4)	5008(4)	115(2)
C(27)	4632(7)	6251(4)	10041(5)	107(2)
C(24)	8903(7)	6619(7)	10843(5)	167(3)
C(32)	2635(5)	6035(5)	6834(5)	120(2)
C(19)	2420(5)	8557(4)	6252(5)	114(2)
C(12)	6735(10)	10904(8)	10495(6)	213(4)
C(11)	7288(7)	10429(4)	9641(4)	118(2)
C(25)	8231(10)	8418(5)	11215(4)	183(4)
C(13)	8670(8)	11032(6)	9913(6)	184(4)

Table A.28 Bond lengths [Å] and angles [°] for **27**.

Mo(1)-C(41)	1.967(4)
Mo(1)-C(44)	2.016(4)
Mo(1)-C(43)	2.029(4)
Mo(1)-C(45)	2.029(4)
Mo(1)-C(42)	2.051(4)
Mo(1)-P(1)	2.5561(8)
P(1)-C(1)	1.697(3)
P(1)-C(21)	1.837(3)
N(1)-C(1)	1.360(4)
N(1)-C(9)	1.443(4)
C(21)-C(22)	1.401(4)
C(21)-C(29)	1.404(5)
O(5)-C(5)	1.363(4)
O(5)-C(6)	1.403(4)
C(1)-C(2)	1.484(4)
C(7)-C(5)	1.348(4)
C(7)-C(8)	1.391(4)
C(2)-C(3)	1.367(4)
C(2)-C(8)	1.371(4)
C(45)-O(45)	1.142(5)
C(44)-O(44)	1.138(4)
C(5)-C(4)	1.363(5)
C(22)-C(26)	1.399(6)
C(22)-C(23)	1.513(6)
C(3)-C(4)	1.382(5)
O(43)-C(43)	1.145(5)
O(41)-C(41)	1.145(4)
C(9)-C(17)	1.391(5)
C(9)-C(10)	1.409(5)
C(29)-C(28)	1.393(5)
C(29)-C(30)	1.505(5)
O(42)-C(42)	1.128(5)
C(10)-C(14)	1.405(5)
C(10)-C(11)	1.508(7)

C(18)-C(17)	1.504(6)
C(18)-C(20)	1.529(6)
C(18)-C(19)	1.530(6)
C(23)-C(24)	1.521(8)
C(23)-C(25)	1.539(8)
C(17)-C(16)	1.403(5)
C(30)-C(32)	1.521(6)
C(30)-C(31)	1.525(6)
C(28)-C(27)	1.378(7)
C(16)-C(15)	1.355(6)
C(14)-C(15)	1.355(6)
C(26)-C(27)	1.355(7)
C(12)-C(11)	1.534(9)
C(11)-C(13)	1.540(10)

C(41)-Mo(1)-C(44)	88.78(16)
C(41)-Mo(1)-C(43)	87.00(16)
C(44)-Mo(1)-C(43)	89.48(15)
C(41)-Mo(1)-C(45)	87.88(16)
C(44)-Mo(1)-C(45)	90.71(16)
C(43)-Mo(1)-C(45)	174.87(15)
C(41)-Mo(1)-C(42)	86.99(16)
C(44)-Mo(1)-C(42)	175.76(15)
C(43)-Mo(1)-C(42)	90.6(2)
C(45)-Mo(1)-C(42)	88.9(2)
C(41)-Mo(1)-P(1)	177.08(13)
C(44)-Mo(1)-P(1)	88.55(11)
C(43)-Mo(1)-P(1)	91.79(11)
C(45)-Mo(1)-P(1)	93.34(11)
C(42)-Mo(1)-P(1)	95.69(12)
C(1)-P(1)-C(21)	106.30(13)
C(1)-P(1)-Mo(1)	130.03(10)
C(21)-P(1)-Mo(1)	123.62(9)
C(1)-N(1)-C(9)	125.2(3)
C(22)-C(21)-C(29)	120.4(3)
C(22)-C(21)-P(1)	119.8(3)

C(29)-C(21)-P(1)	119.7(2)
C(5)-O(5)-C(6)	118.8(3)
N(1)-C(1)-C(2)	117.0(2)
N(1)-C(1)-P(1)	124.7(2)
C(2)-C(1)-P(1)	118.32(19)
C(5)-C(7)-C(8)	120.2(3)
C(3)-C(2)-C(8)	117.4(3)
C(3)-C(2)-C(1)	121.1(2)
C(8)-C(2)-C(1)	121.5(2)
C(2)-C(8)-C(7)	121.4(3)
O(45)-C(45)-Mo(1)	175.3(4)
O(44)-C(44)-Mo(1)	177.0(4)
C(7)-C(5)-C(4)	119.1(3)
C(7)-C(5)-O(5)	125.2(3)
C(4)-C(5)-O(5)	115.7(3)
C(26)-C(22)-C(21)	118.3(4)
C(26)-C(22)-C(23)	118.3(4)
C(21)-C(22)-C(23)	123.4(3)
C(2)-C(3)-C(4)	121.1(3)
O(43)-C(43)-Mo(1)	175.2(3)
C(17)-C(9)-C(10)	122.1(3)
C(17)-C(9)-N(1)	119.5(3)
C(10)-C(9)-N(1)	118.4(3)
C(28)-C(29)-C(21)	118.8(4)
C(28)-C(29)-C(30)	118.0(4)
C(21)-C(29)-C(30)	123.2(3)
O(41)-C(41)-Mo(1)	179.6(4)
C(14)-C(10)-C(9)	116.9(4)
C(14)-C(10)-C(11)	120.3(4)
C(9)-C(10)-C(11)	122.8(3)
O(42)-C(42)-Mo(1)	173.9(4)
C(17)-C(18)-C(20)	113.5(4)
C(17)-C(18)-C(19)	109.1(3)
C(20)-C(18)-C(19)	110.2(4)
C(22)-C(23)-C(24)	110.7(4)
C(22)-C(23)-C(25)	111.4(6)

C(24)-C(23)-C(25)	111.9(5)
C(9)-C(17)-C(16)	117.0(4)
C(9)-C(17)-C(18)	123.7(3)
C(16)-C(17)-C(18)	119.3(4)
C(29)-C(30)-C(32)	112.9(4)
C(29)-C(30)-C(31)	111.1(3)
C(32)-C(30)-C(31)	110.1(4)
C(27)-C(28)-C(29)	120.6(4)
C(15)-C(16)-C(17)	122.0(4)
C(15)-C(14)-C(10)	121.6(4)
C(27)-C(26)-C(22)	121.5(4)
C(14)-C(15)-C(16)	120.5(4)
C(5)-C(4)-C(3)	120.7(3)
C(26)-C(27)-C(28)	120.4(4)
C(10)-C(11)-C(12)	110.8(6)
C(10)-C(11)-C(13)	112.9(5)
C(12)-C(11)-C(13)	108.3(6)

Table A.29 Anisotropic displacement parameters ($Å^2 x\ 10^3$) for **27**. The anisotropic displacement factor exponent takes the form: $-2\pi^2[\ h^2\ a^{*2}U^{11} + ... + 2\ h\ k\ a^*\ b^*\ U^{12}\ ]$

	U^{11}	U^{22}	U^{33}	U^{23}	U^{13}	U^{12}
Mo(1)	47(1)	47(1)	61(1)	25(1)	25(1)	15(1)
P(1)	51(1)	45(1)	55(1)	26(1)	29(1)	14(1)
N(1)	81(2)	54(2)	81(2)	36(1)	59(2)	26(1)
C(21)	63(2)	40(1)	57(2)	23(1)	36(2)	16(1)
O(5)	120(2)	68(2)	77(2)	17(1)	67(2)	-13(1)
C(1)	36(2)	40(1)	35(1)	11(1)	12(1)	3(1)
C(7)	65(2)	59(2)	41(2)	10(1)	23(1)	1(2)
C(2)	39(2)	38(1)	42(1)	14(1)	17(1)	4(1)
C(8)	54(2)	52(2)	48(2)	8(1)	19(1)	-9(1)
C(45)	56(2)	68(2)	93(3)	16(2)	19(2)	11(2)
C(44)	69(2)	62(2)	72(2)	32(2)	22(2)	11(2)
O(44)	123(3)	108(2)	140(3)	81(2)	59(2)	10(2)
C(5)	70(2)	46(2)	58(2)	19(1)	37(2)	1(2)
C(22)	105(3)	54(2)	57(2)	25(2)	42(2)	14(2)
O(45)	70(2)	141(3)	120(3)	5(2)	-7(2)	6(2)
C(3)	84(3)	90(3)	46(2)	-3(2)	30(2)	-37(2)
O(43)	115(3)	132(3)	74(2)	10(2)	2(2)	10(2)
O(41)	135(3)	104(2)	146(3)	30(2)	73(2)	73(2)
C(43)	75(3)	78(2)	64(2)	22(2)	24(2)	25(2)
C(9)	69(2)	46(2)	89(2)	30(2)	53(2)	24(2)
C(29)	64(2)	50(2)	87(2)	33(2)	47(2)	17(2)
C(41)	82(3)	66(2)	84(2)	29(2)	33(2)	28(2)
O(42)	133(4)	240(5)	348(7)	245(5)	176(4)	121(4)
C(10)	88(3)	55(2)	94(3)	19(2)	40(2)	16(2)
C(42)	83(3)	114(3)	167(5)	99(3)	83(3)	60(3)
C(18)	82(3)	61(2)	93(3)	28(2)	33(2)	20(2)
C(6)	105(3)	82(2)	76(2)	27(2)	64(2)	17(2)
C(23)	126(4)	120(4)	49(2)	26(2)	13(2)	-28(3)
C(17)	70(2)	58(2)	88(2)	33(2)	42(2)	27(2)
C(30)	50(2)	77(2)	92(3)	28(2)	29(2)	-2(2)
C(28)	87(3)	79(3)	129(4)	48(2)	77(3)	21(2)

C(16)	97(3)	64(2)	111(3)	41(2)	35(3)	29(2)
C(14)	118(4)	47(2)	129(4)	19(2)	48(3)	11(2)
C(26)	157(5)	83(3)	75(3)	35(2)	74(3)	28(3)
C(15)	122(4)	54(2)	135(4)	42(3)	42(3)	28(2)
C(31)	106(4)	85(3)	120(4)	11(3)	34(3)	7(3)
C(4)	106(4)	80(3)	69(2)	-4(2)	45(2)	-49(2)
C(20)	141(5)	107(4)	94(3)	33(3)	34(3)	30(3)
C(27)	164(6)	98(3)	127(4)	56(3)	118(4)	39(4)
C(24)	127(6)	238(9)	141(5)	105(6)	13(4)	30(5)
C(32)	69(3)	130(4)	162(5)	60(4)	28(3)	27(3)
C(19)	83(4)	105(4)	159(5)	41(3)	46(3)	12(3)
C(12)	246(12)	283(11)	115(5)	34(6)	87(6)	38(9)
C(11)	149(5)	81(3)	100(4)	16(3)	22(4)	10(3)
C(25)	269(10)	141(5)	78(4)	-7(3)	23(5)	-69(6)
C(13)	137(6)	145(6)	186(7)	-7(5)	-14(5)	19(5)

Table A.30 Hydrogen coordinates (x 10^4) and isotropic displacement parameters ($Å^2$x 10^3) for **27**.

	x	y	z	U(eq)
H(7)	7085	7682	4592	66
H(8)	6129	7161	5656	63
H(3)	8537	9381	8059	93
H(18)	4155	7964	6280	91
H(6A)	9509	8861	3894	118
H(6B)	8002	8539	3682	118
H(6C)	9058	7877	4163	118
H(23)	8399	7528	9866	125
H(30)	4530	5941	6849	86
H(28)	3152	5583	8697	101
H(16)	3968	10526	6081	104
H(14)	6603	11982	8822	117
H(26)	6300	6951	11186	112
H(15)	5172	12012	7261	121
H(31A)	3479	4257	6082	163
H(31B)	3241	4202	7097	163
H(31C)	4685	4268	7065	163
H(4)	9457	9911	6987	106
H(20A)	3211	7836	4568	172
H(20B)	4491	8651	4963	172
H(20C)	3096	9023	4791	172
H(27)	4169	6147	10465	129
H(24A)	9813	6933	11176	251
H(24B)	8837	6006	10299	251
H(24C)	8581	6436	11340	251
H(32A)	2723	6771	7133	179
H(32B)	2027	5688	7053	179
H(32C)	2304	5876	6093	179
H(19A)	1850	7940	5777	171
H(19B)	2037	9156	6111	171

H(19C)	2521	8562	6947	171
H(12A)	7412	11013	11159	319
H(12B)	5991	10440	10438	319
H(12C)	6456	11555	10423	319
H(11)	7393	9709	9637	141
H(25A)	7516	8792	10968	275
H(25B)	9061	8822	11349	275
H(25C)	8213	8285	11841	275
H(13A)	9267	10929	10535	276
H(13B)	8606	11758	10014	276
H(13C)	9000	10785	9357	276
H(1)	5650(30)	8410(20)	8460(20)	38(8)

Table A.31 Crystal data and structure refinement for **24**.

Identification code	**24**	
Empirical formula	C37 H42 Cr N O5 P	
Formula weight	663.69	
Temperature	293(2) K	
Wavelength	0.71073 Å	
Crystal system	Triclinic	
Space group	P-1	
Unit cell dimensions	a = 10.4722(8) Å	α= 84.600(11)°.
	b = 12.1314(11) Å	β= 79.559(10)°.
	c = 14.7650(13) Å	γ = 71.687(10)°.
Volume	1749.9(3) $Å^3$	
Z	2	
Density (calculated)	1.260 Mg/m^3	
Absorption coefficient	0.414 mm^{-1}	
F(000)	700	
Crystal size	0.66 x 0.32 x 0.12 mm^3	
Theta range for data collection	2.81 to 25.68°.	
Index ranges	-12<=h<=12, -14<=k<=14, -17<=l<=17	
Reflections collected	24645	
Independent reflections	6226 [R(int) = 0.1282]	
Completeness to theta = 25.68°	93.8 %	
Max. and min. transmission	0.9520 and 0.7717	
Refinement method	Full-matrix least-squares on F^2	
Data / restraints / parameters	6226 / 0 / 415	
Goodness-of-fit on F^2	0.884	
Final R indices [I>2sigma(I)]	R1 = 0.0402, wR2 = 0.0931	
R indices (all data)	R1 = 0.0641, wR2 = 0.1010	
Largest diff. peak and hole	0.236 and -0.194 $e.Å^{-3}$	

Table A.32 Atomic coordinates (x 10^4) and equivalent isotropic displacement parameters ($Å^2$x 10^3) for **24**. U(eq) is defined as one third of the trace of the orthogonalized U^{ij} tensor.

	x	y	z	U(eq)
Cr(1)	-532(1)	8402(1)	7108(1)	42(1)
P(1)	1391(1)	7275(1)	7842(1)	42(1)
N(1)	3477(2)	5377(1)	8144(1)	40(1)
O(41)	-2837(2)	9855(2)	6167(2)	87(1)
O(42)	-1427(2)	6301(2)	6906(2)	79(1)
O(43)	1231(3)	8305(2)	5224(2)	82(1)
O(44)	4(3)	10612(2)	7474(2)	92(1)
O(45)	-2688(2)	8862(2)	8807(2)	76(1)
C(1)	2334(2)	5854(2)	7751(1)	34(1)
C(2)	1897(2)	5079(2)	7236(2)	37(1)
C(3)	1503(3)	4137(2)	7656(2)	48(1)
C(4)	1157(3)	3417(2)	7149(2)	55(1)
C(5)	1175(3)	3593(2)	6212(2)	49(1)
C(6)	819(4)	2792(3)	5658(2)	77(1)
C(7)	1546(3)	4538(2)	5799(2)	50(1)
C(8)	1901(3)	5271(2)	6297(2)	43(1)
C(9)	4149(2)	4146(2)	8255(2)	39(1)
C(10)	3920(2)	3602(2)	9121(2)	42(1)
C(11)	3138(3)	4258(2)	9970(2)	49(1)
C(12)	3948(4)	3938(3)	10767(2)	74(1)
C(13)	1760(3)	4077(3)	10263(2)	76(1)
C(14)	4465(3)	2399(2)	9190(2)	54(1)
C(15)	5214(3)	1783(2)	8446(2)	61(1)
C(16)	5493(3)	2336(2)	7625(2)	58(1)
C(17)	4968(3)	3531(2)	7502(2)	45(1)
C(18)	5387(3)	4117(2)	6595(2)	60(1)
C(19)	6790(4)	4229(4)	6579(3)	101(1)
C(20)	5349(4)	3485(3)	5767(2)	88(1)
C(21)	2363(2)	7988(2)	8372(2)	41(1)
C(22)	2108(3)	8132(2)	9331(2)	43(1)
C(23)	1190(3)	7565(2)	9995(2)	52(1)

C(25)	1785(3)	7063(2)	10876(2)	67(1)
C(26)	2691(3)	8840(2)	9681(2)	56(1)
C(27)	3524(3)	9380(2)	9121(2)	62(1)
C(28)	3814(3)	9210(2)	8198(2)	60(1)
C(29)	3263(3)	8517(2)	7799(2)	49(1)
C(30)	3700(3)	8319(3)	6779(2)	67(1)
C(31)	3501(4)	9450(4)	6190(3)	104(1)
C(32)	5155(4)	7549(3)	6583(3)	90(1)
C(24)	-225(3)	8414(3)	10244(2)	69(1)
C(41)	-1950(3)	9292(2)	6519(2)	60(1)
C(42)	-1020(3)	7048(2)	6969(2)	52(1)
C(43)	607(3)	8300(2)	5937(2)	53(1)
C(44)	-164(3)	9765(2)	7335(2)	56(1)
C(45)	-1811(3)	8648(2)	8199(2)	54(1)

Table A.33 Bond lengths [Å] and angles [°] for **24**.

Cr(1)-C(41)	1.846(3)
Cr(1)-C(45)	1.881(3)
Cr(1)-C(44)	1.883(3)
Cr(1)-C(43)	1.904(3)
Cr(1)-C(42)	1.906(3)
Cr(1)-P(1)	2.4260(7)
P(1)-C(1)	1.700(2)
P(1)-C(21)	1.836(2)
N(1)-C(1)	1.363(3)
N(1)-C(9)	1.445(3)
O(41)-C(41)	1.144(3)
O(42)-C(42)	1.133(3)
O(43)-C(43)	1.135(3)
O(44)-C(44)	1.138(3)
O(45)-C(45)	1.146(3)
C(1)-C(2)	1.484(3)
C(2)-C(8)	1.383(3)
C(2)-C(3)	1.389(3)
C(3)-C(4)	1.369(3)
C(4)-C(5)	1.377(3)
C(5)-C(7)	1.379(3)
C(5)-C(6)	1.497(4)
C(7)-C(8)	1.378(3)
C(9)-C(17)	1.392(3)
C(9)-C(10)	1.399(3)
C(10)-C(14)	1.391(3)
C(10)-C(11)	1.511(3)
C(11)-C(13)	1.508(4)
C(11)-C(12)	1.525(4)
C(14)-C(15)	1.362(4)
C(15)-C(16)	1.359(4)
C(16)-C(17)	1.387(3)
C(17)-C(18)	1.514(3)
C(18)-C(19)	1.513(5)

C(18)-C(20)	1.516(4)
C(21)-C(22)	1.409(3)
C(21)-C(29)	1.415(3)
C(22)-C(26)	1.380(3)
C(22)-C(23)	1.519(4)
C(23)-C(24)	1.518(4)
C(23)-C(25)	1.535(4)
C(26)-C(27)	1.367(4)
C(27)-C(28)	1.361(4)
C(28)-C(29)	1.381(4)
C(29)-C(30)	1.511(4)
C(30)-C(32)	1.508(5)
C(30)-C(31)	1.531(4)

C(41)-Cr(1)-C(45)	86.12(12)
C(41)-Cr(1)-C(44)	89.55(12)
C(45)-Cr(1)-C(44)	87.62(12)
C(41)-Cr(1)-C(43)	87.23(12)
C(45)-Cr(1)-C(43)	173.14(11)
C(44)-Cr(1)-C(43)	90.64(12)
C(41)-Cr(1)-C(42)	89.91(12)
C(45)-Cr(1)-C(42)	87.55(12)
C(44)-Cr(1)-C(42)	175.16(13)
C(43)-Cr(1)-C(42)	94.14(11)
C(41)-Cr(1)-P(1)	177.65(10)
C(45)-Cr(1)-P(1)	95.61(8)
C(44)-Cr(1)-P(1)	88.95(8)
C(43)-Cr(1)-P(1)	90.99(8)
C(42)-Cr(1)-P(1)	91.75(8)
C(1)-P(1)-C(21)	106.75(10)
C(1)-P(1)-Cr(1)	130.36(8)
C(21)-P(1)-Cr(1)	121.08(7)
C(1)-N(1)-C(9)	125.07(18)
N(1)-C(1)-C(2)	117.66(17)
N(1)-C(1)-P(1)	122.95(16)
C(2)-C(1)-P(1)	119.39(16)

C(8)-C(2)-C(3)	117.6(2)
C(8)-C(2)-C(1)	119.79(18)
C(3)-C(2)-C(1)	122.56(19)
C(4)-C(3)-C(2)	120.7(2)
C(3)-C(4)-C(5)	122.0(2)
C(4)-C(5)-C(7)	117.2(2)
C(4)-C(5)-C(6)	121.8(2)
C(7)-C(5)-C(6)	121.0(2)
C(8)-C(7)-C(5)	121.6(2)
C(7)-C(8)-C(2)	120.8(2)
C(17)-C(9)-C(10)	121.94(19)
C(17)-C(9)-N(1)	119.68(19)
C(10)-C(9)-N(1)	118.4(2)
C(14)-C(10)-C(9)	117.4(2)
C(14)-C(10)-C(11)	119.4(2)
C(9)-C(10)-C(11)	123.20(18)
C(13)-C(11)-C(10)	112.2(2)
C(13)-C(11)-C(12)	110.2(2)
C(10)-C(11)-C(12)	111.5(2)
C(15)-C(14)-C(10)	121.0(2)
C(16)-C(15)-C(14)	120.6(2)
C(15)-C(16)-C(17)	121.4(3)
C(16)-C(17)-C(9)	117.4(2)
C(16)-C(17)-C(18)	119.5(2)
C(9)-C(17)-C(18)	123.0(2)
C(19)-C(18)-C(17)	108.9(2)
C(19)-C(18)-C(20)	111.1(3)
C(17)-C(18)-C(20)	112.8(3)
C(22)-C(21)-C(29)	119.6(2)
C(22)-C(21)-P(1)	120.72(18)
C(29)-C(21)-P(1)	119.23(18)
C(26)-C(22)-C(21)	118.7(2)
C(26)-C(22)-C(23)	118.4(2)
C(21)-C(22)-C(23)	122.9(2)
C(24)-C(23)-C(22)	111.0(2)
C(24)-C(23)-C(25)	109.8(2)

C(22)-C(23)-C(25)	112.4(2)
C(27)-C(26)-C(22)	121.4(3)
C(28)-C(27)-C(26)	120.1(3)
C(27)-C(28)-C(29)	121.7(3)
C(28)-C(29)-C(21)	118.4(2)
C(28)-C(29)-C(30)	118.2(2)
C(21)-C(29)-C(30)	123.3(2)
C(32)-C(30)-C(29)	110.8(2)
C(32)-C(30)-C(31)	110.8(3)
C(29)-C(30)-C(31)	113.1(3)
O(41)-C(41)-Cr(1)	178.9(3)
O(42)-C(42)-Cr(1)	173.9(2)
O(43)-C(43)-Cr(1)	175.7(3)
O(44)-C(44)-Cr(1)	177.2(3)
O(45)-C(45)-Cr(1)	172.9(2)

Table A.34 Anisotropic displacement parameters ($Å^2 x\ 10^3$) for **24**. The anisotropic displacement factor exponent takes the form: $-2\pi^2[\ h^2\ a^{*2}U^{11} + ... + 2\ h\ k\ a^*\ b^*\ U^{12}\ ]$

	U^{11}	U^{22}	U^{33}	U^{23}	U^{13}	U^{12}
Cr(1)	39(1)	39(1)	48(1)	-6(1)	-13(1)	-8(1)
P(1)	38(1)	37(1)	54(1)	-9(1)	-16(1)	-7(1)
N(1)	40(1)	32(1)	51(1)	-2(1)	-15(1)	-11(1)
O(41)	71(2)	84(1)	101(2)	9(1)	-47(1)	0(1)
O(42)	59(2)	65(1)	126(2)	-19(1)	-19(1)	-29(1)
O(43)	82(2)	112(2)	59(1)	-16(1)	3(1)	-45(1)
O(44)	114(2)	55(1)	116(2)	-22(1)	-15(2)	-34(1)
O(45)	57(2)	84(1)	74(2)	-6(1)	4(1)	-9(1)
C(1)	34(1)	38(1)	32(1)	-2(1)	-2(1)	-13(1)
C(2)	34(1)	36(1)	40(1)	-5(1)	-4(1)	-10(1)
C(3)	58(2)	54(1)	40(1)	2(1)	-10(1)	-28(1)
C(4)	73(2)	53(1)	53(2)	2(1)	-15(1)	-35(1)
C(5)	51(2)	51(1)	51(1)	-8(1)	-13(1)	-18(1)
C(6)	106(3)	71(2)	70(2)	-15(2)	-25(2)	-43(2)
C(7)	62(2)	53(1)	36(1)	-7(1)	-9(1)	-19(1)
C(8)	47(2)	41(1)	42(1)	0(1)	-6(1)	-15(1)
C(9)	36(1)	35(1)	48(1)	-2(1)	-12(1)	-10(1)
C(10)	40(2)	36(1)	48(1)	0(1)	-8(1)	-10(1)
C(11)	54(2)	42(1)	47(1)	-1(1)	-10(1)	-9(1)
C(12)	68(2)	93(2)	62(2)	-16(2)	-20(2)	-18(2)
C(13)	53(2)	103(2)	62(2)	-19(2)	-5(1)	-11(2)
C(14)	61(2)	38(1)	59(2)	4(1)	-11(1)	-11(1)
C(15)	66(2)	36(1)	76(2)	-3(1)	-13(2)	-7(1)
C(16)	55(2)	46(1)	67(2)	-16(1)	-4(1)	-4(1)
C(17)	38(2)	46(1)	50(1)	-5(1)	-6(1)	-10(1)
C(18)	55(2)	64(2)	52(2)	-2(1)	3(1)	-12(1)
C(19)	76(3)	133(3)	95(3)	10(2)	10(2)	-50(2)
C(20)	98(3)	93(2)	55(2)	-15(2)	-3(2)	-7(2)
C(21)	36(1)	34(1)	53(1)	-5(1)	-14(1)	-8(1)
C(22)	43(2)	35(1)	51(1)	-7(1)	-12(1)	-8(1)
C(23)	57(2)	48(1)	53(2)	-12(1)	-5(1)	-18(1)

C(25)	83(2)	59(2)	54(2)	-2(1)	-9(2)	-17(1)
C(26)	62(2)	54(1)	56(2)	-17(1)	-15(1)	-18(1)
C(27)	71(2)	55(1)	75(2)	-11(1)	-24(2)	-31(1)
C(28)	60(2)	62(2)	69(2)	1(1)	-17(1)	-32(1)
C(29)	46(2)	52(1)	55(2)	2(1)	-19(1)	-18(1)
C(30)	62(2)	96(2)	57(2)	3(2)	-17(1)	-44(2)
C(31)	100(3)	135(3)	72(2)	34(2)	-19(2)	-36(2)
C(32)	87(3)	103(2)	75(2)	-23(2)	4(2)	-27(2)
C(24)	53(2)	78(2)	73(2)	-14(2)	-3(1)	-18(1)
C(41)	63(2)	55(1)	60(2)	-6(1)	-15(1)	-14(1)
C(42)	40(2)	52(1)	64(2)	-9(1)	-14(1)	-8(1)
C(43)	57(2)	54(1)	55(2)	-7(1)	-16(1)	-21(1)
C(44)	56(2)	49(1)	61(2)	-8(1)	-10(1)	-11(1)
C(45)	51(2)	48(1)	61(2)	-1(1)	-15(1)	-7(1)

Table A.35 Hydrogen coordinates (x 10^4) and isotropic displacement parameters ($Å^2$x 10^3) for **24**.

	x	y	z	U(eq)
H(1)	3824	5845	8341	48
H(3)	1475	3994	8288	57
H(4)	902	2790	7446	66
H(6A)	1639	2234	5381	115
H(6B)	334	3233	5184	115
H(6C)	256	2394	6053	115
H(7)	1558	4684	5168	59
H(8)	2147	5901	5998	52
H(11)	2988	5088	9817	59
H(12A)	3465	4423	11275	111
H(12B)	4825	4052	10572	111
H(12C)	4064	3139	10958	111
H(13A)	1189	4435	9809	113
H(13B)	1348	4421	10846	113
H(13C)	1864	3259	10319	113
H(14)	4315	2009	9754	65
H(15)	5537	977	8500	73
H(16)	6048	1903	7134	70
H(18)	4745	4902	6566	72
H(19A)	6797	4602	7122	152
H(19B)	7016	4685	6042	152
H(19C)	7448	3470	6561	152
H(20A)	5497	3945	5215	131
H(20B)	4476	3361	5823	131
H(20C)	6050	2749	5738	131
H(23)	1100	6921	9684	62
H(25A)	1726	7687	11252	100
H(25B)	2722	6612	10715	100
H(25C)	1279	6577	11213	100
H(26)	2513	8953	10311	67

H(27)	3894	9863	9370	75
H(28)	4397	9569	7827	72
H(30)	3125	7904	6598	80
H(31A)	4096	9854	6321	155
H(31B)	2572	9930	6330	155
H(31C)	3708	9274	5549	155
H(32A)	5746	7924	6765	135
H(32B)	5402	7411	5936	135
H(32C)	5242	6822	6924	135
H(24A)	-169	9041	10570	103
H(24B)	-803	8021	10627	103
H(24C)	-596	8717	9691	103

Table A.36 Crystal data and structure refinement for **28**.

Identification code	**28**	
Empirical formula	C37 H53 N2 P	
Formula weight	556.78	
Temperature	293(2) K	
Wavelength	0.71073 Å	
Crystal system	Monoclinic	
Space group	P2(1)/n	
Unit cell dimensions	a = 11.7267(7) Å	α= 90°.
	b = 18.8194(16) Å	β= 90.249(7)°.
	c = 15.8220(9) Å	γ = 90°.
Volume	3491.7(4) $Å^3$	
Z	4	
Density (calculated)	1.059 Mg/m^3	
Absorption coefficient	0.104 mm^{-1}	
F(000)	1216	
Crystal size	0.30 x 0.25 x 0.20 mm^3	
Theta range for data collection	2.05 to 26.00°.	
Index ranges	-14<=h<=14, -23<=k<=23, -19<=l<=18	
Reflections collected	27651	
Independent reflections	6692 [R(int) = 0.0745]	
Completeness to theta = 26.00°	97.3 %	
Absorption correction	None	
Refinement method	Full-matrix least-squares on F^2	
Data / restraints / parameters	6692 / 0 / 381	
Goodness-of-fit on F^2	0.790	
Final R indices [I>2sigma(I)]	R1 = 0.0434, wR2 = 0.0952	
R indices (all data)	R1 = 0.0970, wR2 = 0.1095	
Largest diff. peak and hole	0.145 and -0.171 $e.Å^{-3}$	

Table A.37 Atomic coordinates (x 10^4) and equivalent isotropic displacement parameters ($Å^2$x 10^3) for **28**. U(eq) is defined as one third of the trace of the orthogonalized U^{ij} tensor.

	x	y	z	U(eq)
P(3)	6174(1)	1558(1)	947(1)	56(1)
N(2)	7396(1)	1927(1)	2381(1)	45(1)
N(1)	5455(1)	1983(1)	2560(1)	43(1)
C(2)	4310(2)	1933(1)	2265(1)	43(1)
C(1)	6298(2)	1872(1)	2068(1)	41(1)
C(3)	3685(2)	2571(1)	2205(1)	48(1)
C(10)	3778(2)	1272(1)	2124(1)	50(1)
C(26)	7529(2)	1851(1)	472(1)	49(1)
C(7)	2552(2)	2532(1)	1949(1)	59(1)
C(31)	9499(2)	1575(1)	188(1)	63(1)
C(22)	7989(2)	3001(1)	3127(1)	51(1)
C(14)	7640(2)	2291(1)	3162(1)	45(1)
C(27)	8471(2)	1390(1)	570(1)	51(1)
C(15)	7544(2)	1921(1)	3924(1)	54(1)
C(33)	8675(2)	2621(1)	-391(2)	70(1)
C(9)	2632(2)	1273(1)	1883(1)	62(1)
C(34)	7629(2)	2475(1)	-23(1)	57(1)
C(8)	2038(2)	1891(1)	1785(2)	66(1)
C(20)	8120(2)	2989(2)	4649(2)	71(1)
C(21)	8231(2)	3339(1)	3890(2)	66(1)
C(19)	7784(2)	2296(1)	4663(1)	68(1)
C(32)	9601(2)	2183(2)	-282(2)	73(1)
C(11)	4225(2)	3280(1)	2416(2)	62(1)
C(5)	4197(2)	42(1)	1540(2)	82(1)
C(16)	8154(2)	3374(1)	2284(2)	65(1)
C(4)	4374(2)	564(1)	2275(1)	59(1)
C(37)	8226(3)	88(1)	387(2)	102(1)
C(17)	9349(2)	3228(1)	1942(2)	85(1)
C(28)	6624(2)	2963(1)	-209(2)	74(1)
C(35)	8400(2)	686(1)	1031(2)	63(1)
C(23)	7264(2)	1136(1)	3956(1)	68(1)

C(6)	3974(2)	233(2)	3107(2)	88(1)
C(36)	9420(2)	545(2)	1607(2)	94(1)
C(29)	5982(3)	2698(2)	-980(2)	111(1)
C(12)	3427(2)	3778(1)	2901(2)	90(1)
C(25)	8348(3)	710(2)	4096(2)	104(1)
C(13)	4672(3)	3647(2)	1647(2)	110(1)
C(24)	6394(3)	952(2)	4630(2)	120(1)
C(18)	7928(3)	4175(1)	2315(2)	99(1)
C(30)	6946(3)	3737(2)	-303(3)	144(2)

Table A.38 Bond lengths [Å] and angles [°] for **28**.

P(3)-C(26)	1.845(2)
P(3)-C(1)	1.8733(19)
N(2)-C(1)	1.381(2)
N(2)-C(14)	1.440(2)
N(1)-C(1)	1.279(2)
N(1)-C(2)	1.423(2)
C(2)-C(10)	1.408(3)
C(2)-C(3)	1.410(3)
C(3)-C(7)	1.389(3)
C(3)-C(11)	1.514(3)
C(10)-C(9)	1.396(3)
C(10)-C(4)	1.523(3)
C(26)-C(27)	1.413(3)
C(26)-C(34)	1.416(3)
C(7)-C(8)	1.373(3)
C(31)-C(32)	1.370(3)
C(31)-C(27)	1.396(3)
C(22)-C(21)	1.393(3)
C(22)-C(14)	1.399(3)
C(22)-C(16)	1.519(3)
C(14)-C(15)	1.396(3)
C(27)-C(35)	1.513(3)
C(15)-C(19)	1.393(3)
C(15)-C(23)	1.514(3)
C(33)-C(32)	1.373(3)
C(33)-C(34)	1.388(3)
C(9)-C(8)	1.364(3)
C(34)-C(28)	1.522(3)
C(20)-C(19)	1.364(3)
C(20)-C(21)	1.376(3)
C(11)-C(13)	1.496(4)
C(11)-C(12)	1.531(3)
C(5)-C(4)	1.535(3)
C(16)-C(17)	1.530(3)

C(16)-C(18)	1.532(3)
C(4)-C(6)	1.531(3)
C(37)-C(35)	1.532(3)
C(28)-C(30)	1.511(4)
C(28)-C(29)	1.516(4)
C(35)-C(36)	1.524(3)
C(23)-C(24)	1.519(4)
C(23)-C(25)	1.519(4)

C(26)-P(3)-C(1)	103.22(8)
C(1)-N(2)-C(14)	121.68(17)
C(1)-N(1)-C(2)	121.35(15)
C(10)-C(2)-C(3)	120.81(16)
C(10)-C(2)-N(1)	121.81(17)
C(3)-C(2)-N(1)	117.04(17)
N(1)-C(1)-N(2)	119.39(17)
N(1)-C(1)-P(3)	124.80(13)
N(2)-C(1)-P(3)	115.60(15)
C(7)-C(3)-C(2)	118.07(19)
C(7)-C(3)-C(11)	120.61(19)
C(2)-C(3)-C(11)	121.31(17)
C(9)-C(10)-C(2)	117.85(19)
C(9)-C(10)-C(4)	119.0(2)
C(2)-C(10)-C(4)	123.08(16)
C(27)-C(26)-C(34)	120.24(19)
C(27)-C(26)-P(3)	116.50(16)
C(34)-C(26)-P(3)	123.10(16)
C(8)-C(7)-C(3)	121.4(2)
C(32)-C(31)-C(27)	121.4(2)
C(21)-C(22)-C(14)	117.4(2)
C(21)-C(22)-C(16)	121.6(2)
C(14)-C(22)-C(16)	120.99(18)
C(15)-C(14)-C(22)	122.36(18)
C(15)-C(14)-N(2)	119.17(18)
C(22)-C(14)-N(2)	118.45(18)
C(31)-C(27)-C(26)	118.4(2)

C(31)-C(27)-C(35)	118.44(19)
C(26)-C(27)-C(35)	123.10(18)
C(19)-C(15)-C(14)	117.1(2)
C(19)-C(15)-C(23)	120.6(2)
C(14)-C(15)-C(23)	122.20(18)
C(32)-C(33)-C(34)	121.8(2)
C(8)-C(9)-C(10)	121.5(2)
C(33)-C(34)-C(26)	118.2(2)
C(33)-C(34)-C(28)	118.9(2)
C(26)-C(34)-C(28)	122.8(2)
C(9)-C(8)-C(7)	120.23(19)
C(19)-C(20)-C(21)	120.0(2)
C(20)-C(21)-C(22)	121.2(2)
C(20)-C(19)-C(15)	121.8(2)
C(31)-C(32)-C(33)	119.9(2)
C(13)-C(11)-C(3)	112.0(2)
C(13)-C(11)-C(12)	110.0(2)
C(3)-C(11)-C(12)	113.2(2)
C(22)-C(16)-C(17)	110.45(18)
C(22)-C(16)-C(18)	113.8(2)
C(17)-C(16)-C(18)	110.3(2)
C(10)-C(4)-C(6)	110.35(19)
C(10)-C(4)-C(5)	112.40(18)
C(6)-C(4)-C(5)	110.5(2)
C(30)-C(28)-C(29)	111.2(3)
C(30)-C(28)-C(34)	114.1(2)
C(29)-C(28)-C(34)	109.7(2)
C(27)-C(35)-C(36)	113.32(19)
C(27)-C(35)-C(37)	109.31(19)
C(36)-C(35)-C(37)	111.9(2)
C(15)-C(23)-C(24)	113.1(2)
C(15)-C(23)-C(25)	109.8(2)
C(24)-C(23)-C(25)	110.0(2)

Table A.39 Anisotropic displacement parameters ($Å^2 x\ 10^3$)for **28**. The anisotropic displacement factor exponent takes the form: $-2\pi^2[\ h^2a^{*2}U^{11} + ... + 2\ h\ k\ a^*\ b^*\ U^{12}\ ]$

	U^{11}	U^{22}	U^{33}	U^{23}	U^{13}	U^{12}
P(3)	42(1)	86(1)	40(1)	-9(1)	6(1)	-13(1)
N(2)	34(1)	62(1)	41(1)	-9(1)	4(1)	-1(1)
N(1)	32(1)	56(1)	40(1)	-3(1)	4(1)	2(1)
C(2)	35(1)	59(1)	35(1)	-2(1)	4(1)	1(1)
C(1)	38(1)	43(1)	41(1)	1(1)	-2(1)	0(1)
C(3)	41(1)	61(1)	42(1)	-2(1)	3(1)	6(1)
C(10)	40(1)	64(1)	45(1)	-1(1)	4(1)	-1(1)
C(26)	44(1)	66(1)	37(1)	-8(1)	8(1)	-7(1)
C(7)	45(1)	75(2)	56(1)	0(1)	3(1)	13(1)
C(31)	43(1)	83(2)	63(1)	-5(1)	12(1)	0(1)
C(22)	42(1)	55(1)	57(1)	-10(1)	-4(1)	6(1)
C(14)	35(1)	56(1)	44(1)	-10(1)	-3(1)	4(1)
C(27)	44(1)	64(1)	45(1)	-8(1)	9(1)	-6(1)
C(15)	46(1)	67(1)	48(1)	-4(1)	-6(1)	-1(1)
C(33)	67(2)	80(2)	62(2)	8(1)	17(1)	-13(1)
C(9)	45(1)	77(2)	64(1)	-5(1)	1(1)	-13(1)
C(34)	57(1)	70(2)	42(1)	-5(1)	9(1)	-4(1)
C(8)	35(1)	97(2)	67(2)	-2(1)	-4(1)	4(1)
C(20)	69(2)	89(2)	56(2)	-25(1)	-6(1)	-1(1)
C(21)	61(1)	59(1)	77(2)	-19(1)	-6(1)	-1(1)
C(19)	68(2)	87(2)	49(1)	-6(1)	-4(1)	-5(1)
C(32)	52(1)	98(2)	70(2)	-2(2)	22(1)	-20(1)
C(11)	56(1)	62(2)	67(2)	-3(1)	1(1)	11(1)
C(5)	82(2)	70(2)	93(2)	-18(1)	3(2)	-6(1)
C(16)	66(2)	56(1)	72(2)	2(1)	-7(1)	-3(1)
C(4)	55(1)	56(1)	65(1)	1(1)	4(1)	-3(1)
C(37)	124(3)	73(2)	109(2)	-21(2)	29(2)	-18(2)
C(17)	78(2)	87(2)	91(2)	4(2)	19(2)	-7(1)
C(28)	76(2)	85(2)	62(2)	9(1)	20(1)	11(1)
C(35)	56(1)	63(2)	69(2)	-3(1)	13(1)	-1(1)
C(23)	78(2)	75(2)	53(1)	8(1)	-14(1)	-13(1)

C(6)	103(2)	81(2)	81(2)	17(2)	13(2)	7(2)
C(36)	81(2)	94(2)	108(2)	26(2)	-1(2)	6(2)
C(29)	83(2)	173(3)	78(2)	3(2)	-7(2)	34(2)
C(12)	104(2)	70(2)	98(2)	-18(2)	19(2)	16(2)
C(25)	107(2)	74(2)	130(3)	-6(2)	-14(2)	4(2)
C(13)	132(3)	98(2)	99(2)	-16(2)	44(2)	-35(2)
C(24)	117(3)	113(3)	130(3)	28(2)	29(2)	-25(2)
C(18)	116(2)	67(2)	115(2)	10(2)	-16(2)	9(2)
C(30)	137(3)	83(2)	211(4)	33(3)	13(3)	19(2)

Table A.40 Hydrogen coordinates (x 10^4) and isotropic displacement parameters ($Å^2$x 10^3) for **28**.

	x	y	z	U(eq)
H(7)	2134	2948	1888	70
H(31)	10129	1280	254	76
H(33)	8752	3028	-720	84
H(9)	2265	842	1787	74
H(8)	1282	1878	1606	80
H(20)	8274	3226	5153	86
H(21)	8472	3810	3887	79
H(19)	7714	2066	5181	81
H(32)	10296	2299	-527	88
H(11)	4880	3184	2785	74
H(5A)	3406	-85	1502	123
H(5B)	4645	-378	1637	123
H(5C)	4430	262	1021	123
H(16)	7607	3167	1884	77
H(4)	5194	657	2326	70
H(37A)	7481	128	137	153
H(37B)	8294	-363	666	153
H(37C)	8794	123	-46	153
H(17A)	9908	3413	2328	127
H(17B)	9433	3454	1402	127
H(17C)	9456	2725	1880	127
H(28)	6104	2930	272	89
H(35)	7720	702	1388	75
H(23)	6944	1000	3406	82
H(6A)	4163	545	3567	133
H(6B)	4346	-216	3189	133
H(6C)	3164	164	3087	133
H(36A)	10099	511	1273	141
H(36B)	9305	108	1908	141
H(36C)	9498	929	2004	141

H(29A)	6452	2750	-1472	167
H(29B)	5296	2970	-1052	167
H(29C)	5792	2206	-905	167
H(12A)	3850	4180	3103	136
H(12B)	3103	3528	3371	136
H(12C)	2827	3936	2531	136
H(25A)	8882	815	3655	156
H(25B)	8171	212	4086	156
H(25C)	8675	832	4633	156
H(13A)	5229	3350	1378	165
H(13B)	5018	4089	1807	165
H(13C)	4055	3736	1260	165
H(24A)	6695	1071	5177	180
H(24B)	6230	453	4608	180
H(24C)	5706	1216	4530	180
H(18A)	7164	4258	2506	149
H(18B)	8021	4373	1761	149
H(18C)	8458	4395	2699	149
H(30A)	7490	3863	127	215
H(30B)	6277	4026	-246	215
H(30C)	7275	3812	-850	215
H(2)	7887(16)	1964(9)	2017(12)	36(5)
H(3)	5469(19)	2060(12)	703(13)	78(7)